National Library
of Canada

Bibliothèque nationale
du Canada

Canadian Theses Service

Service des thèses canadiennes

Ottawa, Canada
K1A 0N4

NOTICE

The quality of this microform is heavily dependent upon the quality of the original thesis submitted for microfilming. Every effort has been made to ensure the highest quality of reproduction possible.

If pages are missing, contact the university which granted the degree.

Some pages may have indistinct print especially if the original pages were typed with a poor typewriter ribbon or if the university sent us an inferior photocopy.

Reproduction in full or in part of this microform is governed by the Canadian Copyright Act, R.S.C. 1970, c. C-30, and subsequent amendments.

AVIS

La qualité de cette microforme dépend grandement de la qualité de la thèse soumise au microfilmage. Nous avons tout fait pour assurer une qualité supérieure de reproduction.

S'il manque des pages, veuillez communiquer avec l'université qui a conféré le grade.

La qualité d'impression de certaines pages peut laisser à désirer, surtout si les pages originales ont été dactylographiées à l'aide d'un ruban usé ou si l'université nous a fait parvenir une photocopie de qualité inférieure.

La reproduction, même partielle, de cette microforme est soumise à la Loi canadienne sur le droit d'auteur, SRC 1970, c. C-30, et ses amendements subséquents.

NL-339 (r. 88/04) c

Canadä

UNIVERSITY OF ALBERTA

Petroleum Hydrogeology of the Pechelbronn-Soultz Basin in the Upper Rhine Graben, France: Ramifications for Exploration in Intermontane Basins

by

© Claus J. Otto

A thesis submitted to the Faculty of Graduate Studies and Research in partial fulfillment of the requirements for the degree of DOCTOR OF PHILOSOPHY.

DEPARTMENT OF GEOLOGY

EDMONTON, ALBERTA

Spring, 1992

National Library
of Canada

Canadian Theses Service

Ottawa, Canada
K1A 0N4

Bibliothèque nationale
du Canada

Service des thèses canadiennes

The author has granted an irrevocable non-exclusive licence allowing the National Library of Canada to reproduce, loan, distribute or sell copies of his/her thesis by any means and in any form or format, making this thesis available to interested persons.

The author retains ownership of the copyright in his/her thesis. Neither the thesis nor substantial extracts from it may be printed or otherwise reproduced without his/her permission.

L'auteur a accordé une licence irrévocable et non exclusive permettant à la Bibliothèque nationale du Canada de reproduire, prêter, distribuer ou vendre des copies de sa thèse de quelque manière et sous quelque forme que ce soit pour mettre des exemplaires de cette thèse à la disposition des personnes intéressées.

L'auteur conserve la propriété du droit d'auteur qui protège sa thèse. Ni la thèse ni des extraits substantiels de celle-ci ne doivent être imprimés ou autrement reproduits sans son autorisation.

ISBN 0-315-73280-6

Canadä

UNIVERSITY OF ALBERTA

RELEASE FORM

NAME OF AUTHOR: Claus J. Otto

TITLE OF THESIS: Petroleum Hydrogeology of the Pechelbronn-Soultz Basin in the Upper Rhine Graben, France: Ramifications for Exploration in Intermontane Basins

DEGREE: Doctor of Philosophy

YEAR THIS DEGREE GRANTED: 1992

Permission is hereby granted to the UNIVERSITY OF ALBERTA LIBRARY to reproduce single copies of this thesis and to lend or sell such copies for private, scholarly or scientific research purposes only.

The author reserves all other publication and other rights in association with the copyright in the thesis, and except as hereinbefore provided neither the thesis nor any substantial portion thereof may be printed or otherwise reproduced in any material form whatever without the author's prior written permission.

Claus Otto
(Claus J. Otto)

CSIRO, Division of Water Resources
Private Bag, PO Wembley, WA 6014
Perth, Australia

Date: 21 April 1992

UNIVERSITY OF ALBERTA

FACULTY OF GRADUATE STUDIES AND RESEARCH

The undersigned certify that they have read, and recommend to the Faculty of Graduate Studies and Research for acceptance, a thesis PETROLEUM HYDROGEOLOGY OF THE PECHELBRONN-SOULTZ BASIN IN THE UPPER RHINE GRABEN - FRANCE: RAMIFICATIONS FOR EXPLORATION IN INTERMONTANE BASINS submitted by Claus, Jürgen Otto in partial fulfillment of the requirements for the degree of Doctor of Philosophy in Geology.

J. Tóth
Dr. J. Tóth, supervisor

Philippe Erdmer
Dr. P. Erdmer

Dr. F.W. Jones

Hans G. Machel
Dr. H. Machel

Dr. K. Muehlenbachs

Dr. R.N. Farvolden, external examiner

Date: 1992 March 24

Dedication

gewidmet

meinen Eltern

(to my parents)

Abstract

The Pechelbronn-Soultz Basin oil deposits in the intermontane valley of the Upper Rhine Graben are the first petroleum accumulations in Europe known to have been commercially exploited. The deposits, originally discovered as oil seeps, are associated with hydrogeological phenomena that are characteristic of groundwater discharge such as relatively high salinity in formation waters (> 100 000 mg/l TDS), positive geothermal anomalies (11 ^{o}C/100 m), flowing artesian wells, and seeps of brine and oil. Oil deposits in Mesozoic and Tertiary reservoirs originated from Lower Jurassic source rocks located in deeper parts of the graben to the northeast, east and southeast. Since the beginning of the Oligocene period, oil has migrated at least 8 km from the graben centre towards the tectonically uplifted reservoirs in the basin. Oil is trapped by faults in structural highs of the Middle Triassic carrier beds and in Eocene and Oligocene strata and sand lenses.The oil deposits have been chemically altered by degradation processes implemented by groundwater of regional and local flow systems. Observed hydraulic head patterns show that the formation waters move from recharge areas in the graben shoulders, the Vosges and Black Forest mountains to discharge areas in the Rhine Valley. The waters discharge in the valley by cross-formational ascent through intensively fractured fault blocks. Within the Pechelbronn-Soultz Basin, which is a region of highest fault density, the two basinal flow systems converge and groundwater is forced to flow up the conductive fault zones to shallower depths. Local flow systems generated by topographic relief can reach depths of several hundred metres and merge with the regional flow system. Distribution patterns of water salinity and temperature are consistent with the regional flow configuration. Furthermore, formation waters are of meteoric origin and are relatively young (< 30 000 years ^{14}C age) even in the deepest hydrostratigraphic units. The synthesis of the above observations in light of the theory of gravity-induced regional groundwater flow results in a unified picture of basin evolution, fluid dynamics and petroleum migration and accumulation within the Pechelbronn-Soultz Basin.

Acknowledgements

Foremost, I wish to express my sincere thanks and appreciation to my supervisor and teacher Dr. József Tóth for providing the opportunity, direction and inspiration for this study. His constant interest in the project, his critical evaluations and encouragement as well as financial support made completion of this graduate study possible.

The input of my supervisory committee has been invaluable. I thank Dr. P. Erdmer and Dr. K. Muehlenbachs of the Department of Geology and Dr. F. Jones of the Department of Geophysics, University of Alberta, for their critical review of my thesis and their valuable suggestions.

Without the professional assistance and financial support of the Federal Institute for Geosciences and Natural Resources (BGR), Hannover, FRG this work would not have been possible. Special thanks are due to Dr. P. Gerling and Dr. D. Plöthner for allowing me to use their geochemical and shallow temperature data, and to Dr. K. Trippler for the organization and co-ordination of the field and office activities in France and Germany. Original well data were supplied by Service Géologique Régional d' Alsace et de Lorraine in Strasbourg. Additional recent well reports were made available by Dr. M. Comte of TOTAL-C.F.P., Paris. Dr. P. Schwoerer's hydrogeological and geological expertise of the area was indispensable in the data acquisition.

I would like to thank my wife Emi. Not only did she assist me with the final drafting of the figures, but she has been a continual source of support and encouragement in every way.

I also wish to thank my friends and colleagues of the Petroleum Hydrogeology Group. To Dan Barson, Diane Edmond, John Horgan, Steve Holysh, Morris Maccagno, Duke Ophori, Kevin Parks, Ben Rostron, Kriensgak Srisuk, Liane Schlickenrieder and Joanne Thompson, I hope to see you all again.

Finally, my deepest appreciation goes to my parents, my family in Holland, Germany, England, Malaysia and Japan.

Table of Contents

1. Introduction 1
    - 1.1 Background to the Study 1
    - 1.2 Literature Review 2
    - 1.3 Purpose and Objectives of the Study 4
    - 1.4 Structure of Thesis 4
    - 1.5 Location, Definitions and Terminology 5
2. Petroleum Geologic Framework 7
    - 2.1 Introduction 7
    - 2.2 Taphrogenic Evolution of the Upper Rhine Graben 8
    - 2.3 Basin Analysis 10
        - 2.3.1 Lithostratigraphy and geohistory 10
        - 2.3.2 Tectonic Structure 11
            - 2.3.2.1 Principal Structure Zones 11
            - 2.3.2.2 The Fault Complex in the Pechelbronn-Soultz Basin 12
            - 2.3.2.3 The Soultz Horst 16
        - 2.3.3 Petroleum Formation and Occurrences 17
            - 2.3.3.1 Source Rocks 17
            - 2.3.3.2 Oil Fields, Reservoir- and Carrier-Beds 21
    - 2.4 Some Tentative Conclusions and Statements 29
3. The Hydrogeologic Environment 32
    - 3.1 Introduction 32
    - 3.2 Topography 32
    - 3.3 Depth and Width 33
    - 3.4 Climate 33
    - 3.5 Hydrostratigraphic Units (HSU's) 34
        - 3.5.1 Hydrostratigraphy of the Upper Rhine Graben 35
            - 3.5.1.1 The Granitic basement - Aquitard (HSU 1) and Aquifer (HSU 2) 35
            - 3.5.1.2 The Permo - Triassic Multi-Aquifer System (HSU 3) 36
            - 3.5.1.3 The Lettenkohle Aquifer (HSU 4) 37

3.5.1.4 The Keuper Aquitard (HSU 5) 38
3.5.1.5 The Grés à Roseaux Aquifer (HSU 6) 39
3.5.1.6 The Jurassic Aquitard (HSU 7) 39
3.5.1.7 The Cenozoic Aquifer - Aquitard Complex 39
3.6 An Aquifer Connectivity Model 41
4. Observed Hydrogeological Phenomena related to Groundwater Flow 43
4.1 Introduction 43
4.2 Analysis of the Hydrochemical Regime 43
4.2.1 Theoretical Considerations 43
4.2.2 Database 45
4.2.3 Hydrochemistry and Classification 47
4.2.3.1 Hydrochemical Overview 47
4.2.3.2 Formation Water Characteristics 48
4.2.3.3 Schoeller Classification 55
4.2.3.4 Trace Elements 57
4.2.4 Isotopic Composition of Formation Waters 60
4.2.4.1 Stable Oxygen and Hydrogen Isotopes 61
4.2.4.2 Radioactive Isotopes Tritium and Carbon-14 68
4.2.5 Interpretation of the Water Chemistry in Terms of Groundwater Flow 77
4.2.6 Conclusions 83
4.3 Analysis of the Subsurface Temperature Regime 85
4.3.1 Theoretical Considerations 85
4.3.2 Database 87
4.3.3 Subsurface Temperature Distribution 88
4.3.4 Temperature and Heat Flow Anomalies caused by Groundwater Flow 90
4.3.5 Conclusions 96
5. Analysis of the Gravity-Driven Groundwater Flow Regime 97
5.1 Theoretical Considerations 97
5.2 Database 99
5.3 Interpretation of the Steady-State Groundwater Flow Regime 101
5.3.1 Hydraulic head distribution and inferred groundwater flow patterns 102
5.3.2 p(d) and p(z) diagrams 105
5.4 Conclusions 106

6. Petroleum Hydrogeological Synthesis 107
7. Applied Petroleum Hydrogeology in the Pechelbronn-Soultz Basin........................111
  7.1 Observed crude oil compositions in relation to groundwater flow...........111
  7.2 A Shallow-Depth Hydrochemical and Temperature Survey across the Pechelbronn - Soultz Basin..114
8. Concluding Statements..120

Bibliography 209

Appendix 1 Notes on Tóth's Generalized Hydraulic Theory of Petroleum Migration 229
Appendix 2 Fault Terminology and Construction Techniques 234
Appendix 3 A Fault Permeability Model - A Critical Review of Permeability Characteristics of Faults in the Upper Crust 235
Appendix 4 Faults and Aquifer Connectivity 241
Appendix 5 Seals and Sealing Mechanisms to Petroleum 246
Appendix 6 The Petroleum Exploration and Production History of Northern Alsace from 1735 to 1961 247
Appendix 7 Hydraulic data 249
Appendix 8 SAEM hydrochemistry data 257
Appendix 9 PREPA hydrochemistry data 266
Appendix 10 BGR hydrochemistry data 269
Appendix 11 GL-BW hydrochemistry data 285
Appendix 12 Schoeller classification data..288
Appendix 13 Trace elements concentrations of formation waters in the Pechelbronn-Soultz Basin 300
Appendix 14 Isotope data (BGR)..309
Appendix 15 Subsurface temperature data..315
Appendix 16 Cumulative thermal resistance and calculated heat flow values for for various depths in the Pechelbronn-Soultz Basin and Internal Zone..323
Appendix 17 Equivalent and environmental hydraulic head data derived from pressure and water level measurements. Data sources: SAEM, PREPA and TOTAL)..350

List of Tables

Table:

1 Average uplift- and elevation-rate for graben shoulders of the middle segment of the Upper Rhine Graben study area from the Late Eocene to present. Data source: Roll, 1979 188

2 Nomenclature of structural units in the Pechelbronn-Soultz Basin and approximated dip angles of principal faults 189

3 Organic characteristics and maturation levels of Tertiary and Jurassic source rocks (see also Figure 78) 190

4 Vitrinite reflectance values for Oligocene and Jurassic source rocks at various depths.Data source: Robert 1985 191

5 Mesozoic reservoirs in the study area 192

6 Permeability and porosity values of the upper Muschelkalk in the Soultz region. Ddata source: SAEM well reports 193

7 Summary of Mesozoic oil producing reservoirs beyond the Pechelbronn-Soultz Basin.Data sources: SAEM, PREPA well reports 194

8 Cumulative oil production in Mesozoic reservoirs at the end of 1961 in the Upper Rhine Graben study area.Data source: Sittler, 1974 194

9 Tertiary reservoir rocks, carrier beds and oil field in the Upper Rhine Graben 195

10 Average porosity and permeability values for Tertiary reservoirs and carrier formations taken from PREPA well reports 196

11 Summary of oil producing Upper Pechelbronner Schichten reservoirs in the Pechelbronn-Soultz Basin. Data source: SAEM well reports 197

12 Summary of Lower Pechelbronner Schichten reservoirs in the Pechelbronn-Soultz Basin. Data source: SAEM well reports 197

13 Equivalent hydraulic conductivity and intrinsic permeability values ranges for freshwater at 15 °C characteristic for aquifers and aquitards (modified after Todd, 1959) 198

14 Assigned porosities, hydraulic conductivities and transmissivities to Mesozoic hydrostratigraphic units 199

15 Assigned porosities, hydraulic conductivities and transmissivities to Tertiary hydrostratigraphic units in the Pechelbronn-Soultz Basin 200

16 Assigned porosities, hydraulic conductivities and transmissivities to Tertiary hydrostratigraphic units in the Upper Rhine Graben 201

17 Groundwater flow across and along juxtaposition faults 202

18 Connectivity factors for aquifers (HSU's) at two principal faults in the Pechelbronn-Soultz Basin 202

19 Groundwater chemistry in hydraulic regimes of flow systems 203

20 Generalized Schoeller classification of formation waters in the Pechelbronn-Soultz Basin 204

21 Iodide and ammonium concentrations for formation waters in the Hochwald and Pechelbronn-Soultz Basin 205

22 Methane content of formation waters in the Vosges, Hochwald and Pechelbronn-Soultz Basin 206

23 Apparent velocities in m/y for groundwater flowing west to east from the Vosges to wells Romaine, Morsbronn and Helion 206

24 Assigned thermal conductivity values for Mesozoic and Tertiary formations in the Upper Rhine Graben study area 207

25 Chemical and physical characteristics of oil pools at Pechelbronn-Soultz in Tertiary and Mesozoic formations at various depths and

reservoir temperatures; O1 is a unaltered oil sample from Ohlungen oil field, 17 km south of the basin. Data source: SAEM oil distillation reports, SGAL, Strasbourg, France) 208

Appendix 7 Hydraulic data 249

Appendix 8 SAEM hydrochemistry data 257

Appendix 9 PREPA hydrochemistry data 266

Appendix 10 BGR hydrochemistry data 269

Appendix 11 GL-BW hydrochemistry data 285

Appendix 12 Schoeller classification data 288

Appendix 13 Trace elements concentrations of formation waters in the Pechelbronn-Soultz Basin 300

Appendix 14 Isotope data (BGR) 309

Appendix 15 Subsurface temperature data 315

Appendix 16 Cumulative thermal resistance and calculated heat flow values for for various depths in the Pechelbronn-Soultz Basin and Internal Zone 323

Appendix 17 Equivalent and environmental hydraulic head data derived from pressure and water level measurements. Data sources: SAEM, PREPA and TOTAL) 350

List of Figures

Figure:

1 Physiography and schematized tectonic structure of the Upper Rhine Graben 124

2 A petroleum hydrogeological analysis requires the implementation of various geo-scientific disciplines which will result in an inter-disciplinary petroleum hydrogeological synthesis and exploration for petroleum in a basin 125

3 The Upper Rhine Graben and its regional geologic setting 126

4 Regional stress patterns in the Upper Rhine Graben; the study area is located in an area of compression and uplift 127

5 Locations of 4 SAEM wells which encountered the granitic basement, and outcropping formations in the Vosges, Hochwald and Black Forest shown on a simplified isohypse map of the top of the basement (modified after Walgenwitz, 1979) 128

6 Simplified isohypse map of the base of the Tertiary for the Upper Rhine Graben (modified after Walgenwitz, 1979) 129

7 Schematic longitudinal section of the Upper Rhine Graben (modified after Sittler, 1967) 130

8 Vitrinite reflectance values (R_o) versus depth for Oligocene and Jurassic source rocks in the Upper Rhine Graben study area; reflectance gradients are higher than the "normal gradient" for passive basins and off-set at the Cretaceous Unconformity (data source: Table 6) 131

9 Oil producing wells in the Grés à Roseaux at the Kutzenhausen Fault near Kutzenhausen 132

10 Oil producing wells in the Grés à Roseaux at the Hoelschloch Fault near Pechelbronn 133

11 Definition of the Tertiary hydrostratigraphic units in the Pechelbronn-Soultz Basin and Upper Rhine Graben 134

12 Above: Schematized geology of displaced hydrostratigraphic units A, B, C, D (aquifers) by two normal faults I and II with different throw; white filed between aquifers represent aquitards. Below: the conceptual diagram of the aquifer connectivity model shows unblocked pathways for groundwater flow and possible sites of petroleum entrapment (Appendix IV) 135

13 An aquifer connectivity model for the Pechelbronn-Soultz Basin (Appendix IV) 136

14 Two water types A and B are identified on a Piper Diagram 138

15 Two water types A and B are identified on a Schoeller diagram 139

16 Formation water density vs. depth plot 140

17 TDS vs. formation water density plot 140

18 Relative frequency distribution of TDS values in the study area 141

19 Relative frequency distribution of sodium + potassium concentrations for formation waters in the Pechelbronn-Soultz Basin; a) SAEM data, b) BGR data 142

20 Relation of sodium vs. chloride concentrations for formation waters in the Pechelbronn-Soultz 143

21 Relation of potassium vs. chloride concentrations for formation waters in the Pechelbronn-Soultz Basin 144

22 Relative frequency distribution of calcium concentrations for formation waters in the Pechelbronn-Soultz Basin; a) SAEM data, b) BGR data 145

23 Relation of calcium vs. chloride concentrations for formation waters in the Pechelbronn-Soultz Basin 146

24 Relative frequency distribution of magnesium for formation waters in the Pechelbronn-Soultz Basin; a) SAEM data, b) BGR data 147

25 Relation of magnesium vs. chloride concentrations for formation waters in the Pechelbronn-Soultz Basin 148

26 Relative frequency distribution of chloride for formation waters in the Pechelbronn-Soultz Basin; a) SAEM data, b) BGR data 149

27 Relative frequency distribution of sulfate for formation waters in the Pechelbronn-Soultz Basin; a) SAEM data, b) BGR data 150

28 Relation of sulfate vs. chloride concentrations for formation waters in the Pechelbronn-Soultz Basin 151

29 Relative frequency distribution of hydrogencarbonate + carbonate for formation waters in the Pechelbronn-Soultz Basin; a) SAEM data, b) BGR data 152

30 Relation of hydrogencarbonate + carbonate vs. chloride concentrations for formation waters in the Pechelbronn-Soultz Basin 153

31 Lithium vs. chloride concentrations for deep and shallow formation waters in the Vosges, Pechelbronn-Soultz Basin and Black Forest 154

32 Strontium vs. chloride concentrations for deep and shallow formation waters in the Vosges, Pechelbronn-Soultz Basin and Black Forest 154

33 Bromide vs. chloride concentrations for deep and shallow formation waters in the Vosges, Pechelbronn-Soultz Basin and Black Forest 155

34 Iodide vs. chloride concentrations for deep and shallow formation waters in the Vosges, Pechelbronn-Soultz Basin and Black Forest 155

35 D vs. ^{18}O plot for deep and shallow formation waters in the Vosges, Hochwald, Pechelbronn-Soultz Basin and Black Forest 156

36 Schoeller diagram showing no significant chemical variations of the formation waters for well Helion from 1978 to 1987 157

37 Changes in flow rate, salinity, temperature and isotopic composition of formation waters in HSU 3 for well Helion recorded from the year 1978 till 1987 158

38 δ ^{13}C vs. ^{14}C-activity plot for deep and shallow formation waters in in the Vosges, Hochwald, Pechelbronn-Soultz Basin and Black Forest 159

39 Modified Schoeller diagram displaying ionic ratios of formation waters in the Vosges, Hochwald and Black Forest recharge area; a) cation ratios, b) anion ratios 160

40 Modified Schoeller diagram showing hydrochemical evolution of groundwater in HSU 3 from the Vosges to the Pechelbronn -Soultz Basin; a) cation ratios, b) anion ratios 161

41 Modified Schoeller diagram showing hydrochemical variations of formation waters in Tertiary formations at Pechelbronn and Soultz in comparison to groundwaters in recharge regions 162

42 Modified Schoeller diagram displaying hydrochemical differences and similarities of groundwaters from shallow wells in Tertiary formations in comparison to deep formation waters in the Kutzenhausen-Soultz region 163

43 Tritium vs. chloride concentration plot showing a decreasing TU/Cl ratio from the western recharge region towards the Pechelbronn-Soultz Basin 164

44 Schematic diagram showing the change in grad T and temperature regime affected by the transport of heat of ascending and descending groundwater........165

45 Temperature vs. depth plot for the study area........166

46 Temperature vs. depth plot for the Pechelbronn, Kutzenhausen and Soultz area........167

47 Geothermal gradients for 3 wells in the Pechelbronn-Soultz Basin and Internal Zone showing negative and positive temperature anomalies........168

48 Heat flow vs. depth for well 4515 calculated for intervals bounded by by successive BHTs........169

49 Heat flow vs. depth for well 4616 calculated for intervals bounded by by successive BHTs........170

50 Heat flow vs. depth for well 4776 calculated for intervals bounded by by successive BHTs........171

51 Calculated subsurface temperatures for given basal heat flow values of 82, 130 and 200 mW/m^2 in comparison to a measured temperature profile of well 4616........172

52 Temperature log for well 4616 recorded by BRGM in 1988........173

53 Diagrammatic representation of hydraulic-, elevation- and pressure heads showing relavent subsurface well data........174

54 Pressure vs. depth plot for all available stabilized DST pressure data........175

55 Pressure vs. depth plot for formation pressures measured in HSU 3 in the Kutzenhausen-Soultz-Hermerswiller Compartments........176

56 Pressure vs. elevation plot for formation pressures measured in HSU 3 in the Kutzenhausen-Soultz-Hermerswiller Compartments........177

57 Graphical summary of the hydraulic theory of petroleum migration and associated natural phenomena (modified after Tóth, 1980)........178

58 Schematic representation of regional groundwater flow between the graben's shoulders with observed phenomena and ^{14}C values 179

59 Geological, geothermal, hydrogeological and petroleum geological history of the Upper Rhine Graben study area 180

60 Maturation-geohistory diagram (Lopatin's method) for well Rohrlach-1 showing that Jurassic source rocks reach the oil window about 25 Ma ago 181

61 a) Schematic representation of the effects of bacterial alteration and water washing on the Correlation Index plot; b) Correlation index plot for altered oils at Pechelbronn, P1-P4; c) Correlation Index plot for altered oils at Soultz, S1-S4, O1 represents a unaltered oil from a Jurassic reservoir at Ohlungen south the study area 182

62 Schematized locations of sampled oil pool, P1-P4 and S1-S4 in the Pechelbronn-Soultz Basin and emplaced oil alteration-degradation processes by the hydrodynamic, geochemical and geothermal system 184

63 Near-surface temperatures vs. depth plot for wells 3, 12 and 31 185

64 Definitions of fault descriptive variables (Appendix II) 186

65 Fault plane construction from two observation points (Appendix II) 186

66 Classification diagram for sealing mechanisms and seal types related to faults (Appendix V) 187

the following Figures are located in the map pocket:

67 Location of the Pechelbronn-Soultz and Upper Rhine Graben study area, relevant towns, rivers and geologic - tectonic features

68 Lithostratigraphy, petroleum geology, hydrostratigraphy and geohistory of the study area

69 Regional simplified cross-section (A"-A"') of the Upper Rhine Graben study area (data sources: SAEM, PREPA well reports, Sittler '85) and definition of structural zones and elements

70 Location Base Map: principal faults, definition of structural zones and compartments, fault-controlled oil pools (data sources: SAEM well reports, Schnaebele '48, Levi '62) and vitrinite reflectance values of Jurassic and Oligocene sourcerocks (data source: Robert '88)

71 Complex structure contour of top of Muschelkalk (HSU 3), principal faults, structural compartments, producing oil wells, formation water salinity distribution and other hydrogeological phenomena (see also Figure 88 ; data sources: SAEM well reports, BGR)

72 Structural contour of top of Zone Dolomitique (HSU 8), principal faults, structural compartments, fault-controlled oil pools, formation water salinity distribution and other hydrogeological phenomena (data source: SAEM well reports)

73 Profiles Ia and Ib south at Kreuzecke and Reimerswiller, respectively, showing geology, oil pools, formation water salinities, subsurface temperatures, hydraulic heads and inferred groundwater flow directions

74 Profiles IIa, IIb and IIc south of Preuschdorf and at Hoelschloch showing geology, oil pools, formation water salinities, subsurface temperatures, hydraulic heads and inferred groundwater flow directions

75 Profiles IIIa, IIIb, IIIc, IIId south of Pechelbronn and near Kutzenhausen showing geology, oil pools, formation water salinities, subsurface temperatures, hydraulic heads and inferred groundwater flow directions

76 Profile B-B': General increase in formation water salinity and subsurface temperatures towards the Kutzenhausen-Soultz discharge area with groundwater flow direction, modified by the channelling-effect of fault zones in the Pechelbronn-Soultz Basin

77 Profile IV at Kutzenhausen and Soultz showing a complex geology, oil pools, formation water salinities, subsurface temperatures, isotherms, hydraulic heads and inferred groundwater flow directions

78 ProfileV at Soultz showing a complex geology. oil pools, formation water salinities, subsurface temperatures, isotherms, hydraulic heads and inferred groundwater flow directions

79 Profiles VIa, VIb and VIc north of Pechelbronn and Soultz showing geology, oil pools, formation water salinities, subsurface temperatures, hydraulic heads and inferred groundwater flow directions

80 Profile VII shows a schematized NNW-SSE cross-section of the Pechelbronn-Soultz Basin

81 The Lettenkohle is productive in the up-dip section of the formation the footwall of the Kutzenhausen and Soultz Faults

82 A locally scaled showing oil pools and the formation water salinity distribution in the Pechelbronner Schichten in relation to principal fault zones dissecting the Tertiary formations and to the superimposed local topography; as well as a shallow-depth survey profile with to the near-surface outcropping faults as detected by shallow-depth chemical and temperature anomalies (Chapter 7.2)

83 Regional salinity distribution pattern (TDS in g/l) in HSU 3 (Muschelkalk) of the Pechelbronn-Soultz Basin and Hochwald

84 Tritium content and uncorrected, conventional ^{14}C age of deepand shallow formation waters in the Vosges, Hochwald and Pechelbronn-Soultz Basin

85 Regional subsurface temperature and geothermal gradient distribution pattern in HSU 3 (Buntsandstein, Muschelkalk) in the Pechelbronn-Soultz Basin and Internal Zone superimposed on top of Buntsandstein and principal faults

86 a) Contoured of subsurface temperatures at about -500 m depth showing an increase in temperature from the west and east towards the Kutzenhausen-Soultz region (data sources: SAEM, PREPA well reports, Hass and Hoffmann '29); b)

variation of temperature at -500 m depths shown across the graben on a simplified cross-section C-C' (data sources: SAEM, PREPA well data, Sittler '67)

87 a) Contoured regional of heat flow in interval between surface and depth of HSG I; wells marked are those with deepest BHT taken mainly in Buntsandstein and Muschelkalk; b) Insignificant variation of cumulative thermal resistance to 1000 m depth, and significant variation of heat flow in HSG I with a maximum at Soultz is shown along a simplified structural cross-section D-D' (data sources: SAEM, PREPA well reports, Sittler '67)

88 Inferred from dominant equivalent hydraulic head values obtained at points of measurements within specified elevation ranges, groundwater flow is focussed from the west and east toward the Pechelbronn-Soultz Basin

89 Equivalent hydraulic head values obtained at points of measurements within specified elevation ranges and inferred groundwater flow trends in HSU 3 at the Kutzenhausen-Soultz region; groundwater direction are dominantly upward along/across fault planes; the connectivity factor indicates that the fault-severed HSU 3 is continuous

90 Shallow-depth chemical and temperature survey along the Pechelbronn-Soultz Basin: data and results on hydrochemistry and temperature (see Figure 82 for well locations)

List of Symbols and Abbreviations

BGR	Bundesanstalt für Geowissenschaften und Rohstoffe Hannover, FRG
BRGM	Bureau de Recherches Géologique et Miniéres, Orleans, France
GL-BW	Geologisches Landesamt, Baden-Württemberg, Freiburg
PREPA	Société de Prospection et Exploitations Pétrolières en Alsace
SAEM	Société Anonyme d' Exploitations Minirés, Pechelbronn
SGAL	Service Géologique Régional d' Alsace et de Lorraine, Strabourg, France

Geology:

NS	Niederroederner Schichten (Niederroederner Beds)
SG	Serie Grise (Grey Series)
PS	Pechelbronner Schichten
Ps	Pechelbronner Schichten Superieur (Upper)
Pm	Pechelbronner Schichten Moyen (Middle)
Pi	Pechelbronner Schichten Inferieur (Lower)
CD	Complexe Dolomitique (Dolomitic Complex)
CR	Couches Rouches (Red Beds)
ZD	Zone Dolomitique (Dolomitic Zone)
J	Jurassic
RH	Rhaetian
GR	Grés à Roseaux (Reed sandstone)
K	Keuper
LK	Lettenkohle

MK	Muschelkalk
Bsdst.	Buntsandstein
B	Basement

HdF	Heidenboesch Fault
PF	Pechelbronn Fault
HlF	Hoelschloch Fault
KF	Kutzenhausen Fault
SF	Soultz Fault
HwF	Hermerswiller Fault

Hydrogeology:

HSU	hydrostratigraphic unit
HSG	hydrostratigraphic group

k	intrinsic permeability (md)
n	porosity (%)
b	thickness of HSU (m)
ρ	density (kg/m^3)
T	Transmissivity (m^2/s)
μ	viscosity Pa s
K	hydraulic conductivity (m/s)
T°	temperature (°C)

Symbols used on maps and profiles:

⌒	fault
➘	dip direction
70°	dip angle
r	vertical displacement (m)
✦	producing oil well
✷	gas well
✦	eruptive oil well

●	well location or data point
◐	oil-stained formation water
☼	formation water with gas traces
ø	free flowing well
⚲	artesian well
○	fresh formation water
⊙	saline formation water
I	oil impregnated
T	warm or hot formation water

1. Introduction

1.1 Background to the Study

Exploration for petroleum in sedimentary basins and development of known oil/gas fields is mostly based on geological, geophysical and geochemical principles. Factual knowledge concerning the migration of petroleum is lacking and there seems to be a tacit assumption in the oil industry that oil and gas migration occurred during certain evolutionary stages of sedimentary basins. A contemporary problem of petroleum geology is, in my view, the reconciliation of geochemistry and fluid mechanics. Once petroleum has been generated, its movement is governed by physical laws within geological constraints. The most fundamental of these is that fluids lose potential energy while in motion. If the source postulated for an accumulation has less energy than the accumulation, then it must be established that it could have had higher energy at the time of migration, or that there was a source of energy, i.e., a transporting medium. No real progress can be made in understanding petroleum generation and migration until this central problem is recognized. So far, the petroleum geologist has been concerned only with two deposition components, the source rock and the reservoir. Application and integration of hydrogeological principles and techniques to petroleum exploration and basin analysis, defined here as Petroleum Hydrogeology, complements the third neglected component, the transport of petroleum in a basin, based on the effects of groundwater flow on the subsurface distribution of petroleum hydrocarbons.

In 1980, J. Tóth introduced the "Generalized Hydraulic Theory of Petroleum Migration" (Tóth, 1980; Appendix I), which states: (1) that gravity-induced cross-formational groundwater flow is the transportation link between the source and destination of petroleum; (2) that well-defined fluid energy conditions are required for accumulation and entrapment of petroleum, and (3) that the petroleum migration avenues and the fluid potentials can be analyzed and evaluated site-specifically from observable and mappable hydrodynamical, physical, geochemical, geothermal and biological data, readily available in the oil industry. Thus, the analysis of groundwater flow regimes in sedimentary basins and the identification of so-called hydrogeological indicators enables us to reconstruct migration trajectories and to predict depository sites of petroleum, thereby potentially improving the present-day efficiency of exploration procedures.

The main purpose of my research was therefore to test the validity of the hydraulic theory of petroleum migration and evaluate its applicability to exploration in an intermontane rift basin. An integrated multi-disciplinary study of a graben-type geologic setting has not been conducted before.

In 1984, in cooperation with, and sponsored by the Federal Institute for Geosciences and Natural Resources, Hannover, Federal Republic of Germany, the study area was selected in the middle segment of the Upper Rhine Graben (Figure 1) for its favourable attributes with respect to the project's objectives. These attributes included: a well defined intermontane topography; a relatively simple history of the basin evolution; well-known conditions and distribution of the petroleum occurrences; and an extensive and accessible data base at the Service Géologique d'Alsace et de Lorraine, Strasbourg, France. Over a period 1985-1987, during the summer months in three consecutive years, I collected and microfilmed 4768 well data reports at the Geologic Survey in Strasbourg; additional data were supplied by Total Exploration in Paris. Also during these months I surveyed and mapped the area and took water samples from water and oil wells in the study area.

1.2 Literature Review

Groundwater has been discussed in various contexts in publication related to petroleum geology since the late 1800's, and since the beginning of this century groundwater movement has been invoked as the cause of migration and accumulation of hydrocarbons.

Munn (1909) introduced in the "hydraulic theory of oil and gas accumulation". The concepy of water descending from the land surface cross-formationally, and transporting (pushing ahead) oil and gas particles. Formation permeability contrasts would then cause entrapment, retaining the oil and gas particles from the advancing water

Rich (1921), introducing the concept of gravity-induced flow, described lateral migration through highly permeable formations over long distances. These carrier beds collected fluids from adjacent formations and conveyed them from topographic high elevations to topographically lower discharge areas.

In 1953, Hubbert presented in his rigorous classical treatise the principles of three-phase fluid flow in the subsurface. He defined the energy conditions required to entrap oil and gas in a hydrodynamic environment. Hubbert did not consider, however, regional migration patterns of groundwater and he thus analyzed the entrapment mechanism only in a one-directional flow field in laterally extensive confined aquifers.

Although these three fundamental papers institutionalized and significantly promoted the development of the hydraulic theory which is based on the recognition that petroleum is transported by moving groundwater in the porous medium, none of these three versions of the theory quantitatively considered the effects of topography on the flow distribution. It was only after the theory of gravity-induced, cross-formational groundwater flow was established (Freeze et al., 1966; Freeze et al., 1967; Freeze et al., 1968; Tóth, 1962; Tóth, 1963; Tóth, 1968) that certain petroleum deposits and observed natural phenomena associated with these deposits were interpreted as being the result of topography-controlled regional groundwater flow (Tóth, 1970b; Tóth, 1980).

By this stage (the late 1960's) Russian geologists (e.g. Bars, 1961) already had a good understanding of the effect of the topographic relief on subsurface fluid migration and had applied its principles to hydrocarbon exploration. Also, a decade later, the role of gravity-driven flow systems on petroleum migration and its significance to exploration was accepted by French petroleum geologists (Chiarelli, 1973; Coustau, 1977). In North America, however, petroleum geologists, especially in industry, are still sceptical and unwilling to apply hydrogeology to petroleum exploration, some years after the "Generalized Hydraulic Theory of Petroleum Migration" (Tóth, 1980) was published. Three main reasons appear to have contributed to this situation: (1) lack of understanding of the hydrogeologic principles and terminology; (2) a wide acceptance of the compaction-migration theory; and (3) a multitude of other concepts and theories of migration (e.g. aquathermal pressuring and sealed fluid pressure compartments).

Recent publications in this field, however, indicate that the concepts of the Hydraulic Theory have been applied to explain petroleum occurrences in some specific geologic environments, such as, e.g., in the interior type Hungarian Basin (Erdélyi, 1985), the platform type Michigan Basin (Vugrinovich, 1988), or offshore Persian Gulf (Wells, 1988). Nevertheless, petroleum hydrogeology has not been widely used as an exploration tool, although Federal research institutes, mainly in Europe, accepted the implications of petroleum hydrogeology with more optimism and put the theory into practice.

The Federal Institute for Geosciences and Natural Resources of West Germany sponsored, from 1984 to 1987, Dr. J. Tóth and myself to investigate the applicability of the hydraulic theory of petroleum migration to exploration for hydrocarbons in the Upper Rhine Graben (Blümel et al., 1989; Tóth and Otto, 1992 submitted). This thesis presents my own research and interpretations of the data collected, with the objective of producing a unified picture of basin evolution, fluid dynamics and petroleum accumulation in the study area..

The TNO Institute of Applied Geosciences, Delft, Netherlands' organization for applied scientific research conducted, in 1989, a comprehensive study on the principles of secondary migration and presented, in addition, qualitative and quantitative approaches for assessing basin-wide secondary hydrocarbon migration patterns, describing also Tóth's generalized hydraulic theory (Verweij, 1989). The project's main objective was to understand the distribution of oil and gas deposits in the southern North Sea Basin by applying principles of secondary migration.

In North America, only the Petroleum Hydrogeology Group at the University of Alberta is actively exercising petroleum hydrogeology, testing the validity of the theory in the Western Canada Basin (Holysh, 1989; Parks, 1989; Rahkit, 1987; Thompson, 1989) and in the Upper Rhine Graben rift basin. The Group is also examining and developing potentially useful hydrogeological principles and techniques (Holysh, 1989; Maccagno, 1991, Rahkit, 1987; Rostron, 1990).

1.3 Purpose and Objectives of the Study

The main purpose of this study was to investigate the applicability and validity of the Generalized Hydraulic Theory of petroleum migration to exploration for hydrocarbons in an intermontane rift basin.

Hence, it was postulated that in an intermontane basin, i.e., in the Upper Rhine Graben a dynamic interrelation must exist between groundwater flow patterns, hydrochemical and geothermal anomalies, the evolution of petroleum migration-deposition and degradation, and the conductance of fault zones.

Therefore, the principal objectives of this thesis are the following:

1) to assess postulated correlations between positions, types and nature of petroleum accumulations; and
2) to assess postulated correlations between distribution patterns of various hydrogeologic and subsurface fluid dynamic parameters;

The specific objectives of the study are:

1) to describe the regional and local hydrogeological conditions in a fault-severed environment by a suite of physical, chemical and fluid dynamic parameters;
2) to describe petroleum migration history and occurrences; and
3) to find and characterize naturally occurring groundwater related phenomena, e.g., geochemical and geothermal anomalies that may be related to and be indicative of petroleum deposits.

1.4 Structure of Thesis

The thesis is structured from a petroleum explorationists point of view; thus, initially, it was assumed that the basin (study area) is unexplored for petroleum and that the oil pools are not known. Figure 2 shows diagrammatically the patterns of interrelation and dependence between the various applied disciplines. The outline of the thesis can serve as a guide for future hydrogeologically oriented exploration projects, demonstrating how to combine and incorporate routinely used exploration methods with hydrogeological techniques.

1.5 Location, Definitions and Terminology

The study area, located north of Strasbourg, France, stretches from the graben shoulders (the Vosges and Black Forest mountains) in the west and the east, over the entire Rhine Valley, and extends to the German border in the north (Figures 1 and 67). This region is described in the thesis as the Upper Rhine Graben. The research was, due to availability and clustering of data, focussed mainly on a local region near the villages of Pechelbronn and Soultz sous Forêts, 40 km north of Strasbourg. The specific study area which reaches from the Hochwald Horst to the Hermerswiller Fault near Hermerswiller over a distance of about 10 km, is here defined as the Pechelbronn-Soultz Basin (Figure 67).

The original German/French formation and stratigraphy terminology, which are commonly used in describing the geology in the Upper Rhine Graben, has been adopted.

All units and values follow the International System of Units (SI) convention.

The Glossary of Geology by the American Geological Institute (Gary et al., 1975) was used as reference to ensure consistency in the geologic terminology.

In this study, the term hydrostratigraphic unit (Maxey, 1964) is used to describe a body of rock having considerable lateral extent and composing a geologic framework of a distinct hydrogeological system. It is a stratum or a complex of strata recognized as a unit in the classification of the rocks of a groundwater basin with respect to the rock's hydraulic character, i.e., hydraulic conductivity, intrinsic permeability and regional continuity.

Terms applied to subsurface waters

A number of descriptive terms have been used to classify subsurface waters. No overall satisfactory classification system exists, due to the fact that subsurface waters can be assessed by several different criteria, such as: salinity of the water, the concentration of dissolved constituents, the origin of the water, and the origin of the solutes (White et al., 1963).

Brines: The definition preferred for this term is water with total dissolved content higher than 100 000 mg/l (Carpenter et al., 1974). Hem's (1989) definition of waters with salinities higher than that of average sea water, i.e., more than 35 000 mg/l TDS would group all oilfield waters together as brines.

Formation water: Formation water is defined as a petroleum-poor liquid enriched in subsurface water and present in rocks immediately before drilling. This term is used extensively in the petroleum industry, but has no genetic or age significance.

Meteoric water: This is considered to be water that was recently involved in atmospheric circulation (White et al., 1963). In this study subsurface water of meteoric origin is redefined as water derived from rain, snow, water courses, and other surface waters that percolate in rocks and displace the interstitial water that may have been connate, meteoric, or of any other origin. The majority of meteoric waters in sedimentary basins are nonmarine and are generally recharged at topographic highs in the margins of the basin.

Connate water: Connate water is here defined as water that was buried with sediments or other rock formation in the basin and which has been out of contact with the atmosphere since its deposition.

2. Petroleum Geologic Framework

2.1 Introduction

This chapter presents the Phanerozoic evolution of the study area in the context of regional depositional and erosional and tectonic events which affected this part of the Upper Rhine Graben. It provides the basic information necessary to comprehend the geometry and lithology of hydrogeologic units as well as their relative positions in the groundwater basin.

As stated previously in section 1.4 , the basin is initially unexplored. Therefore, a first requirement for any further petroleum hydrogeological exploration endeavours is to evaluate the basin's petroleum potential. For the prurpose of this study, sites of oil accumulation are known; this will ultimately enable me in the end to verify the applicability of the Hydraulic Theory.

Aside from Schnaebele (1948), the main data sources used to describe the regional geology and to generate geological and structural maps for the Upper Rhine Graben and the Pechelbronn-Soultz Basin were the 4794 original well reports (in French) from the Service Géologique Régional d' Alsace et de Lorraine in Strasbourg. In general, a well report describes the litho-stratigraphic succession, the occurence of faults, influx of formation waters, fluid levels, petroleum indicators, the drilling history and tentative interpretations.

I was able to look at a few seimic profiles of the study area at the oil company TOTAL-C.F.P. in Paris, but I was not given permission to use or document this information in my thesis.

2.2 Taphrogenic Evolution of the Upper Rhine Graben

The Rhine Graben is the central segment of a meridional rift belt which cuts through the Western European continent. This system is part of an extended rift network with a total length of nearly 9000 km that intersects the Old World from the North Sea to Southeast Africa. The prominent parallelism of its framing escarpments, the upwarped shoulders, and the near equal amount of shoulder elevation underlines the physiographical and geological symmetry of the Upper Rhine Graben proper (Figures 1 and 4). Striking NNE - SSW ("Rheinisch") to N -S at a near 90^0 angle to the Alpine orogenic belt, the Upper Rhine Graben begins near Basel, Switzerland, where graben structures are inferred from the anticlines of the Jura mountains to about 300 km northward near Frankfurt. There, the Holocene rifting is transcurrently interrupted by the Hercynian block of the Rheinish Massif (Figure 3).

Pre-Rift Period

The Hercynian orogeny ceased with the Upper Silurian phase. A period of erosion leading to continental and lagoonal-marine sedimentation followed, and deposits of Permian to Jurassic age covered the granitic basement. Upper Jurassic till Lower Eocene was a period of non-deposition and erosion. Widespread volcanic activity in the Late Cretaceous time, about 80 Ma ago, concurrent with the first compressional deformation in the Alps indicates the break-up of the crust and the first signs of subsidence in the Rhine Graben area .

Two Rifting Stages

The first main rifting stage of taphro-geosynclinal subsidence and subsequent shoulder uplift with displacements along convergent boundary faults occurred during the mid-Eocene, 45 Ma ago until the Lower Oligocene, 37 Ma ago. The southern part of the graben was the primary spreading centre during this rifting stage. Rift valley propagation continued during the sedimentation of the Lower Oligocene beds. Intercalated in the Eocene and Lower Oligocene formations are Jurassic, Triassic and basement pebbles. This demonstrates uplift of the graben shoulders and the sequential denudation of their Mesozoic cover. Graben subsidence and shoulder uplift culminated during this period. The graben's boundary faults served as mobile zones between graben subsidence and shoulder uplift and compensated for lateral extension.The most frequent grabenward fault inclination values range between 60^0 and 65^0. At depth, a flattening can be observed (Erlinghagen et al., 1974). Locally, the boundary fault can be replaced by parallel normal faults. They enclose a zone of foothill structure with synthetic and antithetic step faults.

The Middle and Upper Oligocene was a time of steady graben development. The formations exhibit a uniform thickness over the entire trough, attaining a maximum of about 1000 m in the central segment of the graben (study area). Near the end of the Oligocene the centre of sediment accumulation is shifted northward. The southern part of the Rhine Graben, south of Haguenau became dry land. These paleogeographical changes are accompanied by a reactivation of taphrogenic activity. High rates of subsidence are observed in the northern part of the graben. Internal faults were active as growth faults of antithetic character. Antithetic block faulting is regularly observed. Locally, as is the case in the Pechelbronn-Soultz Basin, the fault planes are dipping antithetically towards the west. Such unilateral tilt of blocks is ascribed to a non-uniformally extensional motion of the two shoulder blocks (Mandl, 1988). During the Aquitan the direction of tension was oriented about WSW-ENE, i.e., oblique to the graben axis.

From the Middle Miocene to Lower Pliocene a period of non-subsidence and tectonic stabilization followed. Parts of the graben fill underwent fluvial erosion and the graben shoulders were further denuded. About 13 Ma ago the Kaiserstuhl volcano erupted and further updoming of the mantle caused large-scale uplift of the Black Forest and Vosges mountains.

The second rift phase began in the middle of Pliocene. With uplift and northwestwards extension of the Alps, the regional stress field was reoriented and the Rhine Graben remodelled into a sinistral shear zone. Substantial shoulder uplift continued in Upper Pliocene to Pleistocene times and tectonic movement of the Graben continues today (Illies et al., 1976; Mälzer et al., 1975).

The axial trend of the Rhine Graben changes twice, the first near Baden-Baden and the second near Heidelberg (Figure 4). The study area is located in the middle segment. Although the graben as a whole acts as a sinistral shear element, the respective tectonic reactions of the individual segments to the regional stress regime are of different character. In the southern segment, active graben tectonics are controlled by a σ_1 direction of about 175^0, which forms an acute angle with the 015^0 trend of the graben axis (Illies et al., 1976). The central segment of the graben trends about 030^0 and the σ_1 direction is about 130^0 which is nearly normal to the local graben axis. Compressive forces control the neotectonic deformations. Here, the sinistral shear operates against the grain of the graben feature causing additional compression. As will be described in detail in the following chapters this middle segment of the graben is characterized by deep thermal, superhydrostatic formation fluid pressures and anomalously high heat flow values. Hot brines, like those of Baden Baden rise along fault-zones that reopened under Holocene stress conditions. Most of them follow the orientation of σ_1.

The compressive motion of the central graben segment resulted in a region of maximum uplift as was revealed by precise levelling measurements (Kuntz et al., 1970). In this region, areas of the deeper Pliocene, Miocene and partly Oligocene strata outcrop and are exposed to erosion.

In the northern section of the graben, sinistral shear and its almost N-S trend favoured crustal extension, giving rise to subsiding basins and sedimentary fill.

Shoulder Uplift

The average uplift rate through geologic time of the western (Vosges) and eastern (Black Forest) graben shoulders can be reconstructed from Roll's geological data (Roll, 1974; Table 1).

Synchronous to the first rifting phase the graben shoulders emerged in Eocene time. In the central part of the Upper Rhine Graben the uplift was more or less equal for both graben shoulders until the Late Oligocene. In the end of the Miocene, however, concurrent with the second rifting phase, substantial shoulder uplift heaved the eastern graben flank to a elevation range between 800 and 1100 m , while the western graben shoulder attained average elevations of only 650 m. Since the Miocene, the uplift rate for both graben flanks has not been uniform; this is also evident in today's elevation difference of approximately 300 m between the Vosges and Black Forest mountains.

2.3 Basin Analysis

2.3.1 Lithostratigraphy and geohistory

The lithostratigraphy and geologic evolution of the study area is explained and summarized in a table (Figure 68). The relative positions, depths and thicknesses of the principal formations in the basin are shown on maps and cross sections (Figures 5, 6, 7, 69, 70, 71, 72, 73-80). The relevant data was extracted from SAEM, PREPA and TOTAL well reports and Schnaebele (1948).

2.3.2 Tectonic Structure

2.3.2.1 Principal Structure Zones

A structural zone is defined by its bounding principal (longitudinal) faults and its sedimentary fill. The structural zones which divide the graben into submonoclinal strips are shown on a regional cross-section and from the graben flanks to the graben centre (Figures 69 profile A"-A"' and 70):

1) Graben Fringe Zone

Bounded by the Vosges and Black Forest main faults, the Vosges and Black Forest mountains form an ancient crystalline massif partly covered by Permian and *Buntsandstein* sandstone formations. The main faults dip synthetic at a mean 70° towards the graben centre.

2) Zone of Fractured Terrain

This zone of outcropping Mesozoic strata is dissected and fractured into partly collapsed compartments. It is positioned between the Graben Fringe Zone and the Rhine Valley. The Saverne Fracture Zone represents a zone of fractured terrain in the western margin of the Rhine Graben; the Kraigau Trough north of the Black Forest (not in this study area) is seen to be its eastern equivalent. The Rhine Fault limits the Saverne Fracture Zone in the east, and divides the Mesozoic fracture zone from the argillaceous Tertiary terrain of the graben valley. The synthetic fault dips between 75-80° to the graben centre.

3) Peripheral Zone

Further to the east, beyond the Rhine Fault, the Peripheral Zone corresponds to a region of outcropping Early Oligocene formations (*Pechelbronner Schichten*) limited at its eastern margin by the Hermerswiller Fault. The fault pattern in the zone is complex and dense. Longitudinal faults of predominantly antithetic inclination and oblique faults cut Mesozoic and Cenozoic sedimentary units into series of sub-monoclinal compartments and tectonic highs (e.g. Soultz Horst). The Pechelbronn-Soultz Basin as well as the Ohlungen Basin with their well-known oil fields constitute Peripheral Zones within the Upper Rhine Graben study area.

4) Internal Zone

Enclosed between the Hermerswiller and the Black Forest Fault, a region of outcropping Late Oligocene (*Série Grise*) and Early Miocene (*Niederroederner Schichten*) defines the Internal Zone of the Upper Rhine Graben. The substrata are displaced by widely-spaced, mostly synthetic faults. To the eastern margin of the Rhine Graben on the German side, the terrain is dissected and upthrown by a set of parallel faults exposing older formations at the surface over a short distance .

2.3.2.2 The Fault Complex in the Pechelbronn-Soultz Basin

Definitions: A group of parallel faults that are related to a deformation episode, is defined as a fault system. A fault complex contains interconnecting and intersecting fault systems having the same or different ages.

In the Pechelbronn-Soultz Basin, the Peripheral Zone of the Upper Rhine Graben study area, the fault pattern is dense and structurally complicated. During the rifting phases older faults were rejuvenated while younger ones were generated in the graben, giving rise to fault systems of synthetic and antithetic block faulting. The fault blocks themselves became dissected with swarms of secondary and younger generation mostly oblique faults, the density of which may significantly vary from one block to another.

Longitudinal normal faults (Figures 5, 9, 70, 71 and 72) strike NNE-SSW parallel to the trend of the graben and divide the basin into submonoclinal compartments. Seven principal longitudinal fault systems in the Pechelbronn-Soultz Basin can be discerned, including the Rhine Fault bounding the Pechelbronn-Soultz Basin to the west (Figures 70 and 76 profile B-B'). In the study area the graben boundary fault is replaced by two parallel master faults, the Rhine Fault and Vosges Fault, respectively.

In the Pechelbronn-Soultz Basin six compartments are discernible (Table 2; Figures 69, profile A''-A''' and 70). Each compartment is confined to the west and east by near-parallel principal faults or fault systems. As far as can be inferred from well reports, each individual principal fault is known to reach the basement. A compartment is a structural unit defined by its bounding fault systems; this does not imply, however, that it is hermetically sealed-off and isolated from externally generated dynamic forces, e.g., fluid flow or heat flux. Governed by factors such as its internal structural complexity, the position of hydrogeologic units in relation to units in adjacent compartments and the sealing capacity and flow-channelling-effect of its fault systems, each compartment can locally modify the regional course of fluid movements and affect deposition of transported matter. As described in the following chapters, these effects can be evaluated by hydrochemical, geothermal and hydrogeological methods which, inversely,make it possbile to discriminate between fluid conductivity and sealing capacity of a fault system and the petroleum entrapment potential of reservoir rocks in a compartment.

The general rule is that when two compartments are displaced by an antithetic principal fault, the eastern compartment is tectonically elevated in relation to its western neighbouring structural unit. For example, the footwall formations in the Soultz Compartment are upthrown in relation to the hanging-wall formation in the western Kutzenhausen Compartment (Figure 76 profile B-B'). When the principal fault is synthetic, e.g., the Hermerswiller Fault, the western compartment (Soultz) is elevated.

Description of the fault types

Normal, longitudinal faults which dip between 45 - 65° to the west opposite to the dip direction of the stratigraphic sequence dominate the tectonic style in the Pechelbronn-Soultz Basin. Synthetic faults which occur more frequently towards the graben centre have an average dip angle of 50° E. The Rhine Fault (strike 015° E) which separates the Saverne Fracture Zone from the graben has an inclination angle between 70 - 85° E (wells Morsbronn 3a and 3b, 70°; well Marienbronn-101, 75°). Sittler (1985) uses an average dip angle of 85°.

"An experienced geologist once stated that nature never created a curved fault" (from Dikkers, 1985, p. 100). No doubt this was an unfounded generalization. Overthrusts in thrustbelts and faults in rollover and synsedimentary fault environments are curved not only on a cross-section but also on a map. This is also true for the principal faults in the study area. Their geometric characteristics (strike, dip and throw) change along the faults' trend and with depth (Figures 69 profile A''-A''', 70, 71, 72, 76 profile B-B', 77 profile IV and 78 profile V).

The magnitude of fault displacement is measured by its throw or vertical separation (v.s.or r): this is the vertical distance between the intersection points of the fault with equivalent markers on either side (see Appendix II). The average throw of the normal faults is between 100 and 500 m with the highest vertical displacement values for principal faults towards the middle of the graben. Notably for antithetic faults in the western compartments (Preuschdorf, Pechelbronn) of the Pechelbronn-Soultz Basin, the throw of an individual principal fault can vary between 70 to 450 m. These faults were synsedimentary active during the distensional motion of the graben. The rate of vertical displacement, generally, decreases from the bottom to the top, from Mesozoic to more recent strata (well SAEM 3956; Figure 75 profile IIIb).

The thickness of a rock unit can be greater on the downthrown side of a synsedimentary fault than that of the correlative unit in the upthrown block. This phenomenon was sometimes observed for the *Zone Dolomitique* and *Couches Rouches* (e.g. Figure 76 profile B-B').

It is commonly believed that normal faults are concave upward or listric (Jackson et al., 1983; Wernicke et al., 1982). This shape can be produced by geometric constraints, either because the faults reactivate curved thrusts, or because they must be curved to accommodate rotations as can be observed in extensional basins. Synsedimentary faults which have been described in the Gulf of Suez, Gulf Coast and Niger Delta (Lowell, 1985) have a listric configuration, and these faults are regarded by most workers (Shelton, 1984) to be sedimentary due to fault-flattening by shale compaction or gravitational sliding (Crans et al., 1980). However, in the Pechelbronn-Soultz Basin the well reports from this study provide no conclusive evidence that the previously described principal faults are listric in configuration. This is mainly due to lack of data on the position of fault surfaces in the subsurface. Some profiles show us that the dip of the Heidenboesch, Hoelschloch and Kutzenhausen Faults are accentuated in Mesozoic formations (Figures 74 profile IIb and 75 profile IIIb). The fault dip is not decreasing but becoming steeper with depth. This phenomenon can be explained by rheologic differences between the rigid and well-consolidated Triassic formations (mainly sand and limestone) and the more ductile Tertiary shaly formations. The Jurassic sequence (mainly shale) can be viewed as a transition zone. Perhaps, these steeper faults also followed and reactivated pre-rift, basement-controlled weakness zones. On the other hand, profiles B-B', IV and V show that the Kutzenhausen and Soultz Faults in the Soultz region are listric. Here, an abundance of well data was available.

Seismic surveys in the region identifed listric antithetic faults close to and in conjunction with the also listric Rhine Fault (pers. comm. D. Comte, Total Exploration, Paris;

Dylikowski, 1985). Block displacement along the listric Rhine Fault which, is assumed to flatten with depth, would create an extension by separation of the blocks on the curved surface. A volume gap would occur between the hanging and footwalls. Rotational block tilting along antithetic listric faults or roll-over folding could compensate for the extension and close the gap. For the Pechelbronn-Soultz Basin the former is more likely to have occurred.

Principal faults often branch off on the downthrown side of the principal fault into smaller parallel faults, e.g. Soultz Fault Zone (Figures 71, 76 profile B-B', 77 profile IV and 78 profile V) fracturing the Triassic formations. This type of branching may reflect reactivation of a fault which was initiated at depth.

Principal faults are often intersected by second generation smaller faults probably of mid-Pliocene age. Mostly, they are encountered in Tertiary formations; they are short in length and die out at shallower and deeper depth (Figure 72 and profiles). A characteristic feature of the faults is that they occur in groups in which the fault planes dip in the same direction. This behavior arises because the faults can not intersect: if they do, one must cease to be active (Roux, 1979). They strike oblique or transverse to the graben's trend (± 30^o), oriented parallel to the mid-Pliocene stress field ($\sigma_1 \pm 130^o$, Chapter 2.2). Their throw is between 10 and 20 m, and their dip between 50 to 65^o. The frequency of their occurrence is variable. From their experience of mining galleries at Pechelbronn, miners described an abundance of accessory faults which dismember the *Pechelbronner Schichten* by ± 10 m vertical separation every 10 to 12 m (Tzschachmann, 1914).

Sites of structural culminations of eastward dipping monoclinal formations between intersecting longitudinal and oblique/transverse faults are potential sites for petroleum entrapment (Chapter 2.3.3.2).

Direction and Inclination of Formations

The main strike-direction is NNE-SSE and NE-SW and the dip is 4 to 9^o to the ESE and SE (Figures 71, 72, 76 profile B-B'). Locally, the strike can change to N-S, even NNW-SSE near Lobsann at the foot of the Hochwald Horst. In the mining galleries strike orientations of E-W or ENE-WSW were measured, and the dip angle can decrease to $0\text{-}3^o$ (Schnaebele, 1948; Sittler, 1974). Near the Rhine Fault in the Preuschdorf Compartment the dip-direction of Tertiary formations can change to the west from the Heidenboesch Fault. This is possibly, caused by block rotation along a listric Rhine Fault.

2.3.2.3 The Soultz Horst

Anomalous hydrogeological, hydrochemical and geothermal phenomena (Chapters 4 and 5) observed in the Kutzenhausen, Soultz, and Hermerswiller Compartments are indirectly related to a structurally complex and tectonically elevated central part. This slightly uplifted zone is termed, a little extravagantly; and the Soultz Horst; the Soultz Fault System is an integral part of it.

Five boreholes drilled before 1948, and sixty others drilled between 1949 and 1951, reached at least the *Muschelkalk* (Figure 71, see also profiles). The basement was reached by wells (SAEM) 4616 and 3956 at 1380 m and 1560 m, respectively.

Good well control made it possible to show the structure of the Soultz Horst (Figures 71, 76 profile B-B', 77 profile IV and 78 profile V). Four auxiliary, antithetic faults (v.s.: 40 - 50 m) branch off from the Soultz Fault dissecting the Triassic formations into smaller blocks. Well reports describe fractured and crushed *Muschelkalk* limestone beds near the fault zone. Drillers have experienced blow-outs and occasionally mud loss when reaching the *Lettenkohle*, *Muschelkalk* and *Buntsandstein* . As I will detail in chapters 2.3.3 2, 4 and 5, these formations produced artesian, hot and saline waters but showed only insignificant oil accumulation, although they have excellent permeability and porosity characteristics and qualify as potential reservoirs.

2.3.3 Petroleum Formation and Occurrences

At this stage of the study and of any basin analysis, identification of potential source-, reservoir- and carrier-formations in the basin is essential to justify continuation of further petroleum hydrogeological exploration efforts.

Attention was directed to the presence of oil deposits in this area by oil seeps (direct indicator) a long time ago. The town's name, "Pechelbronn", is interpreted to mean "pitch spring". An oil seep, described in 1498, produced a mixture of oil and saline water just west of Pechelbronn. It was used by local farmers as lamp fuel and lubricant. In 1735, bituminous sands were discovered, marking the start of industrial oil production in the Pechelbronn-Soultz Basin. Commercial exploration and exploitation ceased in the decade 1953-1963, except for an enhanced recovery project initiated in 1963 (a detailed resumé on the exploration and production history of the study area and for Northern Alsace is given in Appendix VI).

2.3.3.1 Source Rocks

The *Buntsandstein* and lower and middle *Muschelkalk* do not contain organic matter and can be ruled out as source rocks. Upper *Muschelkalk* and *Lettenkohle* contain some marine sapropelic levels but it is doubtful that these very thin bituminous layers are responsible for oil accumulations found in the upper *Muschelkalk* and *Lettenkohle* at Soultz and Kutzenhausen. These deposits can easily be derived by hydrocarbon migration along and across fault- and fracture-zones from neighbouring sources in Jurassic and Tertiary monoclines. The *Keuper* and Rhaetian contain no source rocks.

Part of the 300 m thick sedimentary deposits of the Liassic and Dogger have excellent source rock qualities (Tables 3 and 4; Robert, 1985; Schad, 1962). Deposits of Sinemurian and Hettangian age contain organic matter of kerogen type II (Tissot et al., 1978) indicating a marine organic source. Charmoutian contains sapropelic organic matter (kerogen type II) of good quality. The Toarcian (Lias ε, kerogen type II) has very good source rock qualities (Welte, 1979). The Aalenian, particularly observed in well Reimerswiller-1 (Figure 70) exhibits the richest sapropelic levels found in the basin (internal report Total: Roches Meres Potentielles by A. Noyau). The mixed humic-marine character (kerogen type II & III) suggests continental influence from the highlands in the west.

The Eocene formations (Dolomitic Complex) are not important as source rocks. They are humic, due to a terrestrial supply, and have a low degree of diagenesis. The Oligocene is characterized by an abundance of continental humic matter deposited in a marine environment (kerogen type III); coals are frequent. The Sannoisian source rocks are of medium quality. The Rupelian "Fish Shales" 10 to 30 m thick have a high content of organic matter but reached maturity only in the deeper central part of the Rhine Graben and are immature in the study area.

Maturation

Studies published by Robert (1985), Teichmüller (1979), Welte (1979) and Doebl (1974) contain mean vitrinite reflectance (R_o) data on wells and outcrops in the Upper Rhine Graben. Data reported by Robert (1985) are within the study area.

Vitrinite reflectance (R_o) is a widely used technique in the oil industry for determining the maturation levels of argillaceous and calcareous rocks. The lowest R_o-value associated with known generation of oil is about 0.45%. The beginning of commercial oil generation is generally recognized to be at 0.5-0.6%. At a maturation level of 0.8-1% oil generation peaks, and at higher levels the gas/oil ratios increase with reflectance. Oil generation ends at about 1.3%, condensate at 2%, and methane at 3.5% (Dow, 1977). Price (1985) points out that suppression of R_o by significant concentrations of exinite macerals (kerogen types I & II) in association with vitrinite macerals can result in a serious miscalibration of regional maturation ranks for the onset of petroleum generation. Nevertheless, the use of vitrinite reflectance as a maturation indicator remains a standard exploration tool in the oil industry.

R_o data for Jurassic, Lattorfian and Rupelian source rocks (Table 4) in the study area are plotted on R_o vs. depth diagrams (Figure 8) and on a map (Figure 70). It can be concluded that the Tertiary source rocks are immature in the near vicinity of the Pechelbronn-Soultz Basin (e.g. well Reimerswiller 1). Well Haguenau 2, 18 km to the south of Pechelbronn shows a R_o value of 0.5% indicating first oil generation maturity. Liassic and Dogger source rocks have reached maturity in the basin.

A near-surface geochemical study was conducted across the Pechelbronn-Soultz oil fields by the Federal Institute for Geosciences and Natural Resources (Gerling, 1988). The concentration and isotopic composition of hydrocarbon gases taken from 16 m deep samples were measured (Faber, 1987). From this study it can be concluded, that: (1) the absorbed hydrocarbon gases in near-surface sediments were thermally generated at greater depth from a marine source rock which attained maturation levels of 0.5 - 1.2 % R_o in different parts of the graben; (2) the *Pechelbronn Schichten* (Lattorfian) are immature in the Pechelbronn-Soultz Basin; and (3) Liassic source rocks with a maturity level of approximately 0.7 % R_o in the deeper eastern parts of the graben generated the oils deposited in the Pechelbronn-Soultz Basin.

A rapid increase of R_o and the high vertical gradient of R_o vs. depth in the Jurassic compared to the Tertiary is strikingly apparent on examination of Figure 8. The marked change in R_o gradient and an off-set between Oligocene and Jurassic source rocks provides evidence of a hiatus (Cretaceous unconformity). The large discrepancy in R_o values can not be attributed to burial diagenesis of the Jurassic source rocks since the Jurassic formations were affected by the Cretaceous emersion. In the Eocene, during the first rifting phase, the Jurassic source rocks were buried and affected by a geothermal surge. This thermal event did not affect Lattorfian and Rupelian source rocks, since they do not show similar R_o values and gradients. This suggests that the Eocene geothermal surge which caused anomalously higher subsurface temperatures declined during the tectonically less active period in the Oligocene.

The vertical R_o gradients are related to a "normal" statistical gradient for passive basins (Figure 8). Statistically, a normal R_o gradient was derived for geothermally undisturbed basins with a constant temperature gradient of 3^o/km (Robert, 1985). From Figure 8 it can be seen that, with regard to the depths attained, the Tertiary and Jurassic have abnormally high R_o values throughout: instead of 0.5% at 3000 m, the R_o curves generally reach the same value at about 800 - 900 m. Tertiary formations must have experienced a younger geothermal surge after the Rupelian source rocks were deposited. This second thermal event probably coincided with the second rifting phase in Miocene time, affecting the Tertiary formations as well as reheating the Jurassic source formations.

Well Reimerswiller 1, closest to the Soultz Horst, has higher R_o values relative to depth than do other wells on which reflectance measurements were conducted (Table 4, Figure 70). The depth of the "oil window" at Soultz is at ± 670 m and sinks gradually to the east and south to about 1500 m. From this it can be concluded that burial metamorphism of the source rocks alone can not be considered responsible for the anomalously higher R_o values. Instead, elevated subsurface temperature regimes during the graben's evolution, initiated by an increase in basement heat flux, have accentuated and channelled by forced convective heat transport (Chapter 4.3.4), accelerated the kerogen maturation process.

Bottom hole temperature measurements in the area (Chapter 4.3.3) show that anomalously high temperature gradients still prevail.

2.3.3.2 Oil Fields, Reservoir- and Carrier-Beds

In the study area any porous or fractured/jointed rock formation of Tertiary or Mesozoic age can, under certain controlling conditions (i.e., existing structural, lithological and hydrodynamic entrapment mechanisms), be a hydrocarbon-bearing reservoir rock. The reservoir rocks are mostly consolidated sandstones, partly argillaceous, calcareous and dolomitic. However, quartzose and calcareous conglomerates, oolitic limestones and fractured cavernous dolomites may also become petroleum-bearing reservoir rocks.

Until 1963, most (98%) of the oil produced in the Upper Rhinegraben study area came from Tertiary reservoir formations.. Lenticular sandbodies in the *Pechelbronner Schichten* were the main producers (92 %). Further oil-producing Tertiary formations are found in the *Zone Dolomitique*. Minor oil exploitation occurred near Pechelbronn in the *Grès à Roseaux*, near Kutzenhausen in the *Lettenkohle*, and near Soultz in the *Lettenkohle*, upper *Muschelkalk* and upper *Buntsandstein*. Near Ohlungen to the south of the Pechelbronn-Soultz Basin the oolitic Dogger was productive (Figure 70).

In the following pages I will summarize the geometric properties of the Mesozoic and Tertiary reservoir rocks and associated oil occurrences in the Upper Rhine Graben study area. This chapter also provides some basic hydraulic data necessary to define and characterize hydrogeologic units in Chapter 3.5.1.

The Mesozoic

Table 5 presents the Mesozoic reservoir formations in the region (Figure 70), showing producing reservoirs, oil fields and production wells.

Buntsandstein: The lower and middle *Buntsandstein* formations have good reservoir qualities but are void of any petroleum and are saturated with groundwater. Flowing artesian wells in the Kutzenhausen and Hermerswiller Compartment which reached these beds produced hot, saline water with some oil traces (e.g. wells Helion, 4616, 4515). Twenty wells reached the upper part of the *Buntsandstein* in the study area, but only wells SAEM 4550 and 4590 in the Hermerswiller Compartment were successful and produced oil with hot (100 °C), saline water from fissured sandlayers in the last meters of the upper *Buntsandstein* at depths of 955 and 1000 m, respectively (Figures 71 and 77 profile V). Both pools are situated in the updip section of the eastern footwall close to the Soultz Fault (SF5, Figure 71) but are not connected. The remaining wells in the Pechelbronn-Soultz

Basin are water producers. The PREPA well, Rittershofen-1, situated to the east of Soultz showed flowing groundwater with gas traces (Figure 71).

Measured porosities range between 2 - 12 % (well 4550) at a 971-1050 depth interval in well 4590 a porosity of 6.7 % was measured at 1016 m depth. Permeability values range between 2.5 - 10 md (see also Appendix 7). A high permeability of 175 md was measured on a fissured *Buntsandstein* core sample from 1016 m depth. The values are surprisingly low considering the faulted, fractured and fissured texture of the formations in the Soultz and Hermerwiller Compartments.

Only two small oil pools were discovered. That raises the question, already posed by the geologists who explored the *Buntsandstein* for petroleum in this basin 40 years ago (Sittler, 1985), namely, where is the oil in the *Buntsandstein* and why are the structurally favourable reservoir-highs void of oil deposits? From a "classical" petroleum geologist's view the *Buntsandstein* should show more and/or larger oil pools: it has ideal reservoir qualities the structural trapping mechanisms are in place; and the mature source rocks are not far away at greater depth in the east. The answer must be found in relation to groundwater flow through these Triassic carrier beds and to the conductivity and poor sealing potential of the fault planes in the Soultz Horst.

Muschelkalk: The lower and middle *Muschelkalk* limestone beds are aquifers and contain no petroleum accumulations. The upper *Muschelkalk* limestone beds (54 m thick) are prominent oil producing reservoirs in the Soultz and Hermerswiller Compartments (Figures 70, 71 and 76 profile B-B'). Here, the *Muschelkalk* has secondary porosities and is fractured.

The known porosity and permeability values for Kutzenhausen-Soultz region range between 6-30% and 14-38 md, respectively. A permeability value of 156 md was measured on fractured *Muschelkalk* near the Soultz Fault (Table 6). Near Soufflenheim to the east, at depths below 1670 m, middle and upper *Muschelkalk* porosities and permeabilities are greatly reduced (Appendix 7).

Muschelkalk elsewhere in the study area near Pechelbronn shows oil and gas traces with free flowing saline water and oil impregnation in cores (Figure 71). At the Kutzenhausen Fault, Well 4601 produced gas (10-15 m^3/h) and gaseous water.during a test. At Donau-2, 4214 l/h of saline water with gas traces and at Ritterhausen-3, 4.3 l/h of saline water were produced during tests (Figure 70). Numerous wells encountered the *Muschelkalk* formation in tectonically upthrown or downthrown positions in the foot- or hanging-walls across the principal and/or auxiliary faults. Commonly, these wells are artesian and in the Hermerswiller Compartment at Soultz Fault SF5 they produce oil commercially. Here, the oil is deposited up-dip in a 6-10° eastwards dipping structural monocline bounded by the antithetic SF5 fault and secondary oblique faults (Figures 71 and 78 profile V; wells 4555, 4620, 4554). Oil is produced from the bottom part of the upper *Muschelkalk* which, in this region comprises a fractured dolomitic and a sandy as well as an oolitic and vesicular limestone. Well 4555 was eruptive (blow-out) and produced 550 l/h of oil. In the vicinity, two other eruptive wells (4554 and 4620) were drilled in the same reservoir. All producing wells were water-driven. Saline, hot groundwater flooded the reservoirs and reached the surface.

Lettenkohle: The *Lettenkohle* formation in the Kutzenhausen-Soultz region is dolomitic with fractures and caverns. It is an excellent reservoir rock and carrier bed in the study area. Of the 70 wells which encountered *Lettenkohle*, 40 are within the Hermerwiller Compartment, 7 in the Soultz Compartment (Figure 81), 1 at Marienbronn, 1 at Walbourg, 9 in the Internal Zone to the east and 13 at Ohlungen. In the Pechelbronn-Soultz Basin the *Lettenkohle* lies at a depth of between 800-1000 m; to the graben's centre at Roeschwoog, it is at a depth of 2450 m (Figure 70).

Porosities and permeabilities range between 10-15 % and 2-3 md, respectively. Extremely high porosity values were measured on core at the Soultz Fault (well 4606; Appendix 7).

Oil-producing horizons are found in the bottom part of the 20-25 m thick *Lettenkohle* in the fractured and cavernous dolomitic facies, unique to the Kutzenhausen-Soultz-Hermerswiller Compartments. Wells 4634 and 4589 were eruptive and produced about 12 m^3/h per day; well 4601 near the Kutzenhausen Fault (Figures 75 profile IIIb, 77 profile IV, 78 profile V and 81) was also eruptive and produced 2 m^3/h. Production elsewhere in the study are was minor. For example, the *Lettenkohle* -carrier formation showed only saline water with oil traces, Rittershausen-3 produced 200 l/h of saline water with oil indices, and Donau-5 (eruptive) showed 1 m^3/h of saline water (Figure 70). Further wells which showed oil and gas traces and free flowing saline water are indicated on Figure 81.

Again, it is noted that the producing wells are situated in the up-dip sections of the footwalls east of the Kutzenhausen Fault and Soultz Faults SF3, SF4 and SF5. Exploration wells further down-dip encountered mostly oil-stained groundwater-saturated *Lettenkohle*. That is, they reached the oil-water contact (transition zone) under the *Lettenkohle* oil reservoir. As in the upper *Muschelkalk* reservoirs, the oil pool production rate is low and the pools are, after initially producing only oil, quickly flooded with water.

Grés à Roseaux: Interbedded in the middle *Keuper*, the *Grès à Roseaux* sandstone-marlstone formation is a well-known oil producer in the Soultz and Kutzenhausen Compartments (Figures 11 and 12). Its physical parameters and thicknesses can vary considerably in the basin. In the Pechelbronn-Soultz Basin a sandy facies is developed (wells 3647, 3661, 4477). *Grès à Roseaux* attains an average thickness of 25 m at Pechelbronn, and 15 m at Kutzenhausen-Soultz. It is found at 800-900 m depth in the basin, at 1400-1600 m to the east, at 2350 m at Roeschwoog and at 600-650 m at Marienbronn (Figure 70).

The porosity in the sandy facies varies between 5-25 % and the permeability between 0.5-100 md. For well 4630 a porosity of 20-25 % and a permeability of 33 md was measured (Appendix 7). Vertically, the porosities and permeabilities can change rapidly due to mineralization (rapport de fin de sondage, SAEM).

Oil is produced from the *Grès à Roseaux* in the Soultz and Kutzenhausen Compartments near Pechelbronn and Kutzenhausen, respectively (Figures 11 and 12). Both reservoirs are situated in a structural high of an eastwards inclined monocline upthrown by the respective principal faults. Oil in the Kutzenhausen Compartment was exploited in the 1940's by five SAEM production wells (Tables 10, and 11; Figure 10) and in 1981 by four TOTAL wells. In the Soultz structure, wells 3685 and 4418 (Figure 9) produced oil over a period of five years. As is typical for all Mesozoic oil-producing horizons, the *Grès à Roseaux* reservoirs were water-driven and the production rate of oil was controlled by the influx of saline groundwater. Well report 4418 states specifically that the production *"rythme"* is influenced by the progression of the water front, which itself is governed by the permeability of the lower zones in the compartment.

Other oil-producing formations to the east and south of the Pechelbronn-Soultz Basin are listed in Table 7.

Other petroleum-hydrogeological observations

The total production of oil from Mesozoic reservoirs amounted to 100 900 tons at the end of 1961 (Table 8), which is only 3.8 % of the total oil production in the Pechelbronn-Soultz Basin. The remaining 96.2 % of oil was produced from Tertiary reservoirs. On average a well produced over a period of 5-7 years.

With depletion of an oil reservoir, the production rate of oil by pumping varied. The amount of pumped groundwater also fluctuated over the years, and the pump rate had to be decreased or increased over the production period with changing influx of groundwater. For example, well 3976 (Figure 9) initially produced oil at a rate of 6000-8000 l/d and saline water at a rate of 2000-3000 l/d from the *Grès à Roseaux* reservoir in the Kutzenhausen Compartment (696 m deep) but suddenly dried out after 4 months of production. *Lettenkohle* oil was then produced (80-100 l/d) from the same well at a depth of 984 m (Figure 81) until after 2 1/2 years, groundwater flowed freely to the surface with minor oil traces.

Reaching greater depths by rotary drilling deeper Mesozoic reservoirs became increasingly watered-down and were flushed by saline, often hot water. Numerous wells were initially "eruptive" when drilling into structurally elevated reservoirs close to or in fault planes (Figure 71) and oil and water continued to flow under artesian conditions. Some geological reports for the Hermerwiller Compartment recommended blow-out prevention measures before drilling into the summit of the *Muschelkalk* and *Lettenkohle* east of the Soultz Fault System.

The Soultz region was also known for its marshy ground conditions at planned drill sites. In one instance, well 4636 which was to drill for oil in the *Muschelkalk* in the Soultz Fault Zone had to be relocated because of an unstable drill rig foundation on marsh land. This simple, but meaningful observation is according, to the Hydraulic Theory (see Appendix I), an indication of discharging groundwater flow and an indirect indicator for subsurface oil deposits.

The Tertiary

Of the Tertiary formations, the *Zone Dolomitique* and middle *Pechelbronner Schichten* had important oil producing horizons and lenses.

Table 9 presents the Tertiary reservoirs and carrier beds in the Upper Rhine Graben study region (see Figure 70 for locations). Characteristic of Tertiary oil-bearing sand reservoirs in the Upper *Pechelbronner Schichten* and *Zone Dolomitique* is their predominantly lenticular configuration. Nevertheless, oil-producing sand and conglomerate layers are also observed. Individual reservoir lenses are enclosed argillaceous layers and reach thicknesses ranging from a few decimetres to 2 meters. Lenses do not occur in sequence as evenly arranged horizons, but rather are distributed irregularly as lens-bundles or as stacks. A stack of lenses can be 20-30 m high and 10-20 m wide (Schnaebele, 1948). The sand layers and lentils encased in marls of the *Pechelbronner Schichten* cover areas ranging from some square meters to some hectares. As delineated on the surface by productive wells, the forms, shapes, or sizes of the productive spots are anything but regular (Figure 70).

Porosity and permeability values for Tertiary formations are not available for the Pechelbronn-Soultz Basin. Well reports mention high porosities and high water fluxes in sand lenses and conglomerate layers but also state that interbedded marl-horizons were too tight to take measurements. Interestingly, numerous reports reveal that an increase in porosity and permeability and water flux is observed near fault zones.

A few permeability and porosity measurements were taken in the eastern and deeper part of the Upper Rhine Graben, e.g., at Soufflenheim, Surbourg, Schirrheim (Tables 8 and 10). For the Pechelbronn-Soultz Basin higher values for the shallower Tertiary and an increase in porosities and permeabilities near fault zones can be expected.

Zone Dolomitique : Before 1931, exploration and production in the Pechelbronn-Soultz Basin was focused only on reservoir-carrier formations above the *Couche Rouges* which was also named by SAEM geologists at that time "the wall of (oil) deposits", (*mur des gisements*). The *Couches Rouges*, which attains a maximum thickness at Preuschdorf of 210 m (Chapter 2.3.1.6), is a poor reservoir and carrier bed with no significant petroleum deposits,bearing groundwater only, with occasional with oil traces.

The upper half of the *Zone Dolomitique* is rich in interbedded sands and conglomerate horizons which form an irregularly distributed pattern of oil-bearing lenses and layers. In the Kutzenhausen and Soultz Compartments between the principal faults zones two main oil fields in the *Zone Dolomitique* to the northeast and south of Kutzenhausen (Figure 72) have produced oil since the 1930's. Unlike the Mesozoic reservoir formations the *Zone Dolomitique* reservoirs are laterally discontinuous, with distinguishable production levels 5 to 30 m below the top followed by a sterile zone (no oil, some water) of about 60 m thickness. At 90-120 m below the top of the *Zone Dolomitique* oil-bearing lenses and layers are encountered followed by a water-bearing zone. Oil has accumulated in reservoirs at the down-dip and up-dip section of antithetically faulted monoclines near prinicipal and secondary fault planes. South of Kutzenhausen, oil-bearing levels are dissected and displaced by the Kutzenhausen Fault (Figures 72 and 77 profile IIb). Wells 4514, 4375, 4410, 4503 and 4299 have produced oil from lenses and conglomerate layers at different levels in the up-dip section of the Kutzenhausen footwall; wells 3625 and 3685 have encountered equivalent *Zone Dolomitique* oil reservoirs downthrown by the principal Kutzenhausen Fault in the hanging wall. The vertical separation is about 300 m, and juxtaposed Oligocene marls function as a barrier to oil migrating from the footwall reservoir, while Jurassic formations function as fault-cap rocks to the deeper reservoirs in the hanging wall (Figure 75 profile IIIb). The sealing mechanism is determined by the juxtaposition of low permeable strata (juxtaposition fault seal, see Appendix IV). As was reported for wells 4514 and 3685 which were drilled into the Kutzenhausen Fault Zone, groundwater with an abundance of oil traces flowed freely in the bore hole to higher elevations but remained below the landsurface. Groundwater was able to penetrate the fault plane and flow across and along this fractured zone to higher aquifer formations.

In the oil fields in the northeast of Kutzenhausen a similar situation is observed within the fault blocks. The vertical displacement by auxiliary faults is only a few decametres and reservoir rocks and carrier beds are not entirely separated by fault planes. The reservoirs are hydraulically still connected and oil can migrate between reservoirs across and along the fault plane.

In the middle section of the compartment between the Hoelschloch- and Kutzenhausen Faults the *Zone Dolomitique* dips to the east and is not affected by major faulting, reaching greater depths in this section than in the other compartments. Reservoir rocks are void of oil deposits in the downdip part and function as an aquifer conducting saline, warm groundwater (Figures 72, 76 profile B-B' and 75 profile IIIc). In this part of the Pechelbronn-Soultz Basin the Mesozoic and Tertiary formations are laterally continuous between the bordering principal fault zones. Secondary faults may well be present in these Tertiary formations but the vertical displacement is minor in terms of the formation's continuity. As can be expected, the oil fields in the *Zone Dolomitique* in this compartment are located in the summit of the eastward inclined monocline in the proximity of the Hoelschloch Fault.

Further to the west, oil fields have been found in the Hoelschloch Compartment along the Pechelbronn Fault in a N-S direction. The reservoirs at Hoelschloch and Pechelbronn are noted for their continuity 5 to 10 m below the top of the *Zone Dolomitique*. Two other discontinuous levels are encountered at 50 and 90 m below the top (Schnaebele, 1948).

At Kreuzhecke in the Preuschdorf Compartment numerous lenticular irregularly distributed reservoirs are producing oil 100 m below the top (Figures 72 and 74 profile IIb).

Near Lobsann to the north of Pechelbronn oil production from the *Zone Dolomitique* has been insignificant. Reservoirs were found to contain mostly heavy biodegraded oils and fresh water infiltrating from the Hochwald recharge region (Figures 72 and 79 profile VIa, b).

Exploration efforts in the east compartment of the Soultz Fault as well as north and south of the producing oil fields have been unsuccessful and showed only saline water (Figure 72).

Pechelbronner Schichten : Reservoir rocks in the *Pechelbronner Schichten* are developed as sand lenses, more or less marly and geometrically limited. A stack of lenses constitutes several horizons with lithology that can vary laterally from sandy to marly within a few meters. These lenses of detrital origin in the Pechelbronn region have been mapped and geologically described in detail by SAEM geologists using subsurface drainage mining over the decades (Schnaebele, 1948). Three oil-producing principal levels (stacks of lenses) with variable reservoir qualities extend over the entire Pechelbronn area. It was noted that, depending on the distribution of lenses, porosities and permeabilities varied over short distances and that the production rates are a function of permeability rather than a function of structural position of the lenses in the compartment itself (Schnaebele, 1948). A summary of the estimated oil production capacities of the reservoirs in the upper *Pechelbronner Schichten* is found in Table 11.

Notably, reservoir rocks in the Upper *Pechelbronner Schichten* at Preuschdorf, north of Lobsann and east of Kutzenhausen, are empty.

The Middle *Pechelbronner Schichten* produced only minor amounts of oil in the Pechelbronn-Preuschdorf-Hoelschloch region.

The Lower *Pechelbronner Schichten* are seen as the most prominent oil producer of the Tertiary reservoir formations (Table 12). With the exception of the eastern region of Soultz and Reimerswiller, all other fields constitute several producing levels in this formation. Generally, the lenses appear as bundles similar to these found in the Upper *Pechelbronner Schichten* as.

Other petroleum-hydrogeological observations

Exploration of, and production from the Oligocene petroliferous lenses was focccused mainly in regions parallel to principal faults in a N-S direction. As for reservoirs in the *Zone Dolomitique*, the *Pechelbronner Schichten* reservoirs are concentrated in structural highs near fault zones. In the earlier exploitation stages of the Pechelbronn-Soultz Basin, oil in the Schichten was extracted by subsurface mining. In the galleries miners observed a network of fractures and secondary smaller faults cutting into the Tertiary terrain and the sand lenses (Schnaebele, 1948; Sittler, 1985). Fractures crossing the interlayered marl beds were found to be lined by oil films or, in many cases, by a greenish halo. Marl layers encasing the sand lenses show the same phenomena. From the crushed terrain near the principal Pechelbronn Fault, groundwater poured into the galleries which had to be constantly drained by pumping.

Heavy, oil-impregnated sand lenses (oil sands) were hauled to the surface and oil was extracted by distillation in factories at Pechelbronn. The remaining washed, but chemically contaminated sands were dumped on tailings which now stand as huge cones in the Pechelbronn landscape. Today, hazardous fluids (oils and solvents) still seep from the peripheries of these mounds and leak into the Pliocene shallow aquifer system.

In a later phase, drainage-mining and pumping produced the oil. In the final years of operation pumping by surface wells took over and the mines were closed. Within several weeks of closure the galleries and shafts were inundated by the incoming groundwater from the ever present aquifers.

In the Oligocene 2439 pumps were installed and of the 89.6 % total production in the *Pechelbronner Schichten* 26.1 % was by mining and 63.5 % by well pumping. The *Zone Dolomitique* produced 6.6 % and the remaining 3.8 % was exploited from Mesozoic reservoirs.

2.4 Some Tentative Conclusions and Statements

The simple fact that oil must have migrated from the mature Jurassic source rock located in the graben's centre across and along the faults to reach the structural highs in the Pechelbronn-Soultz Basin proves that the faults are conduits. It also contradicts Hunt's (1990) statement that compartments in general are generally sealed off by their bordering faults.

Even without a detailed knowledge of the hydrogeology of the basin, from observations I have made so far based on subsurface data, i.e., geology, structure and formation fluids I can conclude that the Upper Rhine Graben including the Pechelbronn-Soultz Basin contains a system of structurally disrupted but hydraulically continuous Mesozoic and Tertiary carrier formations saturated with groundwater (aquifers) and holding oil deposits (reservoirs). The principal Fault Zones are conduits to groundwater and its transported matter Formation waters flow cross-formationally from Mesozoic carrier beds and along sand lenses (Schnaebele, 1948; Sittler, 1985). Fractures crossing the interlayered marl beds were found to be lined by oil films or, in many cases, by a greenish halo. Marl layers encasing the sand lenses show the same phenomena. From the crushed terrain near the principal Pechelbronn Fault, groundwater poured into the galleries which had to be constantly drained by pumping.

Heavy, oil-impregnated sand lenses (oil sands) were hauled to the surface and oil was extracted by distillation in factories at Pechelbronn. The remaining washed, but chemically contaminated sands were dumped on tailings which now stand as huge cones in the Pechelbronn landscape. Today, hazardous fluids (oils and solvents) still seep from the peripheries of these mounds and leak into the Pliocene shallow aquifer system.

In a later phase, drainage-mining and pumping produced the oil. In the final years of operation pumping by surface wells took over and the mines were closed. Within several weeks of closure the galleries and shafts were inundated by the incoming groundwater from the ever present aquifers.

In the Oligocene 2439 pumps were installed and of the 89.6 % total production in the *Pechelbronner Schichten* 26.1 % was by mining and 63.5 % by well pumping. The *Zone Dolomitique* produced 6.6 % and the remaining 3.8 % was exploited from Mesozoic reservoirs.

2.4 Some Tentative Conclusions and Statements

The simple fact that oil must have migrated from the mature Jurassic source rock located in the graben's centre across and along the faults to reach the structural highs in the Pechelbronn-Soultz Basin proves that the faults are conduits. It also contradicts Hunt's (1990) statement that compartments in general are generally sealed off by their bordering faults.

Even without a detailed knowledge of the hydrogeology of the basin, from observations I have made so far based on subsurface data, i.e., geology, structure and formation fluids I can conclude that the Upper Rhine Graben including the Pechelbronn-Soultz Basin contains a system of structurally disrupted but hydraulically continuous Mesozoic and Tertiary carrier formations saturated with groundwater (aquifers) and holding oil deposits (reservoirs). The principal Fault Zones are conduits to groundwater and its transported matter Formation waters flow cross-formationally from Mesozoic carrier beds and along fault planes under artesian conditions to the surface. This is especially observed in the Soultz-Hermerswiller Compartments for the Mesozoic formations which are dissected and "crushed" by faults and fractures. Oil traces were observed in a fault plane in the *Pechelbronner Schichten* and middle *Keuper*. Porosity and permeability as well as the flux of water increases toward fault and fracture zones (e.g. well 4512).

None of the *Keuper* reservoirs, (except for the *Grès à Roseaux*, the Liassic, the *Couches Rouges* and Oligocene marl interbeddings) contain oil deposits, but they are known to carry some groundwater. These formations represent regional aquitards and function locally on top of a reservoir and juxtaposed by a fault as sealing cap rocks (see Appendix IV). Any given fault may be a seal at one place and a conduit at another at the same time. This behavior may have changed with geologic time.

In the Keuper, oil has accumulated mainly in tectonically elevated culminations of inclined formations and lenticular sandbodies parallel to the principal faults in a N-S direction. Two possible entrapment mechanisms can be identified: (1) lithological, e.g., sand lenses and conglomeratic horizons in Tertiary formations; (2) structural, e.g., migration of oil from Mesozoic reservoirs being obstructed across the faults by juxtaposed cap rocks. Although not yet established by a hydrogeological flow analysis (Chapter 6), the Soultz Compartment is believed to represent a disaccommodation zone for petroleum, heat and inorganic matter. It constitutes a discharge area in which the regional flow systems from the Vosges and Black Forest Mountains, respectively, converge from opposite directions in the Mesozoic aquifer system at the Soultz Horst then turn vertically up to discharge along the conductive fault zones into shallower Tertiary zones, leaving their organic cargo (oil) in the Mesozoic reservoirs to be retained under the low permeable *Keuper* and Jurassic cap rocks or in Tertiary sand lenses and horizons.

Near oil fields, groundwater carries oil droplets and traces, their abundance decreasing away from the oil pool, often in the downdip direction of the eastward dipping monoclines. The oil/water transition zone can be tilted by 4-6^o to the east indicating a eastward groundwater flow component (Figure 75 profile IIId). Near fault zones, production wells were observed to be flowing, especially in the case of the Mesozoic reservoirs in the Soultz and Hermerswiller Compartments. In this region two wells, initially capped off in the 1950's, are now leaking; they are well 4550 (oil seep at the surface) and well 4616 (Figure 71). From these wells flowing warm, saline water reaches the surface with oil traces. Although these Mesozoic reservoirs in the Soultz region are now depleted of oil in commercial quantity, the regional flow systems remain active and groundwater continues to flow, discharging to the surface.

The formation waters are generally saline and hot. Fresh waters recharging from local topographic highs, e.g. Hochwald, invade the Tertiary carrier beds and reservoirs at shallower depth. When this occurs oils can be expected to be degraded and of lesser quality.

3. The Hydrogeologic Environment

3.1 Introduction

Three main components of the groundwater system: topography, climate and geology are identified as the major controls on the groundwater regime (Tóth, 1970a). A combination of the three components is referred to as the hydrogeologic environment. Each of these components consists of environmental parameters that can be measured, such as topographic relief, regional slope, width and depth of the groundwater basin, rock porosity, precipitation, air temperature and evapotranspiration.

The geology of a basin is related to the groundwater regime through the distribution of the porosity and hydraulic conductivity of the rocks. Spatial variation in the hydraulic conductivity of the rocks framework, caused by the occurrence of strata, lenses and faults of different permeability, modify the flow pattern and the intensity of groundwater flow in the basin.

The relief of the water table influences the distribution pattern and velocity of groundwater flow. In areas with an excess of precipitation and where the water table thusresembles a subdued replica of the surface topography, flow patterns may be calculated by substituting the relief of the land surface for the water table (Tóth, 1963).

In a basin with evenly sloping flanks, a unit pattern of regional groundwater flow (Tóth, 1984) is developed in which, relative to the water table, groundwater flow is descending, lateral and ascending in recharge, midline and discharge areas, respectively. Intensity of movement decreases with increasing depth and away from the midline area. Changes in topographic relief result in modification of flow pattern geometry and intensity, producing flow systems of different order (Tóth, 1963). Each flow system has three regimes: recharge, transfer and discharge. Local and regional slopes, and the width and depth of the basin, control the geometry and intensity of the various flow systems.

3.2 Topography

The Upper Rhine Graben at Pechelbronn is 35 km wide and lies on average 150 m above sea level (a.s.l.). The most salient feature of the regional relief are the mountain ranges of different elevations flanking the graben valley. Regional elevations vary from less than 120 m a.s.l. in the valley of the Rhine River to over 900 m in the Black Forest mountains to the east. The elevations reach up to 500 m in the Hochwald and over 500 m in the Vosges mountains to the west (Figure 1). In the Pechelbronn-Soultz region the undulating hill landscape of Tertiary and Quaternary deposits 150 -200 m above sea level is flanked to the west by the up to 500 m high Hochwald mountain (Figure 82). Two local rivers, the Sauer and the Seltzbach, cut through the landscape and drain into the Rhine River (Figures 70 and 82). The regional slopes of the graben flanks measured from the highest elevation point to the valley floor at an average elevation of 150 m (a.s.l.) are 84 m/km for the Black Forest and about 34 m/km for the Vosges. For the Hochwald, slopes over a distance of less than 2 km may reach 150 m/km. Locally, in the Pechelbronn-Soultz Basin, hills have a topographic gradient of between 50 - 78 m/km. The overall slope of the area, and the drainage of the subsidiary rivers is towards the Rhine River.

3.3 Depth and Width

The Upper Rhine Graben at Pechelbronn is about 35 km wide from the Rhine Fault to the Black Forest Fault. The depths of the groundwater basin to the granitic basement is illustrated on Figure 5 and in a schematized cross-section of the graben (Figure 69 profile A"-A"'). The sedimentary fill is thickest under the Rhine River, and the depth to the basement is in excess of 4000 m. Towards the Pechelbronn-Soultz Basin, upthrown by fault systems, the thickness of the sedimentary fill decreases and the basement is at shallower depths: from 3500 m at Roeschwoog to 1380 m (well 3956) in the Soultz Horst.

3.4 Climate

The climate in the Upper Rhine Graben is humid with mean air temperatures for the summer being 17.5 °C, and for the winter months 5 °C (Steinhause, 1970). In the Black Forest east of Baden-Baden (Figure 70) precipitation increases with altitude to over 1400 mm/y (Deutscher Wetterdienst, 1953). In the Vosges Mountains, an annual rainfall of 800-850 mm/y was measured. On the west side of the Rhine valley annual precipitation is slightly lower. On the east about 900 mm/y of rain have been recorded. In the

Pechelbronn-Soultz region the effective precipitation is about 300 mm/y. About 50 % of the annual precipitation falls over the winter period.

3.5 Hydrostratigraphic Units (HSU's)

A hydrostratigraphic unit is a body of rock that can be distinguished as either water-bearing or water-retarding relative to adjacent rocks. The sequence of sedimentation and tectonic events in the Upper Rhine Graben has resulted in the formation of distinguishable hydrostratigraphic units, with both high permeability (aquifers) and low permeability (aquitards), which are independent of the primarily deposited geologic units. A hydrostratigraphic group (HSG) is a combination of two or more hydrostratigraphic units which together function as either a groundwater conducting or retarding rock complex.

Unconsolidated sands and gravels, sandstones, limestones and dolomites and fractured igneous and metamorphic rocks are examples of rock units known to be aquifers. The most common aquitards are clays, shales and massive crystalline rocks (Table 13; Freeze et al., 1979; Todd, 1980). In a tectonically stressed geologic environment a regionally defined aquitard can function locally near a fault-fracture zone as an aquifer. In a fault-severed geologic environment hydrostratigraphic units can, either completely or in part, be separated by one or more fault planes. The extent of vertical separation by a fault plane, the dip direction and inclination of a hydrostratigraphic unit and the fault plane all govern the lateral continuity of an aquifer, i.e., the conductance of groundwater flow in that unit. If the throw of a fault is less than the total thickness of a hydrostratigraphic unit, hydraulic continuity is maintained across the fault plane to the displaced unit. If vertical separation is greater than the unit's thickness the hydraulic character of the juxtaposed hydrostratigraphic unit determines the lateral hydraulic continuity of the other and affects groundwater flow directions. If a unit adjacent to a fault-plane is an aquitard, flow continuity from a juxtaposed aquifer is impeded and groundwater is deflected into areas of lower flow resistance, e.g., along the fault plane or into other permeable zones (lenses). Therefore, defining a hydrostratigraphic unit in a tectonically stressed groundwater basin based only on its hydraulic characteristics, i.e., hydraulic conductivities and transmissivities, is insufficient for a regional groundwater flow study. Knowledge of the degree of aquifer inter-connectivity and cross-fault hydraulic continuity of disrupted water-bearing formations derived from structure contour maps and cross-sections is essential.

3.5.1 Hydrostratigraphy of the Upper Rhine Graben

In the following the hydrostratigraphic units will be defined. Based on quantitative data, or inferred from indirect information (as, for instance, porosity, water yield, DST recoveries, water occurrences, reportedly dry sections), found in individual well reports, I assigned probable permeabilities and permeability ranges to the hydrostratigraphic units (HSU's) (Tables 8, 20, 21 and 22).

3.5.1.1 The Granitic basement - Aquitard (HSU 1) and Aquifer (HSU 2)

Brace (1980) has reported measurable permeability values in crystalline rocks at any depth accessible by today's drilling technology. In situ permeability measurements on crystalline rocks showed k-values of between 0.1 and 10 md, and no systematic decrease in k with depth. Drilling through igneous and metamorphic complexes, networks of fractures and joints provide excellent avenues for groundwater flow.

A study in the southern part of the Black Forest showed that fresh groundwater flows laterally from the crystalline mountain into the foreland basin (Kanz, 1987). Kanz assumed that the weathered granite and the *Buntsandstein* are the main aquifers and drilling in this area showed the first 500 m of the granite to be weathered. In the Black Forest of the study area the granitic basement outcrops to the surface and constitutes an extensive region of the eastern recharge area. Two geothermal wells drilled in the granite near Baden-Baden encountered fractures and artesian hot waters up to a depth of 230 m and 360 m, respectively.

In autumn 1987 a geothermal drilling project exploring the basement for its geothermal energy potential was conducted by BRGM and BGR (pers. communication, Dr. Jung, BGR-Hannover) in the Soultz Horst, near the former SAEM well 4689, 500 m south of SAEM well 4616. The deep well (GPK, Figure 76 profile B-B') was drilled to the top of the granitic basement at 1376 m depth east of the Soultz Fault. Although a DST in the top of the basement failed, at 1817 m depth a water-bearing joint was encountered, whence hot artesian groundwater flowed at 0.15 l/s. A television camera recorded intensive fracturing and jointing for most part of the granite but there was no significant water yield.

The weathered upper part of the basement is an approximately 300 m thick aquifer (HSU 2) and I assume a probable hydraulic conductivity of less than 10^{-5} m/s. The remaining lower granite is assumed to be a very low permeable aquitard or aquiclude (HSU 1; Table 14).

3.5.1.2 The Permo - Triassic Multi-Aquifer System (HSU 3)

Overlying the basement, the Permian sandstone formation is the first hydrogeologically significant sedimentary series. In the eastern recharge region its thickness varies between 200-600 m. Outcropping in the Black Forest, the hydraulic character of this sandstone formation is comparable to the *Buntsandstein* formation. In the graben, deeply buried Permian was found only locally (Chapter 2.3.1.2) as a discontinuous formation. At Bruchsal, north of Karlsruhe (Figure 70) a transmissivity of $1.0\text{x}10^{-3}$ m^2/s was measured during an aquifer test for coarse-grained Permian at 2440-2470 m depth. This translates into a hydraulic conductivity of $3\text{x}10^{-5}$ m/s (Bertleff et al., 1987). Permian was drilled in the Pechelbronn-Soultz Basin by well 3956 at Kutzenhausen, well 4687 at Ohlungen and Obermodern-1 in the Saverne Fracture Zone. No hydraulic parameters have been measured. West of Wissembourg (Figure 70) at Weiler a pump test (time-drawdown test) gave a transmissivity value of $8\text{x}10^{-4}$ m^2/s and a K-value of $7\text{x}10^{-5}$ m/s for Permian at 50-120 m depth (well Weiler-1, SGAL-Archive). Porosity values are most likely comparable to values in the *Buntsandstein* (n: 3-15 %).

The Triassic is a multi-aquifer system with two main aquifers, the *Buntsandstein* and *Muschelkalk*. The *Buntsandstein* Aquifer is a regional hydrogeologic unit in the Upper Rhine Graben. In the Vosges and Hochwald recharge regions near-surface *Buntsandstein* has an average transmissivity value of $1.9\text{x}10^{-3}$ m^2/s (n: 6, T_{max}: $8.5\text{x}10^{-3}$, St.dev.: $3.3\text{x}10^{-3}$) and a conductivity of K_{mean} $6.5.\text{x}\ 10^{-6}$ m/s (n: 4, K_{max}: $1.0\text{x}10^{-5}$, St.dev.: 4.910^{-6}; Appendix 7).

At Morsbronn (Figure 70, thermal well Mors-3b) *Buntsandstein* at 460-680 m depth has a T-value of $4\text{x}10^{-3}$ m^2/s and a K-value of $2\text{x}10^{-5}$ m/s. Here, 250 m east of the Rhine Fault, the Mesozoic formations are tectonically strained and show higher hydraulic values.

For a flowing thermal well at Pechelbronn (Helion II, SAEM well 1266) the transmissivity of *Buntsandstein* at 1100 m depth is $5\text{x}10^{-3}$ m^2/s and the K-value is about $1\text{x}10^{-6}$ m/s.

At Bruchsal, north of Karlsruhe (Bertleff et al., 1987) a pump test in a geothermal well Bruchsal-1a revealed a T-value of 8×10^{-3} m^2/s and a K-value of 2×10^{-6} m/s for middle *Buntsandstein* at 1742-1875 m depth. A DST in well Bruchsal-2 showed a permeability of 0.026-0.061 md and an effective porosity of 3-6 % at 2345-2349 m depth.

The *Muschelkalk* is the upper aquifer of the Permo-Triassic hydrostratigraphic unit 3. Intensively fractured in the Pechelbronn-Soultz Basin, the *Muschelkalk* limestone formation is a major regional aquifer in the Upper Rhine Graben. In thermal well Morsbronn 3a (SGAL-Archive) an aquifer test produced a transmissivity of 1.0×10^{-3} m^2/s in the upper and middle *Muschelkalk* which translates into a hydraulic conductivity of 4×10^{-5} m/s. The storage coefficient was 1.8×10^{-3} m^3/m^3.

As was also observed in the *Buntsandstein*, hydraulic parameters in the *Muschelkalk* vary significantly with depth and with increasing tectonic strain on the formation in the area (Appendix 7). In the graben centre undisturbed deeper *Muschelkalk* (> 1600 m deep) has porosity and permeability values significantly lower than the tectonically elevated *Muschelkalk* in the Pechelbronn-Soultz Basin (e.g. well Soufflenheim, Tables 8 and 9). Faulting had "crushed" the rigid limestone rocks near fault planes and secondary porosities and permeabilities and a network of fractures cutting through the stratum were observed (Table 6). With a highest fault density in the Soultz Compartment, hydraulic values for the *Muschelkalk* as well as for the hydrostratigraphic unit 3 are expected to be highest in this region.

West of the the Rhine Fault, middle *Muschelkalk* in the Lembach graben (135 m thick) constitutes a shallow-depth drinking-water reservoir for local communities (SGAL-Archives).

Although lithologically heterogeneous (e.g., the lower *Muschelkalk* is more marly and dolomitic and the middle part contains some anhydrite), the entire *Muschelkalk* complex is defined as one hydrogeologic formation and assigned hydraulic parameter ranges (Tables 20).

3.5.1.3 The *Lettenkohle* Aquifer (HSU 4)

No transmissivity or conductivity data are available for the *Lettenkohle* in the Pechelbronn-Soultz Basin. Elsewhere in the Rhine Graben on oil-bearing *Lettenkohle* a drainable porosity of 3-10 % was determined and a transmissivity of 0.01-0.1 m^2/s was given (Nägele et al., 1981) for intensively fractured rigid *Lettenkohle* dolo-limestone and claystone beds. For the *Lettenkohle* I assume a hydraulic conductivity range of between 1×10^{-5} and 1×10^{-6} m/s. Possibly, higher values can be expected in the Hermerswiller and Soultz Compartments where wells in the *Lettenkohle*, *Muschelkalk* and *Buntsandstein* were eruptive and flowing, indicating good groundwater flow conductance in the aquifers and hydraulic communication with the lower hydrostratigraphic units. Similar observations were made in the Hoelschloch Compartment (Figure 71). Permeability measurements on core samples showed values between 1.3 - 10.5 md with a highest value of 157 md on a fractured core sample (well 4541, Appendix 7).

Except for chrono-stratigraphic differences HSU 3 and 4 are, based on their hydraulic parameters, comparable aquifers and I unify these units as one hydrostratigraphic group: The Mesozoic Aquifer Group (HSG I). It is interesting to note that HSU 4, only 20-25 m thick and easily dismembered by principal and auxiliary faults with vertical displacements of even less then 25 m (depends on inclination angles), is regionally laterally discontinuous as an aquifer (Figures 69 profile A"-A'", 75 profile IIIb, c, 76 profile B-B', 77 profile IV and 78 profile V). The *Lettenkohle* Aquifer is laterally hydraulically uninterrupted only within a structurally defined compartment. However, in unifying hydrostratigraphic unit 4 and hydrostratigraphic unit 3 as an aquifer group emphasising vertical hydraulic communication between the units, the *Lettenkohle* Aquifer can be described as hydraulically continuous over the entire basin, as are the lower aquifers. Even the greatest fault displacement along the Kutzenhausen Fault (r=420 m) did not disrupt the regional continuation of the Mesozoic Aquifer Group across the Upper Rhine Graben towards its respective recharge regions, where the Mesozoic Aquifer Group outcrops at the surface.

3.5.1.4 The *Keuper* Aquitard (HSU 5)

The remaining approximately 180 m thick *Keuper* formation capping the *Lettenkohle* Aquifer is an aquitard of low permeable clay-marlstones. Interbedded are dolomite and anhydrite layers. No hydraulic values are available. Instead, a few measurements on core samples indicate horizontal permeabilities between 0.2-3 md and porosities between 2-7 %. Vertical permeabilities are lower and between 0.08-0.4 md (Appendix 7). No significant water influx from the *Keuper* during drilling was reported. Some *Keuper* sections appeared to be dry while others were water-wet. A hydraulic conductivity range of 1.0×10^{-9} to 1.0×10^{-10} and a porosity between 2-7 % is assigned to HSU 5 (Table 14).

3.5.1.5 The *Grés à Roseaux* Aquifer (HSU 6)

"Sandwiched" between hydrostratigraphic unit 5 (Figure 68), the middle *Keuper* Grés à *Roseaux* sandstone formation is a about 20 m thick aquifer and potential reservoir with good permeabilities and porosities in the Pechelbronn-Soultz Basin (Table.8). Interrupted by principal faults, hydrostratigraphic unit 5 is continuous only in the compartments. The displaced aquifer is mainly juxtaposed with the *Keuper* Aquitard deflecting groundwater flow and obstructing petroleum migration (see profiles).

3.5.1.6 The Jurassic Aquitard (HSU 7)

The Early Jurassic and Aalenian aquitard is about 150 m thick in the Pechelbronn-Soultz Basin and contains a low permeable clay-marlstone sequence with intercalations of limestone, dolomite and sandstone beds. For the Middle Jurassic in the graben's centre, permeabilities range between 0.1-5 md and porosities are between 6-18 % (Appendix 7).

In the Pechelbronn-Soultz Basin the Early Jurassic aquitard (wells at Walbourg, Surbourg and Rittershausen, Figure 70) has permeabilities between 0.15-0.31 md and porosities between 6-15 %. Overall, a hydraulic conductivity of 1.0×10^{-9} m/s and a porosity of 10 % is considered to represent a conservative estimate for this particular aquitard's hydraulic character.

Hydrostratigraphic units 6 and 7 are merged together as the Mesozoic Aquitard Group (HSG II).

3.5.1.7 The Cenozoic Aquifer - Aquitard Complex

The Eocene *Zone Dolomitique* as well as the Oligocene *Pechelbronner Schichten* are lithologically dissimilar in the Pechelbronn-Soultz Basin and the Internal Zone of the Upper Rhine Graben to the east. The interbedded Upper Eocene - Early Oligocene *Couches Rouges* has a lithology that is uniform over the entire basin. The following hydrostratigraphic units and groups may be differentiated in the Tertiary for the Pechelbronn-Soultz Basin and Upper Rhine Graben (Figure 11, Tables 21 and 22):

The Tertiary Aquifer Group in the Pechelbronn-Soultz Basin (HSG III)

The Tertiary Aquifer Group comprising clay-marlstones, lenticular and bituminous sandstones and shales of Eocene and Lower Oligocene age include the petroliferous *Zone Dolomitique* (HSU 8 west) and *Pechelbronner Schichten* (HSU 10 west). The matrix permeability of the constituent rock types is normally low, with the exception of lenticular bodies of sandstones and conglomerates. Nevertheless, based on lithologies, reported occurrences and flow rates of water and oil to wells, galleries and shafts (Chapter 2.3.3.2), the combined bulk permeability of these beds appears to be superior to that of the under- and overlying strata. Therefore they qualify as an aquifer, albeit of low hydraulic conductivity (Table 15).

The Tertiary Aquitard Group (HSG IV)

The *Couches Rouges* composed of partly dolomitic-anhydritic marlstones is an aquitard (HSU 9) about 200 m thick, interbedded between hydrostratigraphic units 10 and 8 in the Pechelbronn-Soultz Basin and Upper Rhine Graben (Tables 15 and 16). Well observations indicate that the *Couches Rouges* is devoid of oil deposits and contains only a few water-wet sections, which are found near fault zones and at the top and base. Although no hydraulic data were available, it is deduced from its lithology (which is comparable to the *Zone Dolomitique* and Lower *Pechelbronner Schichten*) and from well observations that the contrast between its permeability and that of the subjacent aquifers is not sharp. Its hydraulic role as an aquitard, even though leaky, is therefore not firmly established.

The Rupelian *Série Grise* Aquitard (HSU 11) overlying the Pechelbronn Aquifer occurs 3-4 km east of the Rhine Fault with 30 m thick marl and clay-siltstones. Towards the graben the *Série Grise* increases in thickness to 450 m (Doebl, 1974). Bulk Permeability and porosity data were obtained from a few wells in the graben centre (Appendix 7); probable hydraulic conductivities range between 10^{-9} and 10^{-10} m/s. The *Niederroederner Schichten* of Chattian age are not present in the Pechelbronn-Soultz Basin and appear near Soufflenheim, attaining as an aquitard (HSU 12) a maximum thickness of 500 m .

The Pliocene - Quaternary Aquifer (HSU 13)

Silty sand-gravel Pliocene sediments occur east of Soultz-Ohlungen with maximal thicknesses of 10-100 m at Soufflenheim. Hydraulic conductivities from two aquifer tests were found to be $6x10^{-5}$ and $3x10^{-4}$ m/s; transmissivities were between $3\text{-}6x10^{-3}$ m^2/s.

Quaternary deposits and alluvium reach thicknesses between 15-30 m in the Rhine Valley at Roeschwoog, and K-values of $2\text{-}3x10^{-3}$ m/s and T-values of 10^{-2} - 10^{-1} m^2/s have been measured (Appendix 7). The Plio-Quaternary Aquifer is an important drinking-water reservoir in the region.

3.6 An Aquifer Connectivity Model

Using on a fault permeability model (Appendix III) as a basis and by formulating two simple methods discerning continuity of carrier beds in the basin (Appendix IV; Table 17), it is possible to approximate the conductivity of fault sections and determine possible sites of petroleum entrapment. Nevertheless, it is obvious that direct field observations are required. The distribution pattern of hydrogeological phenomena, i.e., the groundwater flow-controlled chemical character of formation waters and subsurface temperatures, and a hydrodynamic analysis provide direct methods to evaluate the conductance of fault zones. These techniques will be discussed in the following chapters.

Methods I (connectivity factor) and II (connectivity diagram; Appendix IV) were applied to the Pechelbronn-Soultz Basin for the six main structural compartments and principal faults (Figures 12 and 13; Table 18). Using both the schematic diagram and the fault permeability model, information on aquifer connectivity across fault zones in the basin can be deduced and possible groundwater flow avenues along and across faults can be hypothesized. These hypotheses are set forth below:

(1) the regional aquifer, hydrostratigraphic unit 3 (*Buntsandstein* and *Muschelkalk*), is continuous over the entire basin and groundwater flow is unimpeded by faults. Groundwater will flow across and along fault zones.

(2) the *Lettenkohle* aquifer (hydrostratigraphic unit 4), capped by hydrostratigraphic group II (*Keuper* aquitard) is discontinuous and blocked by HSG II on its upthrown side in the footwall. These are potential sites for petroleum entrapment and accumulation 1).

Downthrown *Lettenkohle* on the hanging wall side is connected to HSU 3, and forms with the *Muschelkalk* and *Buntsandstein* aquifer a continuous hydrostratigraphic group I. Groundwater will flow across the principal faults when the *Lettenkohle* aquifer is juxtaposed with hydrostratigraphic units 4 and 3. Flow along a fault plane on the hanging wall side might occur when flow is blocked by hydrostratigraphic group II.

(3) The *Zone Dolomitique* aquifer (hydrostratigraphic unit 8) is disconnected by the principal faults. Groundwater flow is blocked by hydrostratigraphic group II or hydrostratigraphic unit 9, and thuspossible sites of petroleum entrapment are created.

(4) The *Pechelbronner Schichten* are fully connected over the entire Basin.

[1)] Indeed, oil deposits were discovered only in Mesozoic reservoirs (Chapter 2), i.e., hydrostratigraphic units 3 and 4 in the Hoelschloch, Kutzenhausen, Soultz and Hermerswiller Compartments associated with the Pechelbronn, Kutzenhausen and Soultz Faults, where the carrier bed is fully or partly blocked by hydrostratigraphic group II.

4. Observed Hydrogeological Phenomena related to Groundwater Flow

4.1 Introduction

Groundwater moving through its subsurface environment may dissolve, transport and deposit mineral matter, transport heat and modify pore pressures. Where well-defined flow paths are sustained for sufficiently long times these processes may give rise to systematic variations in the chemical and temperature characteristics of groundwater and the rock framework. Gravity-induced regional groundwater flow is an effective mechanism for the chemical and thermal evolution of groundwater. A knowledge of the interrelation between chemical and thermal properties of groundwater, on the one hand, and its flow pattern, on the other, may therefore be used for: (1) evaluating groundwater flow patterns from observed distribution of hydrogeologic phenomena, i.e., water chemistry and temperature; or (2) reconstructing chemical and thermal conditions from known flow patterns of groundwater.

Practical applications of the analysis of gravity-driven groundwater flow and the distribution patterns of hydrogeological phenomena in the Upper Rhine Graben include: evaluating the effect of faults on groundwater flow and its transported matter; and defining fault zones as conduits and/or barriers to fluid movement and migration and accumulation of petroleum. In this chapter I discern the regional and local groundwater flow systems in the Pechelbronn-Soultz Basin and Upper Rhine Graben by the spatial distribution pattern of hydrogeological phenomena. In chapter 5 I will use direct hydrogeological methods, e.g., hydraulic heads, pressure-depths and pressure-elevation charts to analyze the groundwater flow distributions in the basin.

4.2 Analysis of the Hydrochemical Regime

4.2.1 Theoretical Considerations

The initial chemical composition of groundwater is a function of the lithology of the rock containing it. Beyond this, numerous factors may then control the chemical character of formation water These include:

- Climate;
- Temperature;
- Pressure;
- Contact area;
- Mobility of elements;
- Residence time;
- Saturation of soluble salts; and
- Prior water chemistry.

The major-ion chemistry of groundwater is primarily controlled by the time and distance the groundwater travelled in the flow system. This view holds that, as groundwater moves along its flow path and increases in age, the anions evolve in relative abundance through the sequence:

$$HCO_3^- \Rightarrow HCO_3^- + SO_4^{--} \Rightarrow SO_4^{--} + HCO_3^- \Rightarrow SO_4^{--} + Cl^- \Rightarrow Cl^-$$

This concept, which is exemplified in the works of Chebotarev (1955) and Schoeller (1962), gives little attention to the specific mineral phases with which the water comes in contact or to the order of encounter of minerals along the groundwater flow path.

The changes in water chemistry and characteer is also be related to the hydraulic regimes and the type of flow systems (Tables 19; Tóth, 1984):

In general, the changes in total dissoved solids and cation or anion concentrations may be associated with the direction of groundwater flow:

TDS	increase; mineral dissolution
$SO_4 \div Cl$	decrease; SO_4 reduction and higher solubility of Cl
$SO_4 \div HCO_3$	increase; depletion of CO_2
$Ca \div Na$	decrease; Ca - Na exchange, no Ca added due to CO_2 depletion
$Ca \div Mg$	decrease; Mg-salts more soluble than Ca-salts, no Ca added
$^3H \div TDS$	decrease; Tritium concentration decreases with flow direction (longer residence time, older waters), TDS increases with flow direction
$^{14}C \div TDS$	decrease, ^{14}C activity decreases and TDS increases with flow direction

The chemical composition of groundwater is primarily controlled by the time and distance travelled within a flow system. Therefore, variability in the water chemistry is also a function of the type of flow system. Thus, in a local flow system of short flow paths, variable flow rates and directions, short water residence time, low pressures and temperatures, it would be expected that low TDS and Ca-Mg-HCO_3 water types would predominate.

In intermediate flow systems the water salinity tend to increase slightly with flow direction, and the dominant species will be Na, Mg, SO_4, Cl; mixing with fresher water from local systems or with saline waters from deeper regional flow systems can also occur.

In regional flow systems the residence time of groundwater is higher and the flow path is longer. Na-Mg-Cl type groundwaters with a high TDS will dominate in regional flow systems.

4.2.2 Database

Formation waters have been sampled from near-surface at 16 m depth to very deep, water-bearing formations at 2500 m depths. The hydrochemical database consists of two basic sets: (1) hydrochemical data of formation waters taken from oil wells by the petroleum companies SAEM and PREPA (Appendixes 8 and 9), which were made available by SGAL in Strasbourg; and (2) hydrochemical data of waters taken in the field during the years 1985-1987 from water wells, dug wells, thermal wells, abandoned oil wells and springs (Appendix 10). These water samples were analysed by the Federal Institute for Geosciences and Natural Resources (BGR) laboratories in Hannover, Germany.

The SAEM and PREPA water analyses date back to the years 1931-1956. The analytical data are, with a few exceptions, incomplete. Thus, the PREPA analyses report only sodium, chloride concentrations and densities, while most of the SAEM analyses yield density values only . A quality control on the analyses was rarely possible.

Ninetyfive SAEM well reports give concentration values (mg/l) for all major anions. (Cl, SO_4, HCO_3), but only for Ca, Mg and Fe cations. In these reports, Na+K concentrations were determined by calculating the difference in the ionic balance, although this practice does not give accurate values.

It was noted, that for repeated water sampling in the same oil well, large discrepancies occurred in the analysed chemical composition and mineralization of the waters. These fluctuations are mostly attributed to borehole contamination, due to drilling mud and to sampling "old" unpumped waters standing in the wells over a long time period. High pH values (>10) are indicative of mud contamination.

The following list summarizes the stratigraphic distribution of complete oilfield water analyses available to the study areas:

Basement: Two analyses taken from well 4616 (possibly contaminated) and geothermal well GPK (Appendix 10).

Permian: PREPA oil well (Obermodern-1) in the Zaberner Fracture Zone (Appendix 9)

Triassic: Twenty-two SAEM analyses which are, to a greater part, from the Kutzenhausen-Soultz region; water samples were taken mostly from the *Lettenkohle* and Upper *Muschelkalk* between 800 to 1000 m depth, with 3 samples from the *Buntsandstein*. From the Ohlungen Basin 3 samples were taken. The deepest water sample was taken from the Upper *Muschelkalk* (2085 m) in a PREPA oil well, Niederlauterbach in the Rhine Valley. Three water samples originate from the Grés à Roseaux at Pechelbronn and Soultz.

Jurassic: Of 24 analyses, 10 were from samples taken from the Ohlungen Oilfield. From Haguenau two PREPA samples were analysed.

Eocene: Twenty-seven water samples were taken from the *Zone Dolomitique* at locations distributed over the entire Pechelbronn-Soultz Basin. Three water samples were taken from the *Couches Rouges*.

Oligocene: About 30 SAEM complete water analyses present finding on samples from the *Pechelbronner Schichten* in the Pechelbronn-Soultz Basin. Five PREPA analyses are available from the Rhine Valley. Forty-five near-surface water samples came from the SAEM wells Lobsann 3583, Kutzenhausen 3584 and 3592 as well as Preuschdorf 3643 in the *Pechelbronner Schichten*.

Série Grise water samples were taken in well Dieffenbach 4655 at 26 m depth in the Pechelbronn-Soultz Basin. Samples also came from the Rhine Valley in well Roeschwoog 4749 and PREPA well Niederlauterbach F-2.

In the Pechelbronn-Soultz Basin about 50 wells and springs were sampled and analyzed over the years 1985 - 1987. Thirty water samples were also analyzed for trace elements (Appendix 10). For the Baden-Württemberg side, east of the Rhine River, water analyses of 17 shallow wells were used (Geological Survey, Baden-Württemberg; Appendix 11). Maps (Figures 71, 72 and 82) and profiles B-B' and I to VI (Figures 72 to 79) show the well locations and salinity values for HSU 3, 8 and 10.

4.2.3 Hydrochemistry and Classification

4.2.3.1 Hydrochemical Overview

The dominant water types in the Rhine Graben study area are: Ca-Mg-HCO_3 and Na-Ca-Cl or Na-Cl groundwaters (Figures 14 and 15). Fresh and shallow groundwater in the Pliocene and Quaternary of the Rhine Graben, and groundwater present in aquifers of the Vosges, Hochwald and Black Forest are of a Ca-HCO3 and Ca-Mg-HCO3 water type (cluster A, Figures 14 and type curve A, Figure 15).

Cluster B (including groups I, II, III) and type-curve B (Figures 14 and 15) represent Triassic and Tertiary oilfield waters and thermal formation waters of a Na-Ca-Cl (I) and Na-Cl (II) water type in the Pechelbronn-Soultz Basin. These highly mineralized groundwaters are distinctive for basinal and regional flow systems. We can differentiate thermal waters from the Triassic formation waters at Kutzenhausen and Soultz by their lower degree of mineralization (black triangles in cluster B-I, Figure 14). Geothermal well GPK which reached the granitic basement in the Soultz Horst produced highly saline, hot waters similar in chemical composition to formation waters present in the overlying Triassic hydrostratigraphic units (Figure 76 profile B-B'). Water with lower salinity produced from shallow wells (10 m depths, e.g., wells RG-1, Mattenmühle; see Figure 82 for well locations; Appendix 10), can be separated as a sub-group (B-III) in Figure 14 and the waters are identified by a type-curve B (Figure 15) as having distinctively lower sulfate and higher bicarbonate content. These shallow formation waters are characteristically associated with oilfield waters and with type-B waters of the regional flow system. Discharging groundwaters ascend preferentially along fault and fracture zones to shallower depths.

The lower salinity Ca-Mg-HCO_3 groundwaters of local flow systems mix with saline Na-Cl groundwater of a regional flow system, e.g. group B-III, in comparison to waters from well 4275 (Figure 14, Appendix 10). The SAEM well 4275 produced Na-Ca-HCO_3 groundwater from 120 m depth in the *Pechelbronner Schichten* in the Hoelschloch Compartment (Figures 75 profile IIIa and 82), while the 10 m deep wells of group B-III located in the intensively faulted and fractured Soultz-Hermerswiller Compartment (Figures 76 profile B-B', 77 profile IV and 82) show Na-Ca-HCO_3-Cl waters with oil traces. Obviously, the chemical composition of shallow formation waters in group B-III is controlled by discharging brines ascending to the surface along fault and fracture zones while formation waters in well 4275 are mixed with recharge waters from a local topographic high.

The phenomenon of increasing water mineralization in the direction of formation water flow is well demonstrated by the chemistry of formation waters in the study area (Figure 76 profile. B-B'; Otto et al., 1988) as follows: total dissolved solids (TDS) contents exceed 100 000 mg/l in the deeper faulted zones of the Soultz region. This anomaly is the expression of two gradually increasing regional trends, from the marginal zones towards the centre of the graben. Fresh groundwater generated by the local Hochwald flow system discharges into the Tertiary formations west of Pechelbronn. The gradual salinity increase to the east and the rapid increase upwards is concurrent with the regional flow system shown later in Chapters 5 and 6.

4.2.3.2 Formation Water Characteristics

Densities and Total Dissolved Solids

Densities change laterally within a hydrostratigraphic unit and cross-formationally along hydrostratigraphic units. This has implications for the use of equivalent fresh water head in the analysis of groundwater flow patterns of allegedly isodensity flow systems, as I will see later.

Of 720 reported density values (SAEM, PREPA), about 150 density values are referenced to their respective sampled formational horizon. Extrapolated from cross-sections and contour maps, additional density values could be assigned to their respective horizons of sampling. Water densities were measured in the laboratories at room temperatures and do not reflect in-situ densities of formation waters under subsurface temperature and pressure conditions. On a density vs. depth plot a density - depth relationship is not evident (Figure 16). A positive correlation exists between density and total dissolved solids (TDS) for formation waters. Given TDS values and corresponding densities available for formation waters of major hydrostratigraphic units in the basin (SAEM and BGR water analyses; Appendixes 8 and 10) were plotted on a TDS vs. densities diagram (Figure 17) and the equation for a simple regression line was calculated (least square method; Davis, 1973).

Carpenter's (1978) classification scheme was used to group and characterize the salinity (TDS) distribution in the formation waters of the study area. Figure 18 shows the relative frequency for 172 TDS values and their regional location in the study area.

Freshwater: <1000 mg/l TDS

Twenty per cent of the analyzed TDS-population (n = 172) fall within the fresh water category. This group represents waters from the regional recharge regions in the east and west, the local Hochwald recharge area, shallow oil wells at the foot of the Hochwald (Lobsann, SAEM wells 3583, 3584, 3643) and shallow water wells near Soultz and Reimerswiller.

Brackish: 1000 - 10 000 mg/l TDS

Less than 5 % of the formation waters are brackish, and they are dominated by shallow groundwaters with TDS below 5050 mg/l in the Pechelbronn-Soultz Basin. Most oil wells west of the Pechelbronn Fault and north of Pechelbronn at the foot of the Hochwald produced heavy oils and brackish, flowing formation water from the Pechelbronn Schichten.

Saline: 10 000 - 100 000 mg/l TDS

Twenty-seven % of all formation waters were thoseranging between 10 000 to 85 000 mg/l TDS. They were mainly waters from Tertiary carrier beds in the Pechelbronn - Hoelschloch - Kutzenhausen - Soultz region. A further 11 % range between 85 000 and 100 000 mg/l TDS, representing formation waters from deeper Tertiary and Mesozoic carrier horizons in the Pechelbronn - Soultz oil fields.

Brines: > 100 000 mg/l TDS

Eighteen per cent of the formation waters were of the oilfield waters from Triassic formations with TDS values of 100 000 to 115 000 mg/l. They represent and are characteristic of the Soultz-Hermerswiller Compartments. In the same area, formation waters in the *Zone Dolomitique* are are classified as saline and brines.

A further 19 % of formation waters had TDS values > 115 000 mg/l. These were encountered in the deeper Tertiary in the Graben centre (PREPA Niederlauterbach, Soufflenheim, Appendix 9). Mud contamination of the formation water is possible, here.

In summary, a frequency analysis of all available TDS values shows two salinity ranges for the formation waters (Figure 18): (1) fresh - brackish formation waters typify waters from the recharge areas and shallow wells in the basin; and (2) formation waters related to oil fields in the Pechelbronn-Soultz Basin are saline and brines, with a salinity maximum in the Soultz Compartment. The average salinity (TDS ±90 000 mg/l, n=94) of the oilfield associated formation waters is about 2.5 times that of seawater (TDS 35 100 mg/l, after (Culkin, 1965), implying a net gain of dissolved salts.

Sodium

Figures 19 a and b show the relative frequency distributions for sodium in the formation waters. The Na+K concentrations in Figure 19a were calculated eitehr from differences in the ionic balances or from NaCl concentration data given for SAEM oilfield water analyses (Appendix 8). The dominant sodium concentration of the oilfield waters lies between 10 000 and 31 000 mg/l. A maximum at 31 % iss found in Triassic formation waters in the Soultz-Hermerswiller Compartments. Formation waters with sodium concentrations of 16 000 to 21 000 mg/l are mainly from Tertiary horizons in the Pechelbronn - Soultz region. Concentrations higher than 50 000 mg/l (PREPA data, Appendix 9) are encountered in Tertiary sediments in the graben centre.

Figure 19b shows sodium concentrations for 92 groundwater analyses taken in the field during the years 1984 -1987 (BGR and GL-BW data, Appendixes 10 and 11). High sodium concentrations were measured in water samples taken at shallow depths in the Soultz region and at geothermal wells Morsbronn and Helion.

Figure 20 is a log-log dilution diagram of sodium vs. chloride concentration for formation waters in recharge areas and the basin. The straight line is the dilution - evaporite curve indicating an enrichment of sodium until halite precipitates at about 140 000 mg/l (seawater contains about 19 000 mg/l of sodium). This line is also referred to as the conservative mixing line (Hanor, 1987; Howard et al., 1983). The plotted data points (Figure 20) follow the trend of the conservative mixing line indicating that diagenetic processes, such as ion exchange or membrane-filtration reactions involving clays and/or carbonates, were not operating to deplete the sodium concentration in the formation waters.

Concentrations of sodium and salinity of formation waters increase, in general, from the recharge regions towards the Pechelbronn-Soultz Basin with highest concentrations being encountered in the Kutzenhausen-Soultz region. From the dilution diagram (Figure 20) it can be deduced that subsurface brines originated from the lower end members on the conservative mixing line, i.e., from recharging, meteoric fresh groundwaters.

The concentration mechanism for sodium and chloride is, probably, governed by mineral dissolution of regional groundwater flow from the recharge area towards the basin.

In none of the analyses used in this study did sodium concentrations reach values as high as 140 000 mg/l, the point at which halite precipitates out of solution, although concentrations of over 100 000 mg/l have been measured for brines in the *Zone Dolomitique* at the Soultz Compartment. Nonetheless, it is interesting to note here that thin halite seams and salt impregnated but now water-dry marls have been observed in the *Zone Dolomitique* and *Pechelbronner Schichten* in the mining galleries and in cores (SAEM well 2270, Reimerswiller). Haas and Hoffmann (1933), two local geologists formerly working for SAEM, attributed the occurrence of salts in the Tertiary formation to salt precipitations from subsurface brines flowing along the Tertiary formations. In a recent study Hardie (1990) hypothesized that the thick halite and salt deposits of the Southern Rhine Graben near Mulhouse, 90 km south of Strasbourg, originated from deep circulating hydrothermal brines, rich in Na, K and Ca.

Potassium

Many of the available SAEM chemical analyses of water do not include potassium determination moreover the accuracies of the few SAEM reported values for potassium concentrations appear to be questionable.

On a potassium vs. chloride dilution diagram (Figure 21) the formation waters seem to be enriched in potassium with respect to the normal evaporite curve as is typically observed for oilfield waters (Collins, 1975). Near-surface groundwaters in recharge areas as well as thermal and oilfield waters lie above and parallel to the conservative mixing/evaporite line. It should be noted here, that the plotted potassium values for oilfield and thermal waters which show a linear relationship with chloride, are from the same Triassic sandstone and carbonate hydrostratigraphic group I. No potassium concentration values for Tertiary formation waters were available.

Calcium

In the study area the *Muschelkalk*, *Keuper*, Jurassic, Eocene and Oligocene formations accommodate calcium minerals (Chapter 2.3.1).

Changes in pH of waters containing calcium bicarbonate will cause calcium bicarbonate to precipitate. The solubility increases with salinity and higher P_{CO_2}, but decreases with pH, calcium content and temperature. Solubility of calcium sulfate decreases with temperature. Seawater contains 400 mg/l and subsurface brines, generally, contain 2000-3000 mg/l of calcium. Many authors have observed an increase in calcium and a decrease in magnesium in individual saline formation waters relative to present day seawater, and they attributed this effect to the role played by flowing groundwater in dolomitizing adjacent limestones. Alternative or additional processes may be found in the exchange of cations on clays and ion-exchange reactions whereby sodium-rich waters tend to dissolve calcium from rocks. These processes require considerable water-rock contact time.

Therefore, quasi-stagnant flow conditions promote the existence of high calcium chloride contents in formation waters and are considered to give a hydrodynamic environment favorable for the entrapment and accumulation of petroleum.

Figures 22 a,b show the relative frequency distribution of calcium for the SAEM and BGR data sets (Appendixes 8 and 10). Values <100 mg/l Ca (Figure 22a) represent calcium concentrations in groundwaters from the silicious *Buntsandstein* formation in recharge regions. Thermal wells Morsbronn and Helion have Ca-concentrations of about 1400 -1500 mg/l. Seventy-three per cent of all analysed oilfield waters (Figure 22b) in the study area show Ca-concentrations of more than 3000 mg/l. Lower concentrations represent samples from the Lower Oligocene formations taken at shallow depth between 80 - 370 m. Water samples taken in the Pechelbronn fields from deeper horizons in the *Pechelbronner Schichten*, *Zone Dolomitique*, Jurassic and Triassic have Ca-concentrations between 2000 - 6000 mg/l. Higher concentrations prevail in older and deeper formations. A Ca-concentration maximum is observed for formation waters in the Soultz fields (Figure 26b).

On a calcium vs. chloride diagram (Figure 23), nearly all formation waters are enriched in calcium and show a good correlation between Ca-content and Cl-concentration. Ca-concentrations increase with salinity. This is in agreement with the observations of Collins (1975) for other petroliferous basins in the United States.

Magnesium

Magnesium is dissolved during chemical weathering, mainly as chloride and sulfate. Groundwater associated with igneous rocks or siliceous sandstones may contain less than 5 mg/l of magnesium, whereas those associated with dolomite or limestone may contain over 20 000 mg/l of magnesium (Collins, 1975). In the study area the *Muschelkalk*, *Lettenkohle* and *Zone Dolomitique* hold Ca-Mg carbonates.

The 179 Mg-values in the frequency distribution diagrams (Figures 24a,b) range between 10 - 3300 mg/l. Two thirds of SAEM Mg-data (Appendix 8) are approximate values only, hence this information should be interpreted with caution. Nonetheless, newer water analyses conducted by BGR confirm the trend towards depletion of magnesium in geothermal waters and oilfield brines (Figure 24b).

Plotted on a Mg vs. Cl diagram, oilfield and geothermal waters for the study area (SAEM data points and some BGR data) are depleted in magnesium in comparison to the dilution - evaporite line of seawater (Figure 25). Many oilfield brines are depleted in magnesium (Collins, 1975). Groundwaters of lower salinities, mainly sampled at shallower depth and in recharge regions, are enriched or normal in Mg-content.

Chloride

Petroleum-associated formation waters usually contain relatively high concentrations of chloride; in some brines the content may be 200 000 mg/l or more. Seawater contains about 19 000 mg/l of chloride (Collins, 1975). Schoeller's (1955) scheme for classifying oilfield waters was applied to categorize the chloride content of formation waters in the study area (Appendix 12).

The classification scheme is as follows:

normal (N):	< 10 meq/l, (< 350 mg/l) Cl
low (L):	10 - 40 meq/l, (< 350 - 1400 mg/l) Cl
average (A):	40 - 140 meq/l, (1400 - 5000 mg/l) Cl
high (H):	140 -420 meq/l, (5000 - 15 000 mg/l) Cl
marine (M):	420 -700 meq/l, (15 000 - 25 000 mg/l) Cl
very high (VH):	> 700 meq/l, (> 25 000 mg/l) Cl

According to the Schoeller classification, all formation waters associated with oil fields in the Pechelbronn, Kutzenhausen, Soultz regions are very high in chloride content. This is also shown on the frequency distribution histograms (Figures 26 a,b). The highest peak in Figure 26a represents formation waters from the *Lettenkohle* and Triassic in the Soultz Horst. Waters with marine (M) chloridization are encountered mainly in Tertiary petroleum-bearing horizons. Lower chloride contents are found in Lower Oligocene beds at shallower depths and near the Hochwald recharge area. Here an influx of fresher groundwater from the Hochwald flow system can be expected. Figure 26b shows very low chloride concentrations for groundwaters in the recharge areas and average and high chloride content for samples from shallow oil and geothermal wells.

Sulfate

Potential sulfate sources in the study area are the anhydrite layers in the *Zone Dolomitique*, the anhydrite nodules in the *Couches Rouges* and the gypsum layers in the Upper *Pechelbronner Schichten*.

Relative frequency histograms (Figures 27a,b) show the distributions of sulfate concentration for 198 water samples taken in recharge regions and the Pechelbronn-Soultz Basin. The sulfate content ranges between 1 - 4000 mg/l.

For 89 % of the oilfield waters in the study area, the SO_4/Cl ratio is between 0.0004 and 0.102, indicating sulfate reduction (the SO_4/Cl ratio for seawater is 0.103). Relative to the dilution line for seawater (Figure 28) on a SO_4 - Cl diagram, the SAEM data points representing oilfield waters indicate depletion in sulfate. Sulfate depletion in oilfield brines is a common occurrence in petroliferous basins (Collins, 1975; Krecji-Graf, 1978). Low sulfate concentrations are caused mainly by anaerobic bacterial sulfate reduction (Matthess, 1982), in which bacteria use the oxygen in SO_4^{-2} to oxidize organic matter to CO_2, producing sulfide species as a by-product (e.g. H_2S). If any reactive iron compounds are present, the sulfide species will react with them to form solid sulfides. This phenomenon was observed for the flowing thermal well, Helion, at Pechelbronn (see Figure 82 for location). Thus, the absence or depletion of sulfate in any particular formation water can indicate a reducing subsurface environment and possibly the presence of petroleum (indirect indicator).

Based on Schoeller's (1955) classification scheme the formation water's sulfate content can be divide into the following groups:

normal (N)	< 6 meq/l, (ca. 300 mg/l) SO_4
average (A)	6 -24 meq/l, (ca. 300 - 1150 mg/l) SO_4
high (H)	24 - 58 meq/l, (ca. 1150 - 2800 mg/l) SO_4
very high (VH)	> 58 meq/l, (> 2800 mg/l) SO_4

About two thirds of the formation waters fall into the N -group. Figure 27a shows that the majority of all oilfield waters have a normal SO_4 - content. These waters are characteristic of the *Pechelbronner Schichten* near Pechelbronn and the Triassic in the Soultz region. Formation waters with an average sulfate content (10 %) are mostly encountered in the Tertiary and Jurassic formations. Higher sulfate contents are found in the Lower *Pechelbronner Schichten*, *Zone Dolomitique* and Jurassic. Very high concentrations were found in formation waters from the Upper *Pechelbronner Schichten* at Ohlungen and Surbourg. Figure 27b shows the distribution of normal sulfate concentrations for recharging waters and average contents for thermal waters. Generally, groundwaters in the Tertiary and Jurassic formations have a higher sulfate content than in the *Lettenkohle*, *Muschelkalk* and *Buntsandstein*.

Hydrogen carbonate and carbonate

Data from SAEM water analyses do not always distinguish clearly between HCO_3, CO_3 and CO_2 concentrations. A frequency distribution analysis of the data allows only a tentative and a cautious interpretation. The same applies to Figure 34, which shows no relationship between $HCO_3 + CO_3$ and Cl concentrations.

Oilfield waters can have concentrations between 0 - 2200 mg/l of HCO_3 (Collins, 1975). Krejci-Graf (1978) lists CO_3 concentrations between 617 - 2670 mg/l for formation waters in the Vienna petroliferous basin.

The $HCO_3 + CO_3$ concentration range for SAEM oilfield waters (Figures 29a, 30) is wide spread. Concentrations of up to 300 mg/l are characteristic for Tertiary formation waters, whereas formation water in Triassic aquifers can yield concentrations of up to 600 mg/l of $HCO_3 + CO_3$.

Figure 29b shows the relative distribution for all BGR carbonate data. Recharge groundwaters from silicious sandstone formations (*Buntsandstein*) have concentrations between 15 - 100 mg/l. The $HCO_3 + CO_3$ content of waters in the Tertiary formations and thermal waters from the *Buntsandstein* and *Muschelkalk* ranges between 200 - 450 mg/l.

4.2.3.3 Schoeller Classification

Due to incomplete water analyses by SAEM, missing data on potassium concentrations, estimated values only for magnesium contents and deficient carbonate determinations, a Sulin (Ostroff, 1967) formation water classification was not viable. However, a few SAEM water analyses of oilfield brines and BGR chemical analyses of formation waters (Appendixes 8 and 10) made a Schoeller formation water classification based on anion concentrations (Cl, SO_4, HCO_3+CO_3) and calcium concentrations feasible (Table 20 and Appendix 12).

Table 20 shows the generalized Schoeller classification for recharge waters (top), thermal, shallow and deep formation waters in the Pechelbronn-Soultz Basin (bottom). Schoeller's classification used the chloride concentration to separate the waters into six types (see Chapter 4.2.3, Chloride). The chloride content increases from the Vosges mountains to the Pechelbronn-Soultz Basin from normal to average to very high. Thermal wells, Romaine, Morsbronn and Helion produce average and high chloridized waters. Shallow oil wells have a lower chloride content than deep oil wells.

Using Schoeller's classification for the sulfate concentration of the formation waters in the study was not meaningful since most of the waters fell into the lowest of the four groups, namely, "normal", with a sulfate content of less than 300 mg/l.

For none of the water samples does the $\sqrt{SO_4^{-2} \times Ca^{+2}}$ value exceed 70, indicating that these waters are not saturated with calcium sulfate. Again, the $\sqrt{SO_4^{-2} \times Ca^{+2}}$ value is lowest for fresh groundwaters in the Vosges, Hochwald and shallow wells in the Pechelbronn-Soultz Basin. Petroleum-associated formation waters have distinctively higher values (Table 20). With increasing salinity, the calcium content increases and sulfate reduction is commonly observed. Shallow oil wells show lower $\sqrt{SO_4^{-2} \times Ca^{+2}}$ values which are comparable to values for meteoric waters in the recharge regions.

The $\sqrt[3]{(HCO_3^{-} + CO_3^{-2}) \times Ca^{+2}}$ was used by Schoeller to determine if a water was saturated with calcium carbonate, with a value greater than 7 indicating saturation. This formula is not entirely accurate, but it does indicate if the water contains an excess of calcium, a situation which decreases the carbonate content. All oilfield and thermal waters have values to near or greater than 7 (Table 20; see also Chapter 4.2.3, calcium).

The index of base exchange (IBE) indicates the extent to which of metal ions dissolved in groundwater are exchanged with metal ions on clays. Schoeller assumed that the concentrations of sodium and chloride originally present in groundwater were equal. The IBE is a ratio (Cl-Na/Cl) which has a positive or a negative value according to whether the exchange is of alkali metal ions in groundwater exchanging alkaline earth ions from clays or vice versa. In the former case the ratio (Cl-Na/Cl) is positive, when sodium and potassium in groundwater are exchanging alkaline earth ions from clays. According to Schoeller (1955, p. 823) connate water has an IBE > 0.129 and a Cl/Na ratio > 1.17. Meteoric formation waters will have an IBE < + 0.129 and a Cl/Na ratio <1.17. In general, a positive IBE value is found for oilfield waters.

For the study area a positive IBE (>0.129) is found for formation waters of a high chloride content. Conversely, those of a low salinity can have a negative base exchange value; they correspond to meteoric groundwaters of a sulfate-sodium and bicarbonate-sodium type water. The high IBE values do not imply, however, that the deep and highly chloridized formation waters are of a connate origin as Schoeller's general rule would suggest. Stable isotope analyses (Chapter 4.2.4.1) of oilfield associated formation waters reveal a meteoric origin.

Water samples from the Vosges and Hochwald recharge areas show $\sqrt{SO_4^{-2} \text{ x } Ca^{+2}}$ and $\sqrt[3]{(HCO_3^- + CO_3^{-2}) \text{ x } Ca^{+2}}$ values of less than one. The IBE number is near zero or negative. Lower values are also observed for waters from shallow oil wells (3262, 4275, RG-1) where an influx of fresh groundwater can be expected, possibly along fault zones by local flow systems mixing with saline groundwaters of a deeper flow system.

Using Schoeller 's classification scheme it is possible to differentiate between and recognize formation waters associated with petroleum reservoirs and thermal waters from near-surface waters in the basin and groundwaters in recharge regions. The IBE values and Cl/Na ratios for oilfield waters as well as for highly mineralized thermal waters, e.g., wells Romaine, Morsbronn and Helion, are distinctively higher. A discrimination between oilfield brine from individual hydrostratigraphic units, e.g. Basement, *Buntsandstein*, *Muschelkalk* and Tertiary is not possible, since the Schoeller classification tends to lump highly salinized formation waters together; a Sulin classification would have been more informative.

4.2.3.4 Trace Elements

The trace element content was determined for recently sampled waters from the Hochwald and Pechelbronn-Soultz Basin and by BGR laboratories (Tables 31). The analyzed water samples represent formation waters from the Hochwald recharge area, from shallow water and oil wells as well as from deep thermal and oilfield wells.

Lithium

Lithium, one of the less abundant elements in groundwater, stays principally in solution after its release by weathering of mostly crystalline rocks. Collins (1975) notes that oilfield formation waters usually contain less than 10 mg/l of lithium but that anomalously high lithium concentrations are not uncommon. High lithium concentrations are also observed for thermal waters in active basins and for formation waters in crystalline complexes (Matthess, 1982; Pekdeger et al., 1987). Elevated lithium concentrations in formation waters are thought to originate from an influx of continental, lithium-rich solutions circulating in crystalline formations. Edmunds et al.(1985) interprets a high lithium content as an indication of groundwater solution reactions with micas in crystalline rocks.

From the Hochwald area to geothermal well GPK (see profile B-B', Figure 76) in the Hermerswiller Compartment and geothermal well Bruchsal-1a at the foot of the Black Forest north of Karlsruhe (Figure 70), the lithium concentration increases linearly with salinity. This means that the formation waters in the area are lithium enriched relative to the dilution of sea water (Figure 31). Assuming that the source of lithium is mainly from crystalline rocks, it can proposed: (1) that the granitic basement of the Rhine Graben study area holds lithium-bearing minerals; (2) that basinal groundwaters are flowing through the granitic basement and dissolve these minerals; and (3) that lithium-rich groundwaters reach shallower aquifers. The Vosges, Hochwald and the Black Forest as well as the Pechelbronn-Soultz Basin are underlain by the granitic rift basement. Weathered and fractured in the basement's top 300 m and dissected by principal fault systems most likely extending from the Phanerozoic sediment cover into the basement, the crystalline basement has a hydraulic conductivity and continuity in which groundwater flow can be expected to occur (see Chapters 2.3.1.1, 2.3.2, 3.5.1.1). It seems therefore defensible to assume that in the area being studied basinal groundwater flow has dissolved lithium-bearing minerals and entered the upper aquifer systems cross-formationally, enhanced and deflected by flow-conductive fault zones. From Figure 35 it can be deduced that formation waters in the HSU 2 (GPK-1) and Triassic Aquifers (HSU 3; wells Helion and Morsbronn) are enriched in lithium, but also that shallow oil wells show the same phenomenon. Of special interest is the 10 m deep well RG-1 which was drilled as a reconnaissance well for the GPK-1 geothermal well at the same site near the Kutzenhausen Fault in the Hermerswiller Compartment. The lithium content and salinity are both high (Figure 35). From the piper diagram described previously (Figure 14) it was concluded that a mixing of fresh, shallow type A water and saline, deep type B water had occurred. The high lithium content confirms that deep basinal formation waters ascend along the Kutzenhausen and Soultz Fault to the near-surface formations and that a hydraulic communication between the basement aquifer and upper aquifer systems exists.

Strontium

Strontium is an element common in igneous and carbonate rocks. Dissolved strontium results from water leaching of rocks, and it has been postulated that strontium in oilfield waters may also be a by-product of the organic decay processes which produce petroleum. Sea water contains about 8 mg/l of strontium, but subsurface brines contain up to 3500 mg/l (Collins, 1975).

The strontium content of the formation waters in the study area increases with salinity and the waters are enriched relative to the sea water dilution line (Figure 32). No difference is apparent between samples from carbonate and sandstone hydrostratigraphic units, i.e., wells Morsbronn 3a, 3b, Helion and GPK.

Bromide

The concentration of bromide in sea water is 65 mg/l, and subsurface petroleum-associated brines contain from less than 50 mg/l to more than 6000 mg/l of bromide (Rittenhouse, 1967; Collins, 1975; Krejci-Graf, 1978). The concentration of bromide in a chloride brine can increase as a result of evaporation, even after the solution reaches saturation with respect to sodium chloride.

Although bromide is considered relatively inert, the concentration factor observed in subsurface oilfield brines indicates some transferral to the groundwater, presumably from organic matter. As is known, bromide is, like iodide, a biophile element which is released into pore waters during the decomposition of organic matter.

The formation waters in the Pechelbronn-Soultz Basin carry on average 129 mg/l of bromide (0 - 672 mg/l, after Schnaebele, 1948, Figure 33). More recent data show that the bromide concentration (Appendix 13) for groundwater in the Hochwald (background values) are less than 0.1 mg/l. In analyses of the formation waters being studied it has been found that above a salinity of approximately 50 mg/l the bromide concentration increases linearly with salinity and bromide is slightly enriched relative to the sea water dilution line (Figure 33). Similar observations were made in Northern Switzerland (Edmunds et al., 1985). The bromide content of the Pechelbronn-Soultz oilfield waters when chloride > 100 mg/l shows an increase by a factor of 2-3 relative to the dilution line. Shallow wells in the Pechelbronn field as well as in the Kutzenhausen-Soultz field (well 4275, RG-1) produced formation waters with elevated bromide concentrations.

The source of bromide in the formation waters remains speculative; dissolution of halite minerals, which are randomly distributed in the Oligocene sediments, can not be ruled out.

Iodide

Iodine is a biophile element. It is released into the pore waters during decomposition and maturation of organic matter. Sea water contains about 0.05 mg/l and most petroleum-associated brines contain less than 10 mg/l of iodide, however, concentrations as high as 1400 mg/l of iodide in oilfield waters have been found (Krejci-Graf, 1978).

The formation waters in the Pechelbronn-Soultz Basin contain on average 4 mg/l of iodide (0 - 42 mg/l, n = 354, after Schnaebele, 1948). Analyses show that the iodide content for normal chloridized water samples from the Hochwald region range is below the analytical detection limit of 0.05 mg/l (Appendix 13; Figure 34). Groundwater with a chloride content > 100 mg/l holds iodide concentrations which plot above the sea water dilution line (Figure 38). From this figure no clear correlation between salinity and iodide content is apparent. Formation waters which were sampled from shallow and deep oil wells in the Pechelbronn-Soultz Basin (wells 3262, 3969, 4275, RG-1) contain more iodide than do groundwaters from geothermal wells in the *Muschelkalk* and *Buntsandstein* (wells Morsbronn and Helion) which are not associated with oil deposits.

A high iodide concentration is also associated with a high NH_4 content in oilfield waters (Table 21). Ammonia, NH_3, forms during the anaerobic decay of organic nitrogeneous material and this is then transformed to ammonium in oilfield associated waters. Thus, NH_4-enriched waters confirm the organic source of iodide and the presence of organic matter. It is an indirect indicator for possible petroleum deposits.

In the Pechelbronn-Soultz Basin the high iodide concentrations in groundwaters reveal the presence of organic matter and are thus an indication of possible hydrocarbon accumulations. The high iodide content of formation waters taken at shallow depth in the Soultz area is a good example of this phenomenon.

4.2.4 Isotopic Composition of Formation Waters

On the premise that groundwater flow in the Upper Rhine Graben is gravity-driven and topography-controlled it was postulated that the discharging waters in the Pechelbronn-Soultz Basin are meteoric in origin and that the major topographic highs flanking the basin to the west and the east, the Vosges, Hochwald and Black Forest, function as the main recharge regions. Therefore, it was decided to analyze the stable isotopic composition (^{2}H, ^{18}O and ^{13}C) of and date (^{3}H and ^{14}C) the formation waters in the Pechelbronn-Soultz Basin and in the western and eastern groundwater recharge regions.

Database

All available isotope data for the study area are listed in Appendix 14 which is arranged according to structure zones (see Chapter 2.3.2.1) from the western regions to the Rhine

Valley and Black Forest recharge area. BGR laboratories analyzed a total of 35 water samples for their stable isotope and tritium content, and in 16 samples the carbon-14 content was determined.

Samples were taken in the Vosges mountains, in the Hochwald as well as near the principal Vosges- and Rhine Graben-Faults (Figures, 82 and 84). In the Pechelbronn-Soultz Basin the following wells were sampled for isotope analysis:

wells Morsbronn 3a, 3b, and Helion in the *Lettenkohle -Muschelkalk -Buntsandstein* ; SAEM wells 3262, 3969 in the *Zone Dolomitique* and well 4275 in the Upper *Pechelbronner Schichten;* injection well Mar-101 near the Hochwald; shallow wells RG-1 and Mattenmühle with oil traces in the Soultz Compartment ; shallow wells Schreiner and Aloxan in the Quaternary near Soultz and Betschdorf; SAEM well 4616 in the *Lettenkohle-* to basement (reopened by BRGM) and geothermal well GPK-1 (granite) near Soultz (Vuataz, 1988).

The standard deviations for $\delta^{18}O$, δD, $\delta\ ^{13}C$ and the calculated conventional ^{14}C ages are given in Appendix 14.

For the Black Forest region published isotopic data by (Friedrichsen, 1981) and Matthess (1986) were used.

4.2.4.1 Stable Oxygen and Hydrogen Isotopes

Fundamentals

The stable isotopes oxygen-18 (^{18}O) and deuterium (D) are useful tools in hydrogeology, for they function as environmental tracers. The isotope content of groundwater is generally fixed at the time of recharge, however, as it is transported to areas of low fluid potentials (i.e., discharge areas), the isotopic composition may be modified. Variations in the isotopic composition of recharge water may be caused by four major factors:

climatic effect:

a gradual decrease of the heavy isotope content when going from lower to higher latitudes, i.e., with decreasing temperature continental effect:

a decrease of ^{18}O and D when going from the coast of a continental land - seasonal variations which are comparable to climatic effects

- altitude effect:

a lowering of the ^{18}O and D contents with increasing altitude

The primary reason for these phenomena is isotope fractionation during evaporation and condensation of water since the $HD^{16}O$ and $H_2{}^{18}O$ have lower vapor pressures than $H_2{}^{16}O$, by fractionation factors of 1.085 and 1.010, respectively, at 20 ^{o}C (Fritz et al., 1980). Water vapor is, therefore, lower by about 80 ^{o}/oo in D, and 10 ^{o}/oo in ^{18}O, than liquid water with which it is in equilibrium.

In theory then, stable isotopes may be utilized within the context of integrated regional flow studies to delineate sources and conditions of groundwater recharge. It may be possible to formulate a model of regional groundwater flow and, in addition, to use the unique stable isotope content of a particular groundwater as a tracer.

Stable isotope concentrations are conventionally expressed in δ (del) units. These units represent relative deviations of the heavy isotope fraction in water (R being equal to the ratio of the moles of heavy components to the moles of normal components) from that of some standard, R_{st}:

$$\delta^{18}O = \frac{R(^{18}O/^{16}O) - R(^{18}O/^{16}O)_{st}}{R(^{18}O/^{16}O)_{st}} \times 1000 \text{ (o/oo)}$$

$$\delta D = \frac{R(D/H) - R(D/H)_{st}}{R(D/H)_{st}} \times 1000 \text{ (o/oo)}$$

The symbol $\delta^{18}O$ refers to oxygen-18 concentration, δ D to deuterium concentration. As was proposed by Craig (1961) the standard mean ocean water (SMOW) is taken as a standard. Since 1976 the Vienna-SMOW is being used; its composition is comparable to sea water ($\delta^{18}O = 0$ ^{o}/oo , $\delta D = 0$ ^{o}/oo). Usually δ values are given in per mil units, i.e., δ ^{o}/oo = δx1000.

The numerical correlation between δ D and $\delta^{18}O$ is commonly given in terms of the meteoric water line; i.e., $\delta D = 8 \times \delta^{18}O + d$, where, typically, d = 10 ^{o}/oo (Craig, 1961). The numerical value of the intercept d is called the deuterium excess parameter (Dansgaard, 1964). The δ value can vary according to local conditions. Friedrichsen (1981) gives, for the eastern part of Upper Rhine Graben and northern Black Forest, a meteoric water line equation of $\delta D = 8 \times \delta^{18}O + 8$.

Deep basin isotope effects

Reactions between groundwater and minerals, dissolved species and gases and liquids with which they come in contact, modify the isotopic composition of water and reactants. Mixing between waters of different origin (meteoric and connate) can also complicate the interpretation of isotope data, in fact all of these processes can cause scatter in the isotopic data.

The main processes that modify the isotope composition of groundwater in deep sedimentary basin are as foolows: isotopic exchange between water and rocks; evaporation and condensation; fractionation due to membrane filtration of groundwater by clay sequences; and isotopic exchange between groundwater and other liquids.

In geothermal areas, changes in the isotope composition of flowing groundwaters occur when they are exposed to rocks, particularly limestones, e.g., the Muschelkalk Aquifer. This exposure results in an oxygen isotope shift towards more positive values, i.e., closer to equilibrium with the rock's isotope composition. The absence of a comparable hydrogen isotope shift in most geothermal systems is believed to be due to the fact that minerals in these systems contain little hydrogen and that the water/rock ratios are very high so that the hydrogen in the minerals is a small fraction of the total hydrogen.

Under less extreme temperature conditions the various mechanisms which affect the isotope composition of groundwaters are possibly a combination of membrane filtration (primarily affecting deuterium), chemical exchange with rocks (affecting ^{18}O) and other reactions with clay minerals. All of these reactions occurring under elevated temperatures and pressures and during extended contact between the groundwater and the aquifer's rocks are known to shift isotope composition towards more enriched values. Usually, these changes are accompanied by mineralization of groundwaters.

The D and ^{18}O isotope exchange between H_2S-H_2O and CO_2-H_2O, respectively, will occur in nature when groundwater comes in contact with H_2S-CO_2 rich natural gases as is common in petroliferous basins. The isotopic exchange between water and hydrogen gas may be important because the fractionation factors are very large (Fritz and Fontes, 1980). Generally, organic hydrogen gas derived from the decay and maturation of organic matter is strongly depleted in deuterium (Kaplan, 1983). Methane gas associated with petroleum deposits can have δD values as low as -250 ‰ (Schoell, 1984).

Results and interpretations

On a δ D vs. $\delta\ ^{18}O$ diagram (Figure 35) the deuterium and oxygen-18 values align parallel to the meteoric water line (MWL) demonstrating the groundwater's meteoric origin. A meteoric water line with an intercept at 10.2 shows a better fit to the data points than the meteoric water line of a deuterium excess value of 8 given by Friedrichsen (1981) for the eastern part of the Rhine Graben. This seems to indicate that the groundwater in the Pechelbronn-Soultz Basin did not recharge in the northern Black Forest. Blavoux et al.(1980) derive for the western Vosges mountains, west of the study area a local meteoric water line with a deuterium excess of 12.5 ‰.

The isotopic composition of the groundwater in the study area can be grouped into 4 clusters (Figure 35):

(I) Triassic thermomineral groundwater near the Rhine Fault (Morsbronn 3a and 3b):

$\delta^{18}O$: -9.6 to -10 ‰
δ D : -67 to -69.9 ‰

In March 1978 the flowing geothermal well Helion at Pechelbronn produced water with an isotope composition of $\delta^{18}O$ -9.6 ‰ and δ D -69.9 ‰ which lies within cluster I. Other isotopic values for Hélion II waters sampled in the years from 1985 to 1987 indicate a heavier isotopic composition and do not plot within cluster I (Figure 35).

(II) Thermal waters of the northern Black Forest near Baden-Baden as given by Friedrichsen (1981), (Appendix 14):

$\delta^{18}O$: -9.3 to -10.1 ‰
δ D : -64.4 to 69.7 ‰

(III) Groundwater from the *Buntsandstein* Aquifer (HSU 3) in the Vosges mountains and in the Hochwald, including waters near the Vosges and Rhine Fault:

$\delta^{18}O$: -8.61 to -9.1 ‰
δ D : -60 to -64 ‰

(IV) Deep and shallow oilfield waters, as well as Plio-Quaternary groundwaters from the Pechelbronn-Soultz Basin:

$\delta^{18}O$: -7.9 to -8.6 ‰

δD : -53 to -63 ‰

The following are outside the range of the four clausters:

Geothermal well GPK-1 drilled by BRGM to the granite at 1817m depth in the Soultz Horst produced very heavy waters : $\delta^{18}O$ -0.3 ‰ and δD -25.3 ‰ (Vuataz et al., 1988).

North of Karlsruhe at the foot of the northern Black Forest two thermal wells, Bruchsal 1a and 2, were drilled into the *Buntsandstein* and Lower Permian, respectively. The waters sampled there are heavy in isotopic composition: $\delta^{18}O$ -3 to -3.1 ‰ and δD -36 to 37 ‰.

In general, oxygen-18 and deuterium values for groundwaters from the recharge areas, the Triassic and Tertiary Aquifers, fall close to the meteoric water line indicating that they are isotopically unaltered meteoric waters. However, it is apparent from the data that the thermal waters, especially those analysed for Morsbronn (cluster I), did not originate from "recent" meteoric waters recharging in the Vosges or Black Forest. Most likely, they were derived from "old" meteoric waters, i.e., older than Holocene (>10 000 m.y.). This conclusion is supported by ^{14}C age determinations. The uncorrected age for the Morsbronn waters is given at about 26 900 ±600 years (see chapter 4.2.4.2). The isotope signatures for the Morsbronn waters and one Helion sample indicate depletion by about 1‰ for ^{18}O and 5.5 ‰ for D in comparison to the recent recharge groundwaters. This can indicate that recharge for the Morsbronn and Helion water samples took place when the Vosges and Black Forest mountains and the graben had climates colder then those of the present day from (climate effect), assuming that the topographic conditions at the time of recharge were similar to those of the present. Very similar results and conclusions are published for the Lower Triassic sandstone aquifer of the Lorraine region to the west of the study area (Blavoux et al., 1982). The last cold period in Western Europe occurred during the Würm glaciation period which lasted from 0.075 Ma B.P. to the beginning of the Holocene (0.01 Ma B.P.; Illies, 1965). During this time the uprising of the graben shoulders which began with the rifting of the graben in the Upper Eocene, continued (Roll, 1979; Chapter 2.2.2) and a similar topographic relief of the Upper Rhine Graben to todays topography can be expected (i.e., steady state groundwater flow conditions).

An isotopic enrichment in D and ^{18}O values which plot in cluster III represents groundwaters from springs and shallow wells in the Vosges and Hochwald region (Figure 84). These waters are interpreted to be modern meteoric waters and are comparable in their isotopic composition to recharge waters and sampled precipitation in the Black Forest

(Friedrichsen, 1981, p. 137). The isotopic composition of groundwater from wells Morsbronn 3a & 3b, Hochwald II and Mitschdorf (Appendix 14, Figure 35) which are located near or penetrated the Rhine Fault (Figure 84) are distinctively different. This implies that: (1) no deep "old" meteoric water is ascending along the Rhine Fault to shallower depths at the foot of the Hochwald Horst; and (2) no younger and isotopically heavier water is able to reach the deep confined Triassic Aquifer at Morsbronn.

Two different flow systems control the groundwater flow direction and the age of groundwater, i.e., through-flow time. A regional deep system, the "Vosges Flow System", governs groundwater flow in hydrostratigraphic group I from the Vosges to wells at Morsbronn. A local shallow system, the "Hochwald Flow System", drives groundwater from the Hochwald to wells Hochwald II and Mitschdorf. The travel time for groundwater in hydrostratigraphic unit 3 (*Buntsandstein -Muschelkalk*) to flow from the Vosges to well Morsbronn at the Rhine Fault (Figures 70 and 84) is much longer, than for groundwater to flow in the same but tectonically uplifted Triassic hydrostratigraphic units from the Hochwald recharge area to the wells Hochwald II and Mitschdorf. Obviously, the saline and warm water at Morsbronn is a remnant of the Vosges recharge waters from Late Pleistocene time, while the same "old" water which recharged in the Hochwald has already been flushed through the aquifer system and has been replaced by modern meteoric waters.

The isotope composition of the shallow and deep formation waters (*Zone Dolomitique*, *Pechelbronner Schichten*, Figure 35, cluster IV) in the Pechelbronn-Soultz Basin indicates that, in comparison to clusters I and II, they are enriched in deuterium and oxygen-18.

In the following the isotopic composition of water samples from wells Mar-101, Helion, GPK-1, Bruchsal 1 and 2 will be discussed:

Well Mar-101: At the end of 1982, TOTAL Exploration installed a tertiary oil recovery pilot plant 3 km north of Helion near Marienbronn at the foot of the Hochwald (Figures 70 and 82; pers. comm. J. Comte, TOTAL Exploration, Paris). Steam was injected into the *Pechelbronner Schichten* at shallow depth to recover the heavy oils (tar sands) from their reservoirs. Tertiary oil deposits near the Hochwald are biodegraded and of high viscosity due to freshwater influx from the Hochwald recharge area. The recovered oil-stained water from the Tertiary formations was, after oil extraction and cleaning, reinjected into the *Buntsandstein* at at a depth of 715 m through well Marienbronn 101 (Mar-101; Figures 82, 79 profile VI and 80 profile VII). Due to serious losses of injection steam in the fractured terrain the project was abandoned at the end of 1984 and the installation dismantled. Well-101 remained uncapped and its groundwater is now flowing uncontrolled into a creek nearby! A water sample was taken at the well head in August 1986. The water was of a greenish translucent color and possibly contaminated by chemical additives (Appendix 10). Nonetheless, the chemical composition is comparable to the waters from Morsbronn and Helion (water type B) but of lower salinity (Figure 36). Isotope analyses were conducted in 1986 and 1987 (Appendix 14). The isotope composition differs significantly from the Morsbronn and Helion waters and the tritium content is 13 T.U. (Figure 35). They plot on an evaporation line which intersects the meteoric water line in cluster III which characterizes modern meteoric groundwaters from Tertiary formations. The injected water originated from Hochwald Flow System.

Well Helion: Thermal well Helion at Pechelbronn (Figures 76 profile B-B' and 82) was completed in 1971. Drilled to the top of the *Buntsandstein* Aquifer (HSU 3) at 1146 m depth, the well is cased to the *Lettenkohle* at 904 m. Artesian flowing saline water with a temperature of about 70 ^{0}C at the well head originates from hydrostratigraphic unit 3. The flow rate can be regulated by valves and manometers at the well head. The mineralized and hot water has been piped to a spa facility since 1978.

Systematic chemical water analyses started in 1978. A first stable isotope analysis was conducted by SGAL-BRGM in March 1978; further consecutive samples and analyses were taken during the field work in the years 1985 to 1987 (Appendix 14). From these analyses it is observed that the isotopic content became increasingly enriched in deuterium and oxygen-18 over the years (Figures 35). The path of enrichment follows from cluster I with the lightest isotope content to cluster III and cluster IV.

The Helion water is of water-type B and identical to the groundwaters from hydrostratigraphic unit 3 at Morsbronn and Soultz (Chapter 4.2.3). From a Schoeller diagram (Figure 36) it is concluded that the character of the Helion waters did not change during the years of sampling. The chloride concentration increased since March 1978 (Figures 37). During a period of reduced flow rate the chloride concentration continued to rise slightly while the well head temperature declined. A lower flow rate gives the hot ascending water more time to cool off from its origin of depth (the hydrostratigraphic unit 3) to the surface. Opening the valves to a flow rate of 18.5 m^3/h in March 1986 produced an increase in temperature and chloride content.

Since the flow rate of well Helion was increased for commercial production after 1978 (Figure 37), the thermomineral water has became isotopically heavier. The gradual change in isotopic composition seems to suggest an influx of modern meteoric water to the well from the Hochwald Flow System. The isotope content of the Hélion samples in June 1987 and May 1987 are similar in concentration to the *Pechelbronner Schichten* and *Zone Dolomitique* waters from wells 4275, 3969 and 3262 (Figures 35, 82 and 76 profile B-

B'). A sample taken in December 1987 (Appendix 14; Figure 35), 1 1/2 years after the flow rate was increased, reached the same δ values as those of a sample taken in March 1985. Both water samples are about 30 000 years old (Pleistocene, Würm glaciation period, see next section). This implies that they are "old" meteoric waters of the same origin as the Morsbronn waters.

Geothermal wells GPK-1 and Bruchsal 1a & 2: Water sample from Well GPK-1 and from the reopened SAEM Well 4616 were analyzed by Vuataz et al. (1988; Appendix 14; Figure 35). The water samples were found to be enriched in deuterium and oxygen-18 which indicates that water/rock isotope exchange reactions due to the high subsurface temperatures at Soultz (133 °C at 1817 m) had taken place. Unusually high tritium values of 29 TU (GPK-1) and 6 T.U.(4616) suggest contamination by younger waters.

The sandstone waters from geothermal wells Bruchsal 1a and 2 north of Karlsruhe and west of the Black Forest border fault are less enriched in deuterium and oxygen-18 (Matthess et al., 1986).

4.2.4.2 Radioactive Isotopes Tritium and Carbon-14

^3H and ^{14}C are used as guides to the age of groundwater and as tracers. The law of radioactive decay describes the rate at which the activity of ^3H and ^{14}C or other radioactive substances decreases with time. This is expressed as:

$$A = A_0 e^{-\lambda t},$$

where A_0 is the radioactive level at some initial time, A the level of radioactivity after time, t, and λ is the decay constant of the isotope. The decay constant or the related half-life time, $T_{1/2}$,

$$\lambda = \frac{\ln 2}{T_{1/2}} = \frac{0.693}{T_{1/2}}$$

characterizes a radionuclide.

Radioactive age determination is based on the law of radioactive decay, and the residence time of mass in the hydrogeologic system or the groundwater age (t) is described mathematically as:

$$t = \frac{T_{1/2}}{\ln 2} \ln\left(\frac{A_0}{A}\right).$$

Tritium

Tritium concentrations are reported in terms of tritium units (TU; Fritz and Fontes, 1980). The occurrence of tritium in waters of the hydrogeological cycle arises from both natural and man-made sources. Tritium is produced naturally in the earth's atmosphere by the interaction of cosmic-ray neutrons with nitrogen (Moser et al., 1980). The tritium is oxydized in the atmosphere and reaches the soilthrough precipitation. From hence it penetrates to the groundwater table. The average yearly tritium concentrations in precipitation over Middle Europe is 6 TU (Moser, 1980). However, tritium generated by thermonuclear testing in the atmosphere between about 1952 and 1963 has swamped the natural production of tritium. Tritium levels declined once bomb testing stopped in 1963, but present-day levels remain well above natural background. The age of the waters could in principle be calculated by use of the radioactive decay equation and the half-life time of ^{3}H (12.35 years) to an accuracy of about 50 years. In practice, however, minor mixing of 1952/53 precipitation and recharge to the groundwater saturated zone would result in higher tritium concentrations of the older groundwater and reduce the accuracy of any dating by measuring the radioactive decay of natural tritium. The nuclear tests led to a rise in tritium content of approximately 400 TU in the precipitation over Middle Europe between 1952 and 1959.

The main application of tritium is to differentiate pre-1952 water from younger water. Assuming pre-1952 water to have had an original ^{3}H concentration of 6 TU in Middle Europe (after Geyh, 1980), the concentration in 1985-1987 (years of my field work) would be at a maximum 0.9 TU, which is close to the detection limit using analyses that rely on enrichment techniques. Therefore, detecting tritium in a sample implies that the water contains some component of more recent or post-1952 water, i.e., modern meteoric water.

Results and interpretations

The following paragraphs examine thetritium concentrations in groundwaters from the Vosges recharge region and the Hochwald recharge area to the apparent regional discharge area, the Pechelbronn-Soultz Basin, which also accomodates smaller local recharge areas (Appendix 14; Figure 84). As expected, near-surface groundwaters in the recharge regions have the highest tritium content while ascending groundwaters from deep aquifers are nearly tritium-free.

From the *Buntsandstein* springs in the Vosges and Hochwald, descending waters have tritium concentrations between 20-43 TU, and 43-67 TU, respectively, indicative of post-1952 modern meteoric waters which plot on the D vs. ^{18}O diagram in cluster III (Figure 35). My previous supposition that, in cluster III, δ-values represent recent waters is herewith confirmed.

Wells Four à Chaux (artesian) and Liebfrauental in the Lembach Graben between the Vosges and Hochwald produce normal chloridized groundwater with tritium concentrations below 2 TU (Appendix 14; Figure 84).

Wells and springs near the Rhine Fault at the foot of the Hochwald yield artesian flowing groundwaters of tritium concentrations between 12 to 2 TU (Appendix 14; Figure 84). The stable isotope compositions of the waters are represented in cluster III of Figure 35.

Shallow Wells RG-1 and Mattenmühle in the Soultz-Hermerswiller Compartment (Figure 84) are tritium-free (<1.9 TU). My previous interpretation that deep saline groundwaters ascend along the Kutzenhausen and Soultz Fault and reach the near-surface, is confirmed by the tritium-free content of the waters in these wells.

The flowing oilfield waters from wells 3262 and 3969 from the *Zone Dolomitique* are tritium-free or tritium-poor (<2.1 - 2.4 TU). The groundwater is dominated by pre-1952 meteoric water. Well 4275, 120 m deep in the *Pechelbronner Schichten*, shows a tritium content of 4.9 TU.

Fresh water from shallow well Schreiner at Soultz (Alluvium) has a tritium content of 28 TU while well Aloxan at Reimerswiller shows low tritium levels for groundwaters in the Plio-Quaternary (<2.5 TU; Appendix 14 ; Figure 82 and 84).

The thermomineral waters in the Triassic Aquifer Group are tritium-free (Romaine, Morsbronn, Helion, Appendix 14).

Carbon-14

Measurements of ^{14}C are reported as percent modern ^{14}C (pmc) determined as the ratio of the sample activity to that of the international standard expressed as a percentage.

Carbon-14 originates naturally in the upper atmosphere through a reaction involving nitrogen and neutrons. As for ^{3}H, atmospheric nuclear testing hasaffected its concentration in recent years. However, except for modern waters, the increase in ^{14}C concentrations does not affect the interpretation.

In theory, groundwater age dating is uncomplicated. It is assumed for groundwater dating that the levels of ^{14}C in precipitation have remained constant until the last 40 years (Mook, 1980). Carbon-14 oxidizes to $CO_{2(g)}$ which is incorporated as dissolved carbon in recharge water, which is isolated from the atmosphere. The activity of ^{14}C is approximately 100 pmc (Fritz and Fontes, 1980). Once carbonate species move below the water table, ^{14}C begins to decay. Since there are no additional sources of carbon-14, by measuring the activity of dissolved carbon in the water sample, one may ascertain the amount of remaining ^{14}C and estimate the uncorrected age. The radioactive half-life of ^{14}C is 5730 years and allows for the valid dating of carbon-containing material up to 50 000 years (Geyh, 1980).

In practice, ^{14}C dating in groundwater is not very straightforward, however. Some reactive minerals contain carbon, and carbon is transferred in and out of the groundwater. The value of the initial activity, A_0, (^{14}C activity at time zero assuming no decay) would be lower than 100 pmc, reflecting the fact that other processes besides radioactive decay influence the ^{14}C activity of the sample. An age determination is meaningful as long as A_0 and A (observed activity) differ only in terms of their rates of radioactive decay.

The following summarizes the most important processes that can alter the ^{14}C activity of groundwater (after Mook, 1980; Moser et al., 1980; Wigley et al., 1978):

- congruent dissolution of carbonate which adds inactive "dead carbon" or carbon without ^{14}C activity to the hydrogeologic system. Because in most groundwater systems calcite and dolomite are much older than 50 000 years, this carbon is devoid of ^{14}C. This will lower the ^{14}C activity measured in the sample.

- incongruent dissolution of carbonate or other Ca-minerals accompanied by precipitation of calcite.

- addition of dead carbon from other sources such as oxidation of organic matter, sulfate reduction, and methan generation. This could occur in a petroliferous basin and would lower the ^{14}C activity of the sample.

- possible isotope exchange reactions between the different carbon-bearing chemical species.

Given thses sources of error, it is fortunate that an accurate age estimate is,often not required for the solution of a hydrogeological problem. In any case, it is felt that an interpretation of the radiometric measurements is rendered meaningful only with an understanding of the concept of regional groundwater flow is. Any geochemical argument is only as good as the hydrogeological framework from which it is developed. In many cases an estimate of important hydrochemical parameters may be made without seriously compromising the overall accuracy of the results, as long as the analyses and conclusions are made with respect to an integrated approach.

I did not attempt to apply the various correction models which have been introduced over the last decade. These models try to estimate the source of carbonate, the amount of dead carbon and the A_0 value in a groundwater system in order to calculate a more precise age of the water. A difference of a thousand years between the absolute and corrected age value is, in a basinal flow system study, of little significance.

Vogel (1967 and 1970) derived by empirical means an A_0 value of 85 ±5 pmc for soil water and shallow groundwater in temperate climates. Since the *Buntsandstein* Aquifer in the Vosges and Hochwald is carbonate free, an initial A_0 value of 100 pmc for the groundwater can be assumed. This is also valid for the crystalline in the Black Forest.

The Ingram-Pearson correction equation (Fontes et al., 1979) was applied to waters with high $\delta^{13}C$ values, when dissolution of carbonates and dilution by dead carbon (e.g., in the *Muschelkalk*, Jurassic hydrostratigraphic units) can be expected.

Ingram-Pearson Correction: The dilution of active carbon, i.e., the initial activity of the total dissolved carbon, is calculated by an isotope mixing model, based on the $\delta^{13}C$ content of each species:

$$A_0 = \frac{\delta^{13}C_T - \delta^{13}C_C}{\delta^{13}C_{CO_2} - \delta^{13}C_C}(A_{CO_2} - A_C) + A_C \quad ,$$

where $\delta\,^{13}C_T$, $\delta\,^{13}C_{CO_2}$ and $\delta\,^{13}C_C$ are the stable isotope compositions of the total dissolved carbon, the soil CO_2, and calcite, respectively,and A_{CO_2} and A_C are the ^{14}C activity of the soil CO_2 and solid carbonate, respectively. The $\delta\,^{13}C$ content of CO_2 gas in the soil zone is -27 ±5 ‰ PDB (Mook, 1980). For practical applications Pearson's model assumes $\delta\,^{13}C_C = 0$ ‰ and $A_C = 0$ % (old marine carbonate), thus, the equation reduces to:

$$A_0 = \left[\frac{\delta^{13}C_T}{-25}\right] \times 100 \text{ pmc}$$

Results and interpretations

Sixteen ^{14}C samples were collected at 15 separate sites in the study area: the Vosges, the Hochwald and the Pechelbronn-Soultz Basin (Appendix 14; Figure 84).

Guidelines for carbon-14 sampling were given by BGR and NLfB, Hannover. Inconsistencies in sampling procedures are expected to have caused most of the discrepancies in the results. Unfortunately, only one control ^{14}C sample was taken for well Helion. Fractionation of ^{14}C could have occurred in the case of a low flow rate from one of the wells which resulted in a prolonged exposure of the sampled water to the atmosphere and substantial loss of CO_2. The ^{14}C samples were analyzed by BGR-NLfB laboratories in Hannover.

To determine the uncorrected "conventional" ^{14}C age of a water sample with regard to the year 1950, the earlier determined radiometric "Libby" half-life of 5570 years (Geyh, 1980) has been used: Adapting Vogel's (1967, 1970) A_0 value of 85 ±5 pmc would have lowered the age of the groundwaters by about 1300 years, so an initial A_0 value of 100 pmc was applied (Appendix 14). The time-residence equation for mass in a hydrogeologic system is then as follows:

$$t_{\text{conv.}} = 8036 \ln\left[\frac{A_0}{A_{\text{sample}}}\right]$$

As mentioned before, $\delta\,^{13}C$ is a measure of the extent of carbonate reaction between the groundwater and aquifer rock and/or non-mineral sources like CH_4 and CO_2. The $\delta\,^{13}C$ values of dissolved total carbon in groundwater range between -20 and -10 ‰ (PDB) when no chemical reactions with the aquifer rock have occurred (Geyh, 1980). In addition, isotopic exchange reactions are expected in the Pechelbronn-Soultz Basin, between thermal CO_2 gas and its transporting medium groundwater; this would result in lower ^{14}C activities and higher $\delta\,^{13}C$ values. Also, chemical reactions with biogenetic methane would increase the ^{13}C content to positive δ-values and increase the ^{14}C age to aberrant estimates. Barker et al. (1978) concluded that thermogenetic methane ($^{13}C_{CH4} > -45$ $^{o}/oo$) had no effect on the carbon-isotope content of groundwater while biogenetic derived methane ($^{13}C_{CH4} < -45$ $^{o}/oo$) did produce an increase in $\delta\ ^{13}C$.

Figure 38 shows a $\delta\ ^{13}C$ vs. ^{14}C-activity plot for the study area. It demonstrates clearly that, with decreasing ^{14}C activity (increasing age of groundwater), the $\delta\ ^{13}C$ values increase. This indicates that secondary chemical reactions with carbonate rocks and an intake of dead carbon have occurred over time.

Figure 38 displays three dominant groups:

Cluster I: Groundwaters infiltrating in the Hochwald and discharging near the Rhine Fault in wells Hochwald II, Mitschdorf and spring Sept Fontaines (Figure 84) have $\delta\ ^{13}C$ values between -19 and -20 $^{o}/oo$. The conventional ^{14}C age is between 1250 and 3200 years. In general, lighter $\delta\ ^{13}C$ values correspond to samples of wells near their recharge areas and thus represent an incomplete equilibrium between soil-zone CO_2 and aquifer carbonate (Pearson et al., 1970). Also, since Lower Triassic sandstone aquifer (HSU 3) is carbonate-free at the Hochwald, an A_0 value of 100 pmc was initially assumed. However, the tritium concentration in the water samples indicates that modern meteoric water is present and that the uncorrected dating is too high. Applying the Ingram-Pearson model corrects the A_0 values to 80 ±5 pmc (this corresponds closely to Vogel's empirically derived A_0 value) and reduces the ^{14}C age for Sept Fontaines groundwater to recent times, the Hochwald II water to about 500 years old and the Mitschdorf water is estimated to be older than 150 years.

Cluster II: The $\delta\ ^{13}C$ values of about -14 $^{o}/oo$ for the near-surface groundwaters in the Pechelbronn-Soultz Basin are higher than the Hochwald $\delta\ ^{13}C$ values (Figure 38; Appendix 14; Figures 82 and 84). Well Schreiner produces groundwater with a conventional age of 835 years. Considering the high tritium content (28 TU) this is surely too high. The water is probably only a few decades old. Well Mattenmühle has Holocene water of a uncorrected age of 6000 years. A correction would lower the groundwater's residence time to about 1600 years.

Cluster III represents the oldest groundwater from thermal wells at the Vosges and Rhine Fault and wells in the Pechelbronn-Soultz Basin, including two thermomineral wells north of Karlsruhe. These waters have a low ^{14}C activity of between 1.3 and 3.6 pmc, and $\delta\ ^{13}C$ values between -6 and -2 $^{o}/oo$. Two oil wells in the *Zone Dolomitique* (SAEM 3262 and 3969) show, in comparison to oil well 4275 (*Pechelbronner Schichten*) much higher δ

^{13}C values (Figure 84; Appendix 14) of +1.1 and - 4.6 ‰. Especially for well 3262, the high ^{13}C content is attributed to subsurface methane generation.

From the west to the east (Vosges - Rhine Fault - Pechelbronn-Soultz Basin) the groundwater in the confined hydrostratigraphic unit 3 (*Buntsandstein* and *Muschelkalk* Aquifers) increases in age, i.e., approximately 20 000 ⇒ 27 000 ⇒ >30 000 years (uncorrected conventional ages for wells Romaine, Morsbronn and Helion (Appendix 14 ; Figure 84). The flowing well Romaine (180 m deep, 18 °C) near the Vosges Fault at Niederbronn in the Zaberner Fracture Zone has a uncorrected age of about 20 000 years which seems very high considering the fact that the Vosges recharge region to the west is only a few 100 m away. The bordering Vosges Fault might function as a conduit for deep circulating, i.e., for older groundwaters to reach shallow horizons, but the low degree of mineralization (Tables 27; Chapter 4.2.3.2) and the fact that the deuterium and oxygen-18 values plot within cluster III of modern meteoric waters in the previously described Figure 35 (Chapter 4.2.3.1) suggests that the groundwater in well Romaine did not originate in a pre-Holocene glacial period alone. Most likely, the groundwater is a mixture of recent and Pleistocene water which ascends along the Vosges Fault to shallower depths. Applying the Ingram-Pearson correction model reduces the groundwater age for well Romaine to a more realistic value of about 8770 years.

Thermal wells Morsbronn 3a (*Muschelkalk*) and 3b (*Buntsandstein*) located near the Rhine Fault (Figure 84) produce about 40 °C warm and mineralized groundwater of similar $\delta\,^{13}$C and ^{14}C values (Appendix 14). The conventional age is about 27 000 years. The regional groundwater flow direction is from the Vosges mountains along the *Buntsandstein* and *Muschelkalk* Aquifer to the east. Dissolution of carbonate in the limestone aquifer and an intake of dead carbon is indicated by the high $\delta\,^{13}$C values (Figure 38); the estimated ages are possibly too high. A corrected age for the groundwaters would be lower at about 15 000 years. Over a linear distance of about 10 km, the migration-time span of groundwater to flow from well Romaine to wells Morsbronn is about 6000 years.

Groundwater from well Helion in the Pechelbronn-Soultz Basin has a conventional age of about 31 000 years. Two ^{14}C samples of near-identical ^{14}C ages were taken in the years 1985 and 1987. A correction would reduce the ^{14}C age to approximately 19 000 years.

The groundwaters from thermal wells Bruchsal 1a and 2, north of Karlsruhe at the Black Forest also plot within cluster III (Figure 38) and have an uncorrected ^{14}C age of > 30 000 years (Matthess et al., 1986).

The ^{14}C activity for wells Helion and Bruchsal are close to the detection limit of ^{14}C and as such the uncorrected ages can only be estimated at > 30 000 years. The relatively high ^{13}C content is indicative of isotopic exchange reactions between the ^{13}C content of the thermal waters and the ^{13}C content of the rocks. In addition isotope exchanges with magmatic or organic CO_2 gas can be expected. Since the methane concentration of the oilfield waters in the Pechelbronn-Soultz Basin (Helion 26 000 ppm CH_4; Table 22) and at Bruchsal are elevated (see also Chapter 7.2) it is likely that the CO_2 gas is also generated by thermally maturing or degrading organic matter.

Groundwater movement and flow velocities

From the ^{14}C ages of groundwater from two observation wells (which are positioned in the same flow system normal to the flow direction) and their lateral distance, a so-called apparent groundwater flow velocity can be estimated. The age of groundwater is proportional to the travelled lateral distance (piston flow model). If no age correction is applied for additional carbon dissolution, significant age differences are observed, and the flow velocity will be underestimated. The flow direction of the groundwater, however, can be established beyond doubt.

For the hydrostratigraphic unit 3 the regional flow direction is from the Vosges to the Pechelbronn-Soultz Basin, i.e., from the west to the east. This conclusion is supported by the facts that: (1) a steady increase in the groundwater's salinity (TDS) from the west to the east is observed; (2) an increase in ^{14}C age of groundwater from the Vosges to the Pechelbronn-Soultz Basin is noted; and (3) groundwater flows from a region of high fluid potential (topographic high, i.e., the Vosges) toward a fluid potential low (topographic low, i.e., the Pechelbronn-Soultz Basin).

I chose the surface water divide in the Vosges mountains which extends near the town Bitche in a north-south direction (Figure 84) as the western regional recharge limit to obtain the lateral distance between the sampled wells and the region of recharge.

The estimates for the apparent flow velocities (in m/y) in the hydrostratigraphic unit 3 for conventional and corrected ^{14}C ages are given in the Table 23.

Such velocities are common for regional groundwater flows. At the same time, they indicate a relatively short throughflow time, i.e., a high rate of groundwater turnover in the hydrostratigraphic unit 3 of the basin. Mean apparent flow velocities for corrected ^{14}C ages are greater than those for conventional ^{14}C ages. Moreover, the fact that the groundwater apparently moves at a steady velocity from the Vosges to the Pechelbronn-Soultz Basin indicates that the principal fault systems do not obstruct and slow down the flow velocities in the aquifer group.

The flow velocity of groundwater from the Hochwald recharge area to the wells 3262 and 3969 (*Pechelbronner Schichten*) near Pechelbronn is about 0.3 m/y.

In the interior of the basin, locally recharged groundwater descends, induced by topographic elevation differences of about 50 m, to the top of the *Couches Rouges* (aquitard) and regenerates the groundwater in the Oligocene of the 150 m deep oil well 4275 and the shallow wells. Assuming the local recharge area to be in the near-vicinity of 1 km, the lateral flow velocity to well 4275 is approximately 0.1 m/y.

4.2.5 Interpretation of the Water Chemistry in Terms of Groundwater Flow

In section 4.2.1 it was stated that the chemical character of formation waters changes systematically with groundwater flow direction and residence time. A three-dimensional distribution pattern of the formation water chemistry in the basin can disclose, on the one hand, regional groundwater flow trends in the study area and, on the other hand, give information on local flow conditions in fault-severed aquifers and possible groundwater flow channelling by principal faults in the Pechelbronn-Soultz Basin. This can be deduced from maps, cross sections and diagrams.

Modified Schoeller diagrams

From the Piper and the Schoeller diagrams (section 4.2.3.1, Figures 14 and 15) I reason that the chemical evolution of the groundwater is from water type A to water type B, i.e., groundwater flows from the Vosges, Hochwald and Black Forest towards the Pechelbronn-Soultz Basin and Rhine Valley.

The disadvantage of the diagrams is that water of the same origin but of different concentration levels, as well as water of different origin but of the same dominant cation-anion pair, may have identical representation on the diagrams. This precludes the use of the diagrams to distinguish between groundwaters of similar hydrostratigraphic units but not of the same recharge area and vice versa (i.e., different levels of mineralization) and also between groundwaters affected by fresh water mixing.

To avoid the problem of dilution of individual constituent concentrations and degrees of mineralization, the Schoeller diagram was modified and I chose to base the hydrochemical characterization on select ionic ratios. Only those ratios of major cations (Ca, Mg, Na+K) and anions (HCO_3, SO_4, Cl) were used. Ionic ratios offer an advantage over individual constituent concentrations, in that ratios are not affected by dilution. It must be pointed out, however, that inherent in the statement that ionic ratios are not affected by dilution, is the assumption that all constituents in the groundwater are diluted at the same rate.

For the following modified Schoeller diagrams (Figures 39a,b, 40a,b, 41a,b and 42a,b), the same chemical data from Appendixes 8 and 10 were used as in Chapter 4.4.2.3. The location of the sample points is given on maps and profiles (e.g. Figures 71, 72, 82, 74 profile II, 76 profile B-B', 77 profile IV and others).

Waters recharging in the Vosges, Hochwald and Black Forest have near-identical chemical composition and concentrations (Figures 39a,b), a high HCO_3/SO_4 ratio and a low (Na+K)/(Ca+Mg) ratio. Locally discharging groundwater from springs in the Vosges valleys as is exemplified by spring Celtic (Appendix 8 and 27, Figures 39a,b and 84), shows a subdued shift toward a lower HCO_3/SO_4 ratio and a higher Na/Ca ratio on the Schoeller diagram. The same observation is made for well Liebfrauenthal at the foot of the Hochwald.

Figures 40a,b demonstrate the lateral hydrochemical evolution of groundwaters in the confined hydrostratigraphic unit 3 (*Buntsandstein* and *Muschelkalk* Aquifer). The curves represent samples of wells from the Vosges to the Hermerswiller Compartment (wells Romaine-Morsbronn-Helion-SAEM 4515 and 4550; Appendixes 8 and 10). The line pattern in Figures 40a and b change from the recharge region towards the Pechelbronn-Soultz Basin. The anion-cation ratios of groundwaters in the Triassic aquifer increase or decrease steadily and systematically toward the Soultz Compartment (Figures 40a,b). Groundwaters from the hydrostratigraphic group I at Soultz show the greatest change in the anion-cation ratios in comparison to groundwater from wells in the west. The anion ratios show a decrease in HCO_3 due to CO_2 depletion in the subsurface (closed system), an increase in chloride content with mineral dissolution and a decrease in SO_4 due to sulfate reduction. The cation ratios seem to be controlled mainly by sodium, potassium and calcium concentrations. This can be due to mineral dissolution and cation exchange mechanisms. The Ca/Mg ratio increases slightly with groundwater flowing to the east. From the Ca, Mg vs. Cl dilution diagrams (Chapter, 4.2.3.2, Figures 23 and 25) an enrichment in calcium and a depletion of magnesium in oilfield brines in comparison to sea water was observed. It is speculated that this phenomenon is caused by dolomitization of limestone horizons in the *Muschelkalk*, *Keuper*, Jurassic and *Zone Dolomitique*. Dolomite formation is thermodynamically and kinetically promoted in aqueous solutions of low Ca/Mg ratios, low Ca/HCO_3 ratios and at high subsurface temperatures (Machel and Mountjoy, 1986). Gravity-driven groundwater flow can generate the necessary volumes of water needed to supply sufficient amounts of magnesium to sites of replacive dolomization. According to a simple stoichiometric reaction describing a possible formation of dolomite:

$2CaCO_3 + Mg^{2+} \leftrightarrow CaMg(CO_3)_2 + Ca^{2+}$, one Mg^{2+} ion would replace one Ca^{2+} ion. Apparently, an increase in groundwater salinity and a subsurface environment with a high geothermal gradient would advance the rate of dolomitization. These subsurface conditions are emplaced by the regional flow system in the Pechelbronn-Soultz Basin.

The gradual changes in anion-cation ratios indicate that groundwater flow in the hydrostratigraphic group I is directed from the west to east towards Soultz. The Black Forest is not the regional recharge area for groundwater west of Soultz. Otherwise the trend in anion-cation ratios would be reversed and the TDS concentrations would increase from the Soultz region towards the west. The same argument applies to the ^{14}C age of the groundwater, i.e., Helion water would be younger than Morsbronn water. Unfortunately, no reliable chemical data were available from deep wells east of Soultz. Thus, the possibility that groundwater in hydrostratigraphic group I east of the Soultz and Hermerswiller Compartments is recharged in the Black Forest and discharges in the Soultz Horst can not be ignored. This would then define the Soultz Horst as a zone of converging regional flow systems from the west and the east. I examine this possibility in Chapters 4.3, 5 and 6.

Figures 41a,b present the changing water chemistry in Tertiary formations at Pechelbronn and Soultz. The solid black line represents the water type in the deep Triassic Aquifer (well Helion) discussed in the previous diagrams (Figures 40a,b).

The line pattern of the cation ratios in the Tertiary formations matches the line of the less mineralized recharge water (Figure 41a). The ratios differ in their higher concentrations of chemical constituents. Groundwaters in the Lower *Pechelbronner Schichten* have smaller Na/Ca and (Na+K)/(Ca+Mg) ratios, while the *Zone Dolomitique* formation waters have higher ratios. On the anion-ratio Schoeller diagram (Figure 41b) groundwaters of the *Zone Dolomitique* with a high Cl and low HCO_3 content can be separated from groundwaters of the *Pechelbronner Schichten* with a high HCO_3, SO_4 and low Cl content. The line for the groundwater in the *Zone Dolomitique* horizons resembles more closely the line of groundwater in the deeper formations, while the line pattern of the groundwater in the Lower Oligocene horizons is more like that of recharged groundwater. This means that the groundwater in the *Pechelbronner Schichten* is diluted by fresh groundwater from the Hochwald Flow System or local flow systems. The *Zone Dolomitique* groundwater is highly mineralized and does not show dilution by fresh groundwater. Groundwater from deeper aquifers flows upward cross-formationally enhanced by fault and fracture zones and enters the *Zone Dolomitique* aquifer, dissolving minerals and thereby further increasing the salinity.of the groundwater.

The final two modified Schoeller diagrams (Figures 42a,b) demonstrate that the type-curves of water samples from shallow wells (Appendix 10; Figure 82) in the Soultz-Hermerswiller Compartment can be used to distinguish between groundwater from local and shallow flow systems in the Pechelbronn-Soultz Basin and from a deeper regional flow system driving saline groundwater cross-formationally upward along/across fault and fracture zones to the near-surface.

Wells Aloxan near Reimerswiller and Schreiner near Soultz, both located in local topographic depressions, produce fresh groundwater from the surrounding local recharge areas. Their type-lines are similar to the lines of the regional recharge regions. Groundwater from shallow wells RG-1 and Mattenmühle at Soultz ascend from deeper formations to the near-surface. The chemical character of the groundwater is comparable to the formation waters in the *Zone Dolomitique* and hydrostratigraphic unit 3. These wells are located in a region of highest fault density (Hermerswiller Compartment) and are in the near-vicinity of the outcropping Soultz and Hermerswiller Fault (Figure 82), i.e., the faults are not a hydraulic barrier but a potential avenue along which groundwater can flow to the surface.

Tritium versus salinity plot

In a basinal groundwater study, in which different gravity-driven flow systems can be expected operate, the tritium content of a water sample can disclose (in relation to an conservative chemical compound, e.g., chloride) information on groundwater flow directions, zones of converging and mixing flow systems. I the case of a fault-severed basin the tritium content can reveal the presence of fluid flow barriers or conduits. The tritium level in groundwater will decline in the flow direction as the water becomes older. On a ^{3}H vs. Cl plot, a curve would decline from high tritium and low chloride levels to low tritium and high chloride levels. This is examplified by Figure 43 for the Rhine Graben study area.

The plot shows a sharp decline in tritium content with increasing chloride concentration towards the Pechelbronn-Soultz Basin, i.e., in groundwater flow direction. It is possible to differentiate between groundwater from the Vosges and Hochwald and fresh groundwater with low tritium content discharging along the Rhine Fault near the foot of the Hochwald and in the Lembach Graben (see also Figure 84). Shallow wells in the Pechelbronn-Soultz Basin produce post-1950 fresh water in local flow systems (well

Schreiner) and saline "old" groundwater fed by conductive faults (well Mattenmühle and well RG-1). The same conclusion was drawn from the previously discussed modified Schoeller diagrams.

Salinity distribution

The spatial distribution pattern of the groundwater's total dissolved solids content (TDS) in the Pechelbronn-Soultz Basin is shown on maps and geologic cross-sections (Figures 71, 72, 82, 83; Figures 73-87 profiles I-VI). Due to data clustering (Appendixes 8, 9 and 10), parts of these maps and sections do not contain TDS values. The structural cross-sections were constructed from SAEM and PREPA well reports.

Profile B-B' (Figure 76) provides a good regional overview of the sub-surface salinity distribution in the hydrostratigraphic units of the basin. Profiles I to VI (Figures 73-87) and salinity-data maps of the *Muschelkalk* (Figures 71, 83), the *Zone Dolomitique* (Figure 72) and the *Pechelbronner Schichten* (Figure 82) present plotted TDS data and their distribution on a more detailed local scale.

The phenomenon of increasing water mineralization in the direction of formation water flow is well documented by the salinity distribution in profile B-B' (Figure 76) and Figure 83 (Otto et al., 1988; Tóth et al., 1989), which show that the TDS values exceed 100 000 mg/l in the deeper faulted and fractured hydrostratigraphic group I of the Soultz and Hermerswiller Compartment. This hydrochemical anomaly is the expression of two gradually increasing trends, from the marginal zones to the Soultz region, and occurs in a region of two converging flow systems from the Vosges and Black Forest, respectively. The principal faults do not hinder a continuous lateral groundwater movement to the east, but rather channel the flow upward along the principal faults Pechelbronn, Hoelschloch, Kutzenhausen and in the Soultz Fault Zone. The Soultz region is interpreted as a zone of vertical groundwater flow and a zone of disaccommodation (Chapters 5 and 6). An uplift of the iso-salinity contours between bordering tectonic compartments is observed, e.g., Pechelbronn - Hoelschloch - Kutzenhausen - Soultz - Hermerswiller Compartments.

The Hochwald Flow System causes fresh water to infiltrate to greater depths and the iso-salinity contour is uplifted to shallow depths towards Pechelbronn and Soultz in areas of regional ascending flow (Figures 76 profile B-B', 75 profile IIIa). From Figures 82 and 83 it can be observed that a plume of fresh water from the Hochwald invades the Pechelbronn region (Figure 79 profile VI). For the Kreuzhecke, Preuschdorf region (profiles I, II, IIIa, Figures 73, 74 and 75) it appears that the fresh water invasion from the

Hochwald had no dilution effect on the TDS concentration of groundwaters in the *Zone Dolomitique* and *Pechelbronner Schichten* (Figures 72 and 82).

Superimposed on the regional flow system are local flow systems in the Pechelbronn-Soultz Basin in which penetrating to shallow depths fresh groundwater mixes with groundwater from a deeper intermediate or regional flow system. The local flow systems are associated with minor topographic elevations in the basin. This is shown on profile II a,b (Figure 74), III b (Figure 75) and VI b,c (Figure 79) as well as on a map (Figure 82). Locally recharging water can descend to depths of 150 m but this phenomenon seems to be restricted to areas north of Pechelbronn (profile VI). Haas et al. (1933) observed incoming fresh water in the mining galleries up to depths of 140 m. In the other more southern part, however, the fresh water infiltration depths of local flow systems are much shallower, generally descending to only a few meters or tens of meters.

As was said before, a groundwater of low mineralization and confined to hydrostratigraphic group I (top Basement, *Buntsandstein*, *Muschelkalk* and *Lettenkohle* Aquifers) flows unrestrained by the Vosges and Rhine Fault from the Vosges mountains to Pechelbronn-Soultz Basin (Profiles B-B', IIa, IIIa, Figures 76; top HSU 3, Figures 71, 83) increasing steadily in TDS content. At the Rhine Fault the TDS concentration (wells Morsbronn) is about 6000 mg/l. In the Soultz-Hermerswiller Compartments the groundwater in the uplifted Triassic aquifer system (HSG I) has gained more than 40 000 mg/l in TDS (Profile IIIb, IV, Figures 75 and 77). The iso-salinity contours are sharply uplifted as is shown by Figure 76 profile B-B'. It is striking that these high TDS concentrations are already observed in the groundwater of the *Zone Dolomitique* of the Preuschdorf and Pechelbronn Compartments west of Soultz. While the TDS concentration in the *Muschelkalk* groundwater is about 20 000 mg/l in these structural blocks, the groundwater in the *Zone Dolomitique* (HSU 8) has TDS concentrations in excess of 90 000 mg/l. This is especially apparent in for the *Zone Dolomitique* oil fields south of Pechelbronn in profiles I, IIa, IIIa (Figures 73-83) and on the *Zone Dolomitique* TDS map (Figure 72). As previosly stated, this phenomenon can be explained by dissolution of minerals in the *Keuper*, Jurassic aquifers by groundwater ascending cross-formationally to shallower depths. The salinity of the groundwater is further increased due to dissolution of halite and anhydrite minerals in the *Zone Dolomitique*. Groundwaters entering the *Pechelbronner Schichten* enhanced by fault and fracture zones can be diluted by fresher groundwater originating from the Hochwald recharge region. This is observed in the northern sections of Pechelbronn.

4.2.6 Conclusions

Hydrochemical analyses of major cation and anion and trace elements were discussed and interpreted in relation to regional annd groundwater flow systems. Hydrochemical anomalies were described which identify areas of recharge and discharge and converging flow systems. A possible indicator for subsurface petroleum deposits was found.

- Two principal water facies can be distinguished: (1) Ca-Mg-HCO_3 waters typify groundwaters in the recharge areas and shallow flow system in the Pechelbronn-Soultz Basin; and (2) Na-Ca-Cl and Na-Cl waters identify deep formation waters of regional flow systems associated with oil fields and to the near-surface discharging groundwater in the basin.

- Oilfield waters are enriched in Ca and depleted in Mg as well as SO_4. This geochemical arrangement has been observed in many petroliferous basins and is attributed to ion exchange (dolomitization) and sulfate reduction.

- Only iodide proved to be a useful indicator for possible hydrocarbon deposits in the subsurface. Other trace elements are less conclusive indicators. The detection of near-surface elevated concentrations of trace elements requires upward groundwater flow directions. Faults and fracture zones as conduits to groundwater flow improve the detection of near-surface anomalies in trace element concentrations.

- Groundwater may attain a TDS content of up to 100 000 mg/l. In principle, the TDS concentration in the groundwater increases from the graben shoulders to the basin. Groundwater flow results in chemical stratification, and faults channelling groundwater result in vertical plumes of high TDS.

- Fresh meteoric water infiltrates the *Pechelbronner Schichten* north of Pechelbronn. It does not reach the *Zone Dolomitique*.

- The composition of stable isotopes in the basinal groundwater reveals clearly its meteoric origin. Thermomineral waters recharged in the Vosges mountains during Pleistocene time. Hochwald waters and shallow groundwaters in the basin were recharged in Holocene time.

- The corrected ^{14}C ages for the groundwater in the hydrostratigraphic unit 3 increase from the Vosges to the Pechelbronn-Soultz Basin from about 8000 to 20 000 years. The groundwater from the Hochwald is modern and less than 800 years old. The apparent flow velocity of the deep groundwater has been roughly estimated at 1.0 to 1.6 m/y. Since some of the ^{14}C values are close to the detection limit, higher water ages are possible.

- The hydrochemical evolution of the groundwater discloses a west to east regional flow direction, from the Vosges to the Pechelbronn-Soultz Basin and from Hochwald to the Basin. Groundwater flows from the Black Forest to the Rhine Valley, but does not reach the Basin west of the Soultz Horst.

- The Soultz Compartment is a region of upward flow and discharging groundwater.

- The principal faults do not impede a continuous lateral flow across the fault zones but rather channel and deflect the groundwater to higher conductive zones.

4.3 Analysis of the Subsurface Temperature Regime

In common with other active rift basins (e.g. Red Sea Basin, East African Rift System), the Upper Rhine Graben is known for its high geothermal gradients and heat flow variations. Numerous papers have been published on the geothermal conditions in the graben and their possible causes. Although in the last ten years the transport of heat by groundwater motion has been discussed and modelled to explain and simulate anomalous subsurface temperatures for the German part of the graben, no detailed geothermal study in the graben has been interpreted in the context of regional groundwater flow and observable hydrogeological phenomena or nor has this been used as an integral part of a petroleum-hydrogeological basin study.

4.3.1 Theoretical Considerations

In exploring for deep groundwaters and interpreting groundwater flow, subsurface water temperatures play an important role in near-surface groundwater surveys. On the one hand, basinal groundwaters can be exploited for their heat content (for thermal spas, geothermal energy), on the other hand, in a regional groundwater study the temperature-dependent physical and chemical parameters of the water (e.g. viscosity, density, solubility) have to be taken into account. High subsurface temperatures can be caused by magmatic intrusions, substantial thermal conductivity differences of the rocks and moving groundwater.

Heat can be transported in a porous medium by way of three processes: conduction, convection and radiation. Heat transfer by radiation does not play a significant role at temperatures below 500 °C (Kappelmeyer et al., 1974).

Conduction of heat follows from a region where the temperature is high to where it is low. In the earth's interior, heat generated by radioactive decay flows by conduction out of the earth. In systems where the pore fluid is moving, convective heat transfer occurs due to this fluid motion. When the flow field is caused by external forces, the theat transfer is said to occur by forced convection. Such is the case where groundwater flow takes place in the absence of density gradients such that Darcy's law applies. A second type of transfer, called free convection, occurs when the motion of the fluid is due exclusively to density variations caused by temperature gradients. Convective heat flow is always coupled with heat conduction, while the latter can occur without convective heat transport.

The conductive heat flow, q, is defined as the amount of thermal energy perpendicularly crossing a unit area per unit time: $\vec{q} = -\kappa \text{ grad } T$, where κ is the thermal conductivity (W $m^{-1}K^{-1}$) and T is the temperature. The SI units of heat flow are W/m^2. Other units in use include cal/cm^2 sec and Heat Flow Units: cal/cm^2 sec x 41.84 = W/m^2; 1 HFU = 41.8 mW/m^2. The minus sign indicates that the flow of heat is in the direction of decreasing temperature. Most heat flow values range between 40 and 80 mW/m^2 (1 to 2 HFU). For Middle Europe an average heat flow value of 60 mW/m^2 is given (Hänel, 1979a). The Upper Rhine Graben has an average basal heat flow value of about 82 ± 20 mW/m^2 (Clauser, 1988; Hoffers, 1981). Higher values of about 130 mW/m^2 were calculated for regions with anomalously high temperature gradients (10°C/100 m) near Landau, 34 km north of the study area (Wohlenberg, 1979).

The thermal conductivity is a physical quantity which depends on the nature of the material constituting the porous medium as well as on its physical conditions such as temperature. For many practical purposes, however, κ can be regarded as independent of temperature. Typical conductivity values range between 1.5 to 5 W $m^{-1}K^{-1}$ (Kappelmeyer et al., 1974). Basement rocks (igneous, metamorphic) are better heat conductors than sedimentary rocks. Dolomite is a better conductor than limestone; shale, clay are poor conductors, evaporites are excellent conductors. Gases and water filling the pore spaces in sediments reduce the thermal conductivity of the porous medium, i.e., thermal conductivity decreases with increasing porosity.

Grad T in Km^{-1}, is the temperature gradient, a vector which represents the magnitude and direction of the steepest change of temperature at every point in the medium with a thermal conductivity, κ. The geothermal gradient is inversely proportional to the thermal conductivity when conduction is at steady state. The average gradient for Middle Europe is 4.1 °C/100 m between 0 - 400 m depth; below 400 m depth the gradient is about 2.4 °C/100 m (Hänel, 1979a).

The temperature of static groundwater is defined by the distribution and intensity of the heat sources, the water's temperature being the same as that of the surrounding rocks. However, if the groundwater is in motion and flows through regions of different temperature, its temperature may differ from that of the surrounding rocks due to convective heat transfer. The rate at which thermal equilibrium is approached and the degree to which it is accomplished depends on the flow velocity, flow volume, geometry of flow systems and thermal conductivity of the rocks.

Descending or ascending groundwater flow can significantly change the geothermal gradient in a sedimentary basin.Two cases can be distinguished (Figure 44):

(1) in regions of groundwater discharge, ascending water will cool down by dissipitating heat into the surrounding rocks thus causing a positive heat flow anomaly at the surface and a high geothermal gradient;

(2) in areas of groundwater recharge, cold water infiltrating to the subsurface, its flow enhanced by fault and fracture zones, will be warmed up when it descends, by removing heat from the surrounding rocks. It causes a heat flow anomaly at the surface which is negative compared to the undisturbed heat flow. The geothermal gradient will be low.

Some general rules can be dereived from these cases. For expamle when the direction of the groundwater flow is determined or estimated:

- negative anomalies imply downward moving water and the motion is directed toward the isotherms of increasing temperature values;
- positive anomalies indicate regions of discharging groundwater and a groundwater flow direction towards isotherms of decreasing temperature values.

4.3.2 Database

From 257 uncorrected bottom hole temperature (BHT) measurements, taken during well logging are available (Appendix 15). Subsurface temperatures were measured by SAEM in the Pechelbronn-Soultz Basin between 1935 - 1950. Sixty per cent of all measurements were taken in hydrostratigraphic unit 3. A few PREPA temperature values are available for the area east of the Pechelbronn-Soultz Basin. Further data were retrieved from two literature sources (Delattre et al., 1968; Lauer, 1976). The quality of the BHT data is difficult to assess since no log reports on the temperature measurements themselves were available. This made a temperature correction after Horner (Jones et al., 1984) impossible. The measured BHT is partly a function of the time lapse between cessation of drilling and the time of logging of the borehole. Circulation of the drilling fluid cools off the bottom portion of the borehole. Measured temperature would thus be too low, and sufficient time is needed after circulation has stopped for the BHT to equilibrate with the formation's fluid temperature.

Since it is impossible to tell the extent to which equilibrium time was allowed for these early well logging measurements, the available BHT data is expected to give temperature values which are tto llow rather than too high.

4.3.3 Subsurface Temperature Distribution

On a temperatures vs. depth plot (Figure 45) it can be readily seen that the subsurface temperatures in the graben are well above the normal statistical geothermal gradient of inactive basins (0.03 °C/m; Robert, 1985). The mean annual surface (z_0) soil temperature (T_0) of approximately 10.5 °C was determined by graphical extrapolation of measured temperature logs to 16 m depth (see Chapter 7.2; shallow survey). Another way to determine the surface temperature is to take the mean annual air temperature from the climatic atlas (Deutscher Wetterdienst, 1953). This temperature is measured 2 m above the earth's surface. Experience has shown that about 1.1 °C must be added to obtain T_0 (Hänel, 1980). For the study area a mean air temperature of 9 °C was obtained, with a T_0 value of 10.1 ±0.5 °C; Clauser (1988) obtained values between 10-12 °C for a region 34 km north of the study area.

From Figure 45 it is also possible to deduce a trend in which temperature increases with depth, although a linear relationship between temperature and depth is not apparent. The subsurface temperatures in the Pechelbronn-Soultz Basin increase faster with depth, than that observed for temperatures in the graben centre. On an additional temperature vs. depth plot (Figure 46), the data points for the Pechelbronn, Kutzenhausen and Soultz areas are shown separately. Two lines, I and II, represent regression lines for temperature data in the Pechelbronn, and Kutzenhausen and Soultz areas, respectively. The regression lines do not delineate the respective geothermal gradients per se, but rather demonstrate the rate of temperature increase with depth over the selected area. Line II for the Kutzenhausen-Soultz region proves to be steeper. Assuming, that forced convection is the dominant mechanism transporting heat in the graben, it is obvious from this simple plot alone that the groundwater flow direction is from the Pechelbronn to the Soultz region, and that the Kutzenhausen-Soultz area is likely to be a region of upward flowing and discharging hot groundwater.

At depth, the flow concentrating effect of fault zones is reflected by the observed distribution of subsurface temperatures. This is shown on isotherm-contour maps and cross-sections (Figures 85, 86a,b & profile C-C', 75 profile IIIb, 76 profile B-B', 77 profile IV and 78 profile V). A pronounced positive temperature anomaly has been known in the Soultz area since the early days of exploration (Haas et al., 1929; Schnaebele, 1948). The "Soultz Horst" between the Kutzenhausen and Hermerswiller Faults is characterized by intensive faulting and by high water yields, usually with artesian levels, fed by faults. Reprocessing of the original bottom hole temperature measurements

(Appendix 15) has shown that the thermal anomaly is even more accentuated than was reported by Schnaebele (op cit). A temperature anomaly located at Pechelbronn between the Heidenboesch and Hoelschloch Faults (Figures 85 and 86a,b) is not as well documented as in the Soultz area, but the presence of athe known thermal artesian well Helion and data from three oil wells attest that anomalously higher temperatures are associated with ascending groundwaters. On detailed examination, the isotherm contours show distinct stepwise changes in the direction and the proximity of faults (Figures 75 profile IIIb, 76 profile B-B', 77 profile IV and 78 profile V). The isotherm-contour maps for -500 m depth superimposed on the top of hydrostratigraphic unit 3 (*Buntsandstein*, Figures 86a,b and 85) and profiles B-B', C-C' (Figures 76 and 94b) show a west to east as well as east to west increase in subsurface temperature towards the Soultz region. Average geothermal gradients, with a maximum of 10-11.5 ^{o}C/100 m at Soultz, reflect the same trend (Figure 85).

It is noted for the western part of the Pechelbronn-Soultz Basin, that the temperature gradient increases toward the Kutzenhausen-Soultz Compartment more steeply than that observed for the internal zone east of Soultz. The contour lines of the isotherms are congested (Figures profile, 75 profile IIIb, 76 profile B-B', 77 profile IV and 78 profile V), and on a profile the isotherms rise rapidly across principal faults to shallower depths, culminating in the Hermerswiller Compartment (Figure 76 profile B-B'). It is further observed that the isotherms of the temperature anomaly at Soultz are not aligned parallel to the trend of the Kutzenhausen and Soultz fault system (NNE-SSW; Chapter 2.3.2), instead they display a NE-SW orientation crossing the principal faults. Also, it appears that the isotherms on the maps (Figures 85, 86a,b) as well as on profiles B-B' and C-C' (Figures 76 profile B-B' and 86b profile C-C') are affected and suppressed by the proximity of the Hochwald and the subsequent influx of colder fresh water discharging into the Pechelbronn-Soultz Basin. Thus, for well Dieffenbach 1, (profile C-C', Figure 86b) closest to the Rhine Fault and the Hochwald, temperatures only 21.5 ^{o}C were found at 415 m depths (negative anomaly); by contrast, its neighboring well, Dieffenbach 2, 180 m west, produced temperatures at the same depth of between 30-35 ^{o}C. It seems that the proximity of the Hochwald recharge region "depresses and protrudes" the isotherms towards the basin, and this results in a right-handed rotation and a NE-SW orientation of the isotherms.

4.3.4 Temperature and Heat Flow Anomalies caused by Groundwater Flow

To determine whether regional and depth variations of grad T, as well as variations of grad T for different geologic units are a result of geothermal conductivity changes of the rock formation, or whether they are related to heat generation or variations in the transfer of heat by forced heat convection, the heat flow distribution must be known. In an ideal steady-state conductive system, heat flow should not vary with depth, and any change in a geothermal gradient across any particular depth interval should be associated with a change in thermal conductivity, κ, to maintain a constant product, $q = -\kappa$ grad T. The amount of heat entering the system from the basement should equal the heat leaving above.

Similar to other rift basins, the Upper Rhine Graben is characterized by a high heat flux from the basement and the mantle due to processes of taphrogenesis. No volcanic activity is presently observed in the vicinity of the Rhine Graben, and heat input by radiogenic mineral decay of sediments and crystalline rocks is negligible in the region (Rybach, 1986). There are no major differences in thermal conductivities in the crust, which could lead to anomalous temperature updoming at the surface (Table 24; Werner et al., 1974). Since external heat sources and extreme thermal conductivity contrasts can be ruled out in the study area, deviations with depth from the regional, basal conductive heat flow of approximately 82 ±20 mW/m^2 (after Clauser, 1988; Hänel, R., 1980) will indicate heat transfer by convection. High heat flow anomalies are attributed to uprising warm water, whereas low heat flow values indicate descending colder groundwater. Thermal studies in other sedimentary basins have shown that downward or upward groundwater movement of the order of a few centimeters per year through formations a few kilometers thick can increase or decrease heat flow up to an order of magnitude (Majorowicz et al., 1985).

The effect of groundwater flow on the geothermal conditions in the basin can be approximated by: (1) temperature vs. depth plots; (2) the thermal resistivity method; and (3) the dimensionless Peclett number.

Temperature vs. depth diagrams

Three wells were chosen to demonstrate the temperature change with depth across the basin (Figure 47). Well Dieffenbach 1 (PREPA) is located farthest to the west near the Hochwald and in the proximity of the Rhine Fault, well 4515 (SAEM) is positioned in the Soultz Compartment of highest fault density, and well 4776 (PREPA) is found 1200 m east of Soultz in the Internal Zone of the graben (Appendix 15; Figures 85 and 86a,b). The temperature vs. depth curves are compared to an average geothermal gradient of 41 °C/km characteristic for Middle Europe (Hänel, 1979a).

The temperature gradients for uncorrected BHT measurements from well 4515 and well 4776 are higher than the normal geothermal gradient (super-geothermal), while the gradient for well Dieffenbach-1 is less steep (sub-geothermal; Figure 47). Defining a temperature increment, ΔT, as the difference between the measured or dynamic subsurface temperature and the nominal temperature (3 °C/km) at any given depth, $\Delta T = T_{obs.} - T_{nom.}$, Figure 47 shows that ΔT values for wells in the Pechelbronn-Soultz Basin and the Internal Zone are positive, while ΔT values for a well at the western periphery of the basin and closest to the Rhine Fault and Hochwald recharge area are negative.

Consequently, it can be concluded that heat transport by forced convection governs the subsurface temperature pattern in the basin. Hence it can be generalized that the region at the foot of the Hochwald, west of Preuschdorf and Lobsann (Figure 70), has a negative temperature anomaly due to downward flowing groundwater channelled by the border fault which recharged in the Hochwald, and that the region of Kutzenhausen-Soultz (which shows the highest positive ΔT values) can be identified as an area of vertically ascending groundwater flow channelled and directed by the fault and fracture zones to the surface. Further to the east, in the graben's internal zone, the temperature gradient remains super-geothermal but is less steep. Hence a vertical flow component of reduced intensity and a dominant lateral groundwater flow component toward the Pechelbronn-Soultz Basin can be expected to obtain here.

Thermal resistivity method

In a sedimentary basin within which transfer of heat is largely governed by conduction and where refraction of heat flow is unimportant, heat flow should be approximately constant with depth. On this assumption, it is possible to derive a heat flow value for each well:

$$q_z = \frac{\Delta T_i}{R_i}, \quad W/m^2,$$

where q_z is the vertical heat flow, ΔT_i is the temperature difference across any particular depth interval i, and R_i is the thermal resistance over the same interval; R_i being defined as follows:

$$R_i = \sum_{i=1}^{n} \left(\frac{l_i}{\kappa_i}\right), \ m^2C/W,$$

where the quantities κ_1, $\kappa_2 ... \kappa_n$ are estimated thermal conductivities based on rock types for discrete layers of thickness l_1, $l_2 ... l_n$. In essence it is necessary to assign values of conductivity to all main lithological units from the surface down to depth z, and to combine this information with the thickness of each to estimate the insulating properties of the sedimentary column as a whole.

No thermal conductivity measurements or data are available for the study area. Conductivities were, however, measured on Miocene and Oligocene formations in the Rhine Valley north of the area by Sattel (1980), and conductivity values for Mesozoic formations were obtained from the literature (Clauser, 1988; Kappelmeyer et al., 1974; Werner, 1975). These conductivity values are not corrected for porosity or temperature (Table 24).

The cumulative thermal resistance at various depths was calculated for selected wells in the Pechelbronn-Soultz Basin and graben centre (Appendix 16) and plotted on a regional profile D-D' (Figure 87b). The thermal resistance curve for -1000 m depth, which depends on both the thickness and thermal conductivity of the overlying rocks, shows no significant variations along the profile D-D'. Variations would reflect both structural and lithological changes.

Heat flow, q_z, is estimated as follows. For a well in which there is only one temperature measurement, interval i is the depth range from the surface down to the depth of measurement, and only one heat flow value may be obtained. When temperature measurements are available for more than one depth, the heat flow across measured depth interval can be calculated. At conductive thermal equilibrium, the heat flow should remain constant over the entire depth range and also laterally over the area (Appendix 16). Heat flow values are estimated for T_i as the difference between the mean surface temperature and the deepest BHT and then plotted on a regional map (Figure 87a) and profile D-D' (Figure 87b).

The estimated heat flow values for the study area exceed the basal calculated heat flow values of 82 ±20 mW/m^2 and vary laterally. Heat flow values are highest in the Soultz region (>200 mW/m^2) and decline to the west and east. Near the Rhine River heat flow values of about 100 mW/m^2 have been calculated. The pattern of the heat flow contours on Figure 87a is comparable to the geothermal gradient distribution outlined in Figure 85. Profile D-D' (Figure 87b) clearly demonstrates the positive heat anomaly at the Soultz-Hermerswiller Compartments. Near the Hochwald, however, heat flow values are lowest (about 50 mW/m^2), reflecting the downward movement and influx of cold meteoric groundwater from this recharge area. The Soultz geothermal anomaly is a local phenomenon and unique in comparison with other observed and discussed anomalies in the Upper Rhine Graben. The Landau region 34 km north of Soultz (Figure 70) is known for its super-geothermal gradients but its estimated heat flow does not exceed values higher than 160 mW/m^2 (Parini et al., 1980; Sattel et al., 1980; Werner et al., 1974; Werner et al., 1980).

A sensitive test for non-conductive heat flow is to examine the variation of heat flow with depth. As previously stated, if conductive equilibrium exists, there should be no variation with depth. Vertical heat flow changes may be studied for boreholes with temperature measurements at different depths. Figures 48, 49 and 50 show heat flow values vs. depth for 3 wells (4515, 4616, 4776) calculated for depth intervals for which temperature measurements were available. The depth-dependent heat flow changes demonstrate the non-conductive thermal conditions in the basin.

Wells 4515 and 4616 are located in the Soultz and Hermerswiller Compartments; profile V (Figure 78) shows the geology and the isotherms associated with these wells. For well 4515 the highest heat flow values are estimated for a shallow depth interval in Tertiary formations (Figure 48). From profile V (Figure 78) it is deduced that the Tertiary is in part incised by secondary faults and hence that the extremely high heat flow values are caused by fault-enhanced ascending groundwater flow movement and transport of heat to shallow depths. The depth-dependent heat flow distribution in well 4616 (Figure 49) is different. Here, high heat flow values coincide with the Soultz Fault and the dissected hydrostratigraphic unit 3 (*Lettenkohle* and *Muschelkalk, Buntsandstein* Aquifers). Obviously, at this depth range the faulted and fractured aquifer is an excellent groundwater conduit for transfering heat upward by convection.

This technique was also used to analyse a third well 4776 located 1200 m east of Soultz at Rittershausen (Figures 70 and 71). The findings show that heat flow does not change significantly over a depth range of 560 to 1300 m. This is due to missing temperature measurements for this depth interval and does not imply heat transport by conduction. For a depth range >1400 m a dramatic heat flow increase associated with a fault zone and hydrostratigraphic unit 3 is observed, indicating ascending flow of groundwater towards Soultz.

Perhaps a more instructive way to examine depth-dependent heat flow changes is to compare the actual temperature log derived from BHT values at different depths in a well with profiles calculated on the basis of what would be expected if the heat flow were at conductive equilibrium. Figure 51 shows the calculated subsurface temperatures for a basal heat flow of 82 mW/m^2 derived by Clauser (1988), for a mean heat flow value of 130 mW/m^2 characteristic for other geothermal anomalies in the Upper Rhine Graben (Hänel, 1979b) and for a heat flow value of 200 mW/m^2, as estimated for the Soultz region. The diagram shows that heat flow must vary with depth and that values of >200 mW/m^2 are required to achieve the subsurface temperature measured in well 4616 and the temperatures in the Soultz-Hermerswiller Compartments in general.

One-dimensional Peclet number and vertical seepage velocities

The temperature distribution in areas of ascending or descending groundwater flow can be characterized by the dimensionless Peclet number, Pe, (Domenico et al., 1973; Kamp, van der , 1983):

$$Pe = \frac{\rho_w c_w v_z L}{\kappa},$$

where, ρ_w is the groundwater density (kg/m^3), c_w is the heat capacity of water (J/kg^oC), v_z denotes the vertical seepages velocity (m/s), L is the depth of the groundwater flow system and κ is the thermal conductivity of the formation (W/m^oC).

The Pe is essentially the ratio of the convective to the conductive heat transfer in a vertical column. If Pe is much smaller than 1.0, the temperature field is not disturbed by vertical groundwater flow. If Pe is much larger than 1.0 the temperature will be strongly affected by ascending or descending groundwater flow.

One method of determining Pe and the discharge velocity is to apply the graphical solution given by Bredehoeft et al. (1965). The suggested method of analysis requires three or more temperature measurements along a vertical section of a semiconfined layer. The values for $(T_z-T_o)/(T_L-T_o)$ are plotted against the depth factor z/L values, using the same scale as the type curves given by Bredehoeft et al. (1965) and superimposed on the type curve set, where: T_z is the temperature measured at any depth z; T_o is the uppermost temperature measurement; T_L is the lowermost temperature measurement; and L is the length of the vertical section over which temperature measurements extend. Well 4616 (Appendix 15; Figure 52) was chosen for this estimation of the Peclet number for the Soultz region, because this was a region in which upward moving groundwater and highest temperature disturbance by convection could be expected. A Peclet number between 0.5 and 1.0 was obtained using the graphical method by Bredehoeft et al. (1965). A Peclet number of 0.5 indicates that one half of the total heat transport is by forced convection. The vertical discharge velocity for groundwater in hydrostratigraphic unit 3 at this depth interval (with $\rho_w = 1070$ kg/m^3, $c_w = 4.2$ kJ/kg^{o}C and $\kappa = 2.7$ W/m^{o}C) is about $7.5\text{x}10^{-9}$ m/s, or 2.3 cm/y.

A rough approximation of the vertical seepage velocity in the region of positive heat flow anomaly at Soultz can also obtained using of the heat transfer equation for depth z, assuming steady-state conditions and uniform permeability (after Lachenbruch et al., 1977):

$$\frac{\partial q}{\partial z} = -q\frac{\rho_w c_w v_z}{\kappa} ,$$

where q denotes heat flow. If the lower boundary of the groundwater system, in which groundwaters circulate, is taken to be at a depth z= L, integration of the equation above leads to:

$$v_z = \frac{\kappa}{L\rho_w c_w} \ln\frac{q_o}{q_L} ,$$

where q_o and q_L are the heat flow values at the upper and lower boundaries of the system, respectively.

For the Soultz region the vertical flow velocity can be approximated by assigning the lower boundary as the top of the unweathered granitic basement at about 1500 m depth with a basal heat flow, q_L, of 82 mW/m^2 and a mean heat flow, q_o, for the Soultz Compartment of 250 mW/m^2, which was derived by the thermal resistivity method. Using further assumptions of an average thermal conductivity of 2.7 W/m^{o}C for the sedimentary column, a density of 1070 kg/m^3 and heat a capacity of 4.2 kJ/kg^{o}C for the groundwater, an approximate velocity of $4.5\text{x}10^{-9}$ m/s or 1.4 cm/y is obtained.

To estimate the vertical seepage velocity were in hydrostratigraphic unit 3 we used the heat flow values from well 4616 (Appendix 16) and obtain a velocity of about $7.9\text{x}10^{-9}$ m/s or 2.5 cm/y.

When these estimated flow velocities were substituted in the above equation Peclet numbers between 1.1 and 0.9 were obtained, indicating that the heat transfer is mainly controlled by convection.

4.3.5 Conclusions

The geothermal gradients and subsurface temperatures in the study area are anomalously high; the thermal positive anomaly in the Pechelbronn-Soultz Basin is even more pronounced than is observed in others parts of the Upper Rhine Graben.

Forced convective heat flow by groundwater movement is a dominant transport mechanism of heat in the entire graben; this is reflected by disturbances of the temperature and heat flow field laterally and with depth.

Subsurface temperatures and heat flow increase radially towards the Kutzenhausen-Soultz region from the west, east and southeast. The observed distribution of thermal phenomena is caused by the groundwater flow channelling effect of fault zones. The Hermerswiller Compartment, known for its highest fault density and fractured Mesozoic formations, constitutes a pronounced positive temperature anomaly and is a region of discharging hot and saline groundwater ascending to the surface with a seepage velocity of about 2 cm/y.

Fault zones in the Pechelbronn-Soultz Basin function as conduits for groundwater to shallower depths and are indirectly responsible for the abnormal geothermal conditions in the basin. It appears that the extent and trend of the principal faults in the basin direct or focus heat flow. The Soultz region seems to function as a "focal discharge area" and as a zone of disposition of heat and inorganic matter.

The proximity of the Hochwald as a local recharge region is reflected by lower thermal gradients and a negative temperature anomaly along the western periphery of the Pechelbronn-Soultz Basin. Cold descending groundwater, topography-driven by the Hochwald recharge region, infiltrates along and across the Rhine Fault into the Pechelbronn-Soultz Basin from the west lowering subsurface temperatures.

The distribution of subsurface temperatures denoted as a hydrogeologic phenomenon, proved to be an excellent tool to determine the groundwater flow pattern in the graben. It confirms the earlier conclusion derived from examination of hydrochemical phenomena that the groundwater flow trend is indeed from the west towards the Pechelbronn-Soultz Basin and, in addition, the subsurface thermal conditions reveal that groundwater flow can also be expected from the east toward the basin.

5. Analysis of the Gravity-Driven Groundwater Flow Regime

5.1 Theoretical Considerations

With depth and laterally the density of formation water can vary regionally within the same hydrostratigraphic unit and from unit to unit due to temperature variations and different concentrations of dissolved solids. Thus, in principle, it is not possible to define a potential field driving groundwater flow, or to derive flow directions using potentiometric surfaces.

Given Darcy's law, the specific discharge or seepage velocity, $\bar{q}$, for steady state conditions can be expressed in the generalized form (de Marsily, 1986):

$$\bar{q} = -\frac{k}{\mu}\left[\text{grad } p + \rho g \text{ grad } z\right],$$

where k is the intrinsic permeability tensor (L^2), μ is the dynamic viscosity of the fluid ($ML^{-1}T^{-1}$), p is the fluid pressure ($ML^{-1}T^{-1}$), g is the acceleration due to gravity (LT^{-2}), z is the vertical axis directed upward, and grad z is a vector of coordinates (0, 0, 1).

By defining a reference constant density, the above relationship can be simplified for incompressible fluids as follows:

$$\bar{q} = -\frac{k\rho_o g}{\mu} \text{ grad } h + \frac{\rho_o - \rho}{\rho_o} \text{ grad } z, \quad \text{or}$$

$$\bar{q} = -K \text{ grad } h + \frac{\Delta\rho}{\rho_o} \text{ grad } z,$$

where $\Delta\rho$ is the density difference with respect to a reference density ρ_o, and h is the hydraulic head (L) and K is the hydraulic conductivity tensor (LT^{-1}). Hydraulic head is defined as the water level, measured relative to a standard datum:

$$h = z + \frac{p}{\rho_o g};$$

and hydraulic head is a measure of fluid potential

$$\Phi = gh .$$

Groundwater flows through a porous medium in response to fluid potential gradients: it moves from positions of high potential to positions of low fluid potential (Hubbert, 1940).

Darcy's law explicitly shows that fluid flow is driven by two forces. The external force is due to hydraulic head differences that` normally originate from the topographic relief. The internal force is the buoyancy caused by density differences within the fluid.

The most common constant density value used is freshwater density $\rho_o = 1000\ \mathrm{kg/m^3}$. The equivalent freshwater hydraulic head is defined as the water elevation, measured relative to a standard datum (mostly sea level) in a well filled with freshwater to a level high enough to balance the existing fluid pressure at a point of measurement. Use of equivalent freshwater head, rather than fluid pressure is discussed by several researchers including DeWiest (1965); Hubbert (1953) and Lusczynski (1961).

Lateral flow in a near-horizontal hydrostratigraphic unit saturated with a variable density fluid can be represented by the hydraulic gradients, q_x and q_y, of a reference potentiometric surface, h:

$$q_x = -\frac{k\rho_o g}{\mu}\frac{\partial h}{\partial x}; \qquad q_y = -\frac{k\rho_o g}{\mu}\frac{\partial h}{\partial y}\ .$$

Lusczynski (1961) showed mathematically that horizontal hydraulic head gradients are unaffected by vertical density variations of groundwater, whereas vertical hydraulic gradients are misrepresented by the use of a hydraulic head based on a reference constant fluid density. Vertical flow in a hydrostratigraphic unit can be due to both external and internal forces:

$$q_z = -\frac{k\rho_o g}{\mu}\left[\frac{\partial h}{\partial z} + \frac{\Delta\rho}{\rho_o}\right]$$

In a system in which z is oriented downward and is negative, the vertical component of specific discharge is:

$$q_z = -\frac{k}{\mu}\left[\frac{\partial p}{\partial z} - \rho g\right],$$

which allows the analysis of vertical groundwater motion in a groundwater flow system by using pressure vs. depth plots. If the slope of the pressure curve as a function of depth is equal to ρg there is no vertical flow and the line is called hydrostatic. The rate at which pore pressures increase with depth, dp/dz, is called the vertical pore-pressure gradient which for freshwater is 9.81 kPa/m.

Tóth (1978) demonstrated how pressure-depth and fluid-density data could be plotted and used to determine the occurrence of ascending or descending groundwater flow based on the distribution and orientation of pressure-depth values relative to the slope of the hydrostatic pressure gradient (see Appendix I). If a flow system contains variations in fluid density with depth, a hydrostatic pressure gradient can be determined which incorporates these variations and, therefore, accounts for the variable density of flow regime. A vertical pressure gradient greater than 9.81 kPa/m is called superhydrostatic and indicates ascending groundwater flow, whereas a vertical pressure gradient lower than 9.81 kPa/m is called subhydrostatic and indicates downward groundwater motion.

5.2 Database

Available data used for the analysis of the groundwater flow regime constituted levels or pressures of formation fluids (Appendix 17). Water level measurements were taken from SAEM well reports, pressures measured by drill stem tests were given by SAEM and PREPA reports, (documented in the 1950's). More recent DST measurements were made available by TOTAL Exploration, Paris.

For these subsurface hydrodynamic fluid parameters to be accepted for interpretation, measured levels and pressures had to satisfy two criteria, namely, that they represented undisturbed and stabilized conditions. It was difficult, if not impossible sometimes, to judge the quality of measurements due to lack of technical details on the measurements themselves. SAEM well reports included pre-flow and shut-in times only. However, PREPA reports did also occasionally document DST pressure charts.

A classification code was implemented based on the quality of the data (Appendix 17). A quality grade 1 indicate that water levels and pressures were measured at stabilized, undisturbed conditions. Grade 3 mean that the values were of poor quality, disturbed and not stabilized due to failed packers, nearby production wells, influx of formation waters from different levels and failed cement casings. Grade 2 indicate that caution should be applied when using this datum point.

The most efficient method of culling the data was to plot the equivalent hydraulic head on potentiometric maps and hydraulic cross-sections for various depth intervals. Data which did not complement a regional hydraulic heads pattern were eliminated, if no apparent geological or hydrogeological causes, e.g., fault barrier, lenses, were given.

Although, the data are of medium quality only, it was possible to derive a general picture of the groundwater flow pattern in the basin.

5.3 Interpretation of the Steady-State Groundwater Flow Regime

The hydrogeological groundwater conditions found in the study area are the same as those often observed in intermontane basins with a mature (i.e., non-compacting) sedimentary fill. The sedimentary rocks are fully saturated with water and the movement of this fluid is gravity-driven induced by the topographically elevated graben shoulders. The present groundwater conditions are at steady state since they represent the youngest stage of an effectively continuous uni-directional evolution driven by gradually increasing topographic-elevation differences between the subsiding graben floor and rising graben shoulders since the first rifting phase about 40 Ma ago (see also shoulder uplift-rate Chapter 2.2).

The groundwater in the basin is of variable density. In practice, if the fluid density is variable, the assumption commonly made is that the fluid flow is nearly horizontal and that buoyancy effects are very small and, therefore, negligible. This assumption had to be evaluated for the variable-density groundwater in the study area. Densities can vary between 1000 to 1070 kg/m^3 in the Pechelbronn-Soultz Basin and can reach values of up to 1100 kg/m^3 in the graben centre (Chapter 4.2.3.2).

Davies (1987) has shown that it is not the absolute magnitude of the density-related error term, but rather the relative magnitude of this term vs. the magnitude of the equivalent freshwater head that determines whether buoyancy effects will be significant in a given situation. A practical measure of the relative magnitude of buoyancy effects is the dimensionless ratio of the magnitude of the equivalent freshwater head, which is a ratio also mentioned by Bear (1972). The Driving-Force-Ratio (DFR) described by Davies (1987) as the relative strength of two driving forces is defined by:

$$\mathrm{DFR} = \frac{\Delta\rho}{\rho_0} \frac{|\mathrm{grad}\ E|}{|\mathrm{grad}\ h_f|} ,$$

where $|\mathrm{grad}\ E|$ is the magnitude of the elevation gradient of the hydrostratigraphic unit and $|\mathrm{grad}\ h_f|$ is the magnitude of the freshwater hydraulic gradient. If flow parallels the upper and lower boundaries of the aquifer, then $|\mathrm{grad}\ E|$ is equal to the slope of the aquifer. Assuming an isotropic medium, Davies (1987) has shown that the value DFR = 0.5 is the approximate threshold at which density-related gravity effects may become significant.

The aquifer system in the Phanerozoic section of the Upper Rhine Graben study area is not horizontal. The general dip is to the east and southeast with an verage angle of 5^0 (Chapter 2.3.2). The density of formation water is variable in the hydrostratigraphic units as well as between hydrostratigraphic units. Therefore, some buoyancy-related effects must be present in the flow. In order to assess the importance of these effects the DFR was computed on a regional scale for hydrostratigraphic group I and III.

The regional hydraulic gradient of 0.02 for the artesian hydrostratigraphic group I can be crudely estimated by calculating the topographic elevation difference between the Vosges recharge area (700 m) and the Soultz recharge (150 m) area over their lateral distance (29 km). Taking the density value to be 1070 kg/m^3, the DFR value is about 0.3, which is less than the threshold value. For the hydrostratigraphic group III the hydraulic gradient between the Hochwald recharge area and the Pechelbronn-Soultz Basin is about 0.035 and the DFR is about 0.2. Locally, the hydraulic gradients can be much higher which means that the DFR values will be even smaller and it can thus be concluded, that buoyancy effects due to density differences of the groundwater in the basin are negligible and that topography-driven groundwater dominates the flow system. Consequently, equivalent freshwater heads can effectively characterize the flow system.

5.3.1 Hydraulic head distribution and inferred groundwater flow patterns

Pressures and water levels were converted to equivalent freshwater hydraulic heads ($\rho_f = 1000\ kg/m^3$) according to the formula:

$$h_f = z + \frac{p}{\gamma_f}, \text{ where } \gamma = \rho_f g .$$

Water levels are measured below land surface and in most cases the density of the water in the well pipe was given, otherwise the density was estimated (see Chapter 4.2.3.2). The real (environmental) hydraulic head and the pressure are calculated, and converted to equivalent freshwater hydraulic head values. Figure 53 defines the parameters involved.

Appendix 17 lists all given and calculated parameters, and the equivalent freshwater head distribution is shown for six depth intervals on a regional distribution map (Figure 88) and a locally scaled map for hydrostratigraphic unit 3 (Figure 89).

Regarding the use of potentiometric surfaces for fault-severed hydrostratigraphic units in rift basins the following two premises should be noted:

(1) A potentiometric map must be related to a single aquifer or to a defined depth range. Other aquifers or the same aquifer but displaced by a fault, deeper or lower in the section will have different potentiometric surfaces which may exhibit heads that are higher and lower than the one of immediate concern. If a potentiometric map is drawn from data obtained from different aquifers, the surface obtained is a composite of potentiometric measurements. In the study area a hydrostratigraphic unit is down or upthrown and can be disconnected by a fault zone. Hydraulic heads measured at the same depth interval in the footwall and hanging wall are not always associated with the same hydrostratigraphic unit. Thus, sudden changes in hydraulic head may identify a fault-barrier or a change in lithology in the foot or hanging wall. It is important to understand the structural position of the investigated hydrostratigraphic units in the basin and a connectivity diagram is a helpful tool to estimate the continuity of the unit and support a potentiometric surface interpretation.

(2) It is assumed that flow in the aquifer is horizontal, that is, parallel to the upper and lower confining layers. Thus, there is an assumed absence of a vertical gradient in the aquifer. If a piezometer is placed in such an aquifer, and hydraulic head is observed, hydraulic head is presumed not to change with increasing depth of piezometer penetration. Hence, the potentiometric surface is a projection of vertical equipotential planes into the horizontal plane. Although there are numerous conditions that give rise to vertical gradients within a single aquifer, it has to be emphasized that the condition of completely horizontal flow (or an absence of vertical gradients) is frequently assumed when using potentiometric surface maps.

This premise, however, should not be used thoughtlessly in the construction and interpretation of potentiometric maps of hydrostratigraphic units in fault-severed groundwater basins. A fault can implement a vertical gradient on groundwater motion when it functions as a conduit to cross-formational movement of groundwater, channelling groundwater vertically up or downwards to adjacent hydrostratigraphic units, or when it operates as a barrier deflecting groundwater flow to lower or higher units. Especially in regions of intensive faulting and fracturing, e.g. Soultz-Hermerswiller Compartments, a strong vertical gradient can be expected, invalidating the use of potentiometric surface maps in this region. Therefore, potentiometric surface maps of hydrostratigraphic units in tectonically disturbed basins are best interpreted in conjunction with hydraulic cross-sections and their geologic-structural framework as well as pressure vs. depth or pressure vs. elevation diagrams.

The basinal flow pattern (Figure 88) in the study area can be inferred on a regional scale from the distribution of equivalent hydraulic head. The hydraulic head distribution map shows dominant head values obtained in points of measurements for specific elevation intervals. Six elevation ranges were chosen according to the depths of original pressure measurements in the wells.

Potentiometric surface elevations show that on a regional scale, hydraulic heads decline toward the valley from the west and east and with decreasing depth of measurement below the land surface: flow appears to be directed towards the Pechelbronn-Soultz Basin and ascending in the graben. Water levels rise to topographic elevations well above the valley's floor (artesian wells), from measurement points at -250 m and lower. It seems that the entire graben acts as a regional discharge region.

Due to lack of hydraulic head data in the eastern part of the graben, the approximation for the basinal Black Forest flow system of hydrostratigraphic units within this part of the graben is based on numerical flow simulations conducted by Garven et al. (1987) and Trippler (1988). Their models confirm my interpretation of the regional flow pattern in the study area. In the Rhine Graben area the two principal flow systems generated by the two major highlands converge towards the Pechelbronn-Soultz Basin. It appears that this sub-basin acts as a focal discharge region. Groundwater is funnelled towards the Pechelbronn-Soultz Basin by the principal fault systems and is deflected upward, ascending mainly along and across the Kutzenhausen-Soultz fault zones. The region of the Soultz-Hermerswiller Compartments, known for their high fault density, is the most prominent discharge area in the graben. Profiles IV and V show the groundwater flow pattern in this region (Figures 77 and 78).

The flow direction, while it appears relatively homogeneous at the regional scale becomes very complex at a local scale, owing to the heterogeneities in the rock's permeability due to stratification, faulting, and lensing. Intermediate and local flow systems associated with depressions in the valley are superimposed and merge with the regional flow system (profiles I, III, IV, V, VI, Figures 73, 75, , 77, 78, 79). Flow systems generated by local topographic relief can reach depths of several hundred meters but do not penetrate the basal Oligocene (*Couches Rouges*).

5.3.2 p(d) and p(z) diagrams

Undisturbed and stabilized pore pressures of the Upper Rhine Graben study area are plotted versus depth on a scatter diagram (Figure 54). The p(d) plot illustrates vertical pore-pressure gradients for densities of freshwater (1000 kg/m^3) and brine (1070 kg/m^3), respectively, and shows that pore pressures increase linearly with depth. Pore pressures are generally superhydrostatic relative to the freshwater vertical hydraulic gradient. Subhydrostatic pore-pressures are encountered only in the *Lettenkohle* formation in the Pechelbronn-Soultz Basin. A linear pore pressure increase with depth indicates that the formations are hydraulically continuous and that groundwater in the water-saturated basin is free to move cross-formationally.

A p(d) diagram displaying a regional pore-pressure pattern of a single hydrostratigraphic unit or several hydrostratigraphic units should not be used in the derivation of groundwater flow directions in the aquifer(s). Rather, p(d) and p(z) plots of locally confined areas with good well control or plots of single wells with multiple pressure measurements should be utilized in the analysis of groundwater flow directions (Maccagno, 1991). This concept was applied to the Kutzenhausen-Soultz region, the only area in the study with good well control. Pore pressures of the *Lettenkohle*, *Muschelkalk* and *Buntsandstein* in the Kutzenhausen-Soultz-Hermerswiller Compartments are plotted on p(d) and p(z) scatter diagrams (Figures 55 and 56).

The patterns of the data point distributions in the p(d) and p(z) diagrams are very similar. This indicates that the groundwater flow system is in equilibrium with present-day land surface boundary conditions, i.e., is at steady state.

On the p(d) plot (Figure 55), vertical pore-pressure gradient lines connect points of multiple pressure measurements of a Mesozoic aquifer taken in one single well or in several wells in nearest vicinity. A local-scaled hydraulic head distribution map superimposed on the structural map of hydrostratigraphic group I shows the position of the points of measurement in the Mesozoic aquifers in relation to the structural complexity of the aquifers and their association to the Kutzenhausen-Soultz fault zones (Figure 89). The slope of the lines determines the directional motion of groundwater. Six vertical pore-pressure gradient lines are shown on the diagram. Superhydrostatic pore pressures and superhydrostatic vertical pore-pressure gradients (lines 1, 2, 2a, 3; Figure 56) indicate ascending flow in the *Buntsandstein* and *Muschelkalk* aquifers of the Hermerswiller Compartment associated with faults SF3, SF4 and SF5 (Figure 89). Line 2a shows upward flow, associated with a fault, from the *Buntsandstein* to the *Muschelkalk* between wells 4585 and 4590 (Figure 89). The vertical pressure gradient 4 is hydrostatic and indicates horizontal flow between wells 4606 and 4613 along the Soultz Fault SF3. These wells are situated in a fault block of lesser fault intensity. Pore pressures in the *Lettenkohle*, overlying the *Muschelkalk* are hydrostatic and subhydrostatic. Production draw-down might have caused a formation pressure reduction at some sites. Nonetheless, line 6 connects points of pressure measurements for a single well 4602 showing a slightly superhydrostatic gradient and upward flow from the *Muschelkalk* to the *Lettenkohle*.

On a p(z) diagram three parallel best-fit curves with the slope of a hydrostatic pressure gradient are drawn through the data points of the Mesozoic aquifers. The vertical hydrostatic gradients intersect the vertical axis at elevations well above the average land surface elevation in the Kutzenhausen-Soultz region, indicating that formation fluids in the wells rise freely to the surface under artesian conditions. Also, the parallel lines confirm that flow in the area is indeed upward from the *Buntsandstein*, *Muschelkalk* to the *Lettenkohle*

5.4 Conclusions

In summary the conclusions are that:

(1) two principal flow systems generated by the Vosges and Black Forest mountains converge from the west and east towards the graben valley;

(2) the Upper Rhine Graben valley functions as a regional discharge area;

(3) faults have a pronounced effect on the direction and pattern of groundwater flow;

(4) associated with a region of highest fault density, groundwater flow is focussed towards the Pechelbronn-Soultz Basin;

(5) the two principal flow systems converge from the west and the east towards the Kutzenhausen-Soultz region and groundwater is directed upward and channelled across and along the Kutzenhausen and Soultz Faults discharging in the region;

(6) the Kutzenhausen-Soultz area is a region of concentrated groundwater discharge and is defined as a focal discharge region;

(7) local flow systems are generated by topographic variations in the basin and groundwater is known to reach the basal Oligocene.

6. Petroleum Hydrogeological Conclusions

In the intermontane Rhine Graben basin a dynamic inter-relationship exists between groundwater flow patterns, hydrochemical and geothermal anomalies, petroleum migration and deposition and the fluid-conductance of fault zones.

In this context, the most significant petroleum hydrogeological phenomena are the spatial relationship and coincidence of oil deposits with locally intensified cross-formational discharge of geologically young groundwaters of meteoric origin and hydrochemical as well as geothermal distribution patterns (e.g. Figure 76 profile B-B'). A genetic role of topography-induced groundwater flow systems is evident, and it provides various keys to hydrogeologically based exploration techniques that are particularly applicable in these environments. In brief, it validates the basic thesis and predicted practical ramifications of the hydraulic theory of petroleum migration, the evaluation of which was one of the principal objectives of this study.

According to the hydraulic theory (Tóth, 1980), geologically mature basins are hydraulically continuous environments in which the relief pattern of the water table generates systems of groundwater flow with patterns modified by permeability differences (see Appendix I). Gravity-induced cross-formational flow is the principal agent in the transport and accumulation of hydrocarbons. The mechanism becomes operative after compaction of sediments and the concomitant cessation of primary migration, allowing subaerial topographic relief to develop. Hydrocarbons from source or carrier beds are then moved along well-defined migration paths toward discharge foci of converging flow systems, and may accumulate en route in hydraulic or hydrodynamic traps. Accordingly, deposits are expected and observed to be associated preferentially with ascending limbs and stagnant zones of flow systems. Hence, they are characterized by relative potentiometric minima, downward increase in hydraulic heads possibly reaching artesian conditions, reduced or zero lateral hydraulic gradients, and relatively high groundwater salinity. Continuous flow of meteoric waters imports hydrocarbons into traps until the trap capacity is reached. The excess becomes source material for new accumulations.

The theory also predicts a genetic relation and spatial correlation between oil deposits, on the one hand, and positive geothermal anomalies, chemically reduced chimneys, sulfide ore formation and marshy and saline surface conditions, on the other. In Figure 57 (Appendix I) a graphical summary of the hydraulic theory is presented in a form slightly modified from the original version (Tóth, 1980, Fig. 44). For comparison, the petroleum hydrogeological conditions as observed in the Upper Rhine Graben in general, and the Pechelbronn-Soultz area in particular, are shown in Figure 58; a convincing similarity between the theoretical and the observed conditions is evident. It must therefore be concluded, that the hydraulic theory offers a viable explanation for the genesis of the oil deposits and associated hydrogeological phenomena in the study area and also, in general, in other geologically mature intermontane basins.

Specifically, the relationships between petroleum accumulation and hydrogeological processes and phenomena in the study area have developed as follows (Figure 59). Source rocks were deposited during the Early Jurassic. These source rocks experienced two episodes of enhanced heat flow during their maturation history which coincided with the two main rifting phases since the submersion of the Rhine Graben. Vitrinite reflectance data has also revealed that the paleothermal gradient in this segment of the Upper Rhine Graben is not older than about 3 Ma (Espitalie, 1979; Teichmüller et al., 1979). Ever since rifting began, the uplifted graben shoulders have functioned as the major recharge regions, and groundwater has been moving from the graben's shoulders towards its centre. After the last main rifting phase in the mid-Pliocene, groundwater flow was allowed to intensify and to focus its flow along and across rejuvenated and open fault systems towards the Pechelbronn-Soultz Basin. The presently observed flow system and phenomena are young (≈ 3 Ma) since they are related to the youngest fractures and faults systems developed during the last rifting phase and the current shear motion in the graben.

The Oligocene and Jurassic source rocks are immature in the Pechelbronn-Soultz Basin, although the geothermal gradients are anomalously high. Wells Reimerswiller 1 and Rohrlach 1 (Figure 70) east and south of the basin contain mature Jurassic source rocks. Migration of Jurassic oil to the Pechelbronn-Soultz region must have occurred over a minimal lateral distance of approximately 8 km. Time-Temperature-Index calculations and a maturation-geohistory diagram based on Lopatin's method (Waples, 1980) using a time-temperature maturation modeling program (Howell (1985), courtesy of Dr. H. Machel) for well Rohrlach-1 revealed that oil migration from Jurassic source rocks started in the Upper Oligocene about 25 Ma ago (Figure 60).

It is likely that in the last ≈ 3 Ma since the cessation of the 2nd rifting phase groundwater flow has been focussed towards the Soultz discharge area, transporting organic and inorganic matter, as well as heat. The transported heat has accumulated in regions where the laterally moving groundwater from the west and east is forced to turn upward: primarily through the heavier fractured fault blocks and along conductive major faults. Similarly, dissolved matter has been transported basinward and close to, and in the vicinity of, areas of intensive discharge, e.g. the Kutzenhausen-Soultz region.

The amount of water that has been available for the transport of matter to date may be estimated in terms of basinal pore volumes. To this end, the time that has elapsed since organic matter maturation (≈ 25 Ma) of Jurassic source rocks is compared with the average subsurface residence time of the groundwater during its travel from recharge to discharge areas (i.e., the duration of one full cycle of pore-volume flushing). Assuming 30 000 years for average residence time, a "water exchange number" (Kartsev et al., 1964) of N = (25 x 10^6/30 x 10^3) = 833 is obtained, indicating that approximately 830 times the basinal rock pore volume of water has been available for hydrocarbon transport, accumulation and degradation in the Pechelbronn-Soultz Basin since maturation. The water exchange number was calculated for the average ^{14}C age travel time of the Vosges flow system (Chapter 4.2.4.2) to the Pechelbronn-Soultz Basin. It is expected that the average groundwater residence time of the Black Forest flow system is higher and the water exchange number slightly lower.

The principal area of collection and deposition of migrated hydrocarbons coincides with the region where the oppositely directed regional flow systems from the Vosges and Black Forest converge in the Pechelbronn-Soultz Basin which functions as a focal discharge area within the regional Rhine Graben discharge region. Since mature Jurassic source rock is situated in the deeper parts of the graben, east and south of the Pechelbronn-Soultz Basin, this implies that groundwater of the Black Forest flow system alone was the main agent of transporting hydrocarbons to their sites of deposition, i.e., the hydrodynamic force is additive to the buoyancy force of the hydrocarbons. En route towards the Pechelbronn-Soultz Basin hydrocarbons are entrapped by fault seals near Schirrhein and Soufflenheim (Figure 70).

In the Pechelbronn-Soultz region groundwater flow is channelled upward and its fluxes increase along principal fault zones which are highly conductive in the hydrostratigraphic group I. Nevertheless, part of the ascending formation fluids will be forced to flow through the intergranular pores of unfractured rocks.

Several entrapment mechanisms cooperate under these circumstances to disaccomodate transported hydrocarbons from the carrier waters. At places where they are locally constricted, fault planes may deflect feed-stock fluids into highly permeable sandstone lenses and horizons that they dissect. Mechanical filtering at, and due to, grain size boundaries as well as capillary pressure differences will tend to retain oil and allow the water to pass through.

Oil is entrapped in structural highs of the *Lettenkohle* (HSU 4) and *Muschelkalk* (HSU 3) reservoirs near Pechelbronn, Kutzenhausen and Soultz by their principal faults (Chapter 2.3.3.2). These faults act locally as sealing faults and juxtaposition faults (see Appendix V on sealing mechanisms). The lower *Keuper* is a low permeability cap-rock seal. Formation waters flow upward in hydrostratigraphic unit 3 and are deflected into the

Muschelkalk and *Lettenkohle* carrier beds of a principal fault's footwall disaccommodating hydrocarbons. Groundwater continues to flow downdip. These oil pool are only a few metres thick and wedge out to the east. It is conceivable that, even today, disaccommodation and remigration of hydrocarbons in these reservoirs continues.

The major oil reservoirs in the *Zone Dolomitique* and *Pechelbronner Schichten* of the Pechelbronn-Soultz Basin are intimately associated with faults and sandlenses.

As was seen earlier, mineralization and temperatures of formation waters increase toward, and are greatest in the Kutzenhausen-Soultz region. Groundwater-related pressure, thermal and chemical conditions greatly enhance the effectiveness of the lithological and structural trapping potential in discharge areas. The sudden and rapid increase in pressure, temperature and salinity owing to the upward turn of the groundwater flow paths in discharging systems causes exsolution of hydrocarbons (Roberts, 1980). The increase in formation water salinity augments the entrapment potential in discharge areas due to an inverse proportionality between hydrocarbon solubility and water mineralization.

In addition to creating hydrocarbon deposits, regional groundwater flow gives rise to phenomena that may be used in exploration. Hydrogeologic phenomena that seem to be related to petroleum deposits in the study area through groundwater flow are: positive temperature anomalies both at depth and near the land surface; oil springs; regional anomalies of formation-water salinities; near-surface occurrence of brines (presumably migration along fractures from depth) and saline springs often containing H_2S; microseeps and/or anomalous contents of hydrocarbons in soils and groundwater (Gerling, 1988); and localized wetlands which, however, are known in the area only from earlier records because land cultivation and urban settlements have eliminated them. Other hydrogeological indicators of petroleum deposits which can be expected in the study area but have not been examined, include: stressed vegetation growth; anomalies of electrotelluric potential and increased electrical conductivity associated with chemically reduced (i.e., organic rich) rock columns; and sulfide ore formation and near-surface anomalies of heavy metals (particularly Ni and V).

7. Applied Petroleum Hydrogeology in the Pechelbronn-Soultz Basin

It was stated in Chapter 1 and explained in Appendix I that the hydraulic theory can be applied to the exploration of petroleum in a basin, or may be utilized for the development of known oil fields. Two case studies will be presented:

7.1 Observed crude oil compositions in relation to groundwater flow

In this section the organic chemistry and character of the oils in Mesozoic and Tertiary reservoirs in the Pechelbronn-Soultz Basin are interpreted in terms of groundwater flow patterns. This petroleum hydrogeological analysis may provide guidelines for the development or exploration of potential reservoirs in a known oilfield district, where it is important to predict the oil quality of possible reservoirs.

Although, the SAEM organic chemistry data made available by SGAL in Strasbourg are outmoded, and the correlation index method used here to classify the oils' compositional characters is outdated, it was possible nonetheless, to detect a distinct pattern in the crude oil composition which can be explained in terms of groundwater flow.

Characteristic patterns related to a crude oil's chemical type can be deduced semi-quantitatively by the Hempel method of distillation using the correlation index (CI) developed by Smith (1940). Typical correlation index curves are obtained when plotting the CI values versus the number of successive distillation fractions (Hempel fraction number, Figure 69a). The CI is zero for linear alkanes, increases for cycloalkanes and is high for aromatics (CI = 100 for benzene). The CI technique has the distinct advantage that it determines the hydrocarbon type of each crude fraction and thus enables identification and removal of hydrocarbon compounds (e.g., paraffins and aromatics) in the lower boiling fractions by the degradation processes. Widely used in the 1950's and 1960's by the U.S. Bureau of Mines (Barbat, 1967), the Hempel distillation procedure was also applied to the crude oils in the Pechelbronn-Soultz Basin during this period.

In my investigation the crude oils were compared by means of correlation indices of fractions 2 to 15, the API gravity of the crude, the percentage of sulphur and asphalt, the percentage of the residuum and the viscosity of the crude. Table 25 gives data for nine oil pools. The symbol O1 represents an unaltered oil sample from a Jurassic oil pool near Ohlungen, south of the study area.

Using the correlation indices, two geochemical oil types can be identified in the area: (1) oil of paraffinic character was found in the Mesozoic (*Lettenkohle* and *Muschelkalk*) pools, Soultz 1 to 3, labeled as S1 - S3; and (2) oil of mixed paraffinic-naphthenic composition was encountered in a middle *Keuper* (*Grès à Roseaux*) reservoir Pechelbronn P4, in *Zone Dolomitique* reservoirs Pechelbronn P3 and Soultz S4, and in the *Pechelbronner Schichten* pools Pechelbronn P1 - P3, (Figure 69a,b,c and 70; Bruderer et al., 1958).

Since only one of the potential source rocks in the study area was mature (Gerling, 1988), the oil found in the Tertiary and Mesozoic reservoirs must have migrated long distances, along and across the fault systems and fractures from the mature Lower Jurassic source rock units to its sites of entrapment. However, this does not explain the different geochemical character of the Mesozoic and Tertiary oil pools in the basin. There are two possible explanations for this:

(1) the differences in the oils' chemistries are a result of hydrocarbon fractionation during secondary migration in the basin's earlier evolution stage; or (2) the chemical differences are caused by secondary alteration processes which have taken place after the oil emplacement.

The migration-fractionation model of Illich et al. (1981) explains the vertical distribution of oil types by differences in ionic solubilities and by transport by formation waters of hydrocarbons during secondary migration. Although the available, semi-quantitative data on the oil's chemical composition are not detailed enough to prove or disprove the applicability of Illich's model to the present case, it appears that the vertical oil type distribution patterns of the Pechelbronn oil pools, P1-P4 (Figure 69b), are inconsistent with the model's predictions. Illich et al. (1981) state that, due to oil migration-fractionation processes to shallower sites of entrapment, an increase in paraffinity and a near-unchanged content of aromatics can be expected for shallower oil pools. This is not the case for the shallower Pechelbronn oils which show an increase in aromatics, a decrease in paraffinity and an increase in sulphur content, density and viscosity (Table 25). There is, however, still the possibility that a migration-fractionation process has taken place during the petroleum's secondary migration phase, and that the initial chemical hydrocarbon composition was later altered by secondary processes.

The chemical heterogeneities of the oil pools in the Pechelbronn-Soultz Basin appear more likely to be the result of the biodegradation and water washing (described below), which occurred after oil emplacement and which continue to the present-day. Also the possibility of hydrocarbon transformations by the processes of mild thermal cracking (maturation) in areas of anomalously high geothermal gradients have to be considered.

Water washing: Water washing preferentially removes aromatics and depresses the correlation index curve for the low boiling fractions (Figures 61 a, b, c; II; Barker, 1986).

The process of water washing acts in the following way in the study area. The oil pools S1 -S3 are situated in the focal discharge area (Figure 69c). Actively flowing formation waters have high salinities, no dissolved oxygen and temperatures between 90^0 and 110 ^{0}C. Under these subsurface conditions aerobic bacterial oil alteration processes can be ruled out (Lafargue et al., 1988). Figure 61c elucidates the effect of water washing by showing depressed curves for the oil pools S1-S3 on the correlation index plot. The oil appears to have lost the low boiling-point fractions, which leaves a relatively high content of paraffins. The expected increases in oil density and porportions of sulphur and carbon-residue, with the process of water washing, is not apparent here (S1-S3, Table 25). However, these distinctive parameters in crude oils can decline with increasing burial depth. For example, temperature increase is a process which is related to moderate thermal maturation (Tissot et al., 1978). Although the pools at Soultz are approximately within the same depth interval as the pools at Pechelbronn (Table 25; Figure 62), the observed geothermal gradient in the Soultz region is higher (11 ^{0}C/100 m). The advective heat transport by the discharging regional flow systems, therefore, causes additional chemical modifications by moderate thermal cracking, mitigating the effects of degradation by water washing.

The oil at pools P3, P4 and S4 are evidently of similar character and their CI curves, located within the paraffinic-naphthenic range, indicate an increase in naphthenic compounds (Figure 61 a,b). These oils are comparable to the unaltered oil, but their physical and chemical parameters (Table 25) show signs of water washing too. The parameters do not reflect thermal alteration effects and the reservoir temperatures are clearly lower.

Biodegradation:: Bacterial alteration has the opposite effect to water washing since the paraffins are preferentially being removed (Figures 61 a, b, c; II; Barker, 1986). A shift of the correlation index curve to high CI values is evidence for bacterial degradation. Generally, a decrease in paraffins, light aromatics and API gravity is observed under these conditions. At the same time, the viscosity and the content of sulphur and asphaltenes in the crude oil increase.

Site P1 is situated near a recharge area of a local flow system at 90 m depth (Figure 62) and is one of several examples in the Pechelbronn region of a bacterial biodegraded oil in the Upper Pechelbronn Beds at shallow depth (Table 25, Figure 61b). The chemical composition and the physical properties of P2 indicate less severe microbial alteration in comparison to P1. At a depth of 370 m, located within an intermediate flow system close the Hoelschloch Fault (Figure 62), this oil seems to have partly preserved its original chemical composition.

The oil alteration processes which have taken place in the Pechelbronn-Soultz basin are directly related to the various groundwater flow regimes, the formation water chemistry and temperatures discussed above. The transporting medium, groundwater, generates the necessary subsurface conditions and alters the oil deposits. In local flow systems biodegradation is expected to be an active alteration process for crude oils. In regional, deeper flow systems, especially in areas of discharge where formation waters have higher temperatures and no dissolved oxygen, water washing and thermal alteration processes can be expected to dominate.

7.2 A Shallow-Depth Hydrochemical and Temperature Survey across the Pechelbronn - Soultz Basin

In 1986 a preliminary interpretation of initial data identified the Pechelbronn-Soultz Basin as a major discharge region of ascending groundwater flow (Otto et al., 1986), and hence, according to the hydraulic theory, a suitable area for petroleum entrapment and accumulation. It was decided in conjunction with BGR-Hannover (Tóth, 1986) to conduct a near-surface geochemical and temperature survey along a profile line across the Pechelbronn-Soultz Basin. The main objective of the survey was to investigate if the hydrogeologic phenomena observed at deeper depths are transmitted to the surface by discharging groundwater which preferentially ascends to shallower depths along conductive fault zones. Near-surface observations of chemical and temperature anomalies can be used as indirect indicators for possible petroleum accumulation in the subsurface (Appendix I).

The present survey could then be seen as the 2nd stage of an exploration campaign to investigate an unknown basin. In the initial stage, a petroleum hydrogeological basin analysis identified a region of fluid potential minimum and also possible sites for petroleum entrapment, e.g. the Pechelbronn-Soultz Basin.

The drilling and sampling program was conducted by BGR in March - June 1987 along a transect approximately 10 km long trending WNW-ESE through the Pechelbronn, Hoelschloch, Kutzenhausen and Soultz oilfields (Figure 82).

Forty-six 18 m deep boreholes were drilled. Gerling (1988) analyzed the hydrocarbon gas content of the sediment core. Water samples were analyzed for their pH, electric conductivity andchloride and trace element (Li, Sr, I, Br) concentrations. Temperatures and water levels were measured in all 46 boreholes (Plöthner, 1988). Shallow boreholes 4 to 42 are aligned along a profile line from Mitschdorf in the west to Hohwiller in the east across the basin. Three shallow boreholes 1-3 were drilled in the Vosges northwest of the Pechelbronn-Soultz Basin to obtain background data. Four additional boreholes 43-46 are situated at the lowest topographic elevations of the basin near Soultz, 500 m north of the profile line (elevations are between 145 to 150 m a.m.s.l.).

By rotary drilling and using tap water as a drilling fluid, a 100 mm diameter borehole was lowered to 17 to 18 m depth. At about 18 m depth a sediment sample was taken for geochemical analysis. The borehole was then temporarily cased with PVC liners.

Water levels

Water levels were measured 48 hours after the well was completed. In general the depth of the water table lies about 2-3 m below landsurface and is a replica of the topography. The depth to the water table is greatest below topographic highs (recharge areas) and near or above the landsurface in regions of topographic depression (discharge areas; Figure 90). A piezometric level above the landsurface was observed for wells 23, 21 and 30, RG-1 and Mattenmühle (artesian flowing). For the Soultz region and to the east the piezometric level rose with increasing drilling depth, a clear indication of upward groundwater flow conditions.

Groundwaters flowing freely to the surface carried oil traces. These direct indicators for subsurface oil accumulations were observed only in local depressions associated with an outcropping fault (Figure 90). Some core samples showed oil-impregnated sandlayers and bituminous fissures and joints in argillaceous sections.

Shallow depth temperatures

In the shallow wells, temperatures were measured in the water column at depth intervals of 0.5 m, 43 hours after well completion. Two measuring devices with an accuracy of 0.01 and 0.1 °C were used (Plöthner, pers. comm.).

Kappelmeyer (1957) and Kappelmeyer et al. (1974) state that seasonal air-temperature fluctuations are negligible below depths of 15 m. The near-surface temperatures are uncorrected and plotted for 16 m depth on Figure 90.

The shallow depth temperatures increase gradually from the west to the east across the Pechelbronn-Soultz Basin and are highest over the Kutzenhausen Soultz Hermerwiller region, coinciding with a region of anomalously high geothermal gradients (Chapter 4.3.3). To the west of Pechelbronn, shallow depth temperatures are generally lower with a minimum of 10.5 °C at well 7. Wells 1 and 3 show background temperature values of 8.5 and 10.1 °C. The higher value in well 3 might be explained by the proximity of the Rhine Fault and possibly higher heat flow due to ascension of groundwater along the fault to shallower depths.

The course of shallow-depth temperatures across the basin is inverse to the topography (Figure 90), i.e., in topographic lows temperatures at 16 m depth are higher, whereas temperatures measured in topographic mounds at 16 m depth are lower. In areas of groundwater recharge the temperature gradients calculated for depths between 11 and 16 m are low, while in local depressions of discharging groundwater the gradients are high (Figure 63). Temperature peaks coincide, and are associated with, outcropping faults in the valleys (Figure 90). The occurrence and magnitude of a sudden rise in shallow depth temperature, indicative of a possible fluid-conductive fault zone, can be subdued or even erased by a local groundwater flow system. Ascending warmer groundwater driven by the regional flow system converges with cooler groundwater driven by a local flow system. This "cooling effect" is observed near the Soultz and Hermerswiller Faults (Figure 90). The Kutzenhausen Fault is an excellent conductor to groundwater flow and its transported matter. Highest shallow-depth temperatures and prominent chemical anomalies are observed. In the field, the area is dominated by phreatophytes and marshy soils.

In summary, the near-surface groundwater temperatures increase basinward and show local anomalies at outcrops of fault planes, the temperature gradients calculated for the depth interval of 11 to 16 m, increase from recharge to discharge areas (Figure 63). Both the magnitudes of the overall anomaly and the observed details of the temperature distribution are strongly suggestive of groundwater flow being focussed and intensified by funnelling through fault zones: the faults have significant modifying effect on both the deep and near-surface distribution of geothermal heat. Similar phenomena have also been observed and measured in regions such as in the Magellan Basin and the Rocky Mountain region (Mcgee et al., 1989; Zielinski et al., 1983).

Hydrochemistry

Water samples were bailed from about 15 m depth after temperature measurements had been taken. The water samples were analyzed for their salinity and trace element content.

Specific electric conductivity (EC): The EC-values of the near-surface waters vary between 100 and 6700 μS/cm. The EC-value of the drilling fluid is 110 μS/cm, and for background well no. 3 the value is 320 μS/cm. The mean EC-value for 32 wells is about 540 μS/cm. Wells 6-11 show an average EC-value of 2200 μS/cm/ These water samples were taken from gypsum-rich horizons in the *Pechelbronner Schichten*. Close to the Kutzenhausen and Hermerswiller Faults, oil-stained groundwater in wells 30, 45, 46, RG-1 and Mattenmühle have the highest EC-values between 1560-6700 μS/cm.

Chloride: The chloride content of the near-surface groundwater varies between 8 and 2070 mg/l. Tap water used for drilling fluid has about 8 mg/l of chloride. Groundwater in 37 wells excluding well 23 show low chloride concentrations of between 8-86 mg/l, while wells 30, 45, 46 and RG-1 show higher values of between 260 and 2070 mg/l (Figure 90). As a comparison, formation waters in the *Zone Dolomitique* (SAEM wells 3262, 3969) have chloride concentrations between 5000-13 100 mg/l. The highest concentrations were measured near the Hoelschloch, Kutzenhausen and Hermerswiller Faults. The water of well 23 appears to be contaminated by leaching fluid from a nearby old mining heap.

Lithium: The lithium content of tapwater is below the analytical detection limit (< 0.005 mg/l). Well 3 has a background value of 0.025 mg/l. The highest concentrations were measured near the Kutzenhausen Fault. High lithium contents are generally observed in oil-stained groundwater rising to the surface near outcropping faults (wells 10, 18, 29, 46, RG-1 and Mattenmühle Figure 90). Oilfield waters in the *Zone Dolomitique* contain lithium contents between 4-14 mg/l.

Strontium: Tap- and background water samples contain about 0.1 mg/l of strontium. High values are observed in the Mitschdorf-Preuschdorf region (Figure 90), where water samples were taken in gypsiferous Tertiary formations. Wells 18 and RG-1 show oil-stained groundwaters with strontium contents of about 9 mg/l.

Bromide and Iodide: The biophile elements bromide and iodide are characteristic components for oilfield formation waters. Tapwater as well as 13 water samples of 20 analyzed samples (including 3) have bromide concentrations below the detection limit of 0.1 mg/l. For iodide, 17 out of 19 samples show values below the 0.05 mg/l detection limit. These values are normal for shallow-depth groundwater. Elevated bromide and iodide contents were noticed for wells 46, RG-1 and Mattenmühle. There is no apparent correlation between the bromide and iodide content and groundwater carrying oil traces, except for the region near the Kutzenhausen Fault zone which appears to transmit deep-seated oilfield water to the surface.

Soil Gases

Gerling (1988) investigated the methane and propane content as well as the carbon isotope ratio of methane for 18 m deep core samples. He concluded that the gases are in generally of thermal origin and have originated from Jurassic (Toarcian) source rocks, suggesting vertical migration to shallow depths. Bacterially generated methane was observed for some wells.

Conclusions

In surface-geochemical exploration, the use of shallow-depth temperatures and hydrochemical parameters as indicators for subsurface petroleum accumulations is viable only under certain hydrogeological conditions:

1) Foremost, the groundwater flow has to be upward, transmitting hydrogeological phenomena to the near-surface. This condition is given in regions of discharge and artesian basins.

2) Conductive fault systems will enhance upward flow and funnel groundwater and its matter to the near surface. Faults are excellent transmitters of direct and indirect indicators of subsurface oil deposits.

3) Elevated concentrations of biophile elements of ascending formation waters appear to be diluted easily by invading freshwaters from local flow systems at shallow depth. Local groundwater flow systems which are generated by the local topography of a basin can alter the temperature and chemistry of the rising deeper groundwaters to an extent that these anomalous hydrogeological phenomena are normalized beyond recognition.

4) Near-surface elevated temperatures are good indicators for warm groundwaters rsing to the surface, and also indicate conductive fault zones and to shallow-depth outcropping faults (Figures 82 and 90).

8. Concluding Statements

The hydraulic theory of petroleum migration was applied, to and its validity tested in, a graben-type intermontane groundwater basin, the Upper Rhine Graben. The study was mainly focussed on the petroliferous Pechelbronn-Soultz Basin, north of Strasbourg, France.

Although the hydraulic theory has been found adequate to explain petroleum occurrences in various environments such as in the interior type Pannonian Basin (Erdélyi, 1985), the platform type Michigan Basin (Vugrinovich, 1988), or offshore Persian Gulf (Wells, 1988) Its predictions can be expected to be most accurate in intermontane basins; it is in this environment that the theoretically required boundary conditions of the flow domain most closely approximate the real boundaries.

The various aspects of the origin, migration and degradation, as well as of the thermal, chemical and fluid-dynamical conditions of petroleum occurrences in the Pechelbronn-Soultz Basin and Upper Rhine Graben can be brought into a genetically linked and unified system of hydrogeological processes and phenomena by the hydraulic theory of petroleum migration.

The Upper Rhine Graben is an intermontane valley flanked by two mountain ranges the Vosges and Black Forest to the west and east, respectively. Hydrocarbon-generating beds and formations of low and high hydraulic conductivity are identified and classified as hydrogeologic units (aquitards or aquifers). Groundwater flow is at steady state.

Underlain by a Hercynian crystalline basement, the Mesozoic and Tertiary formations of the Upper Rhine Graben and Pechelbronn-Soultz Basin are dissected, displaced and fractured by numerous fault systems. The fault pattern is complex and fault-density is greatest in the Pechelbronn-Soultz Basin. Antithetic normal as well as curved faults constitute the principal fault-type in the basin.

A dynamic inter-relationship exists between groundwater flow patterns, hydrochemical and geothermal anomalies, petroleum migration and deposition and the fluid-conductance of fault zones.

Locally intensified cross-formational discharge of geologically young groundwaters (< 30 000 years old) of meteoric origin and hydrochemical as well as geothermal distribution patterns are spatially related and coincide with oil deposits.

The principal area of collection and deposition of hydrocarbons coincides with a region where the oppositely directed regional flow systems from the Vosges and Black Forest converge radially towards the Pechelbronn-Soultz Basin which functions as a focal discharge area and a zone of disaccommodation within the regional Rhine Graben discharge region.

Hydrocarbon migration commenced about 25 Ma from mature Jurassic source rocks situated in the deeper central part of the graben.

Groundwater of the Black Forest flow system was the main agent of transport and additive to the buoyancy force of hydrocarbons migrating to their sites of deposition in the structurally uplifted reservoirs of the Pechelbronn-Soultz Basin.

Fault zones in the study area function mainly as conduits. Their fluid-conductive character is determined by the juxtaposition of aquifers and aquitards as well as fault/fracture density. Fault zones channel and redirect groundwater to shallower or deeper hydrostratigraphic units.

This is expressed by the distribution pattern of hydrochemical and thermal parameters. Water mineralization is highest in the Pechelbronn-Soultz Basin (>100 000 mg/l) and coincides with a discharge area of greatest fault density. Anomalously high geothermal gradients of 11°C/100 m are also observed in this region.

No meaningful relationship can be achieved by attempting to relate flow-affected parameters such as chemical composition, water density and temperature to depth. This is due to factors such as superposition of local and regional flow systems and cross-formational plumes of water mineralization and temperatures along faults.

Flow-affected parameters such as should not be attempted to be related to depth. the no meaningful relation between these parameters and depth can be expected.

Topography-induced groundwater flow systems have an evident genetic role, which provides various keys to hydrogeologically based exploration techniques. These are particularly applicable in intermontane, fault-severed environments. In brief, it validates the basic thesis and predicted practical ramifications of the hydraulic theory of petroleum migration, the evaluation of which was one of the principal objectives of this study.

Similar petroleum hydrogeological conditions are known to occur in other intermontane basins also as, for instance, in Whitney Canyon-Ryckman Creek oil fields in Wyoming, U.S., (Jones, 1983; Zielinski, 1985) and the Mae Soon Oil Field, Fang Basin in N.W. Thailand.

The most relevant properties and consequences of the regional groundwater flow in intermontane basins include:

- well defined regional recharge and discharge regions;
- geometrically defined (i.e., distributed) flow systems;

- well defined and localized cross-formational passage ways ("vents"); and
- short through-flow time, i.e., high rate of groundwater turnover.

As a consquence of the above properties the following phenomena occur in intermontane basins:

- positive temperature anomalies;
- regional anomalies of formation water salinities;
- near-surface indirect and direct indicators for petroleum deposits;
- tilted oil/water interfaces; and
- remigration and degradation of oil pools, also at greater depths.

An analysis based on the correlation between these characteristics and their consequences will lead to an improvement in the success of conventional petroleum exploration; and a better understanding and interpretation of anomalous phenomena detected by near-surface (e.g. geochemical) exploration methods.

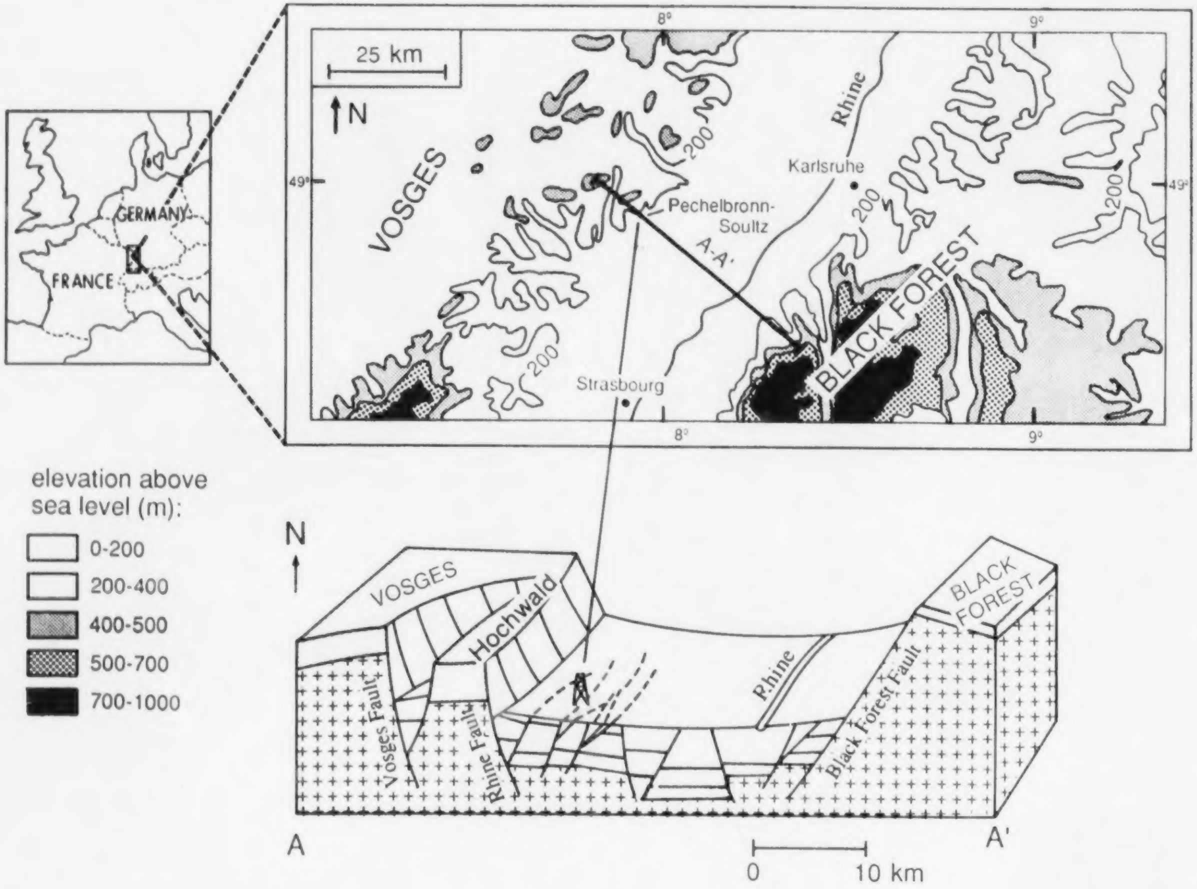
GERMANY
FRANCE
25 km
N
8°
9°
49°
VOSGES
200
Rhine
Karlsruhe
Pechelbronn-
Soultz
A-A'
BLACK FOREST
Strasbourg
elevation above
sea level (m):
0-200
200-400
400-500
500-700
700-1000
N
VOSGES
Hochwald
Vosges Fault
Rhine Fault
Rhine
Black Forest Fault
BLACK FOREST
A
A'
0
10 km

Figure 1 Physiography and schematized tectonic structure of the Upper Rhine Graben

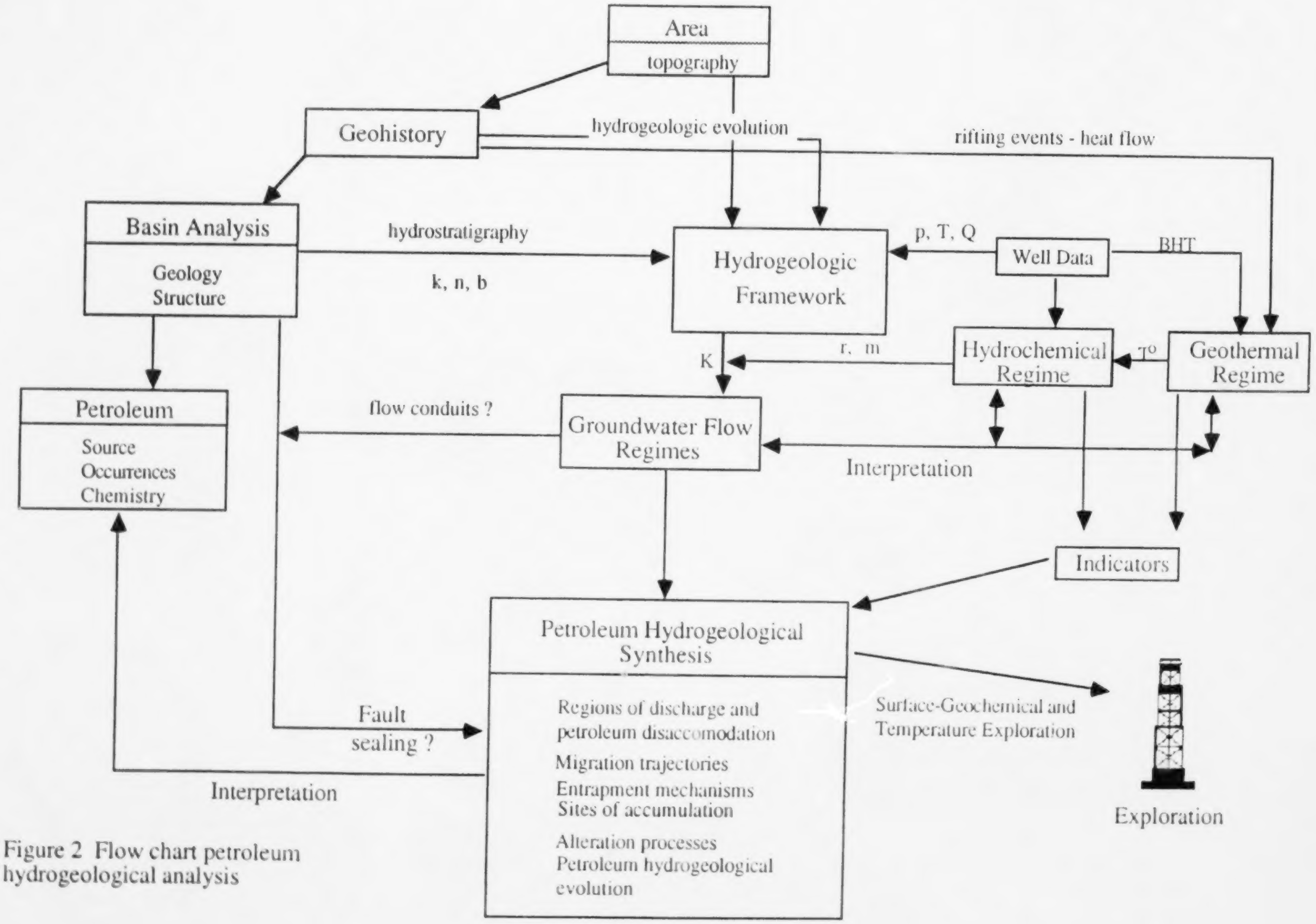
Area
topography
Geohistory
hydrogeologic evolution
rifting events - heat flow
Basin Analysis
Geology
Structure
hydrostratigraphy
k, n, b
Hydrogeologic
Framework
p, T, Q
Well Data
BHT
K
r, m
Hydrochemical
Regime
T°
Geothermal
Regime
Petroleum
Source
Occurrences
Chemistry
flow conduits ?
Groundwater Flow
Regimes
Interpretation
Indicators
Petroleum Hydrogeological
Synthesis
Regions of discharge and
petroleum disaccomodation
Migration trajectories
Entrapment mechanisms
Sites of accumulation
Alteration processes
Petroleum hydrogeological
evolution
Fault
sealing ?
Interpretation
Surface-Geochemical and
Temperature Exploration
Exploration

Figure 2 Flow chart petroleum hydrogeological analysis

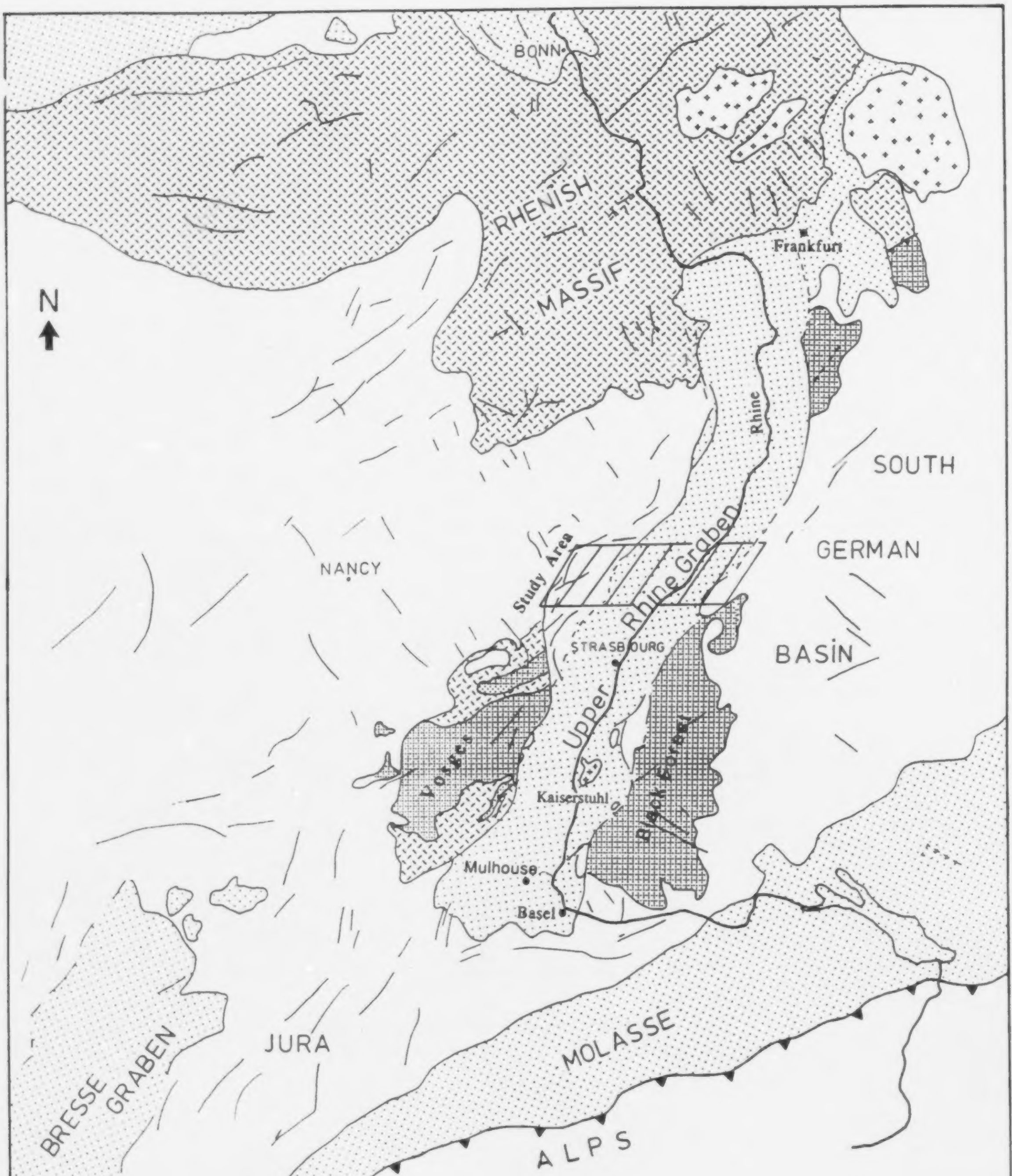
BONN
RHENISH
MASSIF
Frankfurt
N
Rhine
SOUTH
GERMAN
BASIN
Study Area
Upper Rhine Graben
NANCY
STRASBOURG
Vosges
Black Forest
Kaiserstuhl
Mulhouse
Basel
BRESSE GRABEN
JURA
MOLASSE
ALPS
Cenozoic
Mesozoic
Paleozoic
Crystalline Basement
Tertiary Volcanics
Faults
15
45
km

Figure 3 The Upper Rhine Graben an d its regional geologic setting

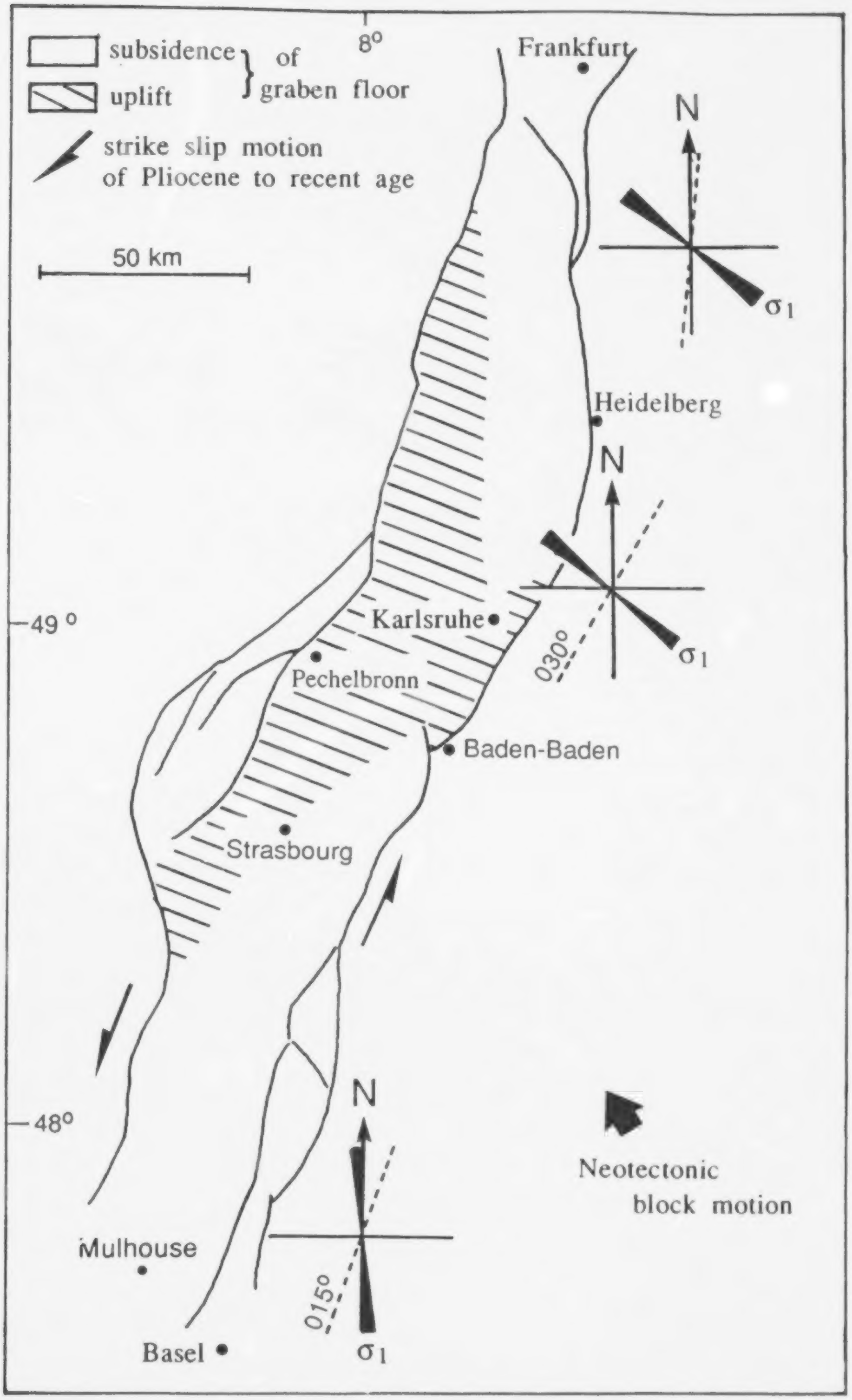
subsidence
uplift
of graben floor
strike slip motion of Pliocene to recent age
50 km
8°
49°
48°
Frankfurt
Heidelberg
Karlsruhe
Pechelbronn
Baden-Baden
Strasbourg
Mulhouse
Basel
N
σ1
030°
015°
Neotectonic block motion

Figure 4 Regional stress pattern in the Upper Rhine Graben; the study area is located in an area of compression and uplift

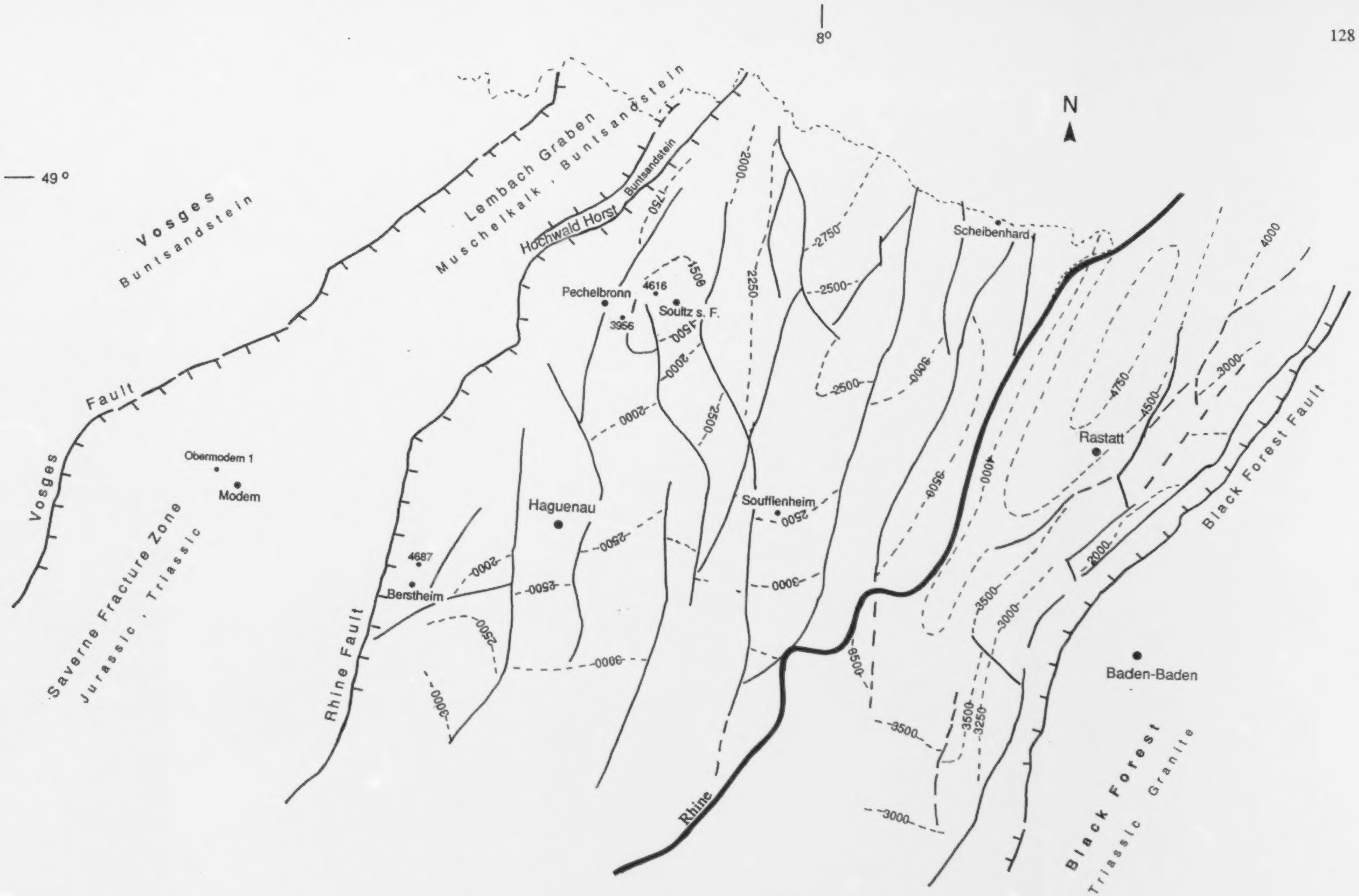
8°
49°
N
Vosges
Buntsandstein
Vosges Fault
Lembach Graben
Muschelkalk, Buntsandstein
Hochwald Horst
Buntsandstein
Saverne Fracture Zone
Jurassic, Triassic
Obermodern 1
Modern
Pechelbronn
4616
3956
Soultz s. F.
Haguenau
4687
Berstheim
Soufflenheim
Scheibenhard
Rastatt
Baden-Baden
Rhine Fault
Rhine
Black Forest Fault
Black Forest
Triassic Granite
750
1500
2000
2250
2500
2750
3000
3250
3500
4000
4500
4750
0
10 km

Figure 5 Location of four SAEM wells which encountered the granitic basement and tooutcropping formations in the Vosges, Black Forest and Hochwald shown on a simplified isohypse map of the top the basement (modified after Walgenwitz '79)

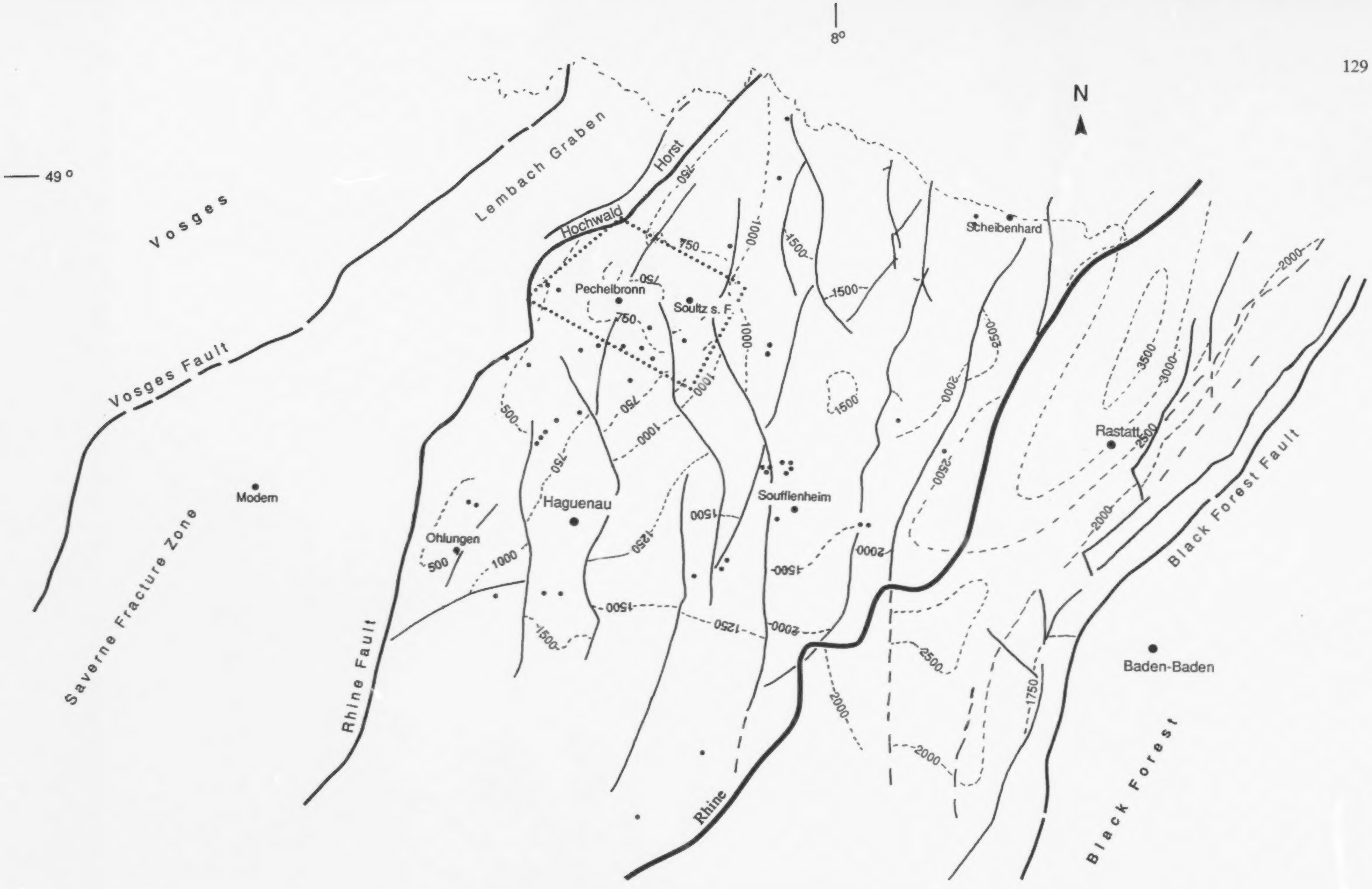
8°
N
49°
Vosges
Lembach Graben
Hochwald
Horst
Vosges Fault
Saverne Fracture Zone
Rhine Fault
Modern
Ohlungen
Haguenau
Pechelbronn
Soultz s. F.
Soufflenheim
Scheibenhard
Rastatt
Baden-Baden
Black Forest Fault
Black Forest
Rhine
500
750
1000
1250
1500
1750
2000
2500
3000
3500
0
10 km

Figure 6 Simplified isohypse map of the base of the Tertiary for the Upper Rhine Graben (modified after Walgenwitz '79)

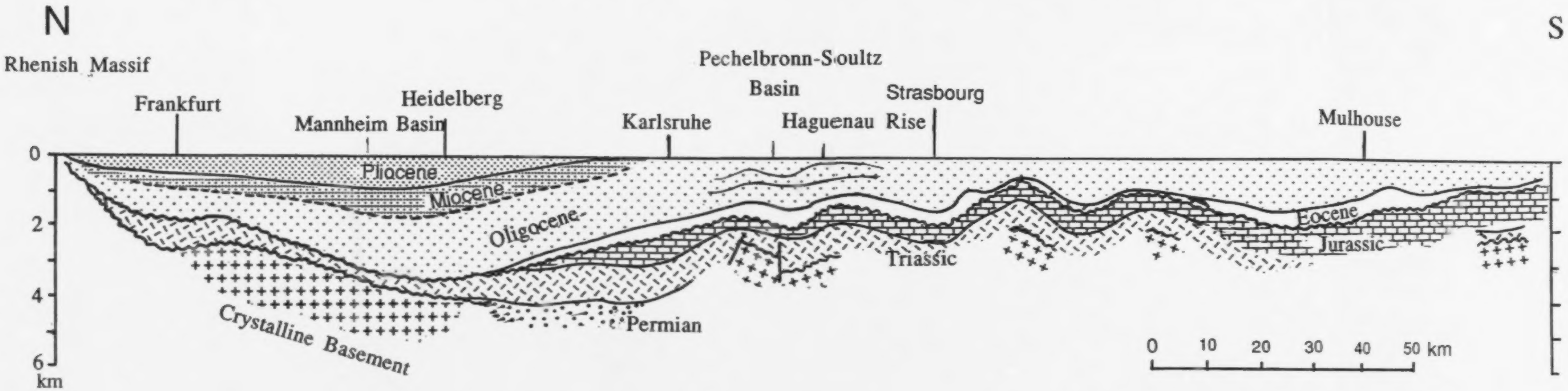
N
S
Rhenish Massif
Frankfurt
Mannheim
Heidelberg Basin
Karlsruhe
Pechelbronn-Soultz Basin
Haguenau
Strasbourg Rise
Mulhouse
Pliocene
Miocene
Oligocene
Eocene
Jurassic
Triassic
Permian
Crystalline Basement
0
2
4
6
km
0 10 20 30 40 50 km

Figure 7 Schematic longitudinal section of the Upper Rhine Graben (modified after Sittler '67)

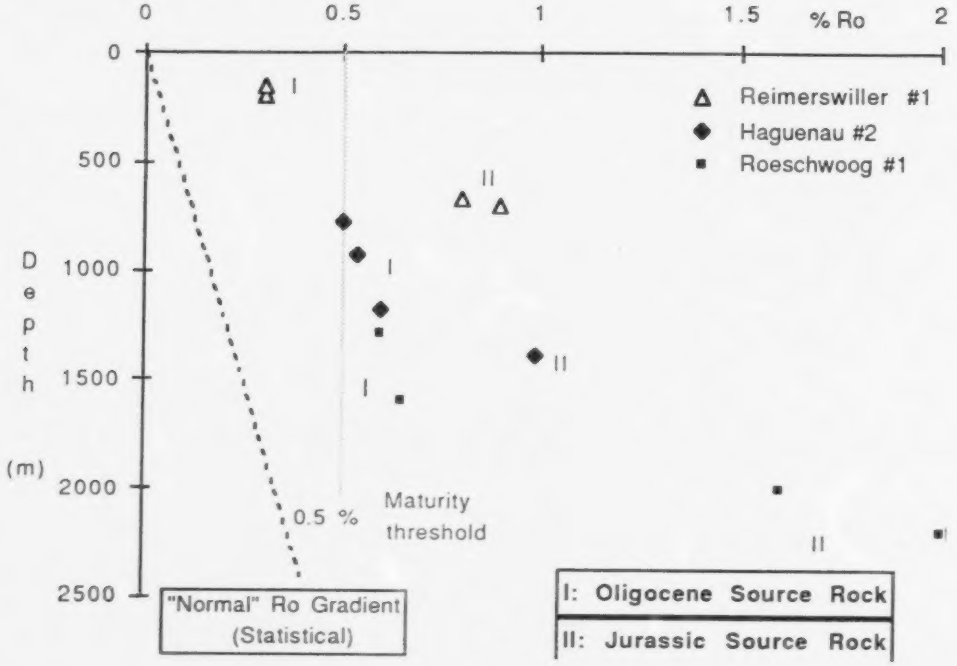

Figure 8 Vitrinite reflectance values (R_o) vs. depth for Oligocene and Jurassic potential source rocks in the Upper Rhine Graben study area. Reflectance gradients are higher then the "normal" gradient for passive basins and off-set at the Cretaceous unconformity. Data source: Table 4.

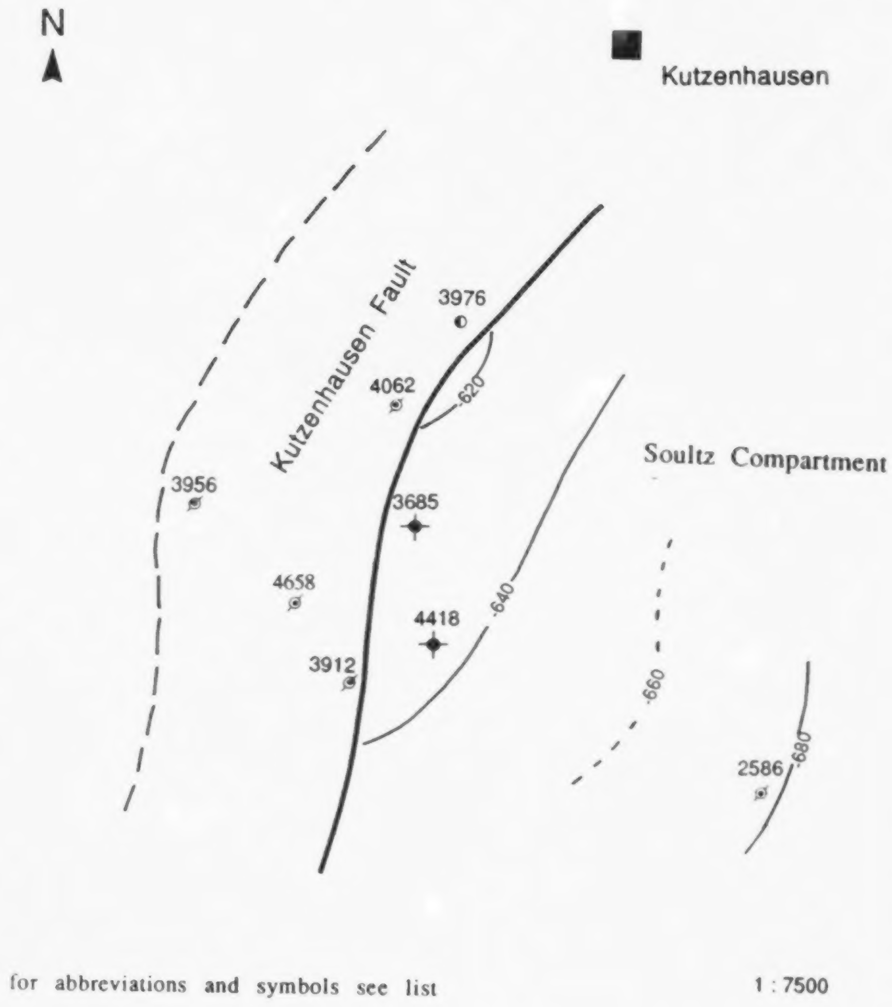
N
Kutzenhausen
Kutzenhausen Fault
3976
4062
-620
Soultz Compartment
3956
3685
4658
-640
4418
3912
-660
2586
-680
for abbreviations and symbols see list
1 : 7500

Figure 9 Oil producing wells in the Grés à Roseaux at the Kutzenhausen Fault near Kutzenhausen

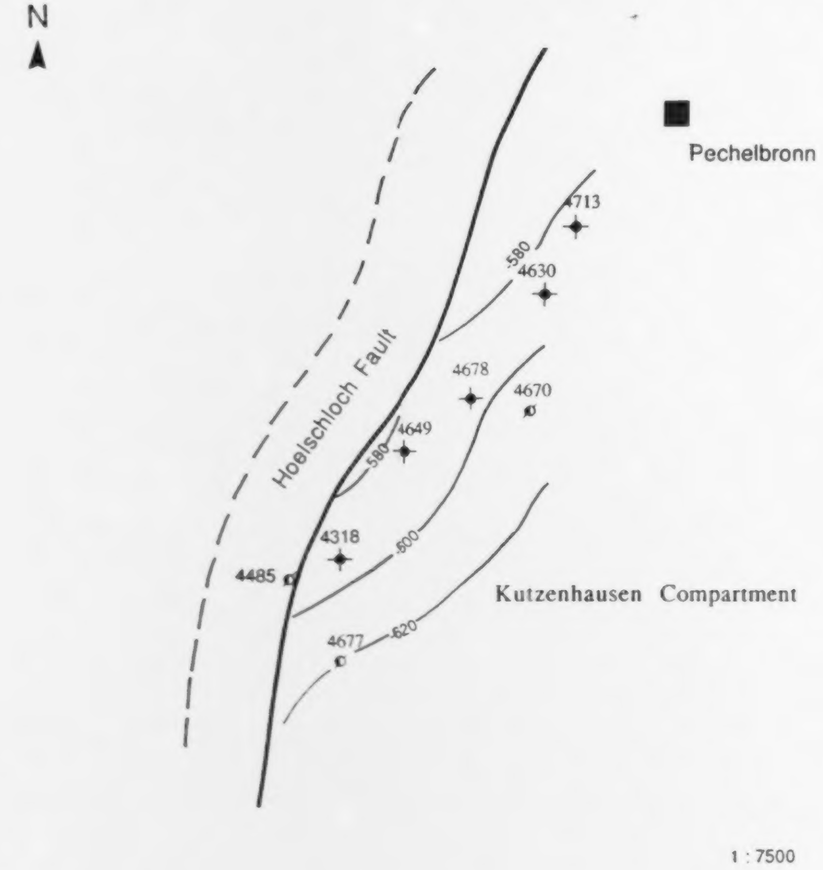
N
Pechelbronn
4713
580
4630
Hoelschloch Fault
4678
4670
4649
580
4318
600
4485
Kutzenhausen Compartment
4677
620
1 : 7500

for abbreviations and symbols see list

Figure 10 Oil producing wells in the Grés à Roseaux at the Hoelschloch Fault near Pechelbronn

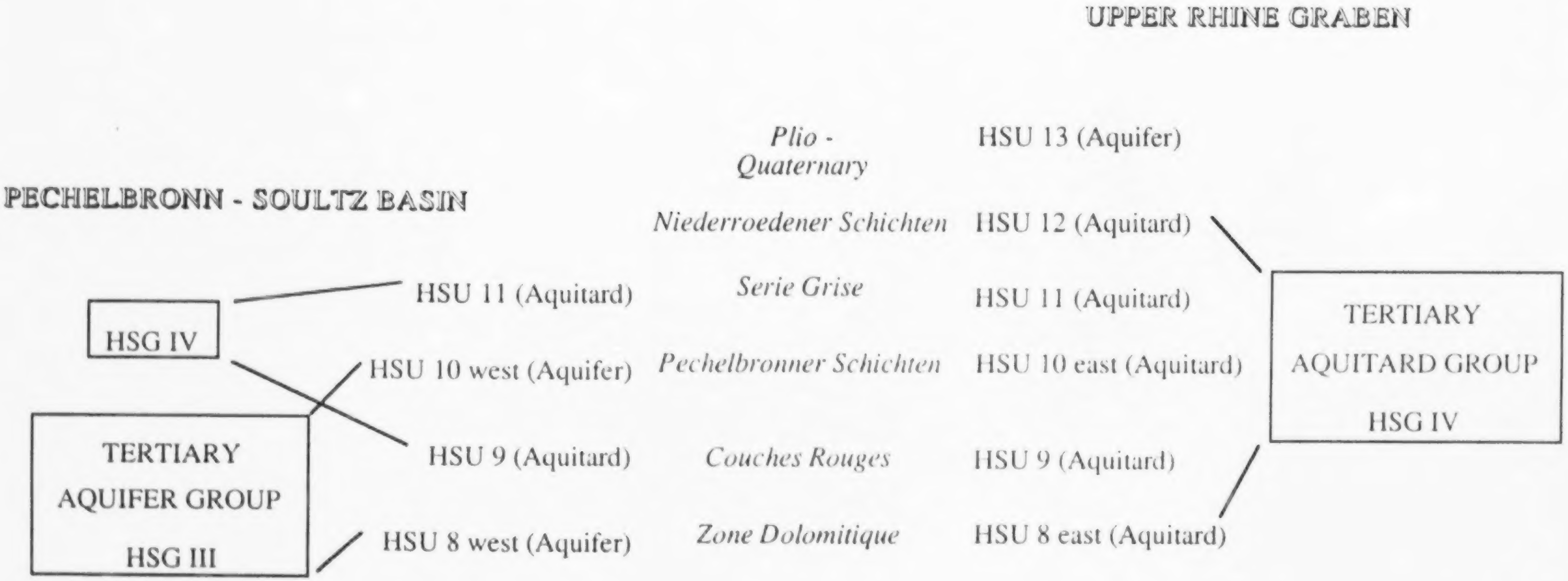
UPPER RHINE GRABEN
PECHELBRONN - SOULTZ BASIN
HSG IV
TERTIARY
AQUIFER GROUP
HSG III
HSU 11 (Aquitard)
HSU 10 west (Aquifer)
HSU 9 (Aquitard)
HSU 8 west (Aquifer)
Plio - Quaternary
Niederroedener Schichten
Serie Grise
Pechelbronner Schichten
Couches Rouges
Zone Dolomitique
HSU 13 (Aquifer)
HSU 12 (Aquitard)
HSU 11 (Aquitard)
HSU 10 east (Aquitard)
HSU 9 (Aquitard)
HSU 8 east (Aquitard)
TERTIARY
AQUITARD GROUP
HSG IV

Figure 11 Definition of Tertiary hydrostratigraphic units in the Pechelbronn-Soultz Basin and Upper Rhinegraben

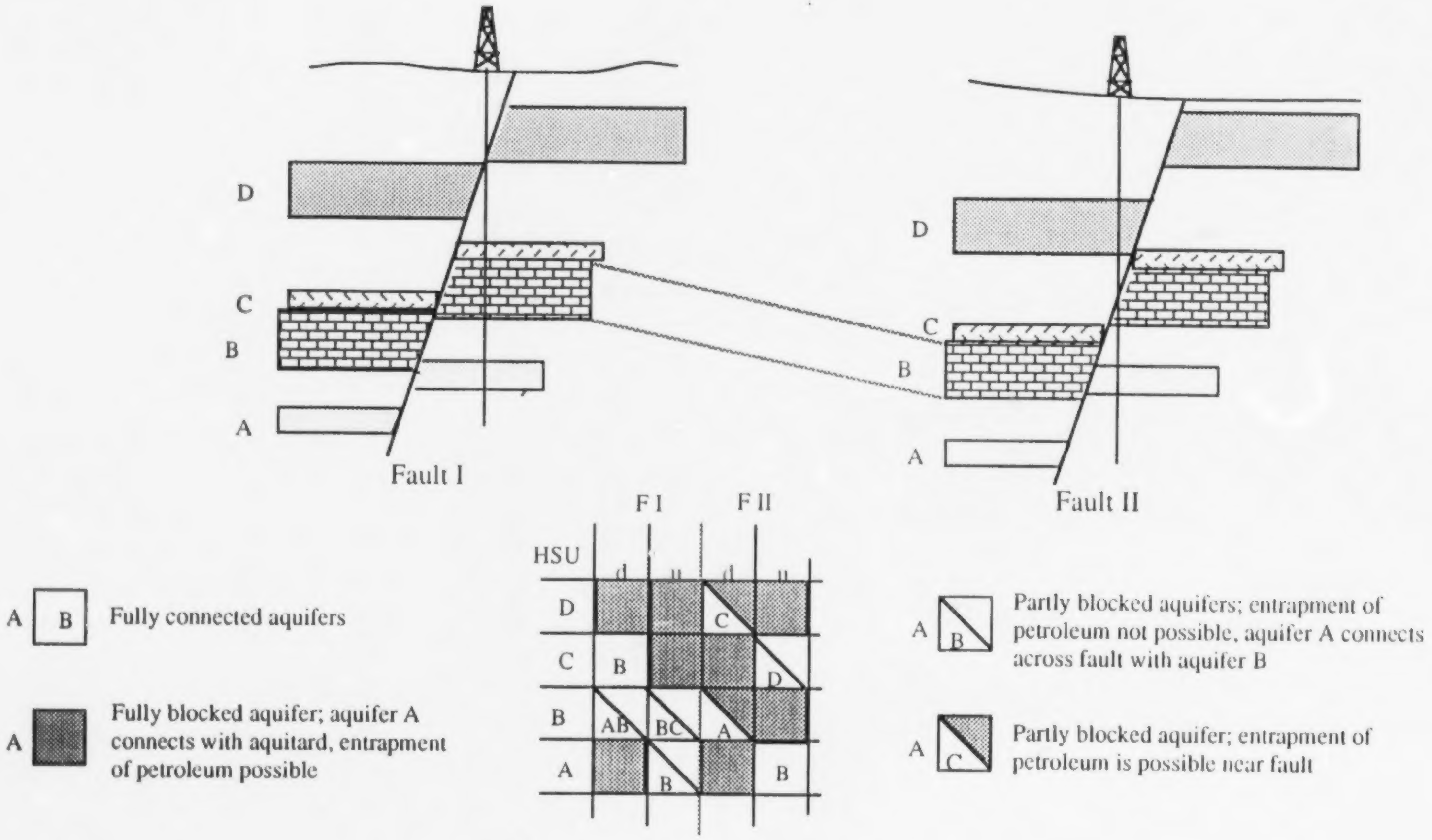
D
C
B
A
Fault I
D
C
B
A
Fault II
F I
F II
HSU
d
u
d
u
D
C
B
A
B
C
D
AB
BC
A
B
B
A
B
Fully connected aquifers
A
Fully blocked aquifer; aquifer A connects with aquitard, entrapment of petroleum possible
A
B
Partly blocked aquifers; entrapment of petroleum not possible, aquifer A connects across fault with aquifer B
A
C
Partly blocked aquifer; entrapment of petroleum is possible near fault

Figure 12 Above: Schematized geology of displaced hydrostratigraphic units A, B, C, D (aquifers) by two normal faults I and II with a different throw; white fields between aquifers represent aquitards. Below: The conceptual diagram of the aquifer connectivity model shows unblocked pathways for groundwater flow and possible sites of petroleum entrapment.

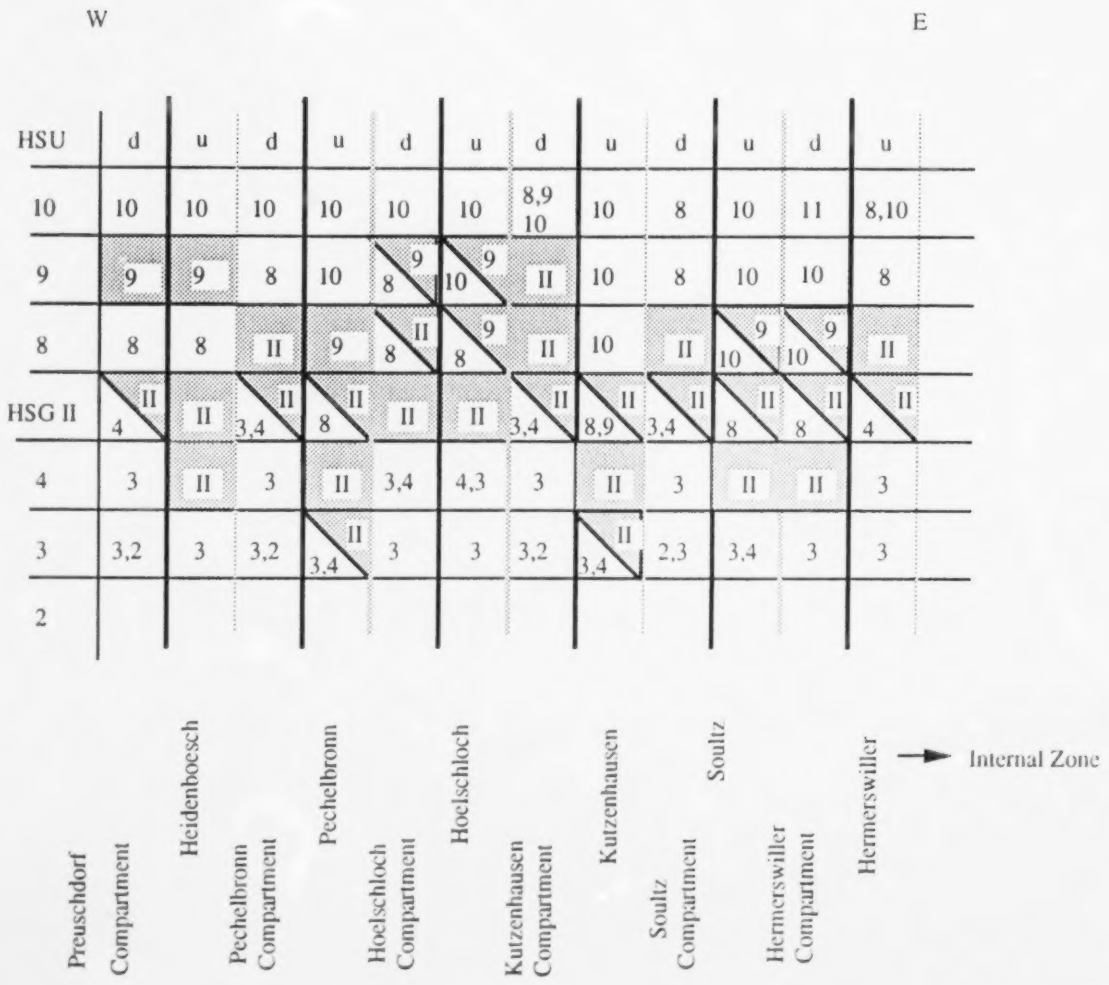

HSU	d	u	d	u	d	u	d	u	d	u	d	u
10	10	10	10	10	10	10	8,9 10	10	8	10	11	8,10
9	9	9	8	10	9 8	9 10	II	10	8	10	10	8
8	8	8	II	9	II 8	9 8	II	10	II	9 10	9 10	II
HSG II	II 4	II	II 3,4	II 8	II	II	II 3,4	II 8,9	II 3,4	II 8	II 8	II 4
4	3	II	3	II	3,4	4,3	3	II	3	II	II	3
3	3,2	3	3,2	II 3,4	3	3	3,2	II 3,4	2,3	3,4	3	3
2												
	Preuschdorf Compartment	Heidenboesch	Pechelbronn Compartment	Pechelbronn	Hoelschloch Compartment	Hoelschloch	Kutzenhausen Compartment	Kutzenhausen	Soultz Compartment	Soultz	Hermerswiller Compartment	Hermerswiller

Figure 13 con't next page

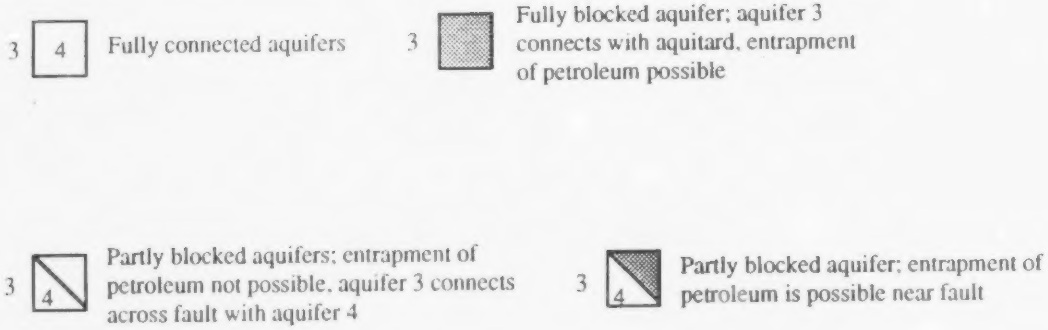
3
4
Fully connected aquifers
3
Fully blocked aquifer; aquifer 3 connects with aquitard, entrapment of petroleum possible
3
4
Partly blocked aquifers; entrapment of petroleum not possible, aquifer 3 connects across fault with aquifer 4
3
4
Partly blocked aquifer; entrapment of petroleum is possible near fault

Figure 13 An aquifer connectivity model for the Pechelbronn-Soultz Basin

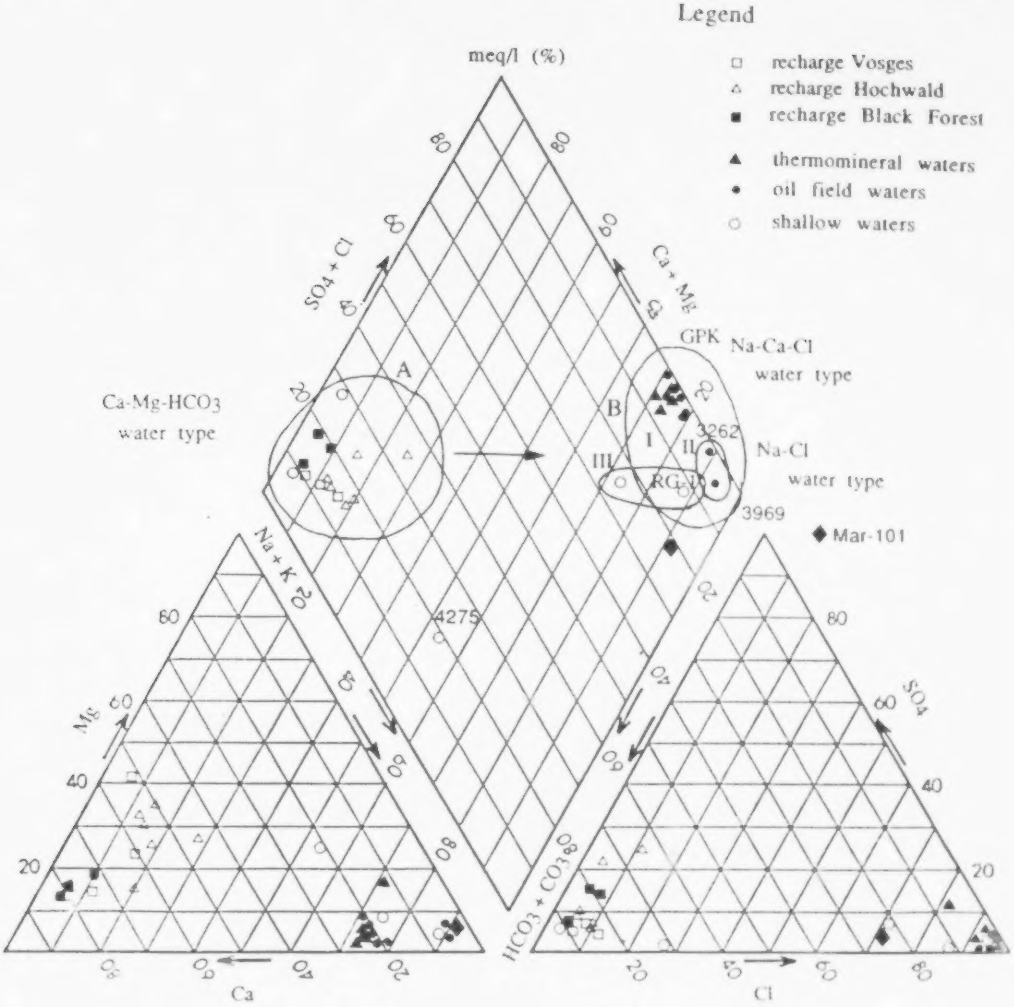

Figure 14 Two water types A and B are identified on a Piper Diagram

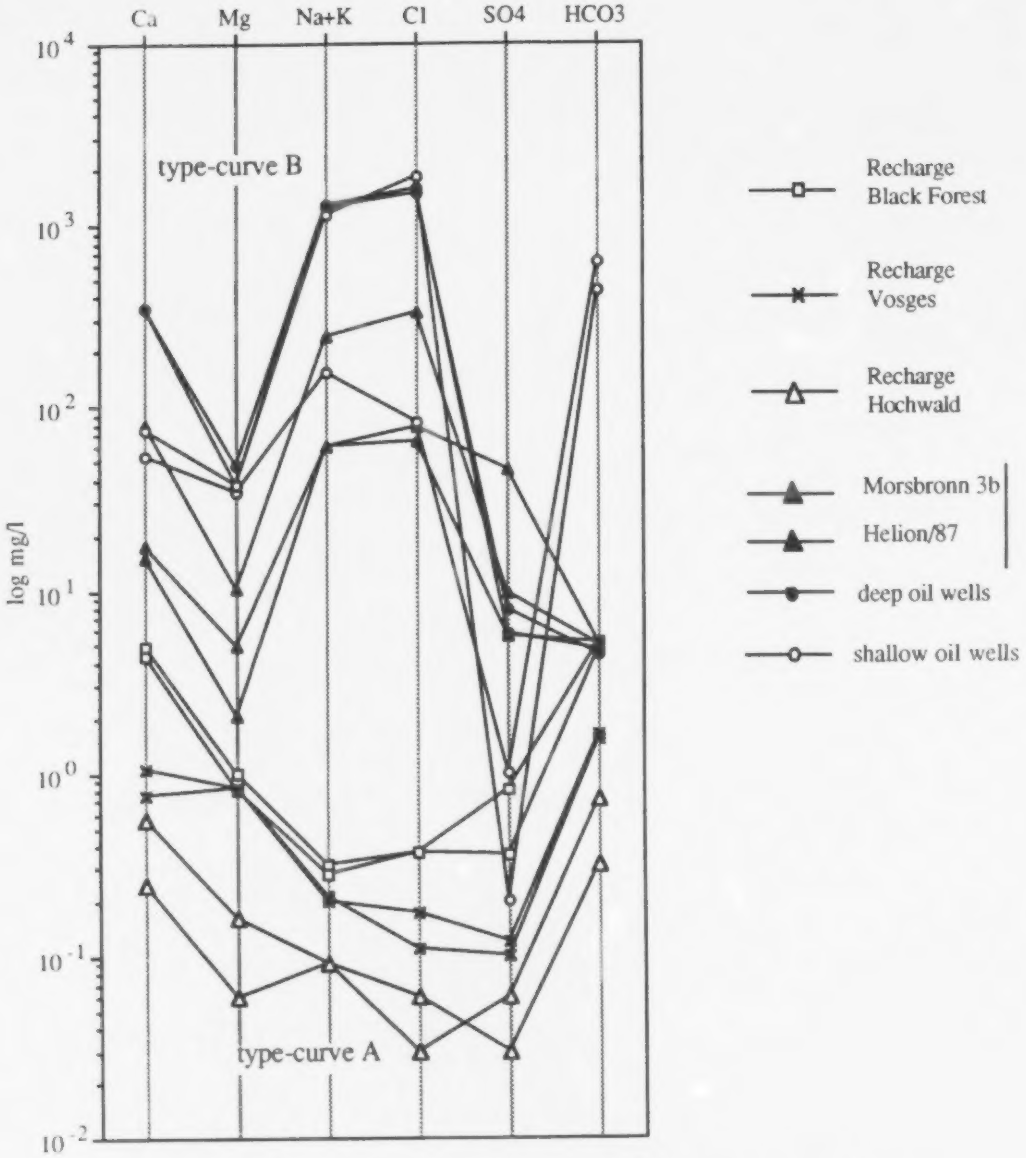

Figure 15 Two water types A and B are identified on a Schoeller Diagram

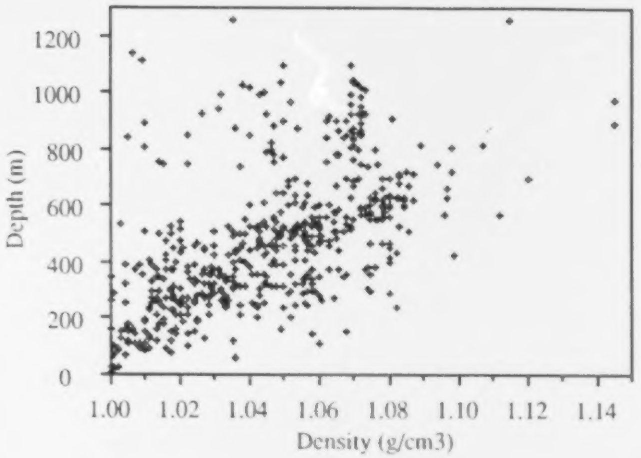

Figure 16 Formation water density vs. depth plot

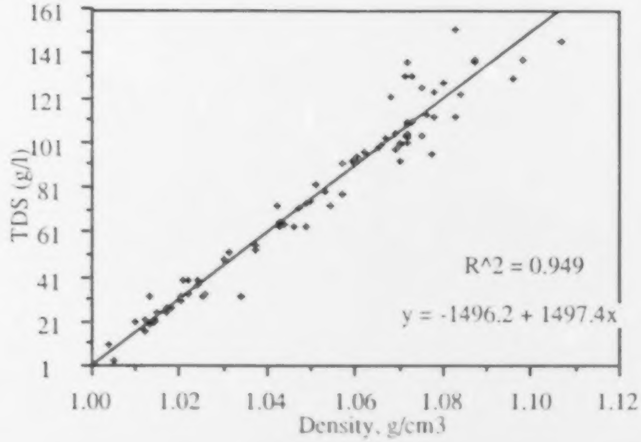

Figure 17 TDS vs. formation water density plot

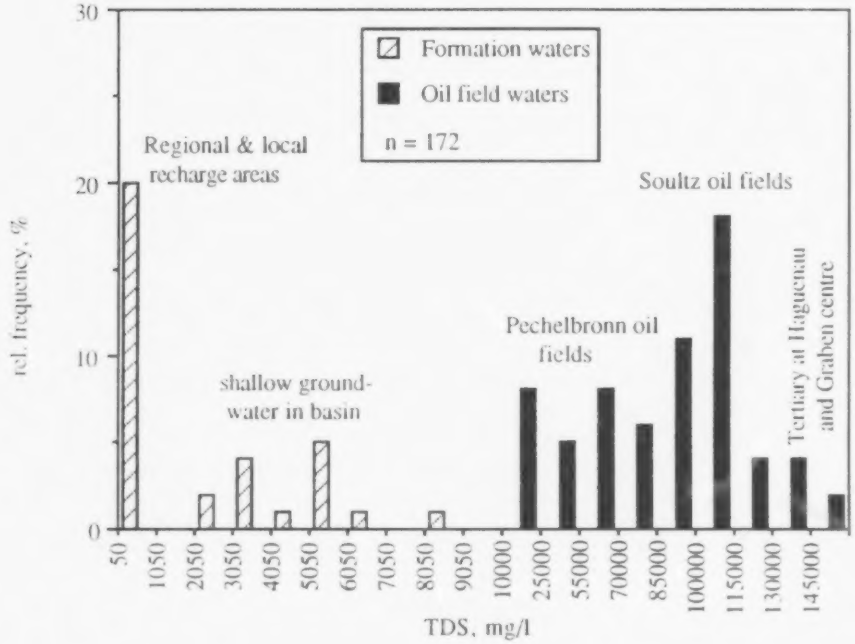

Figure 18 Relative frequency distribution of TDS values in the study area

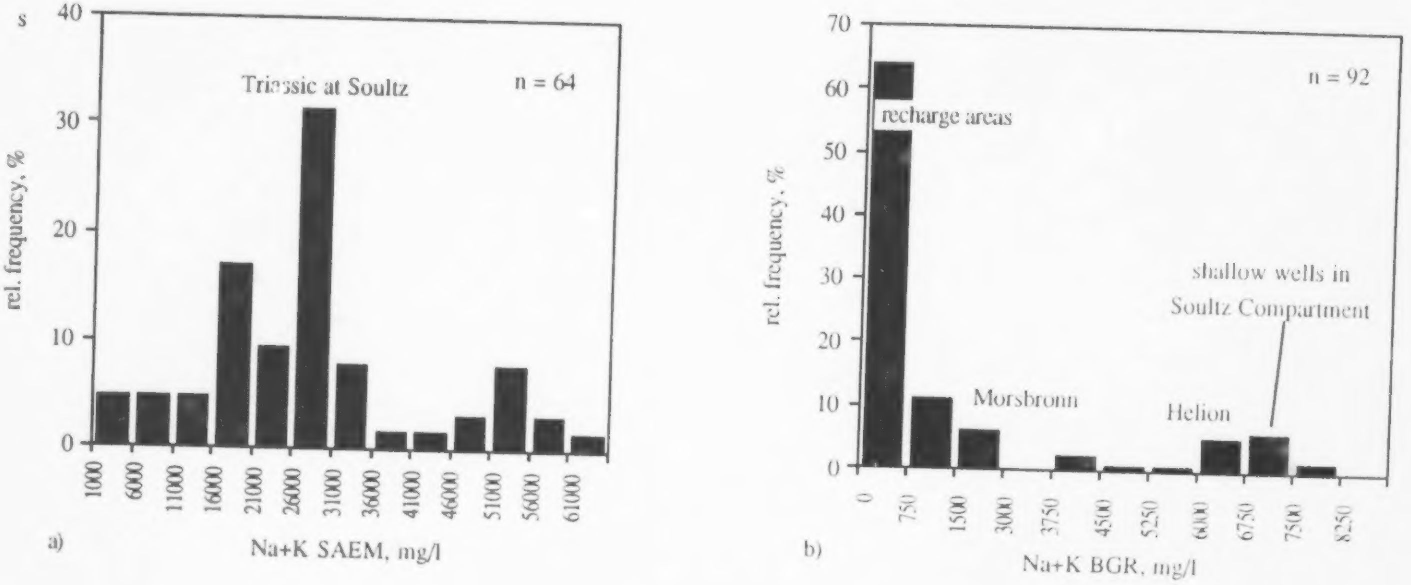

Figures 19 a,b, Relative frequency distribution for sodium + potassium concentration of formation water in the Pechelbronn-Soultz Basin; a) SAEM data; b) BGR data

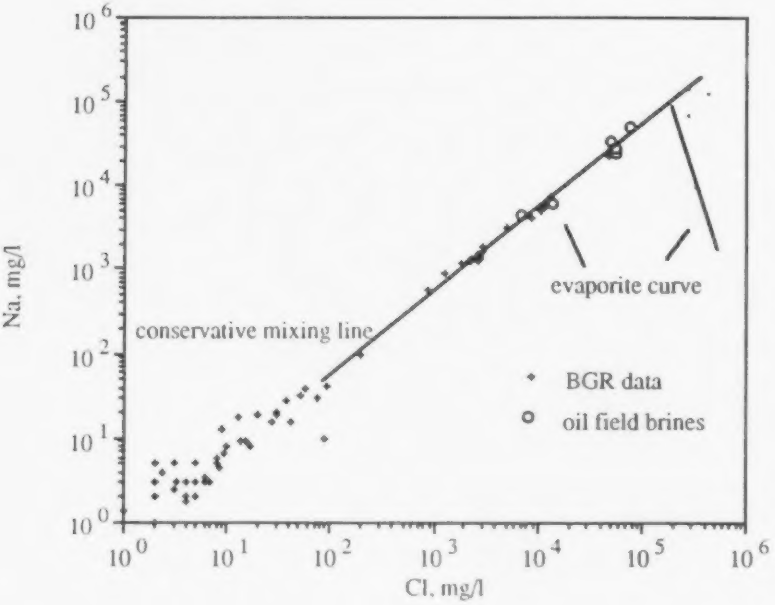

Figure 20 Relation of sodium vs. chloride concentrations for formation waters in the Pechelbronn-Soultz Basin

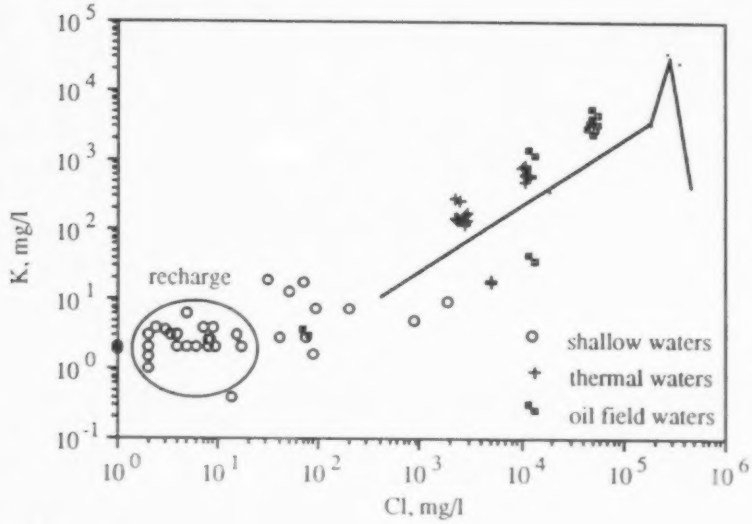

Figure 21 Relation of potassium vs. chloride concentrations for formation waters in the Pechelbronn-Soultz Basin

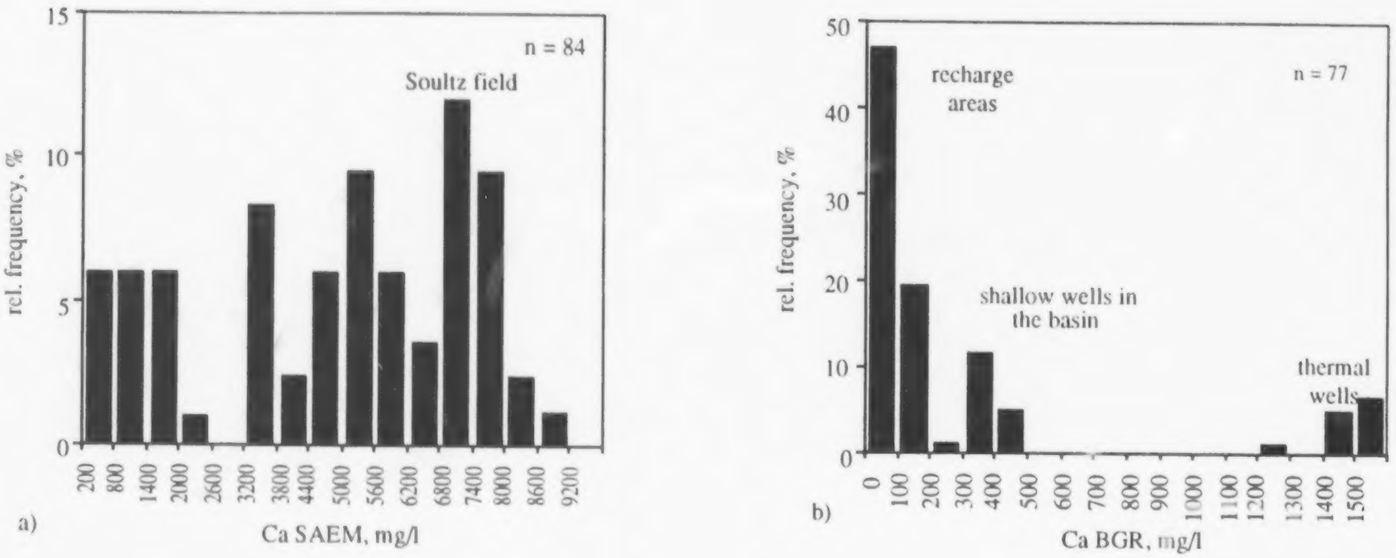

Figures 22 Relative frequency distribution of calcium concentrations for formation waters in the Pechelbronn-Soultz Basin; a) SAEM data; b) BGR data

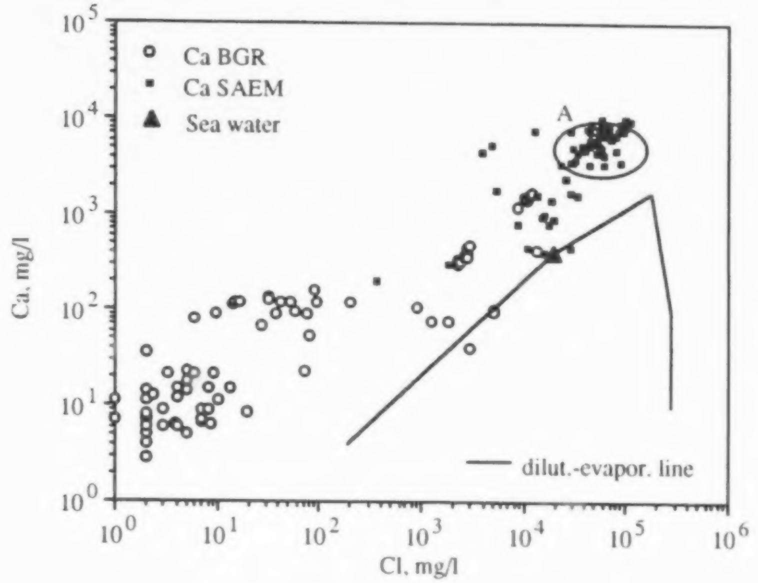

Figure 23 Relation of calcium vs. chloride concentrations for formation waters in the Pechelbronn-Soultz Basin

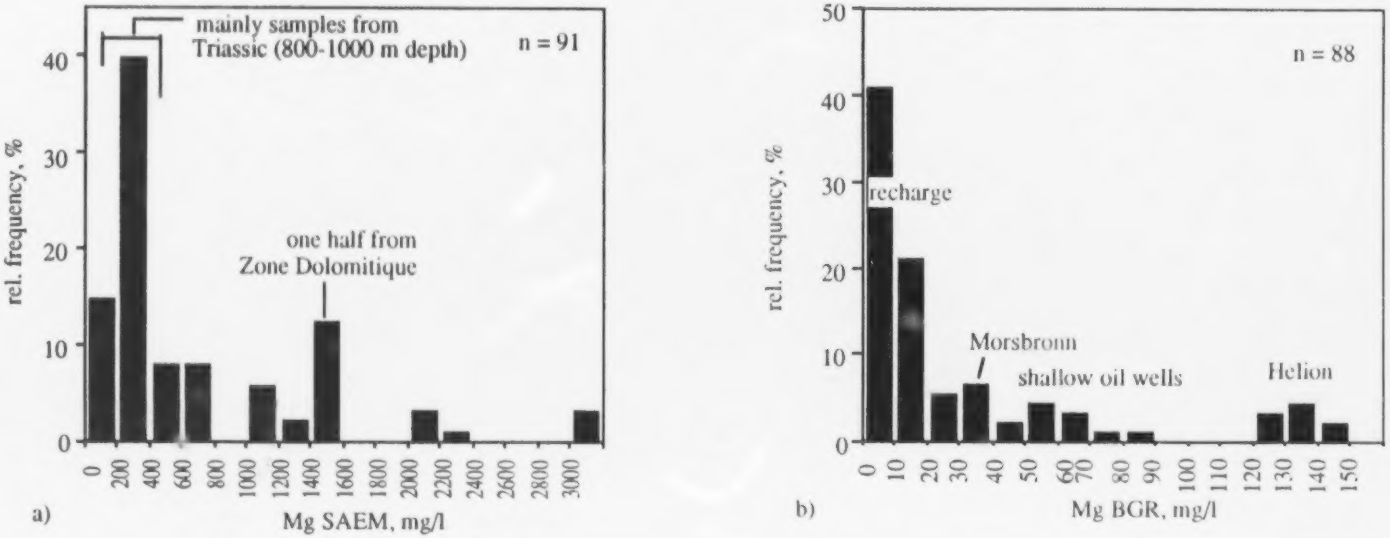

Figure 24 Relative frequency distribution of magnesium concentrations for formation waters in the Pechelbronn -Soultz Basin; a) SAEM data; b) BGR data

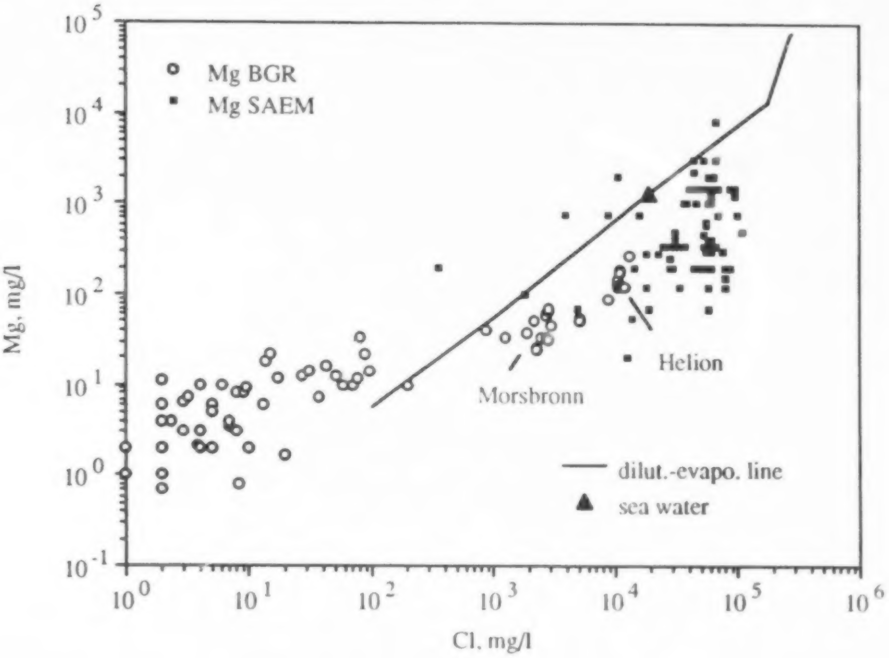

Figure 25 Relation of magnesium vs. chloride concentrations for formation waters in the Pechelbronn-Soultz Basin

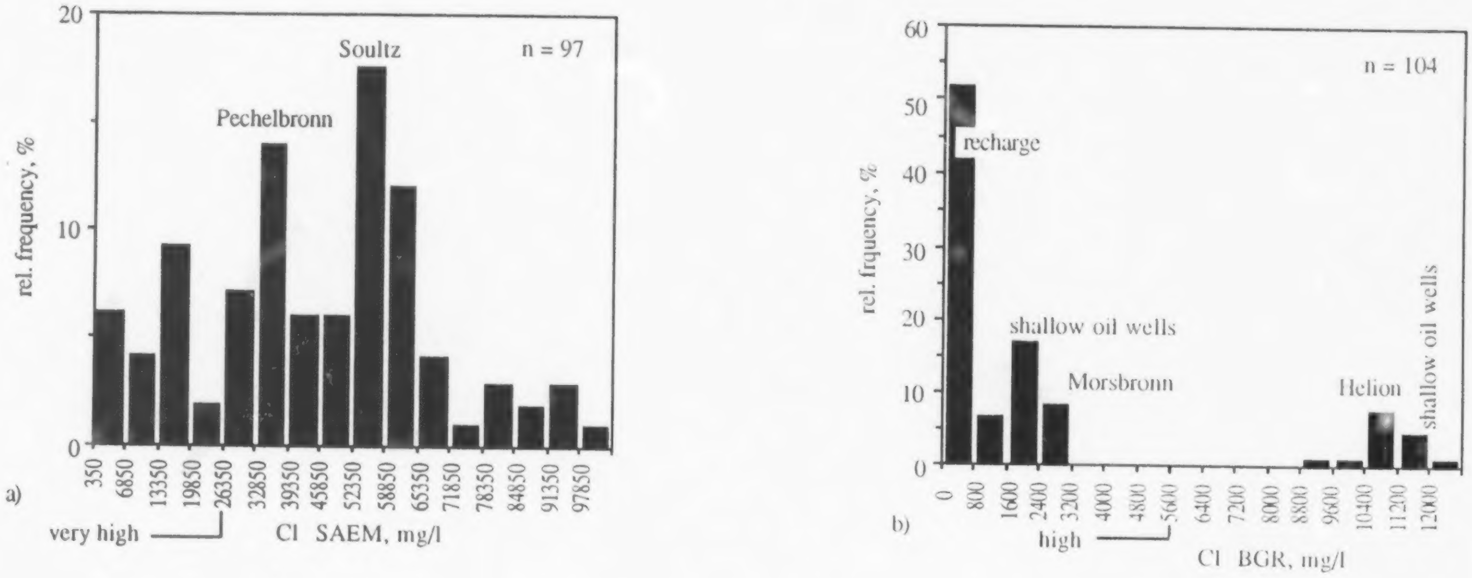

Figures 26 Relative frequency distribution of chloride concentrations for formation waters in the Pechelbronn-Soultz Basin
a) SAEM data; b) BGR data

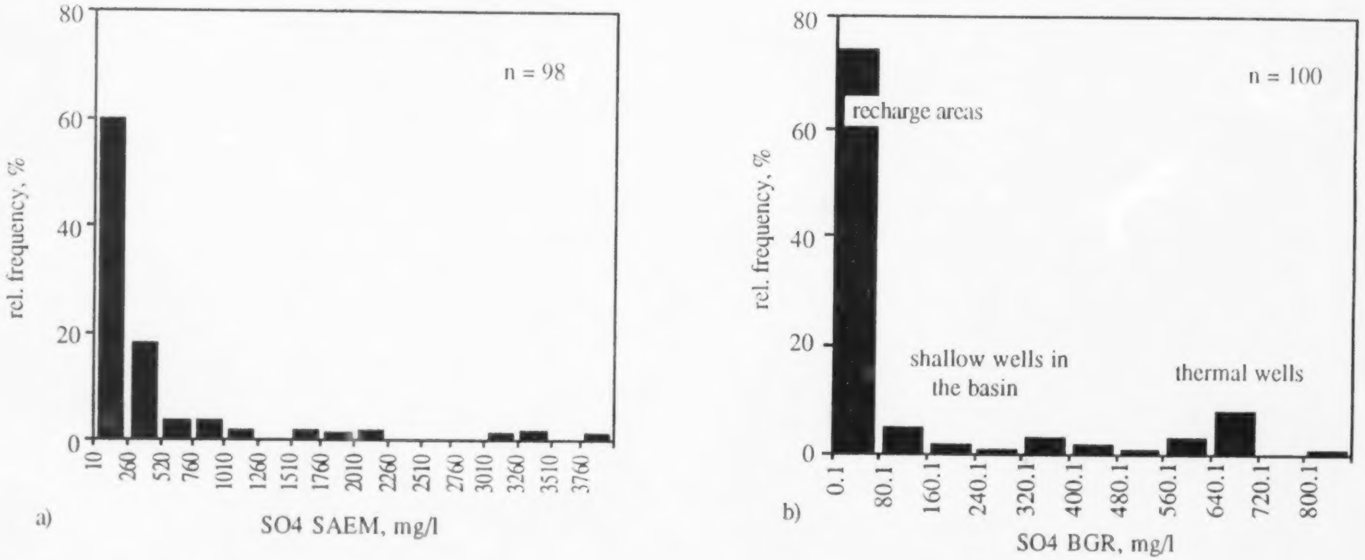

Figures 27 Relative frequency distribution of sulfate concentrations for formation waters in the Pechelbronn-Soultz Basin a) SAEM data; b) BGR data

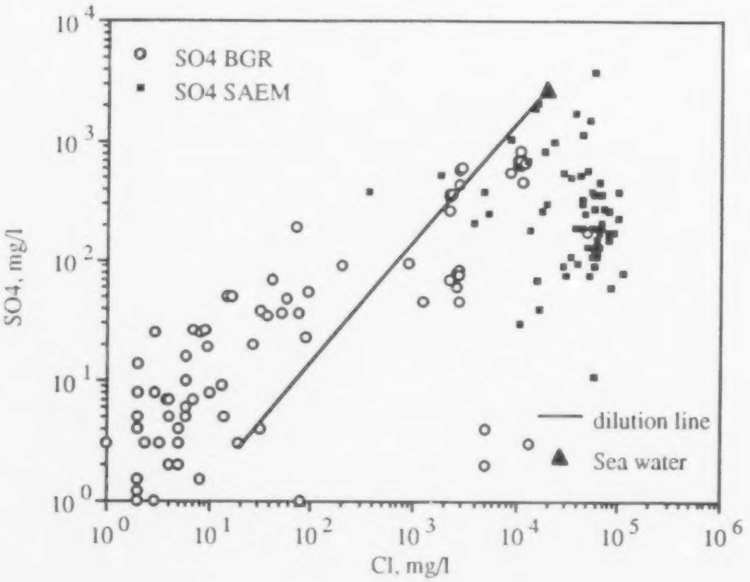

Figure 28 Relation of sulftae vs. chloride concentrations for formation waters in the Pechelbronn-Soultz Basin

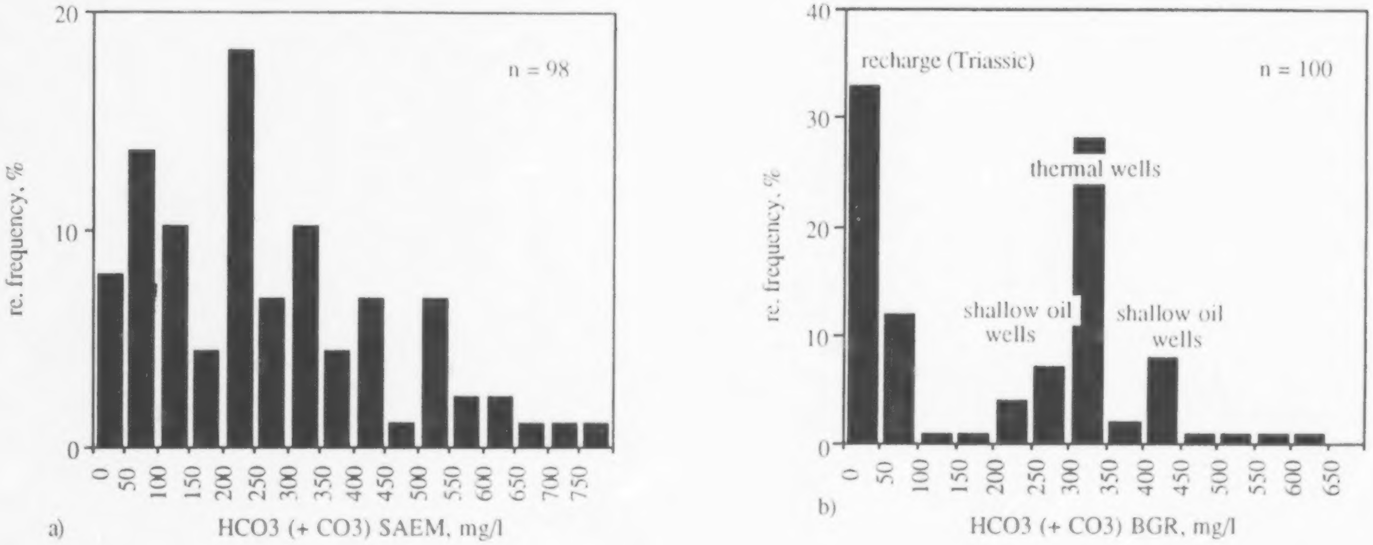

Figures 29 Relative frequency distribution of hydrogencarbonate and carbonate concentration for formation waters in the Pechelbronn-Soultz Basin; a) SAEM data; b) BGR data

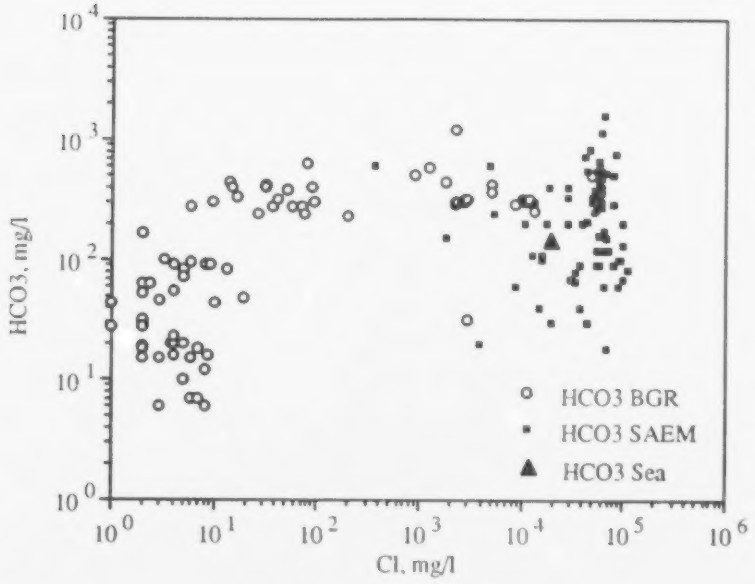

Figure 30 Relation of hydrogencarbonate+carbonate vs. chloride concentrations for formation waters in the Pechelbronn-Soultz Basin

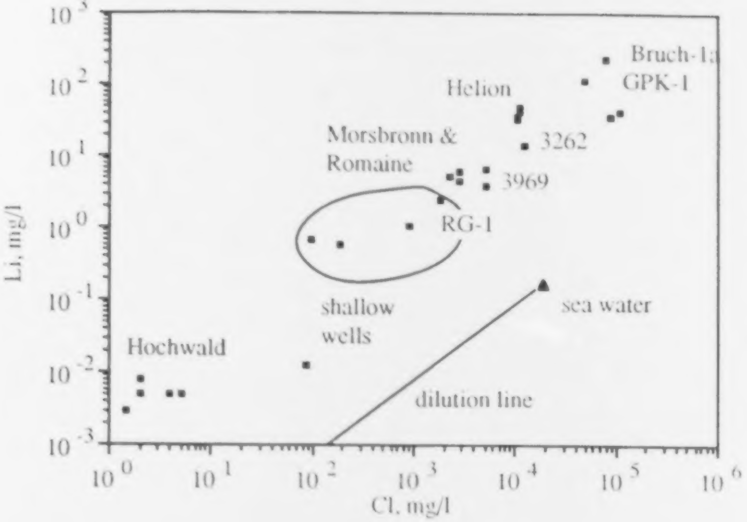

Figure 31 Lithium vs. chloride concentration for deep and shallow formation waters in the Vosges, Hochwald, Pechelbronn-Soultz Basin and Black Forest

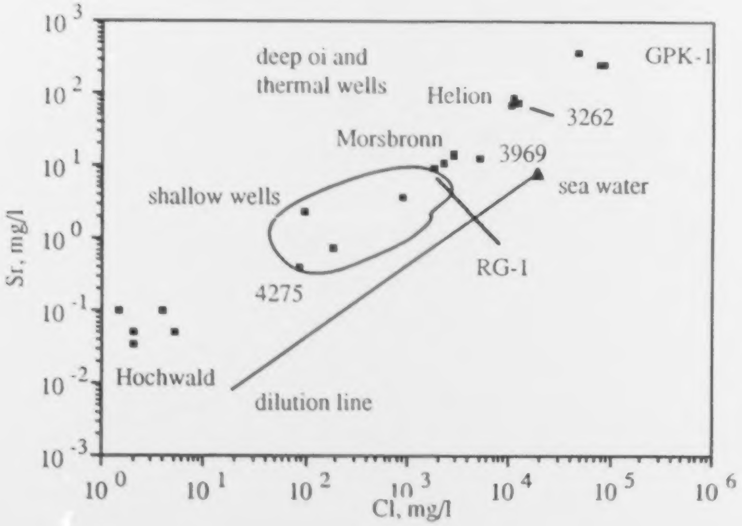

Figure 32 Strontium vs. chloride fro deep and shallow formation waters in the Vosges, Pechelbonn-Soultz Basin and Black Forest

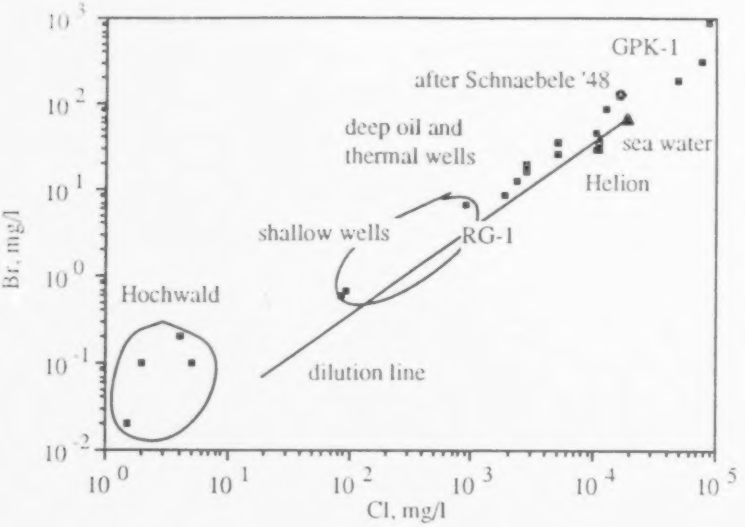

Figure 33 Bromide vs. chloride concentrations for deep and shallow
formation waters in the Vosges, Hoch, Pechelbronn-Soultz Basin

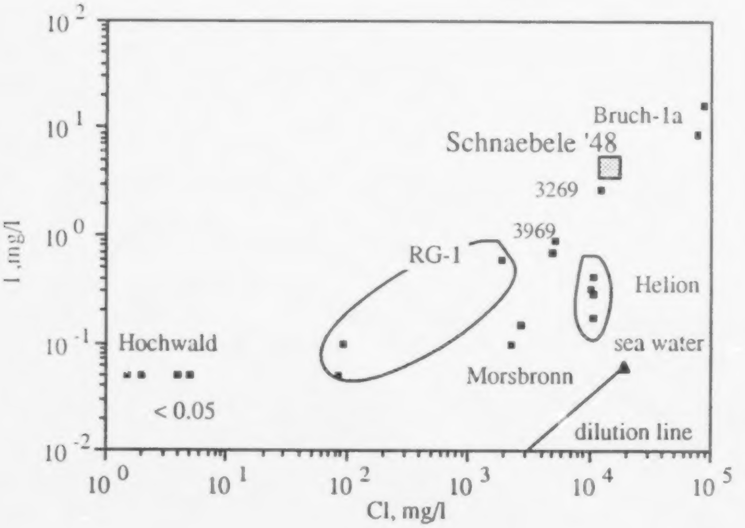

Figure 34 Iodide vs. chloride concentrations for deep and shallow formation waters in the Vosges, Hochwald and Pechebronn-Soultz Basin

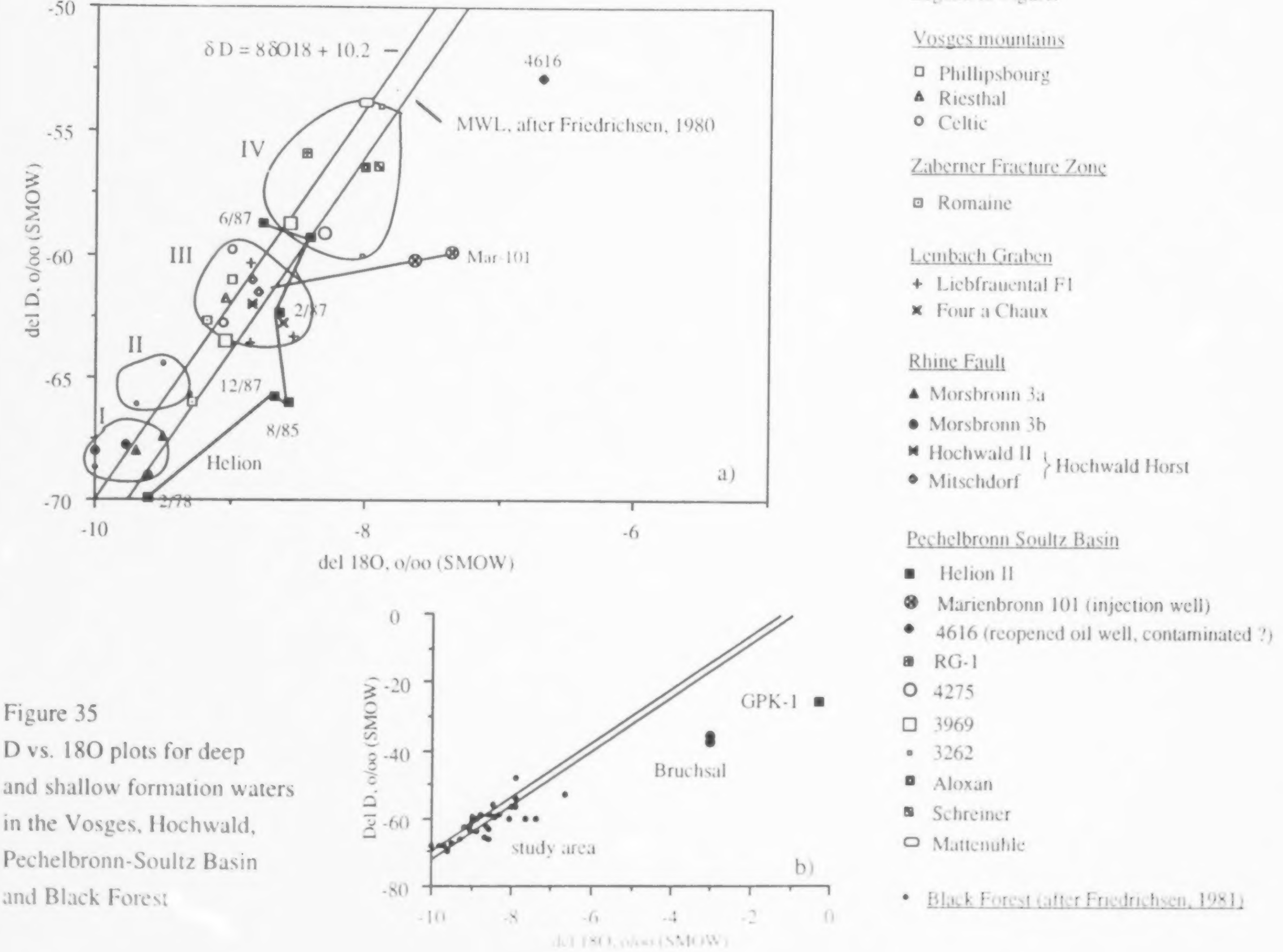

Figure 35
D vs. 18O plots for deep
and shallow formation waters
in the Vosges, Hochwald,
Pechelbronn-Soultz Basin
and Black Forest

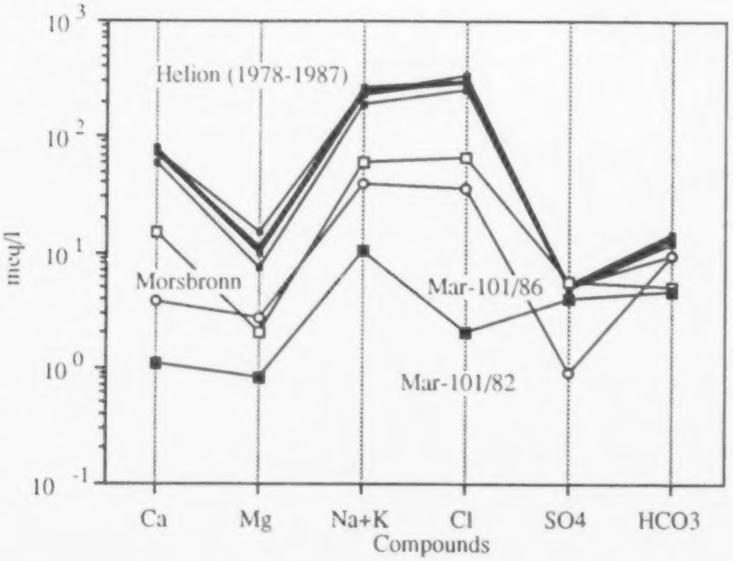

Figure 36 Schoeller diagram showing no significant chemical variation of formation waters for well Helion from 1978 to 1987

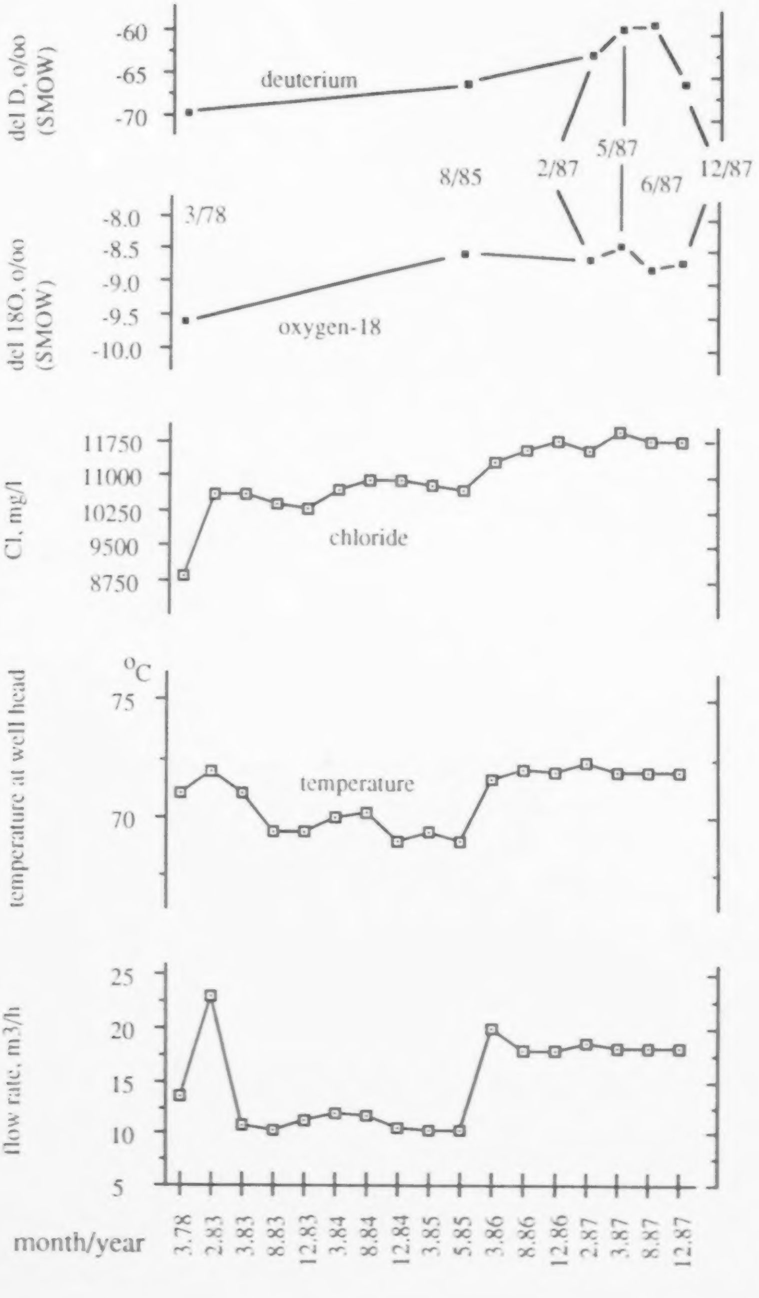

Figure 37 Changes in flow rate, salinity, temperature and stable isotopic composition of formationwater in HSU3 at well Helion II recorded from 1978 to 1987

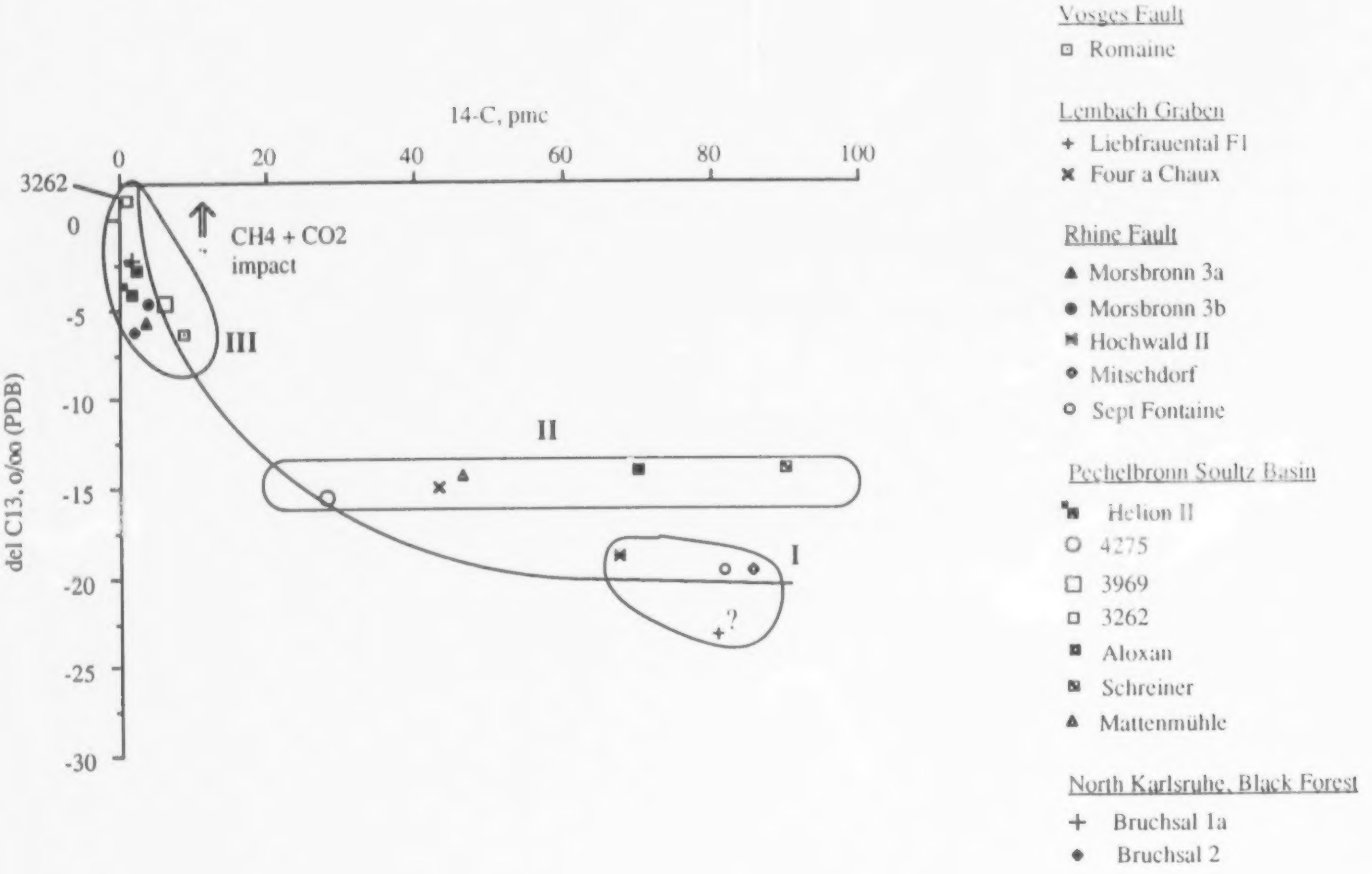

Figure 38 del 13-C vs. 14-C activity plot of for deep and shallow formation waters in the Vosges, Hochwald, Pechelbronn-Soultz Basin and Black Forest

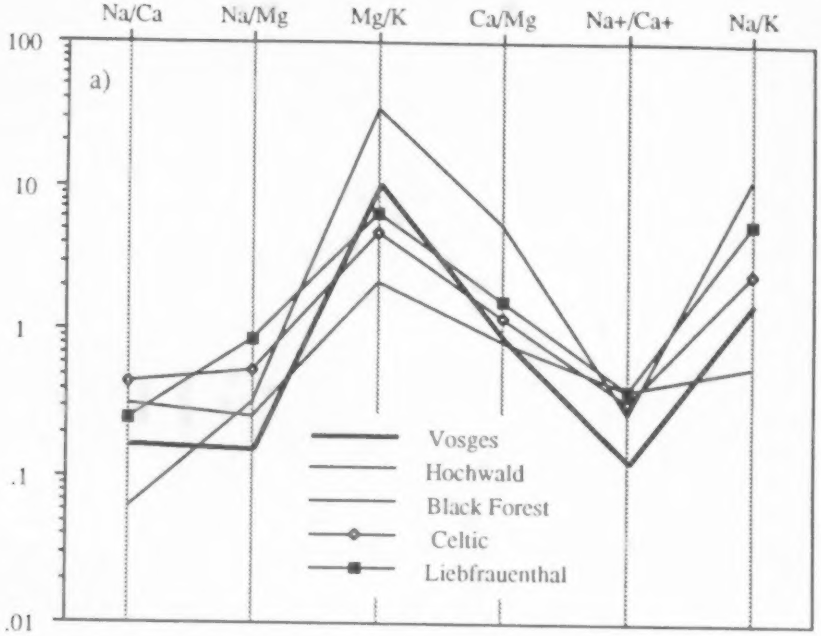

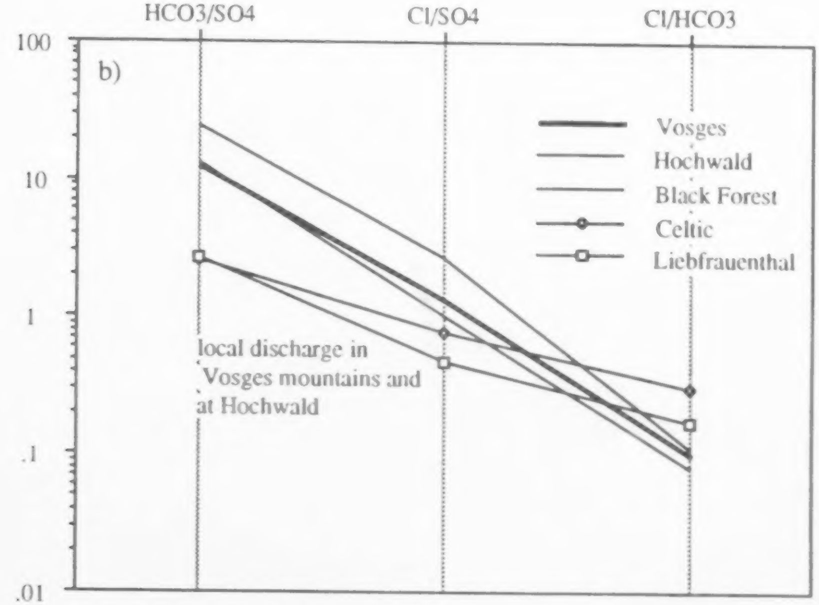

Figures 39 a,b Modified Schoeller diagram displaying ionic ratios of formation waters in the Vosges, Hochwald and Black Forest recharge areas a) cations ratios, b) anion ratios

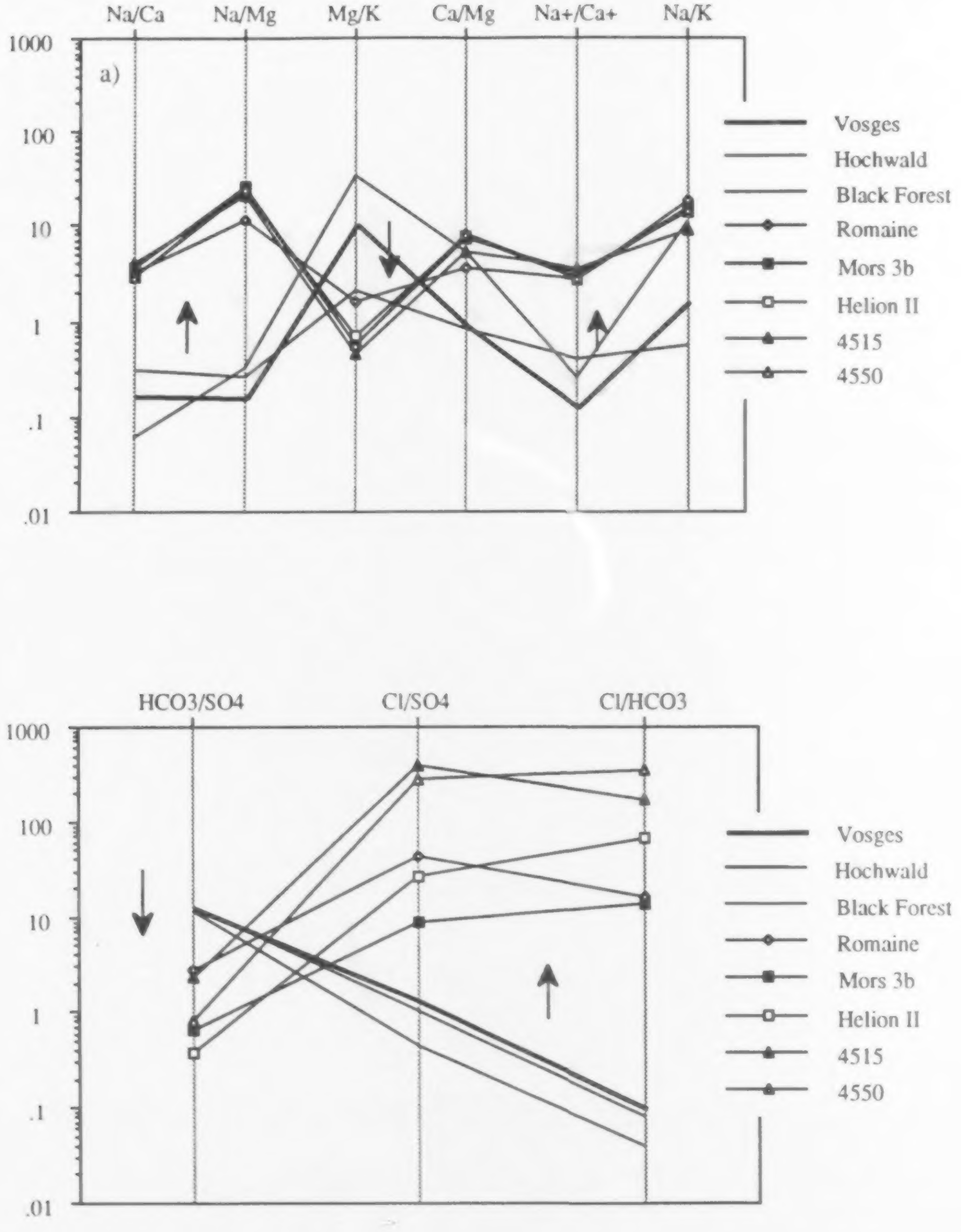

Figures 40 a,b Modified Schoeller diagram showing hydrochemical evolutionof groundwater in HSG 1 from the Vosges to the Pechelbronn -Soultz Basin a) cation ratios, b) anion ratios

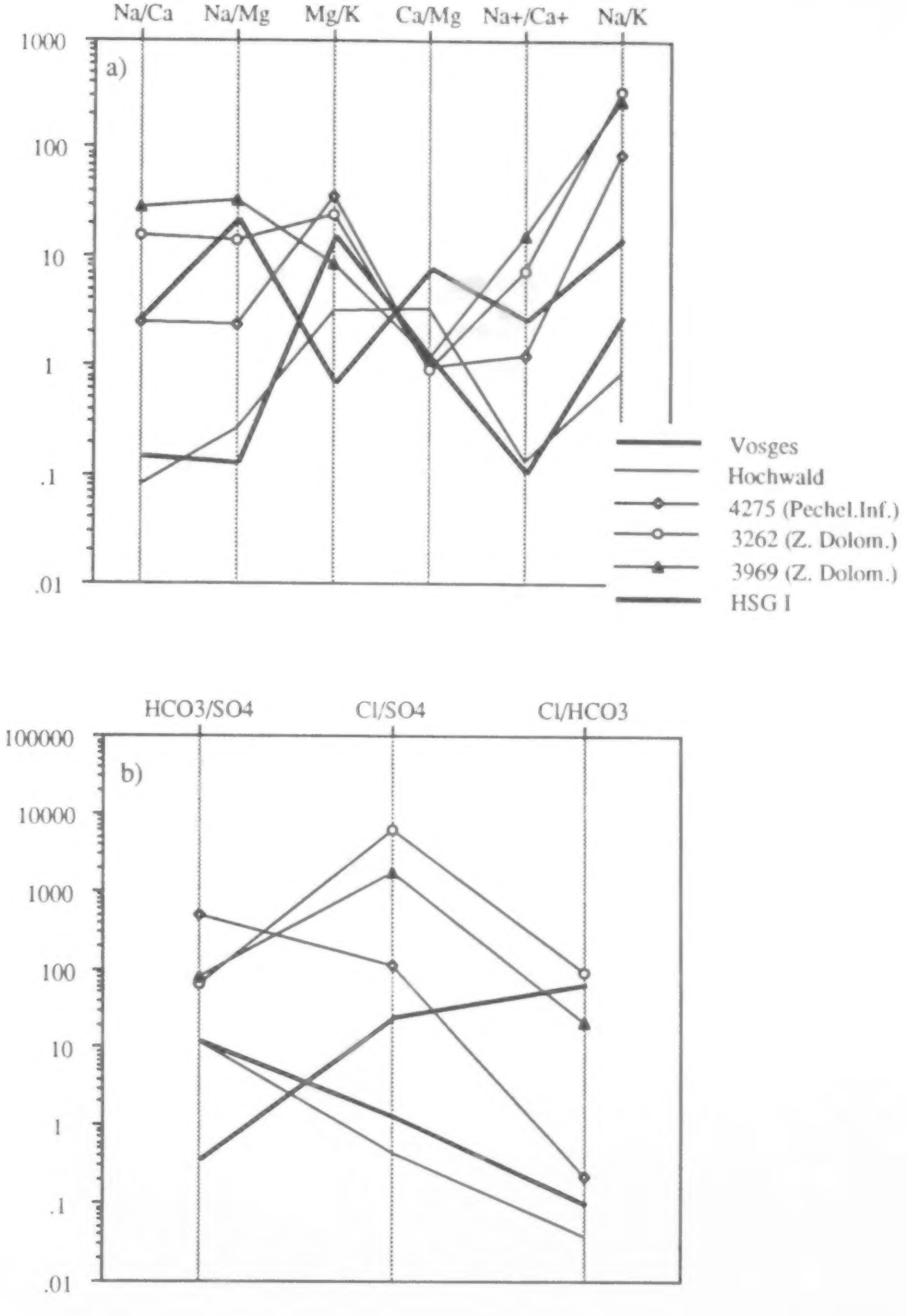

Figures 41 a, b Modified Schoeller diagram showing hydrochemical variations of formation waters in Tertiary formations at Pechelbronn and Soultz in comparison to groundwaters in recharge regions

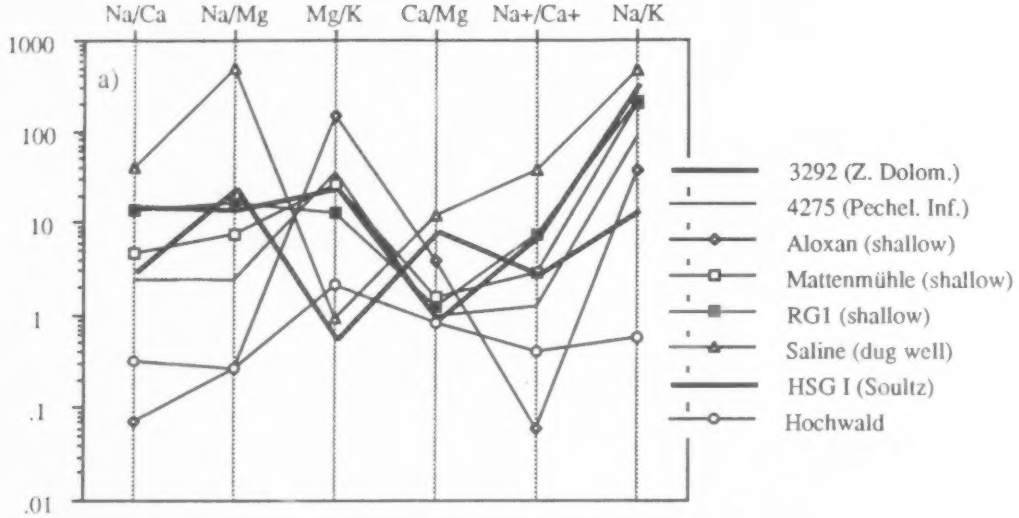

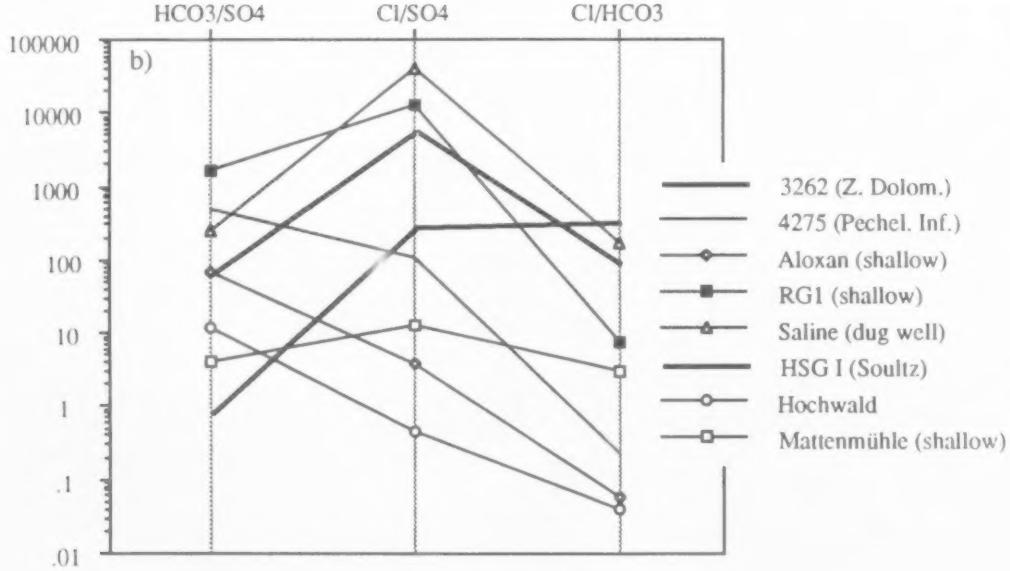

Figures 42 a,b Modified Schoeller diagram displaying hydrochemical differencesand similarities of groundwaters from shallow wells in Tertiary formations in comparison to deep formation waters in the Kutznehausen-Soultz region

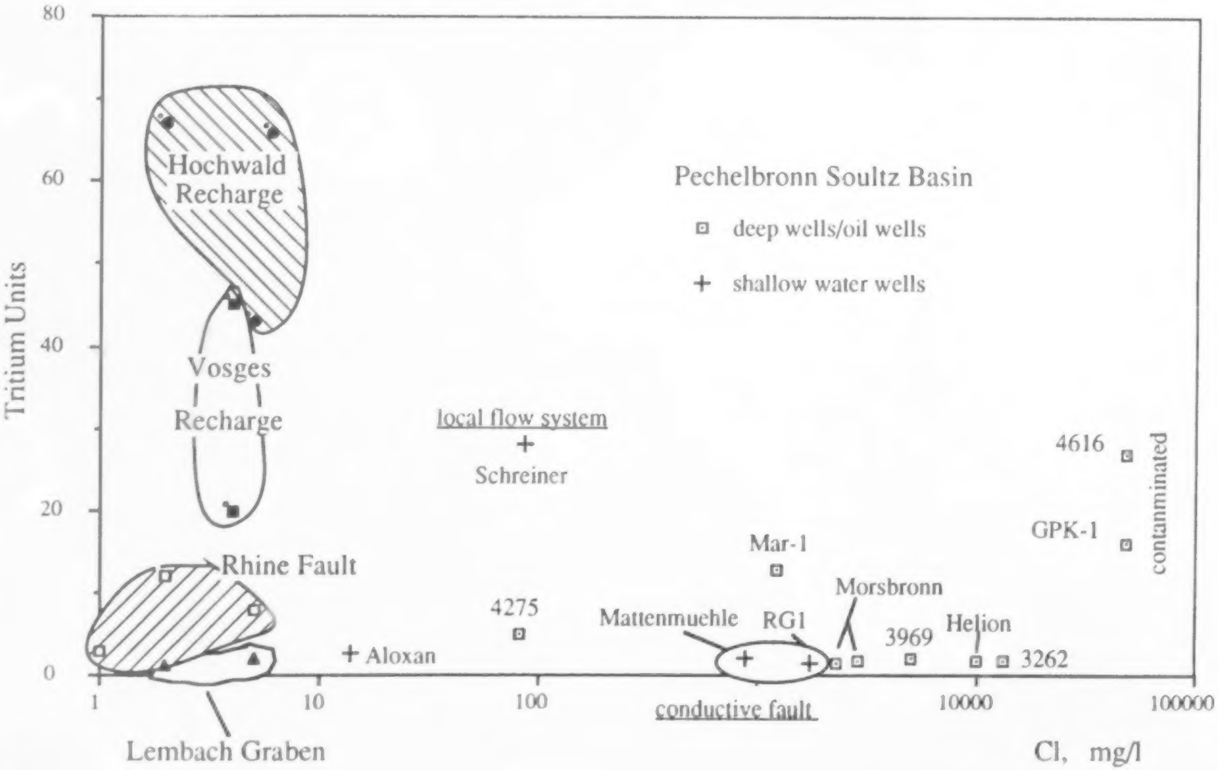

Figure 43 Tritium vs. chloride concentration plot showing a deceasing 3H/Cl ratio for formation waters from the western recharge regions towards the Pechelbronn-Soultz Basin

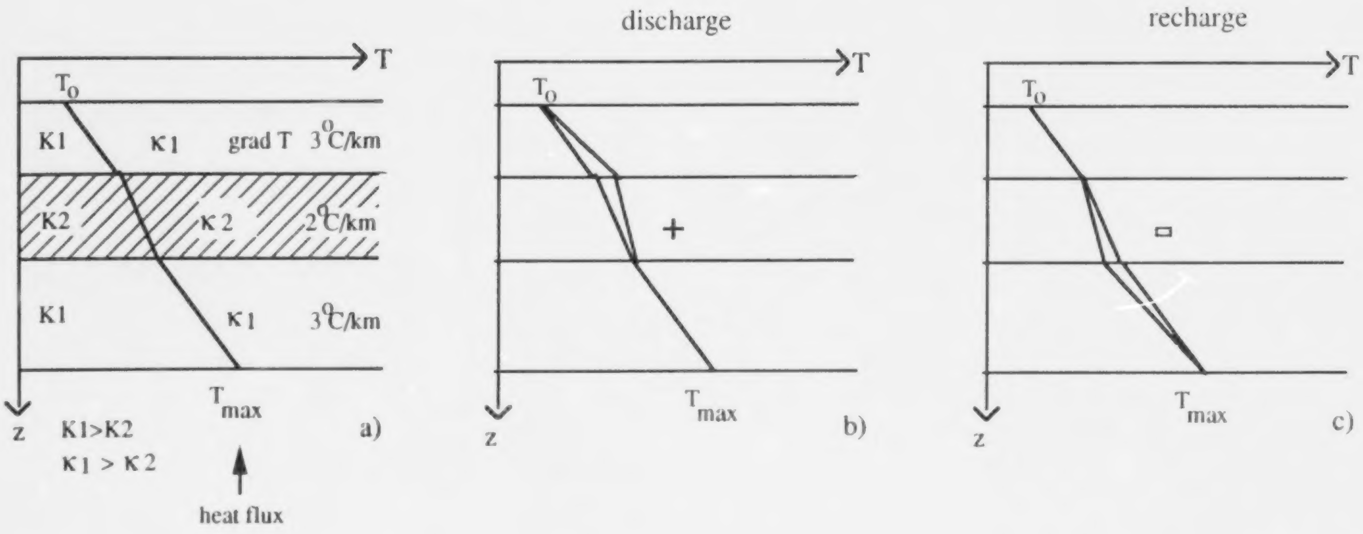
discharge
recharge
T
z
T_o
T_{max}
K1
K2
κ1
κ2
grad T 3°C/km
2°C/km
3°C/km
K1>K2
κ1 > κ2
heat flux
+
□
a)
b)
c)

a) conductive heat flow: geothermal gradient changes in formation of different thermal and hydraulic conductivities

b) additional convective heat transport by ascending groundwater flow, increase in grad T and positive temperature anomalie

c) same as b), but descending groundwater flow results in a grad T decline and negative heat anomaly

Figure 44 Schematic diagram showing the changes in grad T and temperature regimes affected by the transport of heat of ascending and descending groundwater flow

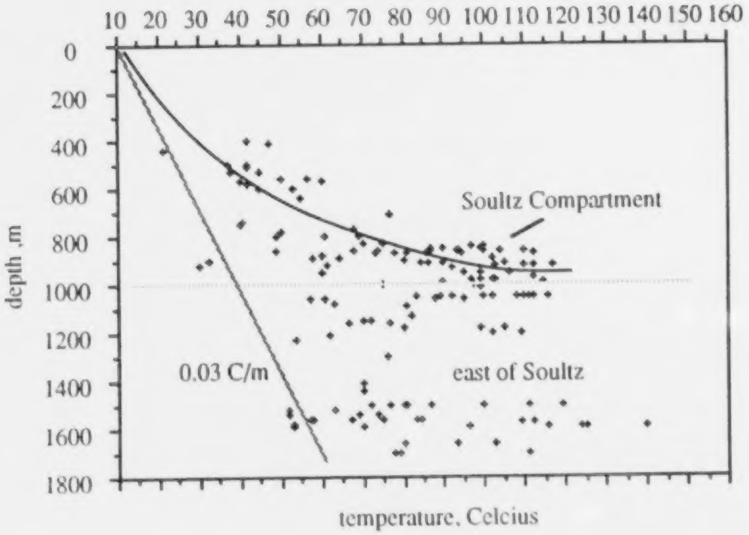

Figure 45 Temperature vs. depth plot for the entire study area

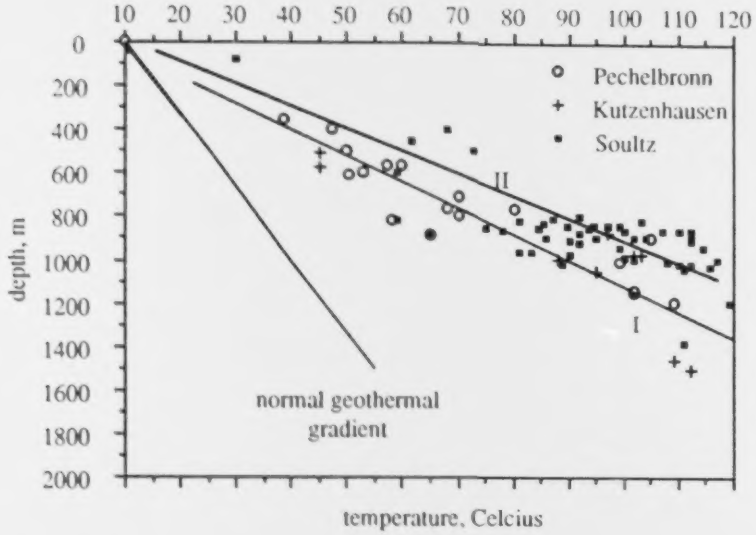

Figure 46 Temperature vs. depth plot for the Pechelbronn, Kutzenhausen and Soultz area

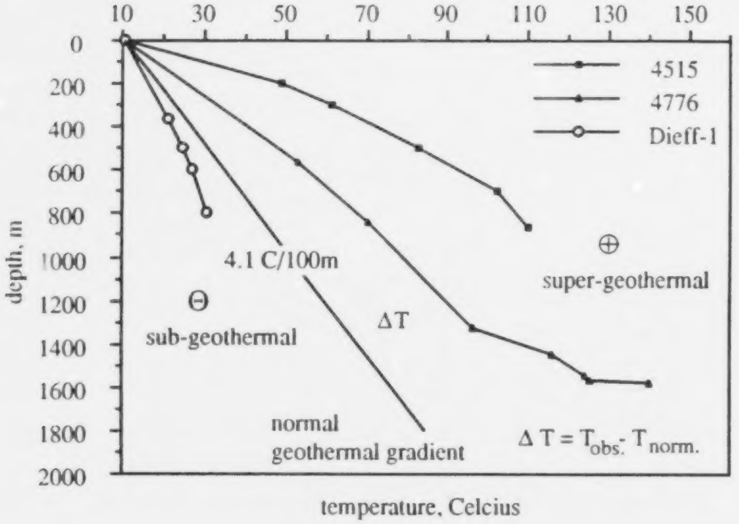

Figure 47 Geothermal gradients for 3 wells in the Pechelbronn-Soultz Basin and Internal Zone showing negative and positive temperature anomalies

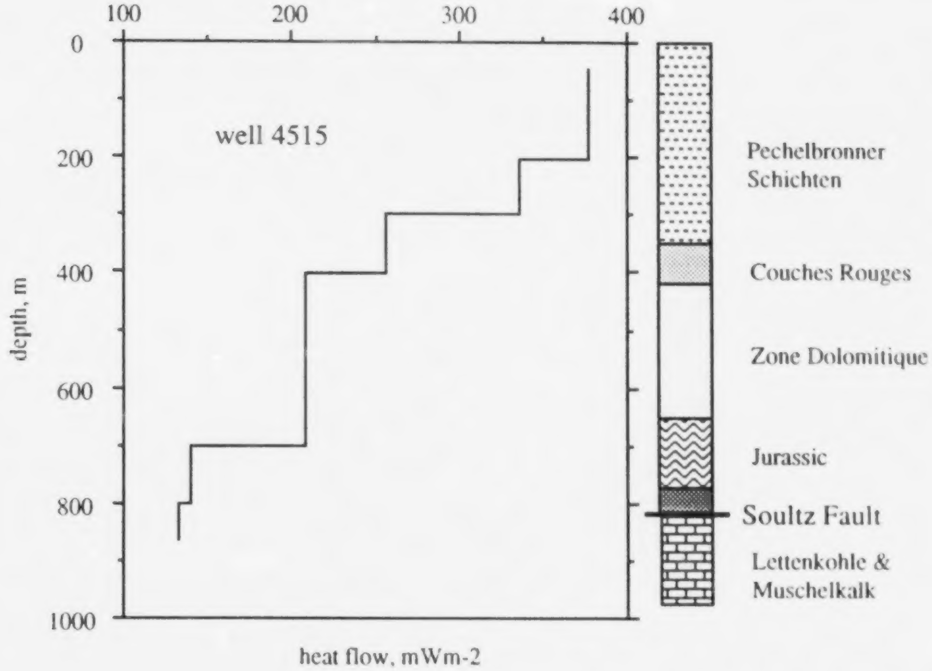

Figure 48 Heat flow vs. depth for well 4515 calculated for intervals bounded by successive BHT

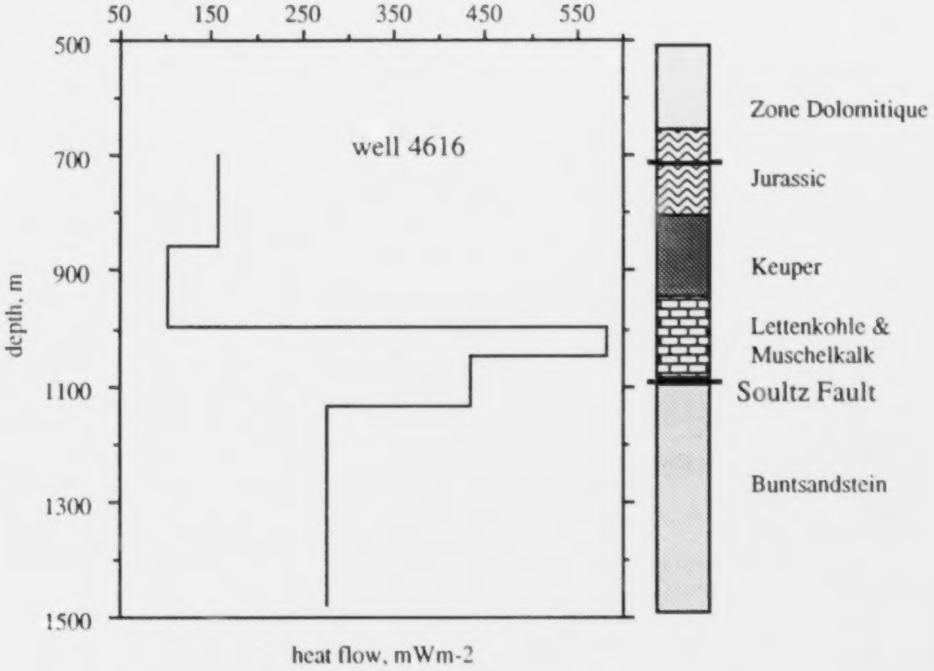

Figure 49 Heat flow vs. depth for well 4616 calculated for intervals bounded by successive BHT

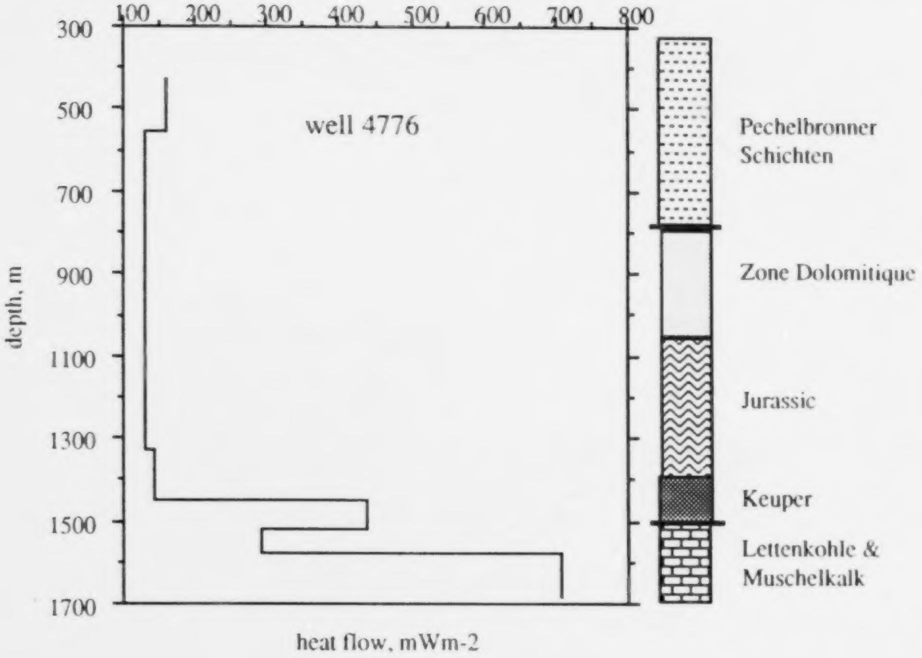

Figure 50 Heat flow vs. depth for well 4776 calculated for intervals bounded by successive BHT

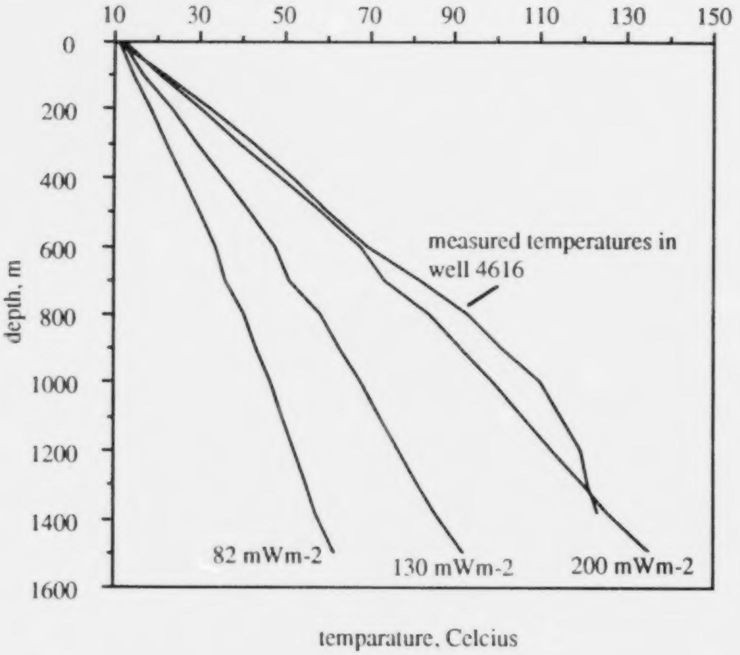

Figure 51 Calculated subsurface temperatures for given basal heat flow values of 82, 130 and 200 mWm-2 in comparison to a temperature profile of well 4616

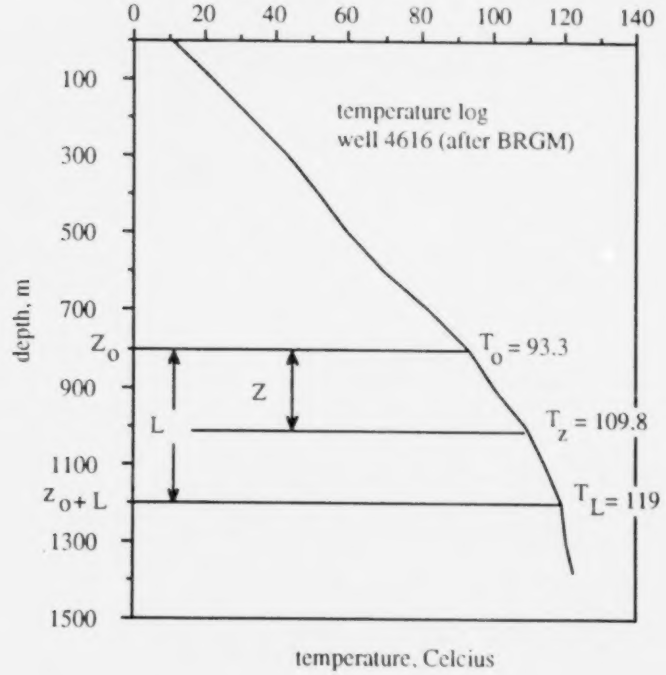

Figure 52 Temperature log for well 4616, measured by BRGM in 1988

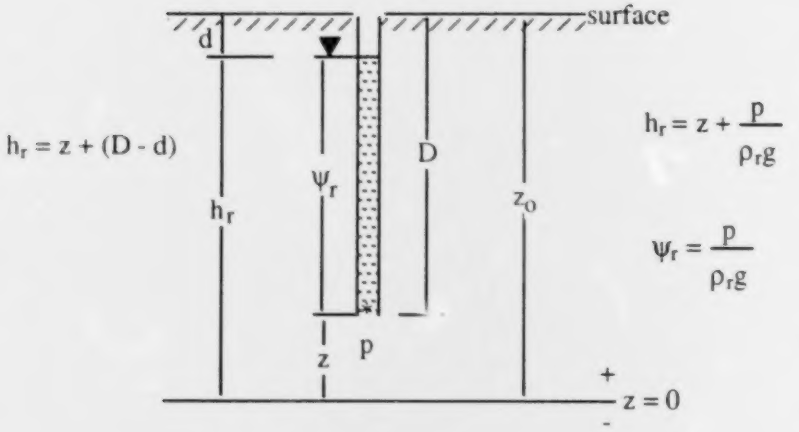
surface
d
$h_r = z + (D - d)$
h_r
ψ_r
D
z_o
z
p
$h_r = z + \frac{p}{\rho_r g}$
$\psi_r = \frac{p}{\rho_r g}$
+
z = 0
-

Figure 53 Definitions of hydraulic-, elevation-, and pressure head and given subsurface well data

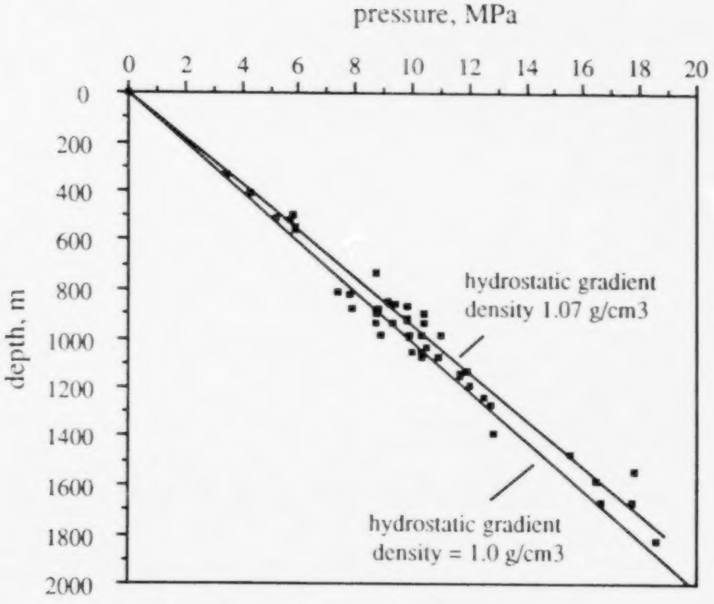

Figure 54 Pressure vs. depth plot for all available stabilized DST pressure data

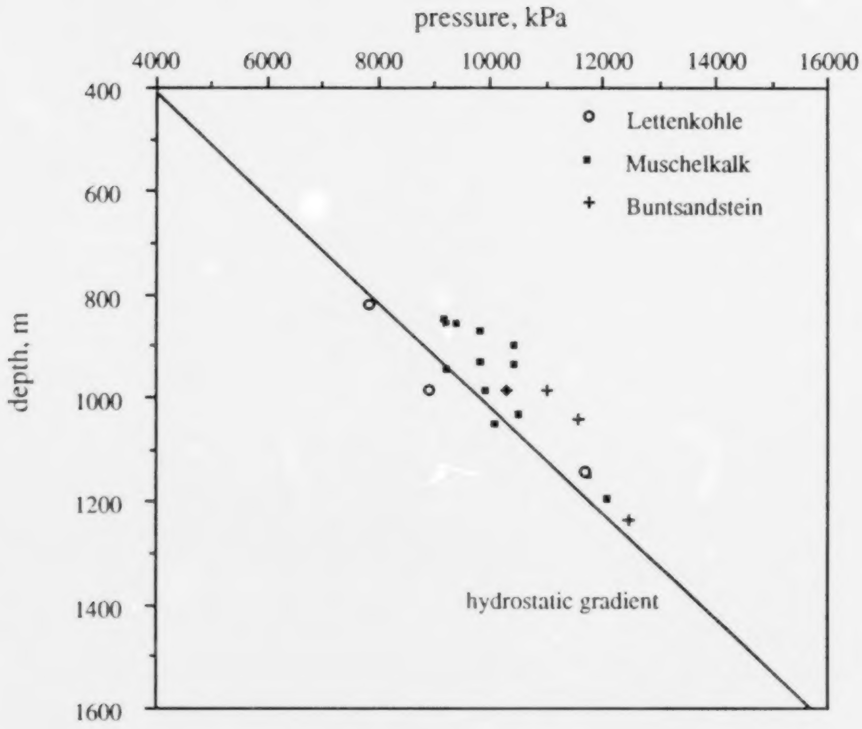

line 1: wells 4515, 4620, 4598, 4555 — SF4, SF5

line 2: wells 4585, 4541

line 2a: wells 4585, 4590

line 3: wells 4550, 4583 — SF3, SF3

line 4: wells 4606, 4613 — SF3

line 5: wells 4602

Figure 55 Pressure vs. depth plot for pressure measurements in HSU3 in the Kutzenhausen-Soultz-Hermerswiller Compartments

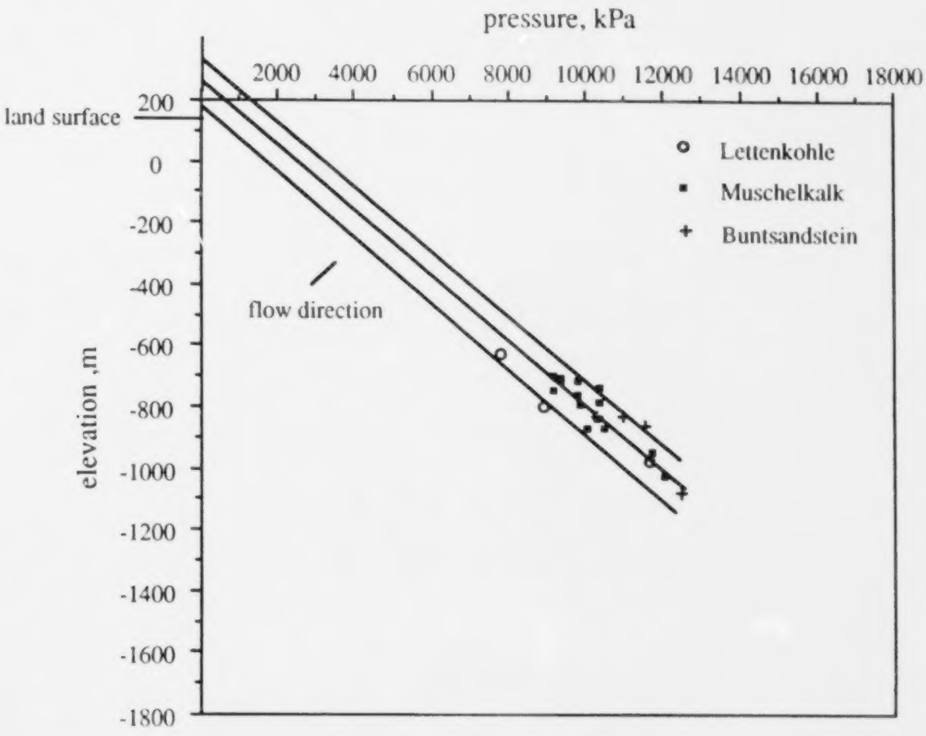

Figure 56 Pressure vs. elevation plot for pressure measurements in HSU 3 in the Kutzenhausen-Soultz-Hermerswiller Compartments

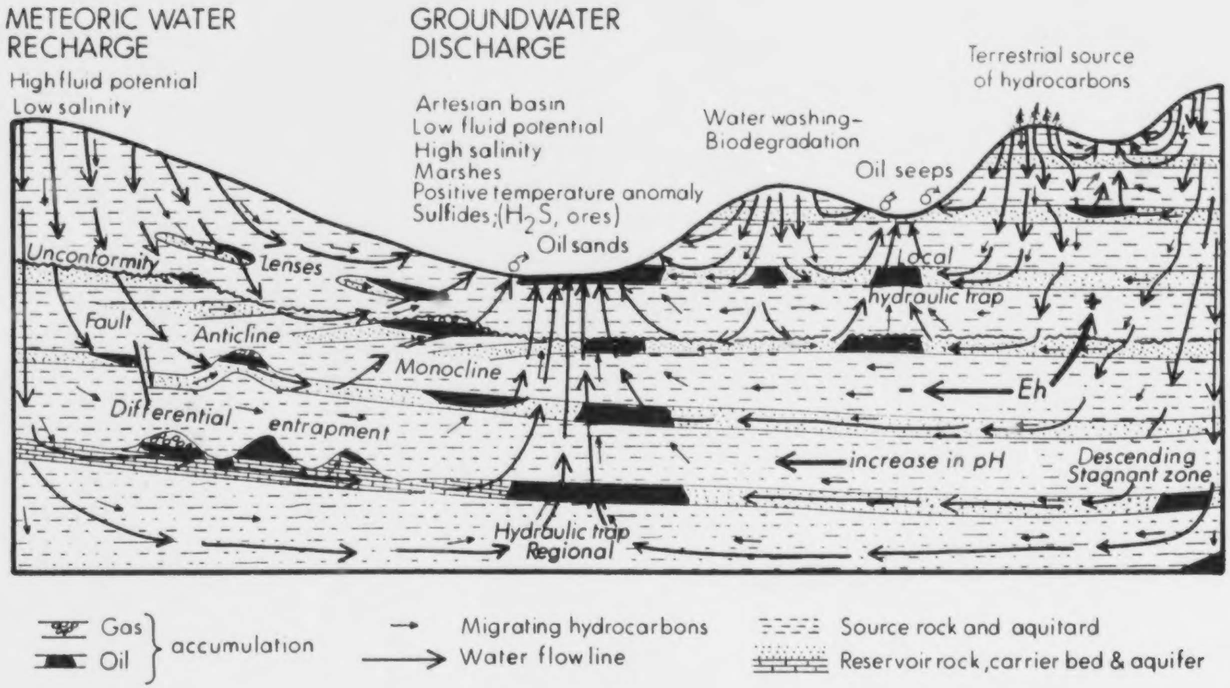
METEORIC WATER RECHARGE
High fluid potential
Low salinity
GROUNDWATER DISCHARGE
Artesian basin
Low fluid potential
High salinity
Marshes
Positive temperature anomaly
Sulfides;(H2S, ores)
Oil sands
Water washing-Biodegradation
Oil seeps
Terrestrial source of hydrocarbons
Unconformity
Lenses
Fault
Anticline
Monocline
Differential entrapment
Local hydraulic trap
Eh
increase in pH
Descending
Stagnant zone
Hydraulic trap Regional
Gas
Oil
accumulation
Migrating hydrocarbons
Water flow line
Source rock and aquitard
Reservoir rock, carrier bed & aquifer

Figure 57 Graphical summary of the hydraulic theory of petroleum migration and associated natural phenomena (modified after Tóth, 1980)

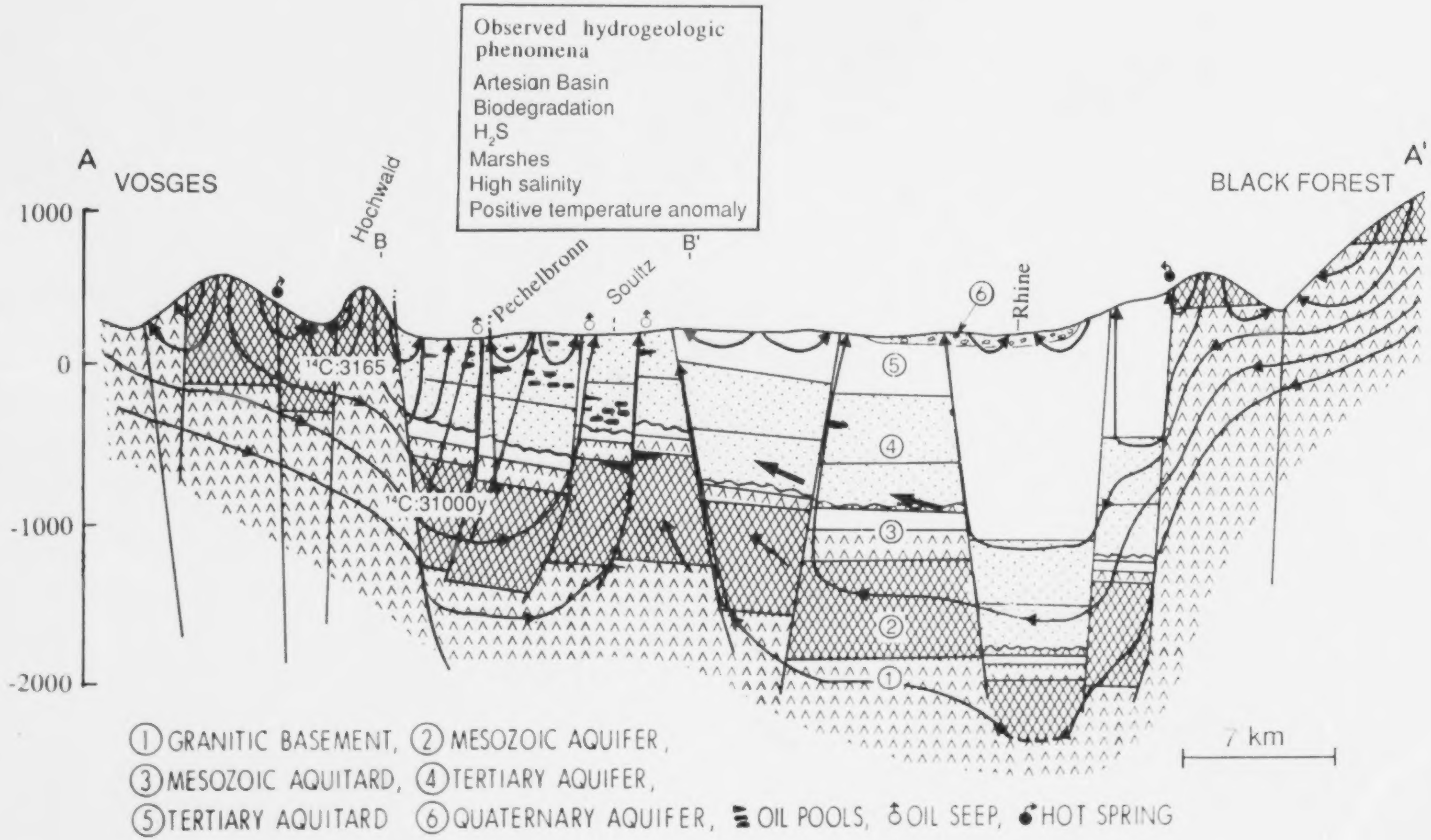
Observed hydrogeologic phenomena
Artesian Basin
Biodegradation
H2S
Marshes
High salinity
Positive temperature anomaly
A
VOSGES
A'
BLACK FOREST
1000
0
-1000
-2000
Hochwald
B
B'
Pechelbronn
Soultz
Rhine
⑥
⑤
④
③
②
①
14C:3165
14C:31000y
7 km
① GRANITIC BASEMENT, ② MESOZOIC AQUIFER,
③ MESOZOIC AQUITARD, ④ TERTIARY AQUIFER,
⑤ TERTIARY AQUITARD ⑥ QUATERNARY AQUIFER, OIL POOLS, OIL SEEP, HOT SPRING

Figure 58 Schematic representation of regional groundwater flow between the graben's shoulders with observed phenomena and ^{14}C values

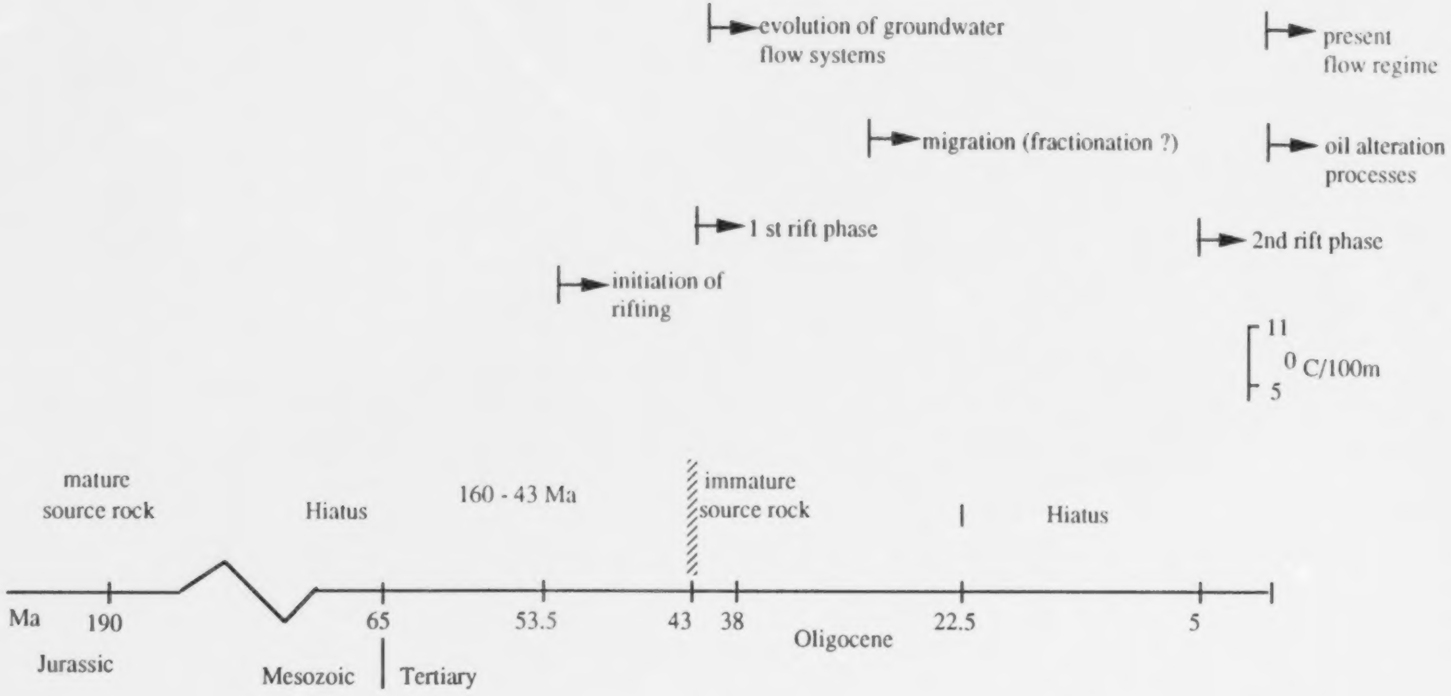
evolution of groundwater flow systems
present flow regime
migration (fractionation ?)
oil alteration processes
1 st rift phase
2nd rift phase
initiation of rifting
11
0 C/100m
5
mature source rock
Hiatus
160 - 43 Ma
immature source rock
Hiatus
Ma
190
65
53.5
43
38
22.5
5
Jurassic
Mesozoic
Tertiary
Oligocene

Figure 59 Geological, geothermal, hydrogeological and petroleum geological history of the Upper Rhine Graben study area

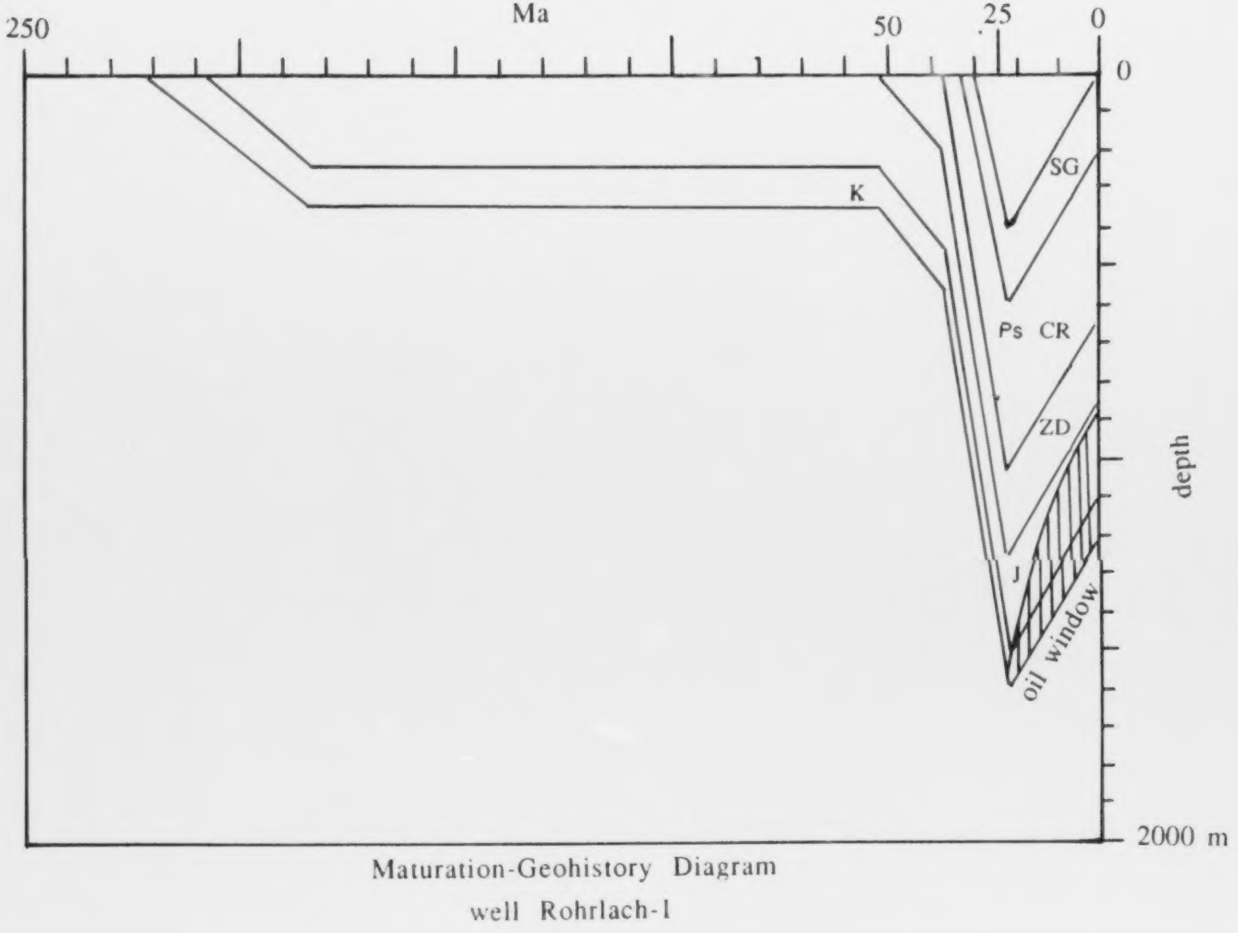

Figure 60 Maturation-Geohistory diagram (Lopatin's method) for well Rohrlach-1 showing that Jurassic source rocks reach the oil window about 25 Ma ago

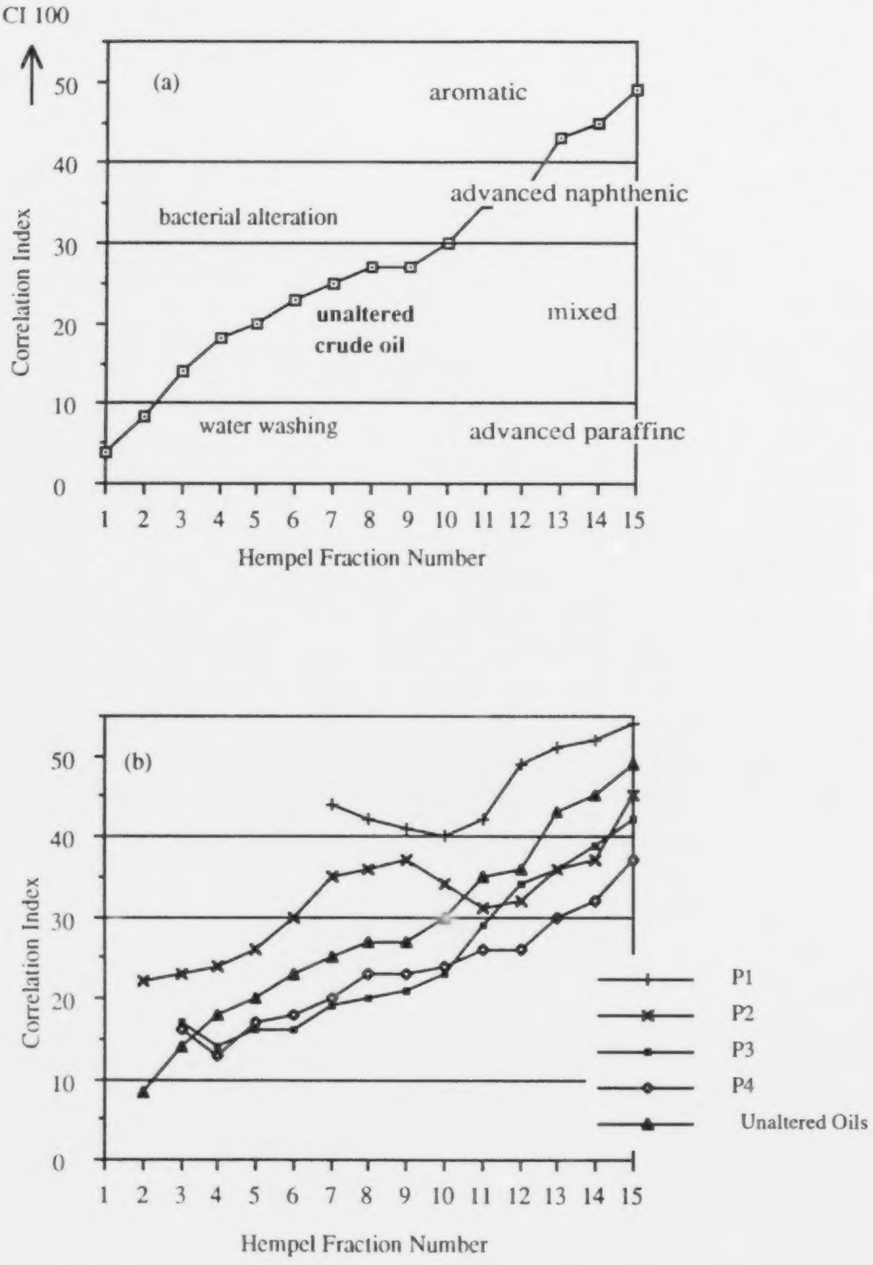

Figure 61 con't next page

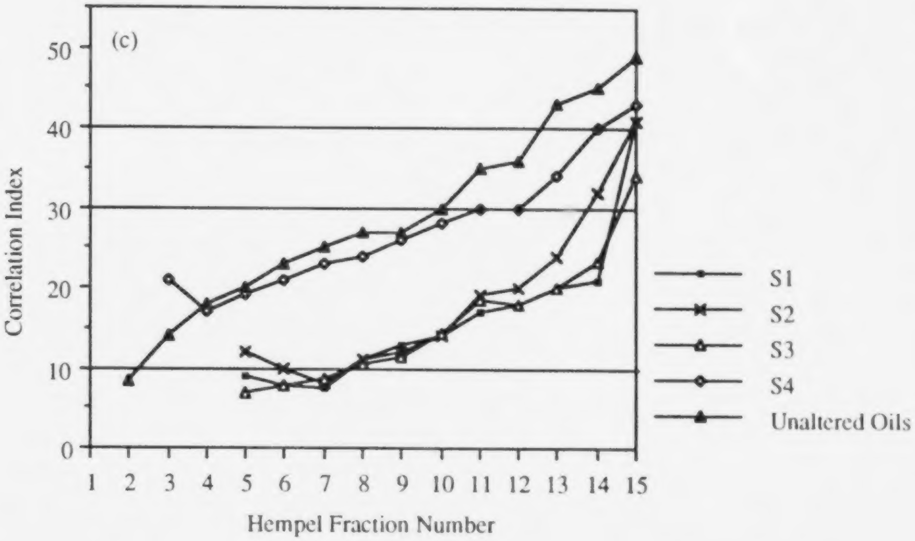

Figures 61 a) Schematic representation of the effects of bacterial alteration and water washing on the Correlation Index plot; b) Correlation Index plot for altered oils at Pechelbronn, P1-P4; and c) Correlation Index plot for altered oils at Soultz, S1-S4, O1 represents an unaltered oil from a Jurassic reservoir at Ohlungen, south of the study area.

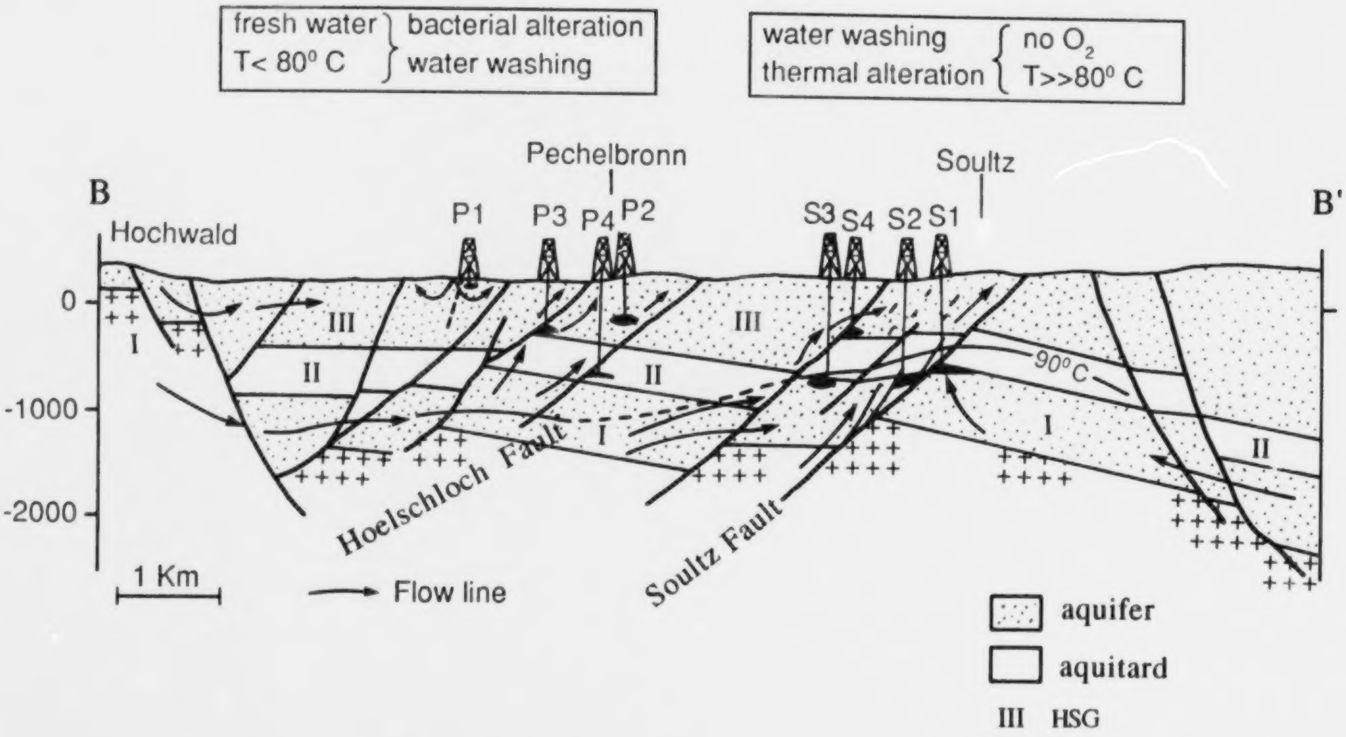
fresh water
T< 80° C
bacterial alteration
water washing
water washing
thermal alteration
no O2
T>>80° C
Pechelbronn
Soultz
B
B'
Hochwald
P1
P3
P4
P2
S3
S4
S2
S1
0
-1000
-2000
III
II
I
90°C
Hoelschloch Fault
Soultz Fault
1 Km
Flow line
aquifer
aquitard
III HSG

Figure 62 Schematized locations of sampled oil pool, P1-P4 and S1-S4 in the Pechelbronn-Soultz Basin and emplaced oil alteration-degradation processes by the hydrodynamic, geochemical and geothermal system

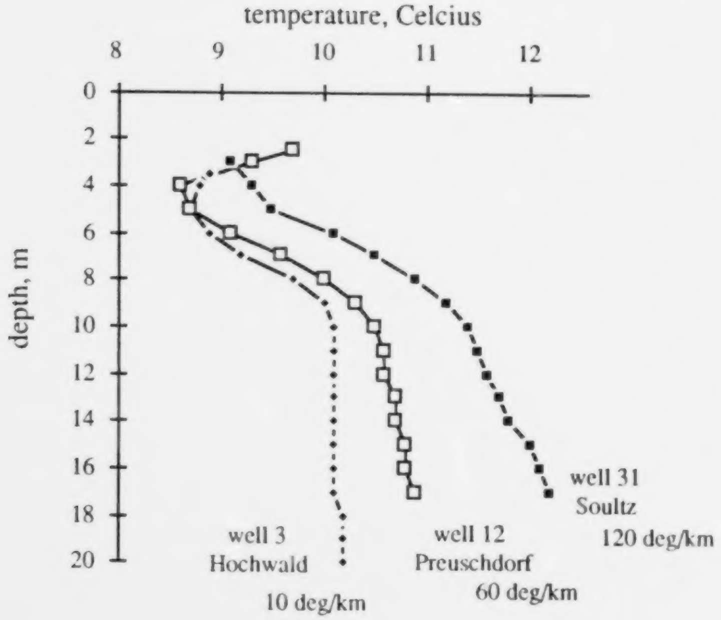

Figure 63 Near-surface temperatures vs. depth plot for wells 3, 12 and 31

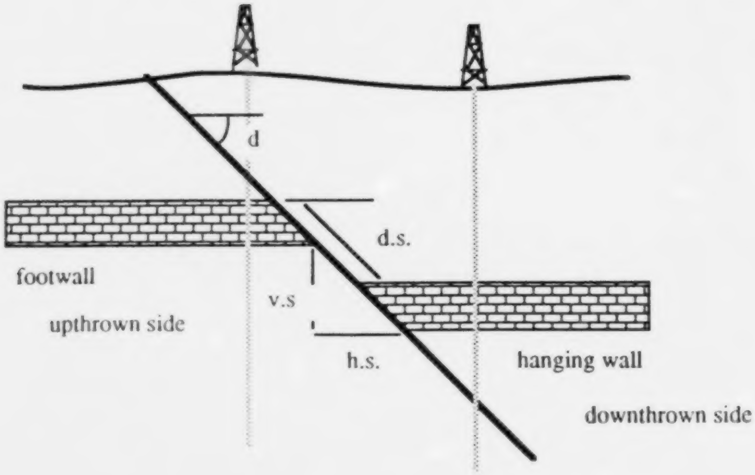
d
d.s.
footwall
v.s
upthrown side
h.s.
hanging wall
downthrown side

Figure 64 Fault descriptive variables

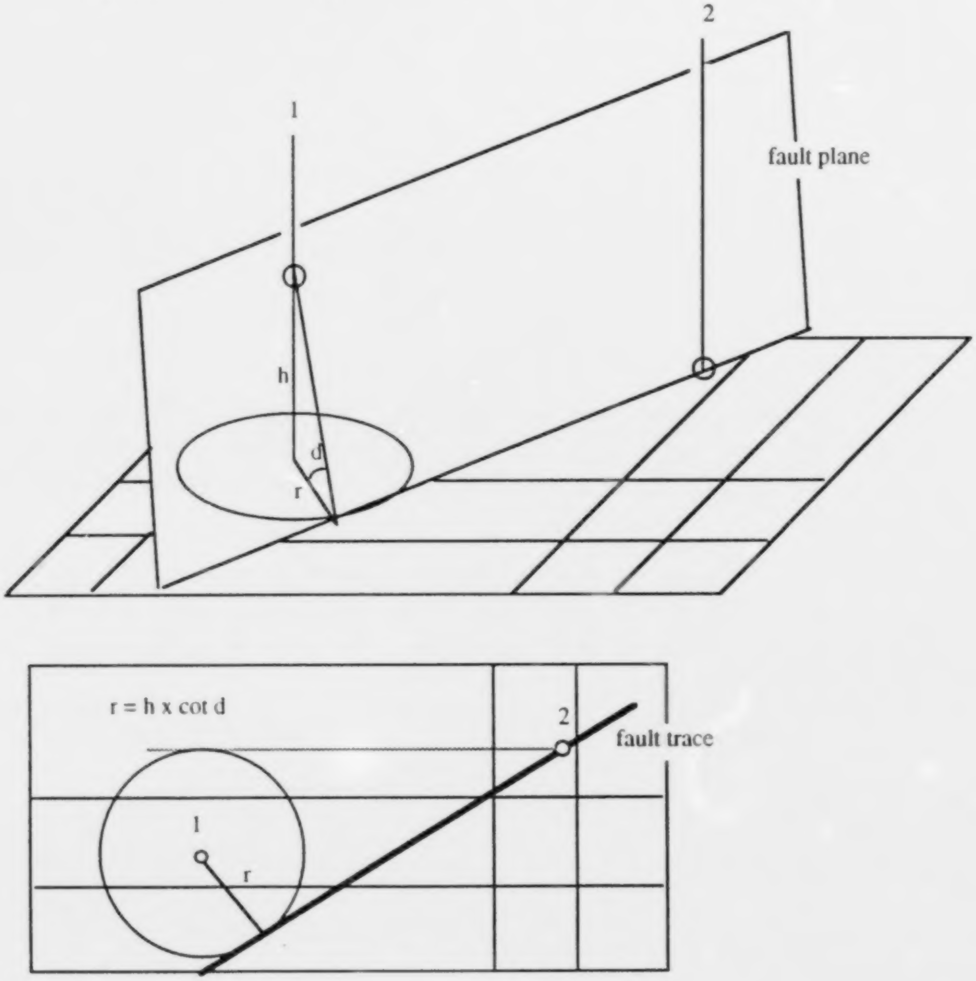
2
1
fault plane
h
d
r
r = h x cot d
2
fault trace
1
r

Figure 65 Fault plane construction

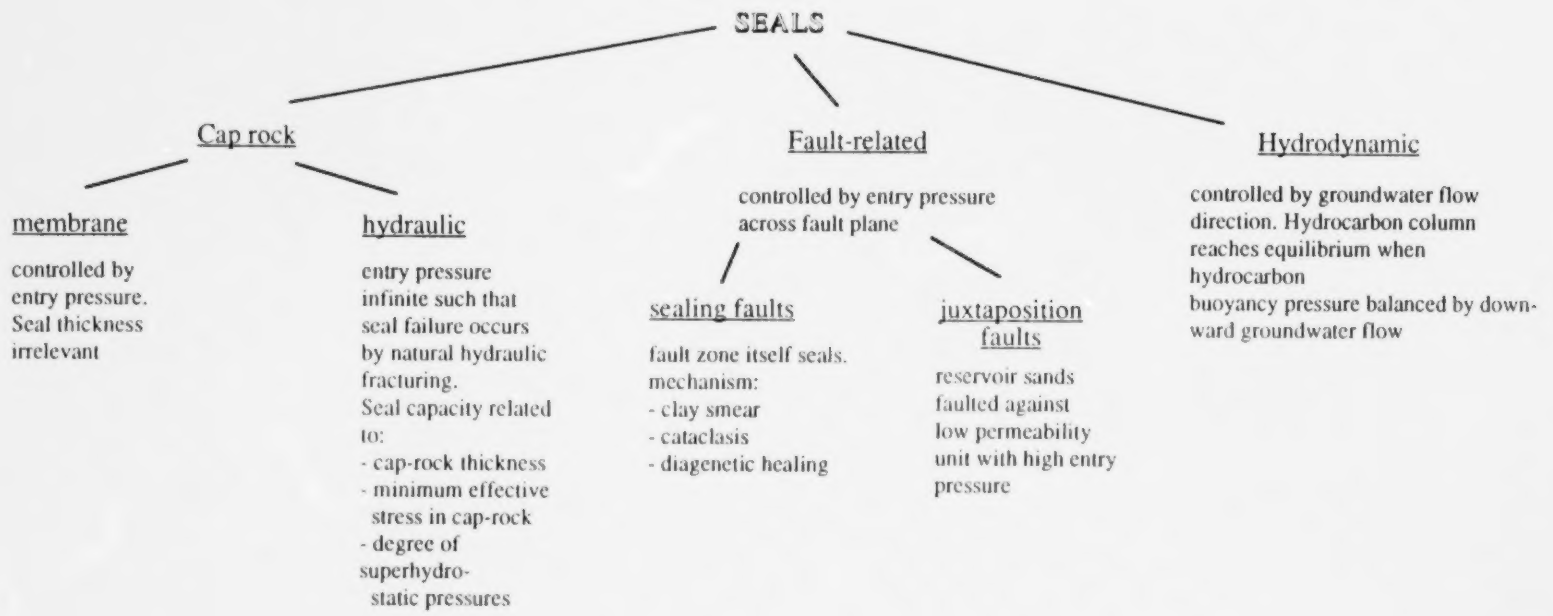

SEALS
Cap rock
Fault-related
Hydrodynamic
membrane
hydraulic
sealing faults
juxtaposition faults

controlled by entry pressure. Seal thickness irrelevant

entry pressure infinite such that seal failure occurs by natural hydraulic fracturing.
Seal capacity related to:
- cap-rock thickness
- minimum effective stress in cap-rock
- degree of superhydrostatic pressures

controlled by entry pressure across fault plane

fault zone itself seals.
mechanism:
- clay smear
- cataclasis
- diagenetic healing

reservoir sands faulted against low permeability unit with high entry pressure

controlled by groundwater flow direction. Hydrocarbon column reaches equilibrium when hydrocarbon
buoyancy pressure balanced by downward groundwater flow

Figure 66 Classification diagram for sealing mechanisms and seal types related to faults

Time Period (Ma)	Vosges West	Black Forest East	average: uplift-rate (m/Ma)
40 - 30	40	35	
	400	350	elevation (m)
30 - 10	15	30	
	650	950	
10 - present	7.5	10	
	700	1000	

Table 1 Average uplift rate and elevation for graben shoulders of the middle segment of the Upper Rhine Graben (study area) from Late Eocene to the present. Data source Roll: (1979).

Compartment	Fault System	
Preuschdorf	Rhine Fault * (± 85°)	Heidenboesch
Pechelbronn	Heidenboesch (45°)	Pechelbronn
Hoelschloch	Pechelbronn (45°)	Hoelschloch
Kutzenhausen	Hoelschloch (58°)	Kutzenhausen
Soultz	Kutzenhausen (55°)	Soultz
Hermerswiller	Soultz (65°)	Hermerswiller * (60°)
	West	East
	Principal fault of compartment	

* synthetic fault; all other principal faults have antithetic style

Table 2 Nomenclature of the tectonic units in the Pechelbronn-Soultz Basin and approximated dip angle of principal faults.

Formation	Type of Organic Matter	Quality	Maturation Level
"Fish Shale"	sapropelic	excellent	immature
upper Pechelbronn Beds	humic	medium	immature at Soultz mature at Scheibenhard
Aalenian	mixed humic	medium - good	immature at Marienbronn & Hoelschloch; mature at Rohrlach & Donau
Toarcian	sapropelic	excellent	immature at Marienbronn & Hoelschloch; mature at Reimerswiller, Rohrlach & Donau
Pliensbachian	mixed sapropelic	medium - good	immature at Hoelschloch; mature at Rohrlach
Sinemurian & Hettangian	mixed sapropelic, humic	good	immature at Hoelschloch; mature Rohrlach; gas at Roeschwoog

Table 3 Organic characteristics and maturation levels of Tertiary and Jurassic source rocks (see also Figure 70: source: SAEM, PREPA, TOTAL reports; Roberts, 1985)

	Scheiben-hardt 101-102	Croetwiller 1	Schaffhausen 3	Reimers-willer 1	Donau 2	Roeschwoog 1	Haguenau 2	Gambsheim 1	Kilstett 1
Liassic	*1750/2					2270/2		1770/0.9	
Dogger				700/0.9			1400/1		1800/0.75
Top Jurassic	1680/1			668/0.8		1880/1.6	1373/1	1455/0.8	15650.5
Lattorfian	1000/0.6	800/0.6	1000/0.6	200/0.3	350/0.6	1500/0.6	1000/0.5	1000/0.45	1500/0.4
Rupelian	900/0.5	600/0.5	600/0.4	153/0.3		1300/0.65		400/0.35	

* depth m/% Ro

Table 4 Vitrinite reflectance data (after Robert 1985)

Reservoir rock	Producing/showing	Oil fields	Reference Wells
Buntsandstein	fresh and salinewater with some oil traces	minor production at Soultz	4590, 4550, 4583, 4616, 4660, 4685
Muschelkalk	oil in upper MK only, fresh and saline water	Soultz and Kutzenhausen	4502, 4555, 4620
Lettenkohle	oil/ fresh and saline water	Soultz, Kutzenhausen and Ohlungen	4560,4660,4623, 4616,4577,4452, 4549
Grès à Roseaux	oil, fresh and saline water	Hoelschloch	4318,4677,4649, 4713,3685
Aalenian	oil prod. and gas traces	Walbourg, Donau and Schirrheim	SAEM
Bajocian	oil prod. and gas traces	Ohlungen, Haguenau, Schirrheim and Donau	SAEM

Table 5 Mesozoic reservoirs in the study area

Well No.	Impreg-nations	Fissures	Permeability md	Porosity %	Depth m	Status
4555		•	38.14	30	863.6	P, erupt.
		•	16.21	21	863.8	P
		•	13.61	24.3	864	P
4515		•			861	P
4620		•			858	P, erupt.
4521	•					P
4642	•	•			837	P
4549	•				883	I
4472	•					P
4500					918	I
4550	•		1.5	2-4	898-971	I
4554	•				864	P, erupt.
	•		0.312	5.7	865	P
4623					867	dry
4541		•	156.7	14	935.7	I
			6.1	8.5-10.5	932	I
			20.7	6.0	937.6	I
4541			1.1	6.5	940	I
4685		•			1089	dry
4607	•	•			862	I
4636		•			855	I
4566	•				921	I
4606		•			944	I
4613		•				I

P = productive; I = indices (water with oil); erupt.= eruptive

Table 6 Permeability and porosity values of the upper *Muschelkalk* in the Soultz region. Data source: SAEM well reports.

Formation	Thickness	porosity/ permeability	Lithology	P.S. Basin	Production	Ref. wells
Rhaetian good reservoir locally	3-13 m	20 %/3 md	sand/marl	Hoelschloch NE Soultz oil traces only	Donau, Ohlungen	4197, Do-1, 3570, Schirr-1, Roe-1
Aalenian medium reservoir	30-35	10-15/ 0.1-3	marl sandy	not present eroded	Walbourg, Ohlungen, Donau, Schirrheim Rittershof.	4471,4768 4761,4768 3288,Hag1 Do1,Schirr 1,Ritt-1
Bajocian Grande Oolithe, irreg., reservoir	33-45 variable	n/a	calcareous, oolithic, marl	not present, eroded	Ohlungen, Haguenau	Hag1-3, Ohlungen

Table 7 Summary Mesozoic oil-producing reservoirs beyond the Pechelbronn-Soultz Basin. Data sources: SAEM, PREPA well reports.

Productive reservoir	Number of pumps	Production (tons)
Dogger	70	60 000
Keuper	5	11 150
Lettenkohle	17	13 250
Muschelkalk	11	16 500
Total	103	100 900

Table 8 Cumulative oil production in Mesozoic reservoirs at the end of 1961 in the Upper Rhine Graben study area. Data source: Sittler, 1974.

Reservoir rock	Producing/showing	Oil fields	Reference Wells
Couches à Melettes	water only	non	PREPA
Upper *Pechelbronner Schichten*	oil & water/traces	Pechelbronn (galleries) Ohlungen, Haguenau, Walbourg, Hochstett	PREPA,SAEM
Middle *Pechelbronner Schichten*	minor oil production, abundance of water	Pechelbronn (galleries) Ohlungen, Hochstett, Donau, Schirrheim, Scheibenhard, Roeschwoog	PREPA, SAEM
Lower *Pechelbronner Schichten*	major oil producer, saline water	Lobsann, Pechelbronn, Marienbronn, Ohlungen	PREPA, SAEM
Zone Dolomitique	oil & water/traces	Kreuzecke, Pechelbronn, Kutzenhausen, Soultz	SAEM

Table 9 Tertiary reservoir rocks, carrier beds and oil fields in the Upper Rhine Graben

Well No.	Location	Depth m	Formation	Porosity %	Permeability md
4716	Soufflenheim	1042-1186	ZD	6.4 ±4	
4755	Soufflenheim	1060-1062	ZD	15	0.61
4755	Soufflenheim	1063-1118	ZD	9.2 ±4	4.3 ±10.4
4760	Surbourg	700-710	ZD	6.6 ±5	0.27 ±0.14
4765	Forstfeld	1236-1240	Ps	4.8	0.1
4765	Forstfeld	1316-1320	Pm	4.7	
4765	Forstfeld	1389	Pi	1.5	
4765	Forstfeld	1477-1790	ZD	8.5 ±2.7	
4774	Beinheim	1119-1427	Ps	3 ±4	
4774	Beinheim	1489-1493	Pi.	3.4	
4774	Beinheim	1735-1740	ZD	5.1	1.2
4778	Beinheim	1017-1070	Ps	11	0.5
4778	Beinheim	1078-1093	Pi	25	50
4788	Schirrheim	350-558	Ps	12.6	0.15 ±0.1
4792	Schirrheim	520-563	Ps	15	2.3 ±4
Mar-101	Marienbronn	256-271	Ps	20-25	

Table 10 Average porosity and permeability values for Tertiary reservoirs and carrier formations taken from PREPA well reports (for abbreviations see list).

Compartments	Oil Fields	Depth range of reservoir(s), m	Production	Comments
N Preuschdorf and Pechelbronn	Lobsann S to Pechelbronn N	30 - 120	oil and water by mining and wells (pumping)	heavy oils and fresh water at Lobsann, others produced lots of saline water
S Preuschdorf and Pechelbronn	Kreuzhecke, Heidenbösch	75 - 250	oil and water by mining and well-pumping	infiltration of fresh water near Heidenbösch
Hoelschloch and Kutzenhausen	S Pechelbronn and Hoelschloch	15 - 260	minor oil production by wells	saline, warm water
Soultz and Hermerswiller	Soultz S	30-50	insignificant production by wells	saline water with oil traces

Table 11 Oil-production capacities of the upper *Pechelbronner Schichten* reservoirs in the Pechelbronn-Soultz Basin. Data source: SAEM well reports.

Compartments	Oil Fields	Depth range of reservoir(s), m	Production	Comments
Preuschdorf	Lobsann N, SE Marienbronn	560 - 600 375 - 550	mining and wells	heavy oil and fresh water
Preuschdorf and Pechelbronn	Lobsann S, Pechelbronn N	275 - 490	mining	saline, warm water
Pechelbronn and Hoelschloch	Pechelbronn S, Hoelschloch	350 - 560	mining and wells	saline water; major oil fields
Kutzenhausen			empty	saline, hot water
Soultz			empty	saline, hot water

Table 12 Oil-production capacities of Lower *Pechelbronner Schichten* reservoirs in the Pechelbronn-Soultz Basin. Data source: SAEM well reports.

Hydrogeologic element	Hydraulic conductivity (m/s)	Intrinsic permeability (darcy)
highly conductive	$> 10^{-1}$ to 10^{-3}	10^{4} to 10^{2}
conductive	10^{-3} to 10^{-6}	10^{2} to 10^{-1}
low conductive	10^{-7} to 10^{-9}	10^{-2} to 10^{-4}
very low conductive	$< 10^{-9}$	$< 10^{-4}$

Table 13 Equivalent hydraulic conductivity and intrinsic permeability value ranges for fresh water at 15 ^{0}C, characteristic for aquifers and aquitards (modified after Todd, 1959).

Hydrogeologic Element				max. Thickness m	Lithology	Porosity %	hydraul. Cond. m/s	Transmissivity m^2/s
HSG IIa	HSU 7	Upper and Middle Jurassic	Aquitard	150	Clay-Marlstones	10	$1x10^{-9}$	
	HSU 6	Upper Keuper	Aquitard	40	Clay - Marlstones	2 - 7	$1x10^{-9}$ - $1x10^{-10}$	
	HSU 5	Grés à Roseaux	Aquifer	20	Sandstones	5 - 25	$1x10^{-5}$ - $1x10^{-6}$	
HSG IIb	HSU 6	Lower Keuper	Aquitard	110	Clay - Marlstones	2 - 7	$1x10^{-9}$ - $1x10^{-10}$	
HSG I	HSU 4	Lettenkohle	Aquifer	25	Dolo-limestone	15	$1x10^{-5}$ - $1x10^{-6}$	
	HSU 3	Muschelkalk	Aquifer	170	Limestones	1.5 - 30	$1x10^{-5}$ - $1x10^{-7}$	$1x10^{-3}$ - $1x10^{-6}$
		Buntsandstein	Aquifer	450	Sandstones	2 - 15	$1x10^{-5}$ - $1x10^{-6}$	$1x10^{-3}$ - $1x10^{-5}$
		Permian	Aquifer	0 - 600	Sandstones	3 - 6	$1x10^{-5}$ - $3x10^{-7}$	$1x10^{-3}$ - $8x10^{-4}$
	HSU 2	weathered Granite	Aquifer	300	Granite	2	$< 1x10^{-5}$	
	HSU 1	Basement	Aquiclude		Granite	2	$1x10^{-12}$	

Table 14 Assigned porosities, hydraulic conductivities and transmissivities to Mesozoic hydrostratigraphic units

Hydrogeologic Element				max. Thickness m	Lithology	Porosity %	hydraul. Cond. m/s	Transmissivity m^2/s
	HSU 13	Plio - Quaternary	Aquifer	sporadic	Sand & Gravels	30	1x10^{-3}- 1x10^{-5}	10^{-3}
H S G I V	HSU 12	Niederroedener Schichten	Aquitard	absent				
	HSU 11	Serie Grise	Aquitard	absent				
H S G I I I a	HSU 10 west	Pechelbronner Schichten	Aquifer	400	Clay-marl-stones with sand lenses	10 - 15	1x10^{-7} - 1x10^{8}	
H S G I V	HSU 9	Couche Rouge	Aquitard	0 - 210	Dolomitic marlstones	10	< 1x10^{-9}	
H S G I I I b	HSU 8 west	Zone Dolomitique	Aquifer	125-300	Marlstones with sand lenses	10 - 15	1x10^{-7} - 1x10^{8}	

Table 15 Assigned porosities, hydraulic conductivities and transmissivities to Tertiary hydrostratigraphic unit in the Pechelbronn-Soultz Basin

Hydrogeologic Element				max. Thickness m	Lithology	Porosity %	hydraul. Cond. m/s	Transmissivity m^2/s
	HSU 13	Plio - Quaternary	Aquifer	130	Sand & Gravels	30	$1x10^{-3}$- $1x10^{-5}$	10^{-3}
HSG IV	HSU 12	Niederroedener. Schichten	Aquitard	500	Clay - Marlstones	10	$1x10^{-8}$ - $1x10^{-10}$	
	HSU 11	Serie Grise	Aquitard	450				
	HSU 10 east	Pechelbronner Schichten	Aquitard	850				
	HSU 9	Couche Rouge	Aquitard	0 - 200	Dolomitic - Marlstones			
	HSU 8 east	Zone Dolomitique	Aquitard	200 - 800				

Table 16 Assigned porosities, hydraulic conductivities and transmissivities to Tertiary hydrostratigraphic unit in the Upper Rhine Graben

Juxtaposition	Conductance to groundwater flow across fault zone	along fault zone
sandstone/sandstone	high	high
carbonate/carbonate	high	high
shale/shale	very low	likely
sandstone/shale	low	likely
carbonate/shale	low	likely

Table17 Groundwater flow across/along juxtaposition faults

HSU	Pechelbronn Fault r = 210 m	Hoelschloch Fault r = 120 m
10	0.5	0.7
8	0.2	0.6
5	-9	-4.7
4	-4	-1.8
3	0.7	0.8
2	0.3	0.6

Table 18 Connectivity factors for aquifers (HSU's) at two principal faults in the Pechelbronn-Soultz Basin.

Recharge Area	Midline Area	Discharge Area
low TDS, high CO_2, cross-flow, low T^o	slightly mineralized source; low CO_2, little cross-flow; const. T^o	mineralized source water; cross-flow; high T^o, mixing with fresh water
Dominant species: Ca, Mg, HCO_3, CO_3, SO_4	Na, Ca, Mg, HCO_3, SO_4, Cl, increase in TDS	SO_4, Cl, Na; high TDS decreasing upward

Table 19 Groundwater chemistry in hydraulic regimes of flow systems

Zone	wellno.	source/ formation*	mean depth	pH	TDS mg/l	chloride	sulfate	root I 1	root II 2	IBE	Cl/Na
Vosges	Bitche	well/Bsdst.	47	5.7	36.5	N	N	0.07	0.27	0.18	1.22
	Pet. Pierre	well/Bsdst.	162	7	134	N	N	0.26	1.39	0.10	1.11
	Phillipsbourg	well/Bsdst.	70	7.9		N	N	0.23	1.19	-0.06	0.86
	Riesthal	spring/Bsdst.		5.7		N	N	0.43	0.17	0.34	1.51
Zaberner Frac.Zone	Romaine	well/Bsdst.	11	6.6	5170	A	N	5.71	7.65	0.26	1.4
	Lichteneck	spring/Bsdst.		6.5		N	N	0.32	0.32	0.29	1.4
Lembach Graben	Liebfrauental	well/Bsdst.	130	7.9	200	N	N	0.45	0.8	0	1
Hochwald Horst	Drachenbronn	well/Bsdst.	140	6.8	80	N	N	0.05	0.38	0.23	1.3
	Sept.Fontain	spring/Bsdst.		7.6		N	N	0.26	1.17	0.07	1.08
Rhine Fault	H I	well/Bsdst.	167	6.6	51	N	N	0.22	0.55	-0.29	0.78
	H II	well/Bsdst.	190	7	52	N	N	0.21	0.74	-0.54	0.65
	Mitschdorf	well/Bsdst.	200	6.4		N	N	0.15	0.41	-1.16	0.46
	Mors 3a	therm./MK	400	6.7	6600	A	A	17	8.6	0.15	1.18
	Mors 3b	therm.Bsdst.	680	7.3	5300	A	A	10.6	7	0.13	1.15
Pechelbronn Soultz Basin	Aluxan	well/Plio	32	7		N	N	0.77	6.53	0.01	1.01
	3262	oil well/ZD	435	7.1		H	N	1.13	7	0.15	1.17
	4275	oil well/Ps	120	7.1	962	N	N	0.24	6.53	-1.8	0.34
	3969	oil well/Pi	490	7.9	8688	A	N	0.45	5.51	0.04	1.04
	4485	oil well/Bsdst.	1214	7.3	24190	H	N	17.3	12.6	0.3	1.43
	4515	oil well/MK	860	7.3	92599	VH	N	32.6	28	0.31	1.46
	4541	oil well/MK	950	7.8	100634	VH	N	57	26	0.23	1.29
	4544	oil well/Pi	250	6	90000	VH	N	21.3	17	0.29	1.4
	4550	oil well/Bsdst.	980	6.9	105300	VH	N	48	20.4	0.25	1.34
	4567	oil well/MK	871	6.8	97314	VH	A	52	13.7	0.22	1.3
	Helion	therm.MK+	1146	6.4	20500	H	A	13.6	12.6	0.24	1.31
	GPK-1	therm.Base	1817	6.4	80000	VH	N	33	27.5	0.29	1.42
	RG-1	well/Ps	10	7	3542	A	N	0.12	5.2	0.05	1.05
Graben centre	Roe S1	well/Plio	28	7	600	N	N	2.6	5.2	0.9	1.5
	Souffl. FII	well/Tert.	64	6.4	72	N	N	0.16	0.65	-0.05	0.7

* for abbreviations see list; 1) near saturation when $\sqrt{SO_4^{-2} \times Ca^{+2}}$ >70. 2) $\sqrt[3]{(HCO_3^- + CO_3^{-2}) \times Ca^{+2}}$. IBE: index of base exchange

Table 20 Generalized Schoeller classification of formation waters in the study area

	I, mg/l	NH_4, mg/l
Hochwald (*Buntsandstein*)	<0.05	0.07-0.3
SAEM 4275 (Merkwiller, 120 m Ps	0.2	1.2
Helion (Pechelbronn, 1140 m MK	0.29	5.8
RG-1 (Soultz, 10 m)	0.6	8.7
SAEM 3969(Kutzenhausen, 490 m Pi)	0.8	5.9
SAEM 3262 (Kutzenhausen, 435 m ZD)	2.7	12.6
GPK-1 (Soultz, BGR, 1817 m Base)	0.1-0.5	28

Table 21 Iodide and ammonium concentration for some formation water in the Hochwald and Pechelbronn-Soultz Basin (for abbreviations see list)

Well No.	BGR No.	Location	CH_4 ppm	δ ^{13}C (CH_4) o/oo (PDB)
Romaine	6015/1	Niederbronn	6	n/a
Sept. Fon	6007/1	Hochwald	1	n/a
H II	6004/1	Hochwald	1	n/a
F 2	6000/1	Mitschdorf	1	n/a
Mors 3	6017/2	Morsbronn	20	n/a
Mors 3b	6018/3	Morsbronn	280	n/a
Mors 3b	6018/4	Morsbronn	20	n/a
Helion	6049/2	Pechelbronn	26 000	-29.8
Helion	6049/2	Pechelbronn	1200	-29.8
3969	6051	Kutzenhausen	45 500	-65.1
3262	6012/1	Kutzenhausen	55 000	-49.3
3262	6012/1	Kutzenhausen	58 500	-71.3

Table 22 Methane content of formation waters in the Vosges, Hochwald and Pechelbronn-Soultz Basin.

from....to	Romaine	Morsbronn	Helion II	Legend:
Vosges	14	24	28	lateral distance [km]
	0.7	0.9	0.9	flow velocity for conv. ^{14}C age [m/y]*
	1.6	1.6	1.6	flow velocity for correct. ^{14}C age [m/y]*
Romaine at Niederbronn		9	14	* apparent mean flow velocity
		1.3	0.8	
		1.4	1.2	
Morsbronn			(8)	> SW - NE direction
			(1.6)	
			(1.6)	

Table 23 Apparent velocities in m/y for groundwater flowing west to east from the Vosges to wells Romaine, Morsbronn and Helion.

			(m)	W/m C		W/m C	
Formation	Age	Lithology	mean thickness	assign.conduct.	reference	report.conduc.	reference
Quartär	Quat./Pleisto	loess	10-20	1.7	1	1.5,1.7,1.8	2 3 4
Nieder.Sch.	Oligocene	claymarl	400	1.8	5	1.5,1.7	2 3
Serie Grise	Oligocene	marl	450	2.1	5	1.8,2.9	2 4
Pechel.Sch.	Oligocene	marl,sandy	400	2.1	5	1.8,2.9	2 4
Couche Rouge	Oligocene	marl,anhydr.	100	2.1	1	1.8,2.9	2 4
Zone Dolom.	Oligocene	carb.dolo.marl	200	2.1	1	1.8,2.9	2 4
Jura	Jura	carb,sand,marl	150	2.7	1	2.4,2.7,2.7	2 3 4
Keuper	Trias	claystone,marl	195	2.7	1	2.4,2.9,2.8	2 3 4
Lettenkohle	Trias	carb.dolo.,clay	25	2.8	1		
Muschelkalk	Trias	limest.marl	170	2.8	1	2.4,2.9,2.8	2 3 4
Buntsandstein	Trias	sandstone	500	2.9	1	2.9,2.9,2.8	2 3 4
Basement		granite		2.3	1	2.7,2.1,	2 3

references:	1 Kappel- meyer '74	3 Delisle 77
		4 Hänel '79
	2 Werner '77	5 Sattel '80

Table 24 Assigned thermal conductivity values for Mesozoic and Tertiary formation in the Upper Rhine Graben study area

Pool	Formation	Depth m	Reservoir temp. ^{o}C	Oil field	^{o}API 15 ^{o}C	Viscosity[1]	Sulfur %	Asphalt %	Residuum[2] wt. %
S1	Lettenkohle	835	90	Soultz	37	1.95	0.14	0.43	26.7
S2	Muschelk.	858	109	Soultz	37	2	0.18	0.40	23.7
S3	Lettenkohle	935	97	Soultz West	37	2.15	0.15	0.28	24.5
S4	Z. Dolom.	450	40	Soultz West	27	6	0.50	6.0	35
O1	Jurassic	465	55	Ohlungen	33	1.55	0.34	2.15	28.4
P1	Pech. Sch.	90	11	Pechelbronn	17	112	0.72	4.3	60
P2	Pech. Sch	370	26†	Pechelbronn	21	28	0.90	11.8	50
P3	Z. Dolom.	401	28†	Pechelbronn	27	5.8	0.74	6.3	43
P4	Gres a Ros.	754	60	Pechelbronn	29	5.3	0.42	6.9	37

1 viscosity is measured in Engler Degrees at 30^{o}C
2 from Hempel distillation analysis
† temperture is calculated from geothermal gradient

Table 25 Chemical and physical characteristics of oil pools at Pechelbronn-Soultz in Tertiary and Mesozoic formatinos at various depths and reservoir temperatures; O1 is a unaltered oil sample from Ohlungen oil field, 17 km south of the basin (data source: SAEM oil distillation reports, SGAL, Strasbourg, France).

Bibliography

Aydin, A. and A.M. Johnson, 1983, Analysis of faulting in porous sandstones: Journal of Structural Geology, 5 (1), p. 519-31.

Barbat, W., 1967, Crude oil correlation and their role in exploration: AAPG Bulletin, 51 (7), p. 1255-1292.

Barker, J.F., P. Fritz and R.M. Brown, 1978, Carbon-14 measurements in aquifers with methane: Isotope Hydrology , IAEA , p. 661-678.

Bars, Y.A., 1961, Genetic relationship of oil-gas basins of subsurface water surrounding them: Petroleum Geology, 5 (11), p. 579-586.

Bear, J., 1972, Dynamics of fluids in porous media: Amsterdam, Elsevier.

Bertleff, B., W. Hammer, H. Joachim, G. Koziorowski, L. Stober, G. Strayle, E. Villinger and J. Werner, 1987, Hydrogeothermiebohrungen in Baden-Würtemberg. - Eine Übersicht: Zeitschrift der Deutschen Geologischen Gesellschaft, 138 (Teil 3), p. 411-425.

Bishop, M.S., 1960, Subsurface mapping: New York, John Wiley & Sons.

Blavoux, B. and P. Olive, 1982, Radiocarbon dating of groundwater of the aquifer confined in the lower triassic sandstones of the Lorraine region, France: In W. Back and R. Létoille (ed.), Symposium on geochemistry of groundwater, Elsevier, p. 167-183.

Blümel, G., M. Eder, P. Gerling, D. Ploethner, U. Ranke and K. Trippler, 1989, Application of hydraulic theory in petroleum exploration: Erdöl und Kohle Erdgas Petrochemie, 42 (1), p. 38.

Boigk, H. and H. Schöneich, 1970, Die Tiefenlage der Permbasis im nördlichen Teil des Oberrheingrabens: In J.H. and S. Müller (ed.), Graben Problems, Scientific Report No.27, Proc. Int. Rift Symposium , Karlsruhe , p. 45-55.

Boigk, H. and H. Schöneich, 1974, Perm,Trias und älterer Jura im Bereich des südlichen Mittelmeer-Mjösen Zone und des Rheingrabens.: In J.H. Illies and K. Fuchs (ed.), Approaches to Taphrogenesis, Scientific Report No. 8, Proc. Int. Rift Symposium , Karlsruhe , p. 60-71.

Brace, W.F., 1980, Permeability of crystalline and argillaceous rocks: Journal of Rock Mech.Min.Sci. and Geomech., 17 , p. 241-251.

Bredehoeft, J.D. and B.B. Hanshaw, 1968, On the maintenance of anomalous fluid pressures: II. Source layer at depth: GSA, 79 , p. 1107-1122.

Bredehoeft, J.D. and S. Papadopulos, 1965, Rates of vertical groundwater movement from the earth's thermal porfile: Water Resources Research , 1 (2), p. 325-328.

Breyer, F., 1974, Die Entstehungsgeschichte des Südteils des Rheingrabens nach refexionsseimischen Messungen, geologische Kartierungen und Tiefbohrungen: Geologisches Jahrbuch, A 20 , p. 3-64.

Bruderer, W. and M.C. Louis, 1958, Conditions governing the distribution and origin of oil in the Rhinegraben of France and Germany: AAPG, Habitat of oil, , p. 1123-1133.

Bryant, W.A., 1978, The Raymond Hill Fault: California Geology, 31 , p. 127-142.

Carpenter, A.B., 1978, Origin and chemical evolution of brines in sedimentary basins: Oklahoma Geological Survey, Circular 79 , p. 60-77.

Cautru, J.P., 1987, The Haguenau-Soultz Project: Orléans, BRGM, (unpublished report).

Cermak, V. and R. Hänel, 1982, Geothermics and geothermal energy: In Symposium joint general assemblies EGS and ESC, Budapest, August 1980.

Chebotarev, I.I., 1955, Metamorphism of natural waters in the crust of weathering, Part 1-3: Geochimica et Cosmochimica, 8 , p. 22-48, 137-170, 198-212.

Chiarelli, A., 1973, Etude des nappes aquiferes profondes, Contribution de l'hydrogeologie a la connaissance d'un bassin sedimentaire et l'exploration petrolier: D.Sc. thesis no. 401, l'Universite de Bourdeaux.

Clauser, C., 1988, Untersuchungen zur Trennung der konduktiven und konvektiven Anteile im Wärmetransport in einem Sedimentbecken am Beispiel des Oberrheingrabens: Fortschritt-Berichte VDI, Reihe 19 (28), p. 1-124.

Collins, A.G., 1975, Geochemistry of oilfield waters.: Amsterdam, Elsevier Scientific Publishing.

Coustau, H., 1977, Formation waters and hydrodynamics: Journal Geochemical Exploration, 7 , p. 213-241.

Craig, H., 1961, Isotopic variations in meteoric waters: Science, 133 , p. 1702-1703.

Crans, W., G. Mandl and J. Haremboure, 1980, On the theory of growth faulting: A geomechanical delta model based on gravity sliding: Journal of Petroleum Geology, 2 (3), p. 265-307.

Culkin, F., 1965, The major constituents of seawater: Chemical Ocennography, 1 , p. 121-161.

Daly, D., J.W. Lloyd, B.D.R. Misstaer and E.D. Daly, 1980, Fault control of groundwater and hydrochemistry in the aquifer system of Castlecomer Plateau, Ireland: Quarterly Journal of Engineering Geology, 13 , p. 167-175.

Dansgaard, W., 1964, Stable isotopes in precipitation: Tellus, 16 , p. 436-468.

Davies, P.B., 1987, Modeling areal, variable-density groundwater flow using equivalent freshwater head - analysis of potentially significant errors: In N.W.W. Association (ed.), Conference on Solving Groundwater Problems with Models.

Davis, J.C., 1973, Statistics and data analysis in geology: New York, John Wiley & Sons.

Davis, S.N. and R.J.M. DeWiest, 1966, Hydrogeology: New York, John Wiley & Sons.

de Marsily, G., 1986, Quantitative Hydrogeology: New York, Academic Press.

Delattre, J.N., R. Hentinger and J.P. Lauer, 1968, A provisional geothermal map of the Rhinegraben (Alsatian Part): In J.H. Illies and S. Müler (ed.), Graben Problems, Scientific Report No. 27, Proc. Int. Rift Symposium , Karlsruhe , p. 107-110.

Deutscher Wetterdienst, 1953, Klima Atlas von Baden-Württemberg: Bad Kissingen.

DeWiest, R., 1965, Geohydrology: New York, John Wiley & Sons.

Dikkers, A.J., 1985, Geology in petroleum production: In G.V. Chilingatian (ed.), Developments in Petroleum Science 30. Amsterdam, Elsevier.

Doebl, F., 1974, Diagenesis of tertiary clayey sediments and included dispersed organic matter in relationship to geothermics in the Upper Rhinegraben: In J.H. Illies and K. Fuchs (ed.), Approaches in Taphrogenesis, Scientific Report No. 8, Proc. Int. Rift Symposium , Karlsruhe , p. 192-207.

Domenico, P.A. and V.V. Palciauskas, 1973, Theoretical analysis of forced convective heat transfer in regional groundwater flow: Geol. Soc. America, 84 , p. 3803-3814.

Dow, W.G., 1977, Kerogen studies and geological interpretations: Journal of Geochemical Exploration, 7 , p. 79-99.

Dunnington, H.V., 1955, Generation , migration, accumulation and dissipation of oil in northern Irak: AAPG Bulletin, 39, p. 1194-1251.

Dylikowski, J., 1985, Etude en stratigraphgie sismique de remplissage tertiare de la région de Pechelbronn (Fossé Rhénan) - Application au développement pétrolier en domaine de fossé d'effondrement: Diss., Universite de Paris-Sud Centre Orsay.

Edmunds, W.M., R. Kay and L.F. MacCartney, 1985, Origin of saline groundwaters in the Carnmenellis Granite, Cornwall, England: Natural processes and reaction during Hot Dry Rock reservoir circulation: Chemical Geology, 49 , p. 287-301.

Erdélyi, M., 1985, Geothermics and the deep flow system in the Hungarian Basin.: Journal of Geodynamics, 4 , p. 321-330.

Erlinghagen, L. and G. Dohr, 1974, Beiträge der Reflexionsseismik zur Frage der Schwarzwaldrandstörung: Approaches to Taphrogenesis, Inter Union Commission on Geodynamics, Scientific Report No. 8 , p. 138-144.

Espitalie, J., 1979, Charakterisierung der organischen Substanz und ihres Reifegrades in vier Bohrungen des mittleren Oberrhein-Grabens sowie Abschätzung der paläogeothermischen Gradienten: Fortschr.Geol.Rheinl.u.Westf., 27 , p. 87096.

Evamy, B.D., J. Haremboure, P. Kamerling, W.A. Knapp, F.A. Molloy and P.H. Rowlands, 1978, Hydrocarbon habitat of the Tertiary Niger Delta: AAPG Bulletin, 62 , p. 1-39.

Faber, E., 1987, Zur Isotopengeochemie gasförmiger Kohlenwasserstoffe: Erdöl Erdgas Kohle, 103 (5), p. 210-218.

Faye, R.E. and D.C. Prowell, 1982, Coastal plain fault affect groundwater flow: In E.G. Kruse, C.R. Burdick and Y.A. Yousef (ed.), Proceedings of the Specialty Conference on Environmentally Sound Water and Soil Management , New York , American Society of Civil Engineers , p. 251-252.

Fontes, J.-C. and J.-M. Garnier, 1979, Determination of the initial C-14 activity of the total dissolved carbon: A review of the existing models and a new approach: Water Resources Research, 15 (2), p. 399-413.

Fowler, W.A., 1970, Pressures, hydrocarbon accumulation, and salinities-Chocolate Bayou Field, Brazoria County, Texas: Jour. of Petroleum Technology, 22 (4), p. 411-423.

Freeze, R. and P. Witherspoon, 1966, Theoretical analysis of regional groundwater flow, 1. Analytical and numerical solutions to the mathematical model: Water Resources Research, 2 (4), p. 641-656.

Freeze, R. and P. Witherspoon, 1967, Theoretical analysis of regional groundwater flow, 2. Effect of water-table configuration and subsurface permeability variation: Water Resources Research, 3 (2), p. 623-634.

Freeze, R. and P. Witherspoon, 1968, Theoretical analysis of regional groundwater flow. Quantitative interpretations: Water Resources Research, 3 (2), p. 623-634.

Freeze, R.A. and J.A. Cherry, 1979, Groundwater: Englewood Cliffs, Prentice-Hall.

Friedrichsen, H., 1981, Geothermal systems in the Upper Rhinegraben and N' Black Forest: A chemical and stable isotope study.: Tectonophysics, 73 , p. 125-140.

Fritz, P. and J.C. Fontes, 1980, Handbook of Environmental Isotope Geochemistry. Volume 1: The terrestrial environment, A.: Amsterdam, Elsevier.

Garven, G. and M. Person, 1987, Final Report: Numerical modelling of regional paleoflow in the Rhine Graben area near Pechelbronn: Bundesanstalt für Geowissenschaften und Rohstoffe, Hannover, Germany and The Johns Hopkins University, Baltimore, USA, (unpublished).

Gary, M., R. McAfee and C.L. Wolf, 1975, Glossary of Geology: Washington, DC, American Geological Institute.

Gat, J.R., 1971, Comments on the stable isotope method in regional groundwater investigations: Water Resources Research, 7 (4), p. 980-992.

Gavrilov, V.P., 1972, Relationship between abyssal fractures in young platforms and gas-petroliferous structures in platform blankets: Int. Geol. Review, 14 (9), p. 917-925.

Gerling, P., 1988, Entwicklung und Anwendung einer erdölgeologisch-geochemischen Explorationmethode unter besonderer Berücksichtigung der Hydraulik im Pechelbronner

Gebiet - Fachbericht: Organisch-geochemische Untersuchungen: Bundesanstalt für Geowissenschaften und Rohstoffe - Hannover (FRG), No. 880013 (unpublished).

Geyh, M.A., 1972, On the determination of the initial C-14 content in groundwater: D 58-59, Proc. VIII International Conference on Radiocarbon Dating , Wellington/New Zealand , Royal Society of New Zealand.

Haas, I.O. and C.R. Hoffmann, 1929, Temperature gradient in Pechelbronn oilbearing region, Lower Alsace.: AAPG Bulletin, 13 (10), p. 1257-1273.

Haas, J.O. and C.R. Hoffmann, 1933, Regime des eaux douces, salees et thermales du Bassin de Pechelbronn: C.R. Géologues Pétroliers de Strasbourg, 3-6 , p. 17-22.

Hänel, R., 1976, Die Bedeutung der terrestischen Wärmestromdichte für die Geodynamik: Geologische Rundschau, 65 , p. 797-809.

Hänel, R., 1979a, Determination of subsurface temperatures in the Federal Republic of Germany on the basis of heat flow values: Geol. Jahrbuch, Reihe E (Heft 15), p. 41-49.

Hänel, R., 1979b, Temperature -und Wärmestromdichtebestimmungen zur Ermittlung von großräumigen Wasserbewegungen im Untergrund der Bundesrepublik Deutschland: NLfB, Ha 934/9 (unpublished).

Hänel, R., 1980, Atlas of subsurface temperatures in the European Community: Luxemburg, Commision of the European Community.

Hanor, J.S., 1987, Origin and migration of subsurface sedimentary brines: SEPM Short Course No. 21.

Hardie, L.A., 1990, The roles of rifting and hydrothermal $CaCl_2$ brines in the origin of potash evaporites: An hypothesis: American Journal of Science, 290 (1), p. 43-106.

Hem, J.D., 1989, Study and interpretation of the chemical characteristics of natural waters, 3rd ed.: United States Geological Survey, Water-Supply Paper 2254.

Hindle, A.D., 1989, Downthrown traps of the NW Witch Ground Graben, UK North Sea: Journal of Petroleum Geology, 12 (4), p. 405-418.

Hobbs, B.E., W.D. Means and P.F. Williams, 1976, An outline of structural geology: New York, Wiley International.

Hoffers, B., 1979, Zusammenhänge zwischen Geothermik und junger Tektonik im Oberrheingraben: Oberrheinische Abhandlungen, 28 , p. 1-5.

Hoffers, B., 1981, Ein Model zur Klärung der geothermischen Anomalien des Rheingrabens durch tiefgehende Wasserbewegungen und dessen tektonischen Voraussetzungen und Folgen.: Diss. Universität Karlsruhe.

Holysh, S., 1989, Petroleum related geochemical signatures and regional groundwater flow, Chauvin Area, East-Central Alberta: M.Sc. Thesis, University of Alberta, (unpublished).

Holzer, T.L., 1976, Ground failure in areas of subsidence due to ground water decline in the United States: In Landsubsidence Symposium, 121, Proceedings of the Second International Symposium on Land Subsidence , International Association of Hydrogeologic Sciences , p. 423-433.

Hontcharenko, B.I., 1937, Methods for developing production from lenses: Oil Weekly, 87 , p. 52-56.

Howard, K.W.F. and J.W. Lloyd, 1983, Major ion characterization of coastal ground waters: Ground Water, 21 (4), p. 429-437.

Howell, J., 1985, From here to maturity - A TTI maturation modeling program: In Platte River Associates and D.W. Waples.

Hubbert, M.K., 1940, The theory of groundwater motion: Journal of Geology, 48 (8), p. 785-944.

Hubbert, M.K., 1951, Mechanical basis of certain familiar geologic structures: Bull. Geol. Soc. of Amer., 62 , p. 355-372.

Hubbert, M.K., 1953, Entrapment of petroleum under hydrodynamic conditions: AAPG Bulletin, 37 (8), p. 1954-2026.

Hubbert, M.K. and W.W. Rubey, 1959, Role of fluid pressure in mechanics of overthrust faulting, I. Mechanics of fluid-filled porous solids and its application to overthrust faulting: Bull.Geol.Soc.Am., 70 , p. 115-166.

Illich, H.A., F.R. Haney and M. Mendoza, 1981, Geochemistry of oil from Santa Cruz Basin, Bolivia: Case study of migration-fractionation: AAPG Bulletin, 65 , p. 2388-2402.

Illies, J.H. and G. Greiner, 1976, Regionales stress-Feld und Neotektonik in Mitteleuropa: Oberrheinsche Geologische Abhandlungen, 25 , p. 1-40.

Illies, J.H. and G. Greiner, 1979, Holocene movements and state of stress in the Rhinegraben Rift System: Tectonophysics, 52 , p. 349-359.

Jackson, J. and D. McKenzie, 1983, The geometrical evolution of normal fault systems.: Journal of Structural Geology, 5 (5), p. 471-482.

Jones, V.T. and R.J. Drozd, 1983, Predictions of oil and gas potential by near-surface geochemistry: AAPG Bulletin, 67 (6), p. 932-952.

Jones, F.W., 1984, Estimates of terrestrial thermal gradients and heat flow variations with depth in the Hinton-Edson area of the Alberta Basin derived from petroleum bottom-hole temperature data: Geophysical Prospecting, 32 , p. 1111-1130.

Kanz, W., 1987, Grundwasserfließwege und Hydrochemie in tiefen Graniten und Gneisen: Geologische Rundschau, 76 (1), p. 265-283.

Kaplan, I.R., 1983, Stable isotopes of sulfur, nitrogen, and deuterium in recent marine environments: SEPM Short Course Notes, 10 , p. 2-108.

Kappelmeyer, O. and R. Hänel, 1974, Geothermics with special reference to application: Berlin, Geb. Bornträger.

Kartsev, A.A. and S.B. Vagin, 1964, Paleohydrogeological studies of the origin and dissipation of oil and gas accumulations in the instance of Cis-Caucasian Mesozoic deposits: Internat. Geol. Review, 6 (4), p. 104-121.

Krecji-Graf, K., 1963, Diagnostik der Salinitätsfazies der Ölwässer: Fortschritte der Geologie Rheinland-Westfalen, 10 , p. 367-448.

Krecji-Graf, K., 1978, Data on geochemistry of oil field waters: Geologisches Jahrbuch, Heft 25 , p. 3-174.

Kreitler, C.W., 1976, Faulting and land subsidence from groundwater and hydrocarbon production, Houston, Galveston, Texas: 121, Proc. 2nd Int. Symposium on Land Subsidence , Int. Assoc.Hydro. Sci. Publ. , p. 435-446.

Kuntz, E., H. Mälzer and V. Schick, 1970, Relative Krustenbewegungen im Bereich de Oberrheingrabens: In J.H. Illies and S. Müller (ed.), Graben Problems, Scientific Report No. 27, Proc. Int. Rift Sympsoium , Karlsruhe , p. 1-4.

Lachenbruch, A. and J.H. Sass, 1977, Heat flow in the United States and thermal regime of the crust: In Heacock, J.G. (ed.), The Earth' Crust - Its nature and physical properties, Geophys. Monogr. no.20, American Geophysical Union, p. 626-675.

Lafargue, E. and C. Barker, 1988, Effect of water washing on crude oil compositions: AAPG Bulletin, 72 (3), p. 263-276.

Lauer, J.-P., 1976, Isothermes profondes et "effets de socle".: Bull. Soc. geol. France, 7 (5), p. 1139-1149.

Levi, v.H., 1962, Die Produktionsgeschichte der Erdöllagerstätten vo Pechelbronn.: Erdöl und Kohle-Erdgas-Petrochemie, 15 (3), p. 169-176.

Levorsen, A.I., 1967, Geology of Petroleum: 2 edition, San Francisco, W.H. Freeman and Co.

Leythäuser, D., 1982, The role of diffusion in primary migration of hydrocarbons.: AAPG Bulletin, 66 (4), p. 408-429.

Louderback, G.D., 1942, Faults and earthquakes: Bulletin Seismic Society of America, 32, p. 305-330.

Lowell, J.D., 1985, Structural styles in petroleum exploration: Tulsa, OGCI Publications.

Lowell, R.P., 1975, Circulation in fractures, hot springs and convective heat transport on mid-ocean ridge crests: Geophysical Journal of Royal Astronomical Society, 40, p. 351-365

Lusczynski, N., 1961, Head and flow of groundwater of variable density: J. of Geophysical Res., 66 (12), p. 4247-4256.

Maccagno, M., 1991, The combined use of pressure-depth and pressure-elevation plots to analyze groundwater flow fields: M.Sc. Thesis, University of Alberta, (unpublished).

Machel, H.-G. and E.W. Mountjoy, 1986, Chemistry and environments of dolomitization - A reappraissal: Earth-Science Reviews, 23 , p. 175-222.

Majorowicz, J.A., F.W. Jones, H.-L. Lam and A.M. Jessop, 1985, Regional variation of heat flow differences with depth in Alberta, Canada: Geophysical Journal Royal Astronomical Society, 81 , p. 479-487.

Mälzer, H. and H. Schlemmer, 1975, Geodetic measurements and recent crustal movements in the southern Upper Rhinegraben: Tectonophysics, 29 , p. 275-282.

Mandl, G., 1988, Mechanics of tectonic faulting: Amsterdam, Elsevier.

Matthess, G., 1982, The properties of groundwater: New York, Wiley.

Matthess, G., A. Pekdeger, D. Schenk and A. Scholtis, 1986, Geothermie Projekt Bruchsal - Interpretation der bisherigen hydrochemischen Analysendaten im Hinblick auf den technischen Betrieb: Geol.-Paläont. Inst. Universität Kiel, (unpublished report).

Maxey, G.B., 1964, Hydrostratigraphic units: Journal of Hydrology, 2 , p. 124-129.

McAuliffe, C.D., 1980, Oi and gas migration: Chemical and physical contraints: In W.H. Roberts and R.J. Cordell (ed.), AAPG Studies in Geology, 10, p. 89-109.

McCullough, E.H., 1934, Structural influence on the accumulation of petroleum in California: AAPG, 38 , p. 735-760.

Miller, J.B., K.L. Edwards, P.O. Wolcott, H.W. Anisgard, R. Martin and H. Andregg, 1955, Habital of oil in the Maracaibo Basin, Venezuela: AAPG Bulletin, 39, p. 601-640.

Mook, W.G., 1980, Carbon-14 in hydrogeological studies: In P. Fritz and J.C. Fontes (ed.), Handbook of Environmental Isotope Geochemistry. Volume 1: The terrestrial environment, part A., Elsevier, p. 48-74.

Moser, H. and W. Rauert, 1980, Isotopenmethoden in der Hydrologie: Berlin, Bebrüder Borntraeger.

Munn, M.J., 1909, The anticlinal and hydraulic theories of oil and gas accumulation: Economic Geology, 4 (6), p. 509-529.

Nägele, R. and H. Tietze, 1981, Geothermische Synthese des Oberrheingrabens zwischen Karlsruhe und Mannheim (Anteil Baden-Württemberg): Geologisches Landesamt Baden-Württemberg.

Newhouse, W.H., 1942, Ore deposits as related to structural features: Princeton, Princeton University Press.

North, F.K., 1985, Petroleum Geology: Boston, Allen & Unwin.

Ostroff, A.G., 1967, Comparison of some formation water classification systems: AAPG Bulletin, 51 (3), p. 404-416.

Otto, C.J. and J. Tóth, 1986. Hydrogeological controls and indicators of the Pechelbronn oil deposits Upper Rhine Graben: A preliminary synthesis: In B. Hitchon, S. Bachu and C.M. Sauveplane (ed.), Third Canadian/American Conference on Hydrogeology,

Hydrogeology of Sedimentary Basins: Application to Exploration and Exploitation , Banff, Alberta, Canada , National Water Well Association , p. 105-106.

Otto, C.J. and J. Tóth, 1988, Hydrogeological controls and indicators for oil deposits in rift grabens - An example from the Upper Rhine Graben, France: AAPG Bulletin, 72 (8), p. 1018.

Parini, M., H. Scriba, C. Sieber and D. Werner, 1980, Geothermal anomalies in the Rhinegraben sediments and their explanation by uprising deep groundwater from the crystalline basement: Proceedings of the 2nd International Seminar on the Results of EC Geothermal Energy Research.

Parks, K., 1989, Groundwater flow, pore pressure anomalies and petroleum entrapment, Belly River Formation, West-Central Alberta: M.Sc. Thesis , University of Alberta, (unpublished).

Pearson, F.J. and B.B. Hanshaw, 1970, Source of dissolved carbonate species in groundwater and their effects on carbon-14 dating: Isotope Hydrology , IAEA , p. 271-289.

Pekdeger, A. and W. Balderer, 1987, The occurrence of saline groundwaters and gases in the crystalline rocks of Northern Switzerland: Saline waters and gases in crystalline rocks: Geological Association of Canada, 33 , p. 157-174.

Price, L., 1985, Geologic time as a parameter in organic metamorphism and vitrinite reflectance as an absolute paleogeothermometer: Reply: Journal of Petroleum Geology, 8 (2), p. 233-240.

Rahkit, K., 1987, Potentiometric anomalies due to flow through highly permeable, lenticular clastic rocks and their application in petroleum exploration: M.Sc. Thesis, University of Alberta, (unpublished).

Rich, J.L., 1921, Moving underground water as a primary cause of the migration and accumulation of oil and gas: Economic Geology, 16 (6), p. 347-371.

Hydrogeology of Sedimentary Basins: Application to Exploration and Exploitation , Banff, Alberta, Canada , National Water Well Association , p. 105-106.

Otto, C.J. and J. Tóth, 1988, Hydrogeological controls and indicators for oil deposits in rift grabens - An example from the Upper Rhine Graben, France: AAPG Bulletin, 72 (8), p. 1018.

Parini, M., H. Scriba, C. Sieber and D. Werner, 1980, Geothermal anomalies in the Rhinegraben sediments and their explanation by uprising deep groundwater from the crystalline basement: Proceedings of the 2nd International Seminar on the Results of EC Geothermal Energy Research.

Parks, K., 1989, Groundwater flow, pore pressure anomalies and petroleum entrapment, Belly River Formation, West-Central Alberta: M.Sc. Thesis , University of Alberta, (unpublished).

Pearson, F.J. and B.B. Hanshaw, 1970, Source of dissolved carbonate species in groundwater and their effects on carbon-14 dating: Isotope Hydrology , IAEA , p. 271-289.

Pekdeger, A. and W. Balderer, 1987, The occurrence of saline groundwaters and gases in the crystalline rocks of Northern Switzerland: Saline waters and gases in crystalline rocks; Geological Association of Canada, 33 , p. 157-174.

Price, L., 1985, Geologic time as a parameter in organic metamorphism and vitrinite reflectance as an absolute paleogeothermometer: Reply: Journal of Petroleum Geology, 8 (2), p. 233-240.

Rahkit, K., 1987, Potentiometric anomalies due to flow through highly permeable, lenticular clastic rocks and their application in petroleum exploration: M.Sc. Thesis, University of Alberta, (unpublished).

Rich, J.L., 1921, Moving underground water as a primary cause of the migration and accumulation of oil and gas: Economic Geology, 16 (6), p. 347-371.

Rittenhouse, G., 1967, Bromine in oil-field waters and its use in determining possibilities of origin of these waters: AAPG Bulletin, 51 , p. 2430-2440.

Robert, R., 1985, Étude de l'histoire géothermique de quelques bassins sédimentaires par l'analyse de la diagenése organique de séries traversées par des sondages: Bull.Centre de Research Expl.Prod. Elf-Aquitan, Pau, Mem. 8 , p. 189-213.

Roberts, W., 1980, Design and function of oil and gas traps: In W.H. Roberts III and R.J. Cordell (ed.), Problems of Petroleum Migration, AAPG Studies in Geology No. 10, p. 121-169.

Roll, A., 1974, Langfristige Reduktion der Mächtigkeit von Sedimentgesteinen und ihre Auswirkung-eine Übersicht.-: Geol. Jahrbuch, Reihe A (Heft 14), 74 pp.

Rostron. B, 1990, Numerical simulationm of oil migration: M.Sc. Thesis, University of Alberta, (unpublished).

Roux, W.F., 1979, The development of growth fault structures: AAPG Structural Geology School Cource Notes, p. 33.

Rybach, L., 1986, Amount and significance of radioactive heat sources in sediments: In Burrus (ed.), Thermal modeling in sedimentary basins, 44, IFP/CNRS Collection Colloques et Seminaires , p. 311-321.

Sattel, G., 1980, Determination of thermal conductivity and diffusivity of Rhinegraben-Sediments with a New Ring Source Device: In A.S. Straub and P. Ungemach (ed.), Proceedings of the 2nd International Seminar on the Results of EC Geothermal Energy Research, London , Reidel Publications.

Sattel, G. and W.O. Fuchs, 1980, Lateral heat flow differences in the Rhinegraben area: Proceedings of the 2nd International Seminar on the Results of EC Geothermal Energy Research, Strasbourg.

Schad, A., 1962, Voraussetzungen für die Bildung von Erdöllagerstätten im Rheintalgraben: Abh.Geol.Landesamt Baden Württemberg, 4 , p. 29-40.

Schnaebele, R., 1948, Monographie géologique du champ petroliférе de Pechelbronn: Mem.Serv. Carte Geol. Als. Lorr., 7 .

Schoell, M., 1984, Wasserstoff- und Kohlenstoffisotope in organischen Substanzen, Erdölen und Erdgasen: Geologisches Jahrbuch, Reihe D, Heft 67 , p. 3-161.

Schoeller, H., 1955, Géochemie des eux souterraines: Revue International Francaise Pétrole, 10 (4), p. 181-213.

Schoeller, H., 1962, Les eaux souterraines: Paris, Mason.

Secor, D.T., 1965, Role of fluid pressure in jointing: American Journal of Science, 263 , p. 633-646.

Shelton, J.W., 1984, Listric normal faults: An illustrated summary.: AAPG Bulletin, 68 (7), p. 801-815.

Shi, L.Q., C. Morrow and J. Byerlee, 1980, Permeability of fault gouges under confining pressure and shear stress (abstr.): EOS, Trans. American Geophysical Union, 61 , p. 1120.

Sittler, C., 1974, Sous-sol et ressources pétroliéres en Basse-Alsace. Aspect géologiques et bilan de deux siécles et demi de recherches et d'exploitations: Saisons d'Alsace, 52 , p. 31-62.

Sittler, C., 1985, Les hydrocarbures d'Alsace dans le contexte historique et géodynamique du Fósse Rhénan: Bull.Centres Res.-Expl.-Prod. Elf-Aquitan, 9 (2), p. 335-371.

Sittler, C. and C. Westphal, 1974, Le recherche du pétrole méne au thermalisme á Pechelbronn: Saisons d'Alsace, 52 , p. 130-140.

Smith, D.A., 1966, Theoretical considerations of sealing and non-sealing faults: AAPG Bulletin, 50 (2), p. 363-374.

Smith, D.A., 1980, Sealing and nonsealing faults in Louisiana Gulf Coast salt basin: AAPG Bulletin, 64 , p. 145-172.

Smith, H.M., 1940, Correlation index to aid interpreting crude-oil analyses: U.S. Bureau Mines Tech. Paper, 610 , p. 34.

Steinhause, F., 1970, Climatic Atlas of Europe: UNESCO.

Teichmüller, M., 1979, Die Diagenese der kohligen Substanzen in den Gesteinen Tertiärs und Mesozoikums des mittleren Oberrhein-Grabens: Fortschr.Geol.Rheinld. u. Westf., 27 , p. 19-49.

Teichmüller, M. and R. Teichmüller, 1979, Zur Geschichte des Oberrhein-Grabens. Zusammenfassung und Auswertung eines Symposiums: Fortschr.Geol.Rheinl.u.Westf., 27 , p. 109-120.

Thompson, T.F., 1966, San Jacinto Tunnel: Association Engineering Geology, Section Los Angeles, p. 105-107.

Tissot, B. and D. Welte, 1978, Petroleum formation and occurence: New York, Springer Verlag.

Todd, D.K., 1980, Groundwater Hydrology: 2 edition, New York, Wiley & Sons.

Tóth, J., 1962, A theory of groundwater motion in small basins in central Alberta: Journal Geophysical Research, 67 (11), p. 4375-4387.

Tóth, J., 1963, A theoretical analysis of groundwater flow in small darinage basins: Journal Geophysical Research, 68 (16), p. 4795-4812.

Tóth, J., 1966, Groundwater geology, movement, chemistry, and resources near Olds, Alberta: Research Council of Alberta, Bulletin 17 , p. 123.

Tóth, J., 1968, A hydrogeological study of the Three Hills Area, Alberta: Research Council of Alberta, Bulletin 24 , Tóth, J., 1970a, A conceptual model of the groundwater regime and the hydrogeologic environment: Journal of Hydrology, 10 (2), p. 164-176.

Tóth, J., 1970b, Relations between electric analogue patterns of groundwater flow and accumulation of hydrocarbons: Canadian Jouranl of Earth Sciences, 7 (3), p. 988-1007.

Tóth, J., 1978, Gravity-induced cross-formational fluid flow in Red Earth region, Alberta.: Water Res. Research, 14 (5), p. 805.

Tóth, J., 1979, Patterns of dynamic pressure increment of formation fluid flow in large drainage basins exemplified by the Red Earth Region.: CSPG, 27 (1), p. 63.

Tóth, J., 1980, Cross-formational gravity-flow of groundwater: A mechamism of the transport and accumulation of petroleum (The generalized Hydraulic Theory of petroleum migration).: In W.H. Roberts and R. Cordell (ed.), AAPG Studies in Geology, 10, p. 121-169.

Tóth, J., 1984, The role of regional gravity flow in the chemical and thermal evolution of groundwater: In B. Hitchon and E.I. Wallick (ed.), First Canadian/American Conference on Hydrogeology, Practical applications of groundwater geochemistry , Worthington, Ohio , National Water Well Association , p. 3-29.

Tóth, J., 1986, Investigation of the applicability of the hydraulic theory of petroleum migration to exploration for hydrocarbons, Pechelbronn-Rhinegraben area, NE France - SW Germany: Progress Report II (unpublished).

Tóth, J. and R. Millar, 1983, Possible effects of erosional changes of the topographic relief on pore pressures at depth.: Water Res. Research, 19 (6), p. 587.

Tóth, J. and C.J. Otto, 1989, Hydrogeology and oil deposits at Pechelbronn-Soultz, Upper Rhine Graben: Ramifications for exploration in Intermontane Basins: In T. Thanasuthipitak and P. Ounchanum (ed.), Proc. Int. Symposium on Intermontane Basins: Geology and Resources , Chiang Mai, Thailand , p. 59-76.

Tóth, J., M.D. Maccagno, C.J. Otto and B.J. Rostron, 1991, Generation and migration of petroleum from abnormally pressured fluid compartments-Discussion: AAPG Bulletin, 75 (2), p. 331-335.

Tóth, J. and C.J. Otto, (submitted), Hydrogeology and oil deposits at Pechelbronn-Soultz, Upper Rhinegraben: AAPG Bulletin.

Trippler, K., 1988, Fachbericht: Stationäres Grundwasserströmungsmodell der BGR längs eines Profilschnittes von den Vogesen über das Pechelbronner Feld zum Schwarzwald - BMFT Forschungsvorhaben 032 6476A: "Entwicklung und Anwendung einer erdölgeologisch-geochemischer Explorationsmethode unter besonderer Berücksichtigung der Hydraulik im Pechelbronner Gebiet": Bundesanstalt für Geowissenschaften und Rohstoffe, Hannover, Germany, Archive Nr. 102457 (unpublished).

Tzschachmann, W., 1914, Die Asphalt -und Erdöllagerstätten im Unter-Elsass.: Petroleum Zeitschrift, 9 (12), p. 841-862.

Van der Kamp, G., 1983, Evaluating the influence of groundwater flow sytems on geothermal conditions`: In Courtis (ed.), Energex Regina Conf. Proc., Regina , Pergamon Press.

Verweij, J.M., 1989, Hydrocarbon migration with special reference to regional secondary hydrocarbon miration and its significance for basin evaluation: TNO Institute of Applied Geoscience, OS 89-67.

Vogel, J.C., 1967, Investigation of groundwater flow with radiocarbon: In Isotopes in Hydrology, Vienna, IAEA, p. 355-368.

Vogel, J.C., 1970, Investigation of groundwater flow with radiocarbon: In Isotopes in Hydrology, Vienna, IAEA, p. 235-237.

Vuataz, F.D., A. Criaud, M. Brach and C. Fouilliac, 1988, Hot Dry Rock Soultz Project: Working Group Geochemistry: Progress report for the meeting of 24th March in Bochum.

Vugrinovich, R., 1988, Relationship between regional hydrogeology and hydrocarbons occurences in Michigan, USA: Journal of Petroleum Geology, 11 (4), p. 429-442.

Wagner, W., 1950, Das Erdöl im Rheintalgraben mit Berücksichtigung der Neubohrungen im Untermiozän Hessens: Zeitschrift deutsche geologische Gesellschaft, 100 , p. 518-544.

Walgenwitz, F., P. Maget, R. Tietze and I. Neeb, 1979, Synthese Geothermique du Fosse Rhenan Supérieur: Commission of the European Community, Brüssel.

Waples, D.W., 1980, Time and temperature in petroleum formation: Application of Lopatin's methods to petroleum exploration: AAPG Bulletin, 66 (3), p. 916-926.

Weber, K.J., G. Mandl, W.F. Pilaar, F. Lehner and R.G. Precous, 1978, The role of faults in hydrocarbon migration and trapping in the Nigerian growth fault structures: Proc. Offshore Technology Conference , p. 2643-2653.

Wells, P.R.A., 1988, Hydrodynamic trapping in the Cretaceous Nahr Umr Lower Sand of the north area, offshore Qatar: Journal of Petroleum Technology, 40 (3), p. 357-362.

Welte, D., 1979, Organisch-geochemische Untersuchungen zur Bildung von Erdöl-Kohkenwasserstoffen an Gesteinen des mittleren Oberrhein-Grabens: Fortschritte Geologie Rheinland Westfalen, 27 , p. 51-73.

Werner, D., 1975, Probleme der Geothermik am Beispiel des Rheingrabens: M.Sc. Thesis, Universität Karlsruhe, Germany.

Werner, D. and F. Doebl, 1974, Eine geothermische Karte des Rheingrabenuntergrundes: In J.H. Illies and K. Fuchs (ed.), Approaches to Taphrogenesis, Scientific Report no. 8, Proc. Int. Rift Symposium , Karlsruhe , p. 182-191.

Werner, D. and M. Parini, 1980, The geothermal anomaly of Landau/Pfalz: An attempt of interpretation: Journal of Geophysics, 48 , p. 28-33.

Wernicke, B. and B.C. Burchfiel, 1982, Modes of extensional tectonics: Jour. of Structural Geology, 4 (2), p. 105-115.

Werveke van, L., 1909, Das Erdölvorkommen im Elsass: In Engeler-Höfer (ed.), Das Erdöl, p. 209-243.

White, D.E., J.D. Hem and G.A. Waring, 1963, Chemical composition of subsurface waters: U.S. Geological Survey Prof. Papers, 440F, p. 67.

Wigley, T.M.L., L.N. Plummer and F.J. Pearson, 1978, Mass transfer and carbon isotope evolution in natural water systems: Geochim.Cosmochim.Acta, 42, p. 1117-1139.

Wohlenberg, J., 1979, The subsurface temperature field of the Federal Republic of Germany: Geologisches Jahrbuch, Reihe E (Heft 15), p. 3-29.

Appendix 1 Notes on Tóth's Generalized Hydraulic Theory of Petroleum Migration

Introduction

Selected concepts and terms used in the study are outlined here.

According to the Hydraulic Theory (Tóth, 1980) regional groundwater flow patterns may be manifested by any, or any combination, of a wide range of natural observable phenomena related to subsurface fluid dynamics, hydrology, geochemistry, and the transport of heat, inorganic and organic matter through porous media. Also, specific petroleum deposits are the result of regional groundwater movement and are associated with definable hydraulic segments of regional flow patterns. Therefore, flow generated natural phenomena which are indicative of those hydraulic segments function as direct or indirect indicators of petroleum deposits.

Modes of petroleum migration

Migration is the process by which hydrocarbons move from low porosity, fine-grained source rocks, where they are generated, to higher porosity reservoir rocks, where they may form a accumulation. During primary migration the newly generated petroleum moves from the lower permeable source rock to higher permeable bed - usually a sandstone or fractured limestone over of 1 km. Secondary migration is the subsequent transfer of petroleum through highly permeable strata known as carrier beds or, in hydrogeological terms, as aquifers. The lateral distance to a potential reservoir can range up to 100 km.

Great uncertainty still exists as to the physical forms and chemical composition of petroleum or its precursors during migration. Early attempts to explain the mechanism of migration were based on the dissolution of petroleum in pore water and/or its diffusion through water-wet rock (McAuliffe, 1980). Attempts to quantify these mechanisms have shown that the solubilities and diffusion constants are far too low to account for the masses of petroleum transported, or the time available (Leythäuser, 1982). However, when groundwater flow is considered as the transport agent of petroleum and its precursors, especially during the secondary migration phase along the carrier beds, sufficient amounts of water are available over geologic time to carry dissolved hydrocarbons to sites of deposition.

So far, petroleum geologists and researchers agree that probably several forms of petroleum can exist during a basin's evolution and that certain forms prevail at one time while others dominate at other stages of the basin's history. The configurations in which petroleum can migrate are: (a) as a continuous oil or gas phase; (b) as oil droplets and gas bubbles; (c) in true solutions; (d) as colloidal or micellar suspension; (e) in a molecularly dispersed form; or (f) as organic acids in solution. It seems, however, that the majority of petroleum geologists in the oil industry consider the bulk fluid phase mode of petroleum migration to be most likely.

Regional groundwater flow conditions relevant to petroleum migration and deposition

The principal interrelationships between petroleum migration, deposition and groundwater flow systems are shown schematically in Figure 57.

Flow originates in a topographica highs, the recharge region, where it descends cross-formationally towards an area of minimum fluid potential, moving subhorizontally under regions of medium elevation, the midline region, and converging toward focally located topographic depressions where it terminates by ascending to the land surface, the discharge region. Cross-formational flow requires that basins be hydraulically continuous and that the rocks be not absolutely impermeable. Hydraulic continuity of a basin is characterized by a time and geometric scale. Iin the Upper Rhine Graben, as in other basins explored world wide, hydrogeologic units, carrier beds and tectonic structures have the ability to transmit pore pressures and hydraulic head changes via connected conduits over a geologic time period. Petroleum, either in solution or as an immiscible fluid phase is transported along with groundwater both in aquitards and aquifers. Depending on the permeability contrast between the aquitard and aquifer, the interfacial tension between water and petroleum and the flow direction, the displacement pressures at the formations' boundary may be too large for the petroleum hydraulic gradients to overcome, and petroleum may accumulate or may be transport along the aquifer, depending on the local flow direction.

Local topographic relief generates flow systems which merge with intermediate and regional flow regimes in a sedimentary basin. Dimensionally, local flow systems are smaller than regional systems and do not necessarily reach the basal impermeable boundary (Tóth, 1963).

In regions where flow systems converge or diverge, quasi-stagnant zones develop. In these stagnant zones no lateral transport of petroleum is possible, thus a region of entrapment exists, a so-called hydraulic trap. This type of trapping mechanism can be found at the convergence of both local and regional systems.

Heterogeneities in permeability of the basin's rock framework modify the flow distribution, according to the law of refraction of flow line across permeability boundaries (Hubbert, 1953). This may result in variations of the flow intensities, in a lateral displacement of recharge or discharge regions, and a channelling effect on fluid migration routes, as is the case for fault-severed aquifers and aquitards.

Dynamic parameters of regional groundwater flow patterns

The regional groundwater flow patterns can be characterized by various fluid dynamic parameters. These parameters include: (a) hydraulic head, h (x, y, z); (b) pressure versus depth relations, p(d), and (c) dynamic pressure increment, Δ p(z', d), (Tóth, 1978).

Hydraulic Head: Hydraulic head, h (length), at any point x in a sedimentary basin is related to the mechanical energy per unit mass of fluid, or fluid potential, Φ (mass^2/time^2), as follows (Hubbert, 1940):

$$h = z + \frac{p}{\rho g} \quad \text{or} \quad \Phi = hg,$$

where z (length) is the elevation (relative to a datum plane, generally sea level) of the point of measurement x, p (mass/length$^{2)}$ is the undisturbed formation pore pressure, ρ (mass/length^3) is the mass density of the fluid and g is the acceleration due to gravity. The hydraulic head distribution in a cross section, h (x, z) is characterized by high values in the recharge region and minimum values in the topographic lowlands. Hydraulic head decreases with increasing depth under recharge area (descending flow), and fluid flow is always from high hydraulic head towards regions of lower hydraulic head. A horizontal distribution of hydraulic head on a map, h (x, y), is termed potentiometric surface, from which information can be derived on the general direction of formation fluid flow the area of flow convergence and the slopes of possible petroleum/water interfaces. Areas of closed or linear depressions on the potentiometric surface map indicate a region of convergent flow, i.e., a hydraulic trap. According to the Hydraulic Theory, petroleum is transported towards regions of minimum hydraulic head. The probability of encountering petroleum accumulations increases in the regional flow direction and is highest in discharge areas, provided petroleum has been generated in the basin.

Distribution of pore pressures in sedimentary basins: In a mature sedimentary basin with a hydraulically continuous rock framework in which the water table is near-horizontal and the pore fluids are at rest, the pore pressures are a function of fluid density and depth. This is defined as a hydrostatic system. The formation fluid pressure at a particular depth may be calculated as the integral of fluid density x depth, i.e.,

$$p = \int_0^d g\rho(d), \text{ per unit area}$$

The rate at which pore pressures increase with depth under hydrostatic conditions is called the vertical hydrostatic pressure gradient, which is 9.80665 kPa/m for a static column of fresh water. Deviations from the hydrostatic gradient towards higher or lower vertical pressure gradients are called superhydrostatic or subhydrostatic gradients, respectively, and are caused by variations in fluid densities in the hydrostatic system.

In a non-deforming sedimentary basin in which the water table is a subdued replica of the land and a gravity-driven flow systems exists, an analysis of the pressure versus depth relations is useful in the determination of upward or downward vertical flow components (Tóth,1978). On a p(d) plot, a subhydrostatic pressure gradient indicates a downward vertical flow component and a superhydrostatic gradient indicates an upward flow component. In regions of lateral flow, vertical pore-pressure gradients will be hydrostatic since the fluid potential is constant with depth. Hence, using p(d) plots, areas of downward and upward flow movement can be determined, i.e, recharge and discharge regions, respectively, in a mature sedimentary basin..

Transient conditions

A change in topographic relief due to erosion for example, must entail an adjustment in the flow patterns. This is because the water table, a subdued replica of the land surface, controls, to a large extent, the geometry of the flow systems. Pore pressures or hydraulic heads will be in disequilibrium with the altered topography and the length of time needed to adjust depends on the permeability and thickness of the intervening aquitards (Tóth et al., 1983). During this time the pore pressures are in a transient state and they may not reflect the contemporary boundary conditions. The adjustment process may take several millions of years, and measured pore pressures which have not yet readjusted to the new land relief can be superhydrostatic relative to the new water table elevation. It is therefore important to have a good knowledge of a basin's geohistory, which can provide valuable information on hydraulic conditions of the basin and the underlying mechanisms responsible for the present flow systems.

Similarly, petroleum deposits may not appear to be situated in hydraulically or hydrodynamically favourable positions with respect to those flow systems adjusted to the prevailing topography. A deposit can be located in a relict, active but decaying or even paleo-flow system and the adapted flow system could be in the process of flushing the reservoir and remigrating the petroleum to hydraulically more suitable sites of entrapment. This has implications for exploration planning, but also for the stability of a petroleum accumulation.

Hydrogeologic indicators of petroleum deposits

According to the Hydraulic Theory, regional groundwater flow is a common generator of various natural phenomena. Consequently, these hydrogeologic phenomena may indicate conditions favourable for, or the actual presence of, petroleum accumulations and thus be used as indirect or direct indicators of petroleum, respectively.

Indirect hydrogeologic indicators reflect groundwater conditions that are potentially suitable for the development of petroleum deposits.

The following phenomena have provedto be useful indirect indicators: (a) regions of discharge ; (b) flowing wells; (c) anomalous formation water chemistry and subsurface temperature distributions; (e) trace metals in formation waters; (f) soil salinization; and (g) type of vegetation.

Direct hydrogeologic indicators are signatures of existing accumulations transmitted to regions beyond the petroleum deposits by groundwater movement.

The following were considered to be useful direct indicators and applied to the study area: (a) oil seeps; (b) thermally generated hydrocarbon gases migrated into soils; and (c) oil stained waters.

Appendix 2 Fault Terminology and Construction Techniques

Figure 64 illustrates a number of parameters which are frequently used in the description of faults (Hobbs, et al., 1976). The dip, d, is the angle between the fault plane and the horizontal. The magnitude of the fault is measured by its throw or vertical separation (v.s. or r); this is the vertical distance between the intersection points of the fault with equivalent markers on either side. The distance between the same points measured along the fault plane is the dip slip, d.s., whereas their horizontal distance is the horizontal displacement or heave, h.d.

A frequent problem in constructing structural contour maps of a basin is the determination of the position of a fault plane from two observation points (Bishop,1960). Figure 65 below shows two wells which penetrate the same fault at different depths. The task is to construct a strike line, i.e., the intersection of the fault plane with a horizontal plane. The fault plane construction makes use of the fact that the locus of a plane with a certain dip passing through a certain point, is a cone with a point as apex and the complement of the dip angle equal to half the apex angle of the cone. Planes tangent to this cone satisfy the condition. Figure 65 shows that this cone constructed around well 1 intersects the horizontal plane through the penetration point of well 2 as a circle. The required strike line then passes through the penetration point in well 2 and is tangent to this circle. Two such lines can be drawn. The dip direction of the fault plane determines which line represents the fault strike line. The radius, r, is determined by the difference in depth, h, between the two penetration points and by the cotangent of the dip angle.

Appendix 3 A Fault Permeability Model - A Critical Review of Permeability Characteristics of Faults in the Upper Crust

Introduction

The following pages present a review of observations of pore fluid flow and distribution near fault. Direct and indirect observations of fluid flow near faults have been made in such varied domains as groundwater resources and oilfield development, tunneling, surface geology and mining (e.g., Pechelbronn mining galleries).

With a knowledge of the factors which affect permeability (e.g., porosity, grain size, sorting and fracture density) and, thus, an aquifer's hydraulic parameters, observations of fluid flow and distribution (e.g., hydraulic heads near faults) can be used to infer the structure of the matrix and fault.

A fault affects the apparent transmissivity of an aquifer in two different ways. First, the throw produces a disturbance of the stream lines near the fault, leading to an increase in hydraulic head loss. The distortion depends on both the fault throw amplitude and the vertical permeability, i.e., the anisotropy of the aquifer. Second, the petrophysical properties can be changed in the vicinity of the fault. If present, this effect produces a change in hydraulic conductivity and head loss. A rapid loss in potential energy will be expressed on a potentiometric surface map as a set of parallel congested equipotential lines indicative of flow obstruction. Similarly, from direct observations of a fault zone's structure and material, groundwater flow directions and distribution can be estimated.

Observations of Fluids near Faults

A fault is a distinct structural element in which parameters which affect groundwater flow and petroleum migration may be markedly different from those in the parent wall rocks. Fault zones may perform two contradictory functions: that of a barrier to fluid flow, and that of a conduit.

Faults as barriers: Several factors may account for faults appearing as barriers to subsurface fluid flow (Davis et al., 1966): (1) fault displacement may tend to pulverize rock in the fault plane, creating a relatively impermeable gouge; (2) faulting may juxtapose permeable and impermeable formations, i.e., aquifers and aquitards; (3) elongated and flat clasts may be rotated parallel to the fault plane reducing permeability to the fault; finally (4) deposition of minerals along the fault surface can reduce permeability. For multiphase fluid flow, barriers to one or more fluid phase may be due to preferential wetting of the matrix by one phase. A barrier to subsurface flow is indicated by abrupt lateral changes in water table elevations, hydraulic heads, fluid pressures, water chemistries and temperatures.

That faults can act as a groundwater flow obstruction has been recognized by hydrogeologists for many decades. Where groundwater resources have been extensively developed, faults are often observed to divide the groundwater basin into distinct subbasins with their own water tables and groundwater yields (Bryant, 1978; Daly et al., 1980; Faye et al., 1982; Tóth, 1966). Fault gouge is thought to play a major role in producing obstructions to flow as is juxtaposition of permeable and impermeable beds.

In exploring for petroleum, faults have been found entirely or in part to form a trap for many petroleum deposits. Most accumulations are discovered in the footwall side of normal faults (Levorsen, 1967). Fault blocks possess their own characteristics as to oil-water contacts, pressure regimes, and quantity and chemistry of oil produced (Fowler, 1970; North, 1985). Evamy et al. (1978), reported that for each major fault block in the Niger Delta, petroleum maturation and migration histories were distinct, implying fluid systems since the beginning of the petrogenic cycle in the Early Eocene.

Fault zones are not always barriers to fluid flow. Smith (1980) concluded that entrapment in sand - shale sequences are in general determined by the amount of slip motion. If the net slip has not been larger than the thickness of the formation, fault entrapment is rarely observed. This seems to imply that a certain amount of displacement along a fault surface is required to ensure the formation of a gouge zone of sufficient thickness and lateral extent to act as a barrier. However, it is a misconception to relate the thickness of a sealing fault zone to the trapping capacity of the fault (op. cit.). The entry pressure of the seal determines the height of the petroleum-column that can be trapped and not thickness of the seal.

Land subsidence and faulting due to aquifer pumping and water withdrawal from the subsurface can also illustrate the role of barrier faults (Holzer, 1976). Kreitler (1976) noted that land subsidence due to aquifer pumping in the Houston Texas area appears to be fault controlled. Observed differential sediment compaction and pressure declines across a fluid barrier is translated to the surface as differential land subsidence rates or fault displacements.

Faults as conduits: Deformation and faulting of consolidated rigid sandstone and carbonate formations will lead to a zone of fault breccia of crushed and fractured rocks, giving rise to a fault-fracture zone of higher permeabilities and greater cohesive strengths.

When exploring for geothermal groundwater in crystalline rocks, fault zones are preferred locations for well sites, due to the increased water yield from fractured rocks associated with the fault zones. Rising hot waters use fault zones as conduits. A close correlation of thermal spring locations and fault zones, which may provide pathways for groundwater flow to depths of about 2000 m is apparent. (this study; Cermak et al., 1982; Lowell, 1975).

Newhouse (1942) presented many examples of ore bodies whose location and distribution were determined by fault zones. Ore bodies were emplaced by liquids at depths of at least several kilometres. Fractures associated with faults and gouge material are controlling factors in the distribution of ore bodies.

Surface evidence for petroleum migration along faults is found as oil seeps associated with faults in such areas as the Ventura Basin in California (McCullough, 1934), the Maracaibo Basin in Venezuela (Miller et al., 1955), basins in Irak (Dunnington, 1955), the Santa Cruz Basin in Bolivia (Illich et al., 1981) and the Pechelbronn-Soultz Basin (this study).

Oil migration along synsedimentary faults in the Niger Delta was postulated by Weber et al. (1978). They observed that single faults exhibit both high and low permeability, with a highly permeable zone parallel to the fault plane, in the hanging wall side, and low permeability perpendicular to the fault zone. If this permeability anisotropy is due to the fault structure, the implications are that the fault itself is structurally anisotropic.

Direct Fault Zone Observations

Fault zones may be directly investigated in tunnels and mines, and at the surface where erosion or excavation has exposed a previously buried fault. In the follwong I will review a few published detailed descriptions of fault zones observed in tunnels and mines and compare these findings with observations of faults made in the Pechelbronn mines and by drilling (Schnaebele, 1948 and SAEM well reports).

In tunnels which cut across the Hayward Fault in California (Louderback, 1942) a fault zone showed a complex succession of fault fractures, crushed belts and breccia, sheared belts and gouge. The clays and clay-sized particles in the fault gouge impede groundwater flow. Permeabilities decrease with decreasing grain size for rock with similar porosities. Clay-gouge may have fairly large porosities, but their permeability should be very low (Shi et al., 1980).

Aydin et al. (1983) studied the development of faults as zones of deformation bands and as slip surfaces in sandstones of southern Utah. Average porosities were found to be 6-10 % in the deformation bands, while undisturbed sandstone beds had an average porosity of 25 %. They observed slip surfaces and high permeabilities on the hanging wall side of normal faults, while on the footwall side nearly impermeable deformation bands were present. Flow to the slip surfaces from an aquifer in the hanging wall would be unimpeded, and slip surfaces as discontinuities in the formation may provide flow paths in a direction parallel to the discontinuity surface. Similar observations were made by Weber et al. (1978) in a coal mine near Cologne, Germany and by Newhouse (1942). They found ore bodies to be emplaced in the hanging wall block, apparently due to fluid migration up the fault zone. Anisotropic in situ permeability and pore fluid distribution was noted in a tunnel excavation near Banning, California (Thompson, 1966). Several faults in igneous and metamorphic rocks intersect the tunnel's course. Large quantities of water were found in open interconnected fractures and joints in the hanging wall; the fault density increased toward the fault zone, from relatively unfractured to highly fractured rocks. By the time the soft, water-saturated gouge and crushed material in the footwall were reached, the influx of water was negligible and water pressure was low.

In the mining galleries of Pechelbronn numerous faults were found to cut through the Pechelbronner Schichten, (Schnaebele, 1948, figures no. 6-8). From his figures it can be deduced that the principal Pechelbronn Fault in the Oligocene formations is several decimeters wide and shows also previously described structural phenomena like anatomizing shear faults, slip surfaces and fault gouges. Oil has migrated along the fault zone on the hanging wall side. Constant water influx from the exposed Pechelbronn Fault into the galleries and shafts could only be contained by pumping (Sittler, 1967; SAEM well reports). In other sections of the galleries auxiliary minor faults displaced Oligocene beds abruptly without the development of a fault, and oil penetrated into the fault plane.

Implications

Interpretation of the observations presented here has yielded a simple model of fault zone permeability and structure. A fault has an anisotropic permeability distribution which differs from that of the surrounding rock. The most commonly noted permeability anistropy had high permeability parallel to the fault zone and low permeability across it. The high permeability zone is most often found on the hanging wall side of the fault zone, with a zone of low permeability on the footwall side. Not all faults exhibit such a simple structure of permeability distribution; many factors may serve to complicate the actual fault system's characteristics in a active basin. These factors include tectonic activity and rejuvenation of faults, geochemical alterations and mineral precipitations by percolating groundwaters.

The model derived here implies that fluids can flow along a fault plane, if faulting and slip motion on the hanging wall side of the fault establishes a region of dilatation. This is most likely to occur in displaced sandstone and other rigid formations. The model also implies that fluid flow across a fault can occur if a low permeable deformation (gouge) zone on the footwall side of the fault zone is absent. This depends on the sheared material involved.

Fault zones will affect petroleum migration and accumulation only if they are continuous on scales required for trapping and vertical migration. It appears that a certain amount of displacement, which depends on the structure and lithology of the unfaulted rock, is required before a fault zone may become important in petroleum migration and entrapment (Smith, 1980). Displacements of the order of the reservoir's thickness were estimated to be responsible for fault sealing in the Gulf Coast basin. If petroleum tends to be trapped by the deformed zone and migrates along slip surfaces and neighbouring dilatational zones, most deposits should be found in the footwall blocks with the deformation zone separating the slip surface and the reservoir rock. Petroleum accumulations at the downthrown side of a fault should be sporadic due to possible vertical migration of hydrocarbons along the high permeability zone on the hanging wall side of the fault zone. In nature, entrapment against the hanging wall side of faults is rarely found, while trapping in the footwall side is fairly common (Levorsen, 1967). In the North Sea Basin (Witch Ground Graben, Hindle, 1989) several oil accumulation were discovered in downthrown fault traps against the hanging wall side. The author states clearly, however, that an inability of the hydrocarbon to escape along the border fault into younger porous and permeable horizons is critical to the entrapment in the downthrown blocks. For the Pechelbronn-Soultz Basin, Mesozoic reservoirs are oil-bearing only in the footwall block (Figures 84 profile B-B') while oil deposits in Tertiary reservoirs are also entrapped in the downthrown blocks.

The presence of fault systems in a sedimentary basin also has implications for the occurrence and maintenance of abnormal pressures in a basin. Bredehoeft et al.(1968)

analyzed the hydraulic characteristics of rock formations containing high pressures and have stated that the maintenance of greater than hydrostatic pressures depends critically on the hydraulic conductivity of the rock formation. Rocks of nanodarcy permeability are required to maintain superhydrostatic pore pressures over geologic times. This implies that the flow of pore waters in a fault-severed basin is obstructed by a thick sedimentary sequence and by a fault barrier. Without discussing the physical or chemical mechanisms which can cause abnormal pressures, their preservation in fault-severed regions is governed by the transmissivity (= hydraulic conductivity x thickness of the hydrostratigraphic unit) and the discontinuity of displaced hydrostratigraphic units. The hydraulic properties of a unit at its site of displacement are a function of the fault's vertical separation and its sealing capacity, i.e., its fault zone material. Thus, applying the fault-permeability model mentioned above, higher pore pressures can be expected to be concentrated in the low permeability (gouge) zone of the fault, i.e., in the footwall block. A pore pressure increase due to tectonism, for example, would dissipate faster in the relatively high permeability zones associated with a fault, than in the footwall. In such a fault zone the effective stress would be low in the gouge zone, possibly to the extent that unstable sliding may take place at very low shear stresses.

However, superhydrostatic pressures in structural compartments of a hydrodynamically active fault-severed basin do not necessarily indicate that the principal faults bordering the compartment are flow barriers. This depends decisively on the location of the allegedly consealed compartment within a groundwater flow system, since the pressure gradient of upward flowing groundwater will be superhydrostatic in any case, when the compartment is positioned in a discharge region.

Appendix 4 Faults and Aquifer Connectivity

For the fault-severed Mesozoic and Cenozoic multi-aquifer system one important question remains unanswered: are the principal fault zones and accessory faults conduits or barriers to groundwater movement and, consequently, are the hydrostratigraphic units connected across and/or along fault zones? It is also an important contemporary debate amongst petroleum geologists whether faults are act as conduits for subsurface fluids, particularly with regard to the migration of petroleum and abnormal pressures (Tóth et al., 1991).

Here, it should be emphasised that a fault is not a sharp planar discontinuity between two adjacent, displaced rock blocks, but rather a band of rock deformations which can be millimetres or meters wide (see Appendix III for a review of faults as conduits or barriers). A fault zone is a tabular region containing parallel or anastomosing faults. A shear zone can be a part of a fault zone across which blocks of rocks have been displaced in a fault-like manner, but without prominent development of visible faults. Shear zones are thus regions of ductile deformation, in contrast to fault zones which are regions of localized brittle deformation. The principal displacement along a fault is usually not confined to a single surface or to conjugate sets of single surfaces. Slip motion can take place along surfaces distributed throughout a shear zone of varying width. The width varies with lithological compositions of the fault walls over the throw interval. If sand is displaced against sand (or limestone/sand) we can expect brittle deformation and a zone of faults. However, if the sand is displaced against softer material, the zones are often wider and include material from different locations along the fault walls. Such shear zones have a lithologically layered appearance. Clay gouge is present where shale beds are sheared off, either by a minor shear or a major fault. This also implies that permeabilities vary along a fault plane, depending on the lithology of the adjacent sediments, and may change with progression of displacement along a fault over geologic time. Hence, a fault can be a conduit and a barrier at the same time (Appendix III).

While it is commonly accepted and well documented that fluids can migrate across faults (Daly et al., 1980; Faye, et al., 1982; North, 1985; Tóth et al., 1989); there are difficulties to be overcome in accepting fault planes as conduits for subsurface fluids. If a fault is to be a conduit for fluid flow then it must have permeability, and there must be a potential gradient in the fault plane. More fundamentally, as the quantity of water that flows through a permeable porous medium is proportional to the area of cross-section normal to flow, a fault plane must have greater permeability and/or a steeper hydraulic gradient in order to move significant quantities of groundwater upwards or downwards through this conduit since the cross-sectional area of a fault is infinitesimal compared to the area of adjacent sediments.

Numerous publications deal with hydrocarbon migration along faults (e.g. Fowler, 1970; Gavrilov, 1972; Mandl, 1988) but they describe and discuss only flow along open fractures in consolidated rocks. For normal faults, however, little detail has been published concerning the properties of fault zones in unconsolidated or semi-consolidated sand/shale sequences or of the exact process of the fluid flow along these zones (see also Appendix III). Two processes that may apply, are discussed in the literature, viz. hydraulic forces opening a pre-existing fault or even forming fractures (Hubbert, et al., 1959; Secor, 1965) and the migration of petroleum into or across a fault zone when the hydrocarbon fluid pressure exceeds the displacement pressure of some marginally permeable material in the fault zone (Smith, 1966). The former process would appear to be generally viable since it demands only that the fluid pressure equal or slightly exceed the total compressive normal stress that presses the fault walls together. The least principal stress is compressive except for relatively shallow depths (some hundreds of meters for consolidated sediments (Hubbert, 1951) and soon exceeds the cohesive strength of the sediments closing any gap. Secor (1965), basing his description on the Griffith theory of failure, puts forward a mechanism of natural tension fracturing expressed in terms of effective stresses which might occur at several thousands of meters depth in the Earth's crust giving rise to migration of groundwater and petroleum along open tension fractures. In extensional basins, tectonic reduction of the least compressive stress will promote extensional and tensional fracturing at greater depth.

For the middle segment of the Upper Rhine Graben (Figure 4; Chapter 2.2.2) the current principal compressive stress is horizontal and at about 130°, near-perpendicular to the 30° trend of the graben axis and the principal faults in the study area. Therefore, it can be assumed that, for the Pechelbronn-Soultz Basin and Upper Rhine Graben study areas, the occurrence of open fractures parallel to principal fault zones at greater depth is rare. Open fractures parallel to σ_1 might occur. Hot brines at Niederbronn (Vosges, Figure 70) and Baden-Baden (Black Forest) rise along fracture zones that re-opened under Holocene stress conditions. Following the trend of σ_1, these fractures or fault zones are of Holocene age and serve as fluid conduits (Illies et al., 1979).

In the study area the fault zones are a porous medium with sections of high or low permeabilities allowing groundwater to move along or across it depending on the hydraulic gradient and permeability of the adjacent rock block. A high permeability zone is most often found on the hanging wall side of the fault, with the low permeability zone on the footwall side (Fault Permeability Model, see Appendix III; Aydin et al., 1983). Relatively good agreement was found between the locatinos of fault zones as predicted by the model and those actually encountered at Pechelbronn through well drilling and observations in the mining galleries.

No details of petrophysical properties for rocks in fault zones or near a fault plane are available for the Upper Rhine Graben or, for that matter, from literature of basins elsewhere in the world (e.g. North Sea, Suez Basin). However, of it is assumed that groundwater is the transport mechanism of heat and matter, the hydraulic behavior of fault zones can be characterized by the use of field observations and applying the Hydraulic Theory. These field observations include measurements of near-surface temperature and geochemical survaeys across faults, subsurface geothermal and hydrochemical studies and regional groundwater flow analysis. The distribution patterns of these so-called hydrogeological phenomena (expressed as iso-salinity lines, isotherms on maps and sections) can reveal the conductance of fault zones to groundwater and its transported matter. Abrupt changes in water chemistry and temperature can indicate a flow-barrier, while a gradual but consistent change along and across a fault zone can indicate flow conductance in a fault zone to other hydrostratigraphic levels.

In an early stage of exploration, detailed information on the manifestation and distribution of hydrogeological phenomena and a regional groundwater flow analysis is not available. It is possible to deduce information on the hydraulic characteristics of fault segments and the connectivity of hydrostratigraphic units as well as on possible sites of petroleum accumulation by applying simple two methods: (1) the calculation of an connectivity factor and (2) the construction and interpretation of an connectivity diagram.

I developed the two methods assuming that:

(1) The ability and ease of groundwater to flow across a fault is a function of its throw. The hydraulic transmissivity of the fault-displaced aquifer is determined by the degree of vertical separation along the fault and lithologic changes in the fault plane, such that cross-flow can only occur when the aquifer is not totally displaced or is in contact with another aquifer across the fault.

(2) The fault zone has an anisotropic three-dimensional structure: flow along a fault zone is likely to occur in the highly permeable zone on the hanging side of the fault zone (see Appendix III).

Thus, depending on the juxtaposition of rock units, the groundwater flow conductance along/across a fault zone is high or low (Table 17).

Method I: Calculation of the Connectivity Factor

The connectivity factor, cf is defined in the following sketch:

$$cf = \frac{b-r}{b}$$

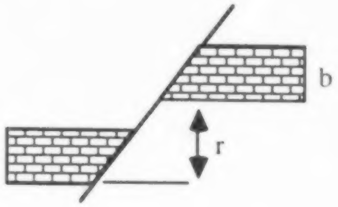

When: $cf \leq 0$ a hydrostratigraphic unit is disconnected; when $1 > cf > 0$ it is partly connected and when $cf = 1$ it is fully connected. The values r and b are inferred from well logs.

For the Pechelbronn and Hoelschloch Faults the connectivity factor for the main aquifers has been calculated (Table 18). The thickness of the hydrostratigraphic units is given in Tables 14 and 15. The representative fault throws for the Pechelbronn and Hoelschloch Fault are taken from wells 4648 and 4713, respectively. It is assumed that the throw is constant with depth. Aquifers 2, 3, 8 and10 are connected across the Pechelbronn and Hoelschloch Faults. The smaller the cf value the larger is the displacement of a hydrostratigraphic unit and flow congestion, lower aquifer transmissivity and loss in hydraulic head can be expected. In plotting the cf values on structure contour maps, the hydraulic continuity of hydrostratigraphic units in a fault-severed groundwater basin can be tentatively interpreted (e.g. HSU 3, Figure 71).

The cf-ratio, particularly for $1 \gg cf < 0$, is also meaningful to petroleum exploration. Small cf-values reflect considerable displacement in and discontinuation of the carrier bed, and can indicate a potential site of petroleum entrapment..

Method I approximates the effect of faults on a basin's hydrogeologic framework, but fails to give information on the juxtaposition of hydrostratigraphic units across a fault zone. Therefore, I have formulated a more advanced procedure which describes the hydrostratigraphy across and along a fault.

Method II: The Aquifer Connectivity Diagram

The diagram illustrates the contiguity of hydrostratigraphic units along and across principal fault zones on a local or regional scale. Along chosen sections of a basin, the diagram displays the up- and downthrown side of a fault, the adjacent positions and hydrogeologic characters of displaced hydrostratigraphic units in relation to other hydrostratigraphic units of the basin's hydrostratigraphic sequence. The same objective to evaluate a basin's hydraulic continuity could be achieved with detailed geologic cross-sections; this procedure is, however, time consuming and requires addition geologic information on the undeformed strata between fault zones. The required data for this method are fault throws, thicknesses of hydrostratigraphic units and juxtaposition across a fault which can be obtained from reference wells along a chosen cross-section.

Procedural Example and Implications

Figure 12 shows the concept of the model. Given the geology of four hydrostratigraphic units (aquifers) penetrated by two wells which encountered two faults (F1 and F2) of different vertical displacements, an aquifer connectivity diagram can be constructed. The vertical axis shows the hydrostratigraphy of a basin, the horizontal axis illustrates a selected cross-section with the up- and downthrown side of the two faults. From the reference well logs it is possible to depict, starting with the deepest hydrostratigraphic unit for the downthrown side, the adjacent hydrostratigraphic unit in the upthrown side. The procedure is repeated for the upthrown side. Partial or complete blockage by adjacent aquitards obstructs and deflects groundwater flow, creating sites for possible petroleum entrapment.

A combination of this initial connectivity diagram (which can always be expanded later by adding further wells) and the fault permeability model (as discussed in Appendix III) provides the petroleum hydrogeologist with a systematic method for hypothesizing potential groundwater flow directions and flow impediments along and across fault zones.

Appendix 5 Seals and Sealing Mechanisms for Petroleum Accumulations

Most subsurface hydrocarbon accumulations are trapped by some kind of physical seal which prevents natural buoyancy-related upward migation. In a hydrodynamic environment groundwater conveying hydrocarbons will pass though the low permeability seal while hydrocarbons are retained. Figure 66 is self-explanatory. It presents a simple classification of seal types which are divided into cap-rock, fault-related and hydrodynamic seals. When hydrocarbons are trapped by a sealing fault or under hydrodynamic conditions, a cap-rock seal must also be present.

The dominant trapping mechanism is the capillary properties of the cap-rock and fault-seal where the minimum displacement (or entry) pressure of the seal equates to the pressure required for hydrocarbons to enter the largest interconnected pore throat of the seal (Berg, 1975; Schowalter, 1979).

The dominant seal types in the Pechelbronn-Soultz Basin to hydrocarbons are fault-seals (a cap-rock must also be present) and membrane seals (lenses).

Appendix 6 The Petroleum Exploration and Production History of Alsace from 1735 to 1961

The following is a synopsis of information of several publications on the petroleum history in the Pechelbronn-Soultz Basin and in Northern Alsace (Hontcharenko, 1937; Levi, 1962; Sittler, 1985; Tzschachmann, 1914; Werveke van, 1909).

Attention was directed to the presence of oil deposits in the Pechelbronn-Merkwiller area by oil seeps some 500 years ago. The town's name "Pechelbronn", is interpreted to mean "pitch spring". An oil seep (direct indicator), described in 1498, produced a mixture of heavy oil and saline water just west of Pechelbronn. It was used by local farmers as lamp fuel and lubricant. Four periods of exploration and production of the Pechelbronn deposits, since the beginning of operation in 1735 up to the present can be distinguished:

Period I. 1735-1888

In 1735 the exploitation of oil sands in the Pechelbronn region began with near-surface mining. From mining galleries and shafts to depths of about 30 m the bituminous sand was excavated and hauled to the surface for oil extraction by hot water. In the year 1865 the galleries reached greater depths and the oil became increasingly viscous. The oil was then produced mainly by drainage mining. In a time period of 150 years 28 shafts were sunk and a total of 18 500 t of oil was produced, 4000 t by washing, 14 500 t by drainage.

Period II. 1889-1916

Following the introduction of the drilling technology in 1882, drainage mining ceased in 1889. In 1898, 23 000 t of oil was produced by bore hole pumping. At the end of the century, Dutch and German oil companies began feverishly to explore the Pechelbronn-Soultz Basin for new oil deposits in Tertiary formations. They met with little success, and by 1906 only the German oil company "Deutsche Erdöl-Aktiengesellschaft" (DEA) was still involved in exploration and production in the region. From 1889 until 1916 about 2850 boreholes were drilled and about 790 000 t of oil was produced. Until 1909, oil was produced exclusively from sandlenses in the Oligocene *Pechelbronner Schichten*. In 1909 the first oil deposit in the Eocene *Zone Dolomitique* was discovered.

Period III. 1917-1953

During the First World War, the demand for oil was very high, and the oil company at Pechelbronn reopened the mines and initiated production by drainage mining on a much wider scale. By the end of the war three deep shafts had been sunk to 400 m depth in the Pechelbronn region to exploit oil from the *Pechelbronner Schichten*. A labyrinth of galleries, tunnels and shafts crisscross the underground at Pechelbronn in a NNE-SSW direction. After the war, Alsace became part of France, and the French government transferred the concession rights to a French oil company, Pechelbronn SAEM. It continued the mining and drilling operations and started constructing a fourth shaft in 1938 in the northern part of Pechelbronn.

The Second World War led to another change in ownership. During the occupation of France, the Pechelbronn oil fields were in control again of the DEA. Minor oil accumulations were discovered in Mesozoic formations at Kutzenhausen, Soultz and Pechelbronn in the *Keuper*, *Lettenkohle* and *Muschelkalk*. However, the production rate was low and the reservoirs were quickly flooded with saline water. During the war, production was interrupted several times and, due to a shortage of skilled workers, the production rate was low. Late in 1944, the entire petroleum complex at Pechelbronn and all the oil rigs were destroyed by allied bombing. French engineers intended to reactivate oil production but found the mining galleries all flooded by groundwater. Only a small part of the mines were reopened. Between 1917 to 1953, 1 292 00 t oil was produced by drilling and 955 99 t by drainage mining.

Period IV. 1953-1961

This last period signaled the decline of the Pechelbronn oil industry. During these nine years only 230 000 t of oil was produced. Further exploration for, and production of, petroleum continued to the east of the Pechelbronn-Soultz Basin. This was carried out by the oil company PREPA in 1954. Minor oil and gas fields were found at Soufflenheim, Scheibenhardt, Schirrheim.

Wellno.	KB	Location	inter.depth	depth (m)	Formation	Comment	vert. Perm. md	horiz. Perm. md	Porosity %
Bisch F4	125	Bischwiller	0-40		alluvium	SGAL 234-4-34			
Hag-67	150	Haguenau	0-6		alluvium	SGAL-Archive			
Hag-Aero	149	Hag. Aerodrome	0-61		Pliocene	SGAL-Archive			
Souff-2	134	Soufflenheim		13	Plio	SGAL-Archive			
4774	116	Beinheim	493-556		CN	mean	0.033	0.038	15 ±2.5
4686	158	Glaswinkel	7-91		SG	low ø			
4774	116	Beinheim	610-1036		SG	mean	0.046	0.07	7.5
Scheib-29	137	Scheibenhardt	555-556		SG	micas	0.73-0.77	64-144	6-18
Scheib-31	165		640-642		SG				10
Scheib-31	165		608-609		SG				10
Scheib-31	165		583-585		SG	fault at 570			17
4632	160	Soultz	250-363		Ps	Conglo./high ø			
4633	150	Walb	266		Ps	very tide			
4765	116	Forstfeld	1236-1240		Ps	mean	0.122	0.088	4.8
4774	116	Beinheim	1119-1427		Ps	mean	0.1		3 ±4
4778	118	Beinheim	1017-1070		Ps	mean	0.5		11
4781	122	Schirrheim	728-733		Ps	mean	0.5	0.12	10.2
4788	121	Schirrheim	360-558		Ps	mean	0.47	0.15±0.1	12.6
4792	122	Schirrheim	520-563		Ps	mean	0.4 ±0.8	2.5 ±4	15
Kalt-1	142	Kaltstett	657-671		Ps		1		11
Oberl-1	170	Oberlach	955-		Ps				28
Obers-1	174	Oberseebach	979-1003		Ps				19.5
Schwab-1	143		400-615		Ps				16
4765	116	Forstfeld	1316-1320		Pm				4.72
4774	116	Beinheim	1489-1493		Pi				3.4
Mar-101	269	Marienbronn	256-271		Pm	Total Expl.			20-25
4600	184	Dieff	218-353		Pi	perm. not measureable			
4604	180	Ohlungen	213267		Pi	rapp.permeable			
4765	116	Forstfeld	1389	1389	Pi				1.5
4778	118	Beinheim	1078-1093		Pi		50		25
4788	121	Schirrheim	558-588		Pi	mean	0.011	0.19	11.8
4512	197	Preus			ZD	ø decreases from fault			
4656	189	Heidenboesch	610-612		ZD	rapp.porous			
4716	131	Soufflenheim	1042-1186		ZD	mean ø,k			6.4 ±4

Appendix 7 Hydraulic Data

Wellno.	hydr. Cond. m/s	Transm. m2/s	Remarks
Bisch F4	1.0 E-3	2 E-2	pump test
Hag-67	1.9 E-5	9.5 E-5	pump test
Hag-Aero	6.4 E-5	3.2 E-3	pump test
Souff-2	3.5E-4	5.9E-3	pump test
4774			plot
4686			
4774			plot
Scheib-29			
Scheib-31			80%H2O
Scheib-31			
Scheib-31			25%H2O
4632			
4633			
4765			E-logs
4774			plot
4778			plot
4781			plot
4788			
4792			fissures
Kalt-1			
Oberl-1			
Obers-1			
Schwab-1			
4765			E-logs
4774			plot
Mar-101			Total; 75 % Oil
4600			
4604			
4765			E-logs
4778			fissure/fault
4788			
4512			SAEM
4656			
4716			

Appendix 7 Hydraulic Data

Wellno.	KB	Location	inter.depth	depth (m)	Formation	Comment	vert. Perm. md	horiz. Perm. md	Porosity %
4755	134	Soufflenheim	1060-1062		ZD/sel gemm	mean	1.4	0.61	15
4755	134	Soufflenheim	1063-1118		ZD	mean	0.6 ±1.8	4.34 ±10.4	9.2 ±4
4760	160	Surbourg	700-710		ZD	mean	0.2 ±0.03	0.27 ±0.14	6.6 ±5
4765	116	Forstfeld	1477-1790		ZD	mean			3.5 ±2.7
4770	121	Schirrheim	768-1115		ZD	mean		0.08	8.5 ±2
4774	116	Beinheim	1735-1740		ZD		0.8	1.2	5.1
4776	137	Rittershofen	1015-1016		ZD				17.2
Kil-1	130	Kilstett	1236-1280		ZD	PREPA, core		0.145	
4755	134	Soufflenheim	1118-1136		ZT	mean	5.2 ±5.9	8 ±17	8.4 ±4.7
4759	134	Soufflenheim	1105-1128		ZT	mean	0.07 ±0.4	0.25 ±0.3	14.1 ±7
4760	160	Surbourg	710-720		ZT	mean	0.12 ±0.19	0.33 ±0.4	12.8 ±3
4776	137	Rittershofen	1102-1039		ZT	mean			7.5±2
4716	131	Soufflenheim	1186-1455		J moy	mean		n/a	7.0 ±2.7
4742	134	Soufflenheim	1122-1150		J moy	mean			27.5
4755	134	Soufflenheim	1136-1255		Bajocian	mean		2.9 ±5.0	9 ±3
4759	134	Soufflenheim	1128-1140		J	mean	0.12 ±0.15	0.14 ±0.3	12 ±5.3
4764	149	Surbourg	712-755		J moy	mean		2.5	12
4765	116	Forstfeld	1886-1900		J moy	mean	1.2	0.5	5.9 ±3.4
4770	121	Schirrheim	1153-1163		Bathonian	mean			10.3 ±1.5
4770	121	Schirrheim	1169-1242		Bajocian	mean	0.19 ±0.2	0.3 ±.3	6 ±1
4776	137	Rittershofen	1043-1101		J moy	mean	0.2 ±0.5	1 ±1.3	9.3 ±1.8
Holz-1	146	Holzheim	1800		J				14
Schwei-2	279	Schweighausen	1653-1666		J moy	PREPA		1.3	6-15
4716	131	Soufflenheim	1440-1455		J inf	mean		0.65 ±0.15	2.6 ±2
4755	134	Soufflenheim	1255-1407		Aalenian	mean, k till 1272	0.22 ±0.3	7.5 ±4.0	8.6 ±3.4
4760	160	Surbourg	720-748		Aalenian	mean	0.06 ±0.1	0.11 ±0.1	12.3 ±3.7
4761	165	Walbourg	522-598		Aalenian	mean/522 fault			10.3 ±4.6
4761	165	Walbourg	700-731		Liassic	single value	0.08	0.31	11.2 ±4.8
4770	121	Schirrheim	1237-1551		Aalen-J inf	mean	0.09	0.16	2.7 ±.6
4776	137	Rittershofen	1287-1337		J inf	mean	0.035	0.15	6.5 ±2.5
Reim-1	186	Reimerswiller	670-692		Aalenian		0-3.0		10-18
4776	137	Rittershofen	1342-1346		Rhät	mean	0.16	0.66	5.8
4606	199	Kutzenhausen		903	K				28.5
4606	199	Kutzenhausen		908	K			2.5	47.4

Appendix 7 Hydraulic Data

Wellno.	hydr. Cond. m/s	Transm. m2/s	Remarks
4755			
4755			E-logs
4760			E-logs
4765			E-logs
4770			E-logs
4774			plot
4776			
Kil-1			
4755			E-logs
4759			E-logs
4760			E-logs
4776			
4716			
4742			gas erup;.
4755			E-logs
4759			E-logs
4764			E-logs
4765			E-logs
4770			E-logs
4770			E-logs
4776			fissures
Holz-1			grand oolith
Schwei-2			
4716			
4755			E-logs
4760			E-logs
4761			E-logs
4761			E-logs
4770			E-logs
4776			fissures
Reim-1			
4776			
4606			
4606			

Appendix 7 Hydraulic Data

Wellno.	KB	Location	inter.depth	depth (m)	Formation	Comment	vert. Perm. md	horiz. Perm. md	Porosity %
4606	199	Kutzenhausen		912	K			1.3	48
4716	131	Soufflenheim	1475-1638		K	mean		0.65 ±0.5	4.8 ±2
4761	165	Walbourg	752-802		K sup.	mean	0.12 ±0.12	0.2 ±0.21	9.9 ±2.9
4761	165	Walbourg	752-802		K	mean	0.17 ±0.4	0.19 ±0.38	13 ±4
4770	121	Schirrheim	1542-1551		K	mean	0.03	0.07	2.2 ±.3
4772	163	Pechelbronn	829-860		K. moy.			1.9-2.3	19-Aug
4776	137	Rittershofen	1373-1510		K	mean	0.08	1 ±1.7	4.7 ±1.1
4630	170	Pechelbronn		781	GR			33	20-25
4761	165	Walbourg	802-827		GR	mean	0.02 ±0.02	0.15 ±0.4	14.4 ±3
4648	194	Pechelbronn	809-833		LK			3	
4716	131	Soufflenheim	1638-1668		LK	mean		1.65 ±0.14	2.5 ±.62
4776	137	Rittershofen	1525-1550		LK	mean	0.04	1.02	3.9
4541	150	Soultz		932	MK			6.1	8.5
4541	150	Soultz		932.1	MK			10.5	
4541	150	Soultz		935.4	MK			156.7	14
4541	150	Soultz		936.3	MK			6.1	8.5
4541	150	Soultz		937.6	MK			20.7	6
4541	150	Soultz		940	MK	silicified		1.1	6.5
4550	150	Soultz	898-955		MK inf			0-1.5	10
4554	156	Kutzenhausen		865	MK	dolomite		0.3	5.7
4555	150	Soultz		854	MK			0	2
4555	150	Soultz		856	MK			0	2.5
4555	150	Soultz		863.5	MK			0	2
4555	150	Soultz		863.6	MK	fissures		38.14	30
4555	150	Soultz		863.8	MK	fissures		16.21	21
4555	150	Soultz		864	MK	fissures		13.61	24.3
4601	169	Kutzenhausen	930-1000		MK	rapp. peu permeable			
4716	131	Soufflenheim	1668-1690		MK sup	mean		1.55 ±0.16	1.65 ±.4
4716	131	Soufflenheim	1809-1834		MK inf	mean		0.11 ±0.13	1.4 ±.3
4776	137	Rittershofen	1585-1602		MK	mean	0.044	0.046	3.4
Mors-3a	190	Morsbronn		400	MK	SGAL-pump test			
Sarre-72	270.5	Sarre-Union	0-350		MK/Bsdst	SGAL 196-3-72			
4550	150	Soultz	955-971		Bsdst sup			2.7	2-10
4550	150	Soultz	971-1050		Bsdst	10md possible		2.8-10	2.5-12

Appendix 7 Hydraulic Data

Wellno.	hydr. Cond. m/s	Transm. m2/s	Remarks
4606			
4716			
4761			E-logs
4761			E-logs
4770			E-logs
4772			Gres a Roseux
4776			fissures
4630			Total
4761			E-logs
4648			Sat. 5%
4716			
4776			fissures
4541			
4541			
4541			
4541			
4541			
4541			
4550			fissures
4554			Total
4555			
4555			
4555			
4555			Total
4555			Total
4555			Total
4601			
4716			
4716			
4776			
Mors-3a		3.0E-3	S=1*E-3
Sarre-72			Vosges/west water di
4550			
4550			175md in fissures

Appendix 7 Hydraulic Data

Wellno.	KB	Location	inter.depth	depth (m)	Formation	Comment	vert. Perm. md	horiz. Perm. md	Porosity %
4590	178	Soultz		1016	Bsdst			2.95	6.7
4609	147	Kutzenhausen		976	Bsdst	close to fault		0.13	4.5
Bitch	231	Bitch/Vosges	0-47		Bdst	SGAL-Archive			
Bruch 1a		Bruchsal	1742-1875		Bsdst	Bertleff et al. 1987			
Bruch 2		Bruchsal	2345-2349		Bsdst	Bertleff et al. 1987		2 E-2 - 6 E-2	3 - 6
Helion II	161	Pechelbronn		1100	Bsdst	Walgenwitz 1979		120	
Hochwald-I	295	Marienbronn	167		Bsdst	SGAL 168-8-22			
Mar-101	269		784-901		Bsdst	Total Expl.			21.6
Mors-3b	190			680	Bsdst	SGAL-pump test			
Phil	220	Philipsbourg	70		Bsdst	SGAL-Archive			
Pierre	245	Petite Pierre	162		Bsdst	SGAL-197-6-20			
Roth-40	196	Rothbach/Vosges	0-133		Bsdst	SGAL 197-4-40			
Weiler-1	170	Wissembourg	0-80		Bsdst	SGAL 168-8-39			

Wellno.	hydr. Cond. m/s	Transm. m2/s	Remarks
4590			
4609			fault gouge?
Bitch		8.5 E-3	pump test
Bruch 1a	2 E-6	8 E-5	pump test
Bruch 2			DST
Helion II	10 E-6	5 E-5	pump test
Hochwald-I	3.0 E-6	1.9 E-4	pump test
Mar-101			Total
Mors-3b	2 E-5	0.7 - 4 E-3	Pump test SGAL
Phil	1.1 E-6	7.3 E-5	pump test
Pierre	3.3 E-6	4.7 E-4	Vosges, pump test
Roth-40		2.6 E-4	pump test
Weiler-1	1.0 E-5	8 E-4	pump test

Appendix 7 Hydraulic Data

Wellnr.	KB	Date	Location	inter.depth	mean.d	Formation	pH	density	TDS mgl	Ca mgl
1850	168	3.3.25	Surbourg		174	Ps			60460	3300.00
2019	188	13.12.34	Lobsann		295	Ps	5.90			0.00
2219	173	3.3.25	Surbourg		397	Ps			60800	3800
2300	189	3.3.25	Surbourg		201	Ps			49200	2400
2364	180	3.3.29	Kutzh.reuz		223	Ps			60460	3630
3005	202	26.6.51	Ohlungen		300	Pi		1.075	125900	4200
3067			Kutzh.N		507	ZD		1.052		
3655	217	27.8.51	Hochstett		395	Ps	7.1	1.004	10000	1800
3670	160	8.5.51	Kutzh.		594	ZD	6.4	1.072	103200	8200
3709	146	16.8.51	Kutzh.		373	ZD	7.8	1.017	25400	1000
3578	154	1.8.34	Soultz	530-532	531	ZD		1.034	32200	1400
3912	158	9.5.38	Kutzh.S		1002	MK	7		99300	4640
4123	164	3.11.50	Pechelbronn		455	ZD	6	1.024	37100	3620
4362	161	8.5.51	Kutzh.S		954	MK	6.4	1.072	109200	7900
4388	162	25.9.50	Soultz		865	LK	5.5	1.072	109800	7620
4418		8.5.51	Kutzh.		784	ZD	6.2	1.066	99800	7400
4445	221	25.2.48	Soufflenh.		321.5	Ps				
4472	173	8.5.51	Soultz		763	LK	6.7	1.07	100500	7800
4485	173	2.1.49	Hoelschloch		1214	Bsdst	7.3	1.015	24190	1626
4502	179	8.5.51	Soultz		829.5	MK	5.9	1.07	101200	7800
4515	147	8.10.51	Soultz		857.7	MK	6.3	1.072	101200	8300
4515	147	8.10.51	Soultz		860	MK	7.3	1.07	92599	5400
4524	168	7.9.50	Preuschdorf		467	ZD	7	1.057	91320	5800
4524	173	3.7.50	Preuschdorf		898	LK	5.5	1.068	121600	7840
4541	150	2.6.50	Soultz		950	MK	7.3	1.07	100654	7500
4542	180		Kreuzecke		913	J	5.5	1.081		
4544	171	3.7.50	Pechelbronn		250	Pi	6	1.057		5800
4549	163		Soultz		856	LK		1.07		7740
4549	163		Soultz		895	MK		1.072		9900
4550	150		Soultz		980	Bsdst	6.9	1.072	101020	6949
4554	156		Soultz		857.4	MK	6.4	1.072	105300	8000
4566	198	28.8.50	Soultz		904	LK	5.5	1.071	107500	8160
4567	147	8.10.51	Soultz		817	LK	6.2	1.07	41300	7300
4567	147		Soultz		871	MK	6.8		97314	7000
4572	170		Dürrenbach		702	ZD	6	1.083		8100
4575	166		Pechelbronn		500	ZD	6	1.056		8720

Appendix 8 SAEM Hydrochemistry Data

Wellnr.	Ca mel	Na mgl	Na mel	K mgl	K mel	Mg mgl	Mg mel	Fe2 mgl	Fe2 mel	HCO3 mgl
1850	164.67					290.00	23.84	0.00	0.00	0.00
2019	0.00					0.00	0.00	0.00	0.00	0.00
2219	189.62					420	34.52		0.00	
2300	119.76					350	28.77		0.00	
2364	181.14					476	39.13		0.00	
3005	209.58					350	28.77	80	2.86	300
3067	0.00						0.00		0.00	
3655	89.82					350	28.77		0.00	240
3670	409.18					120	9.86	50	1.79	440
3709	49.90					750	61.65		0.00	100
3578	69.86					280	23.02	130	4.65	400
3912		34620		with Na		200		340		160
4123	180.64					200	16.44		0.00	330
4362	394.21					350	28.77		0.00	60
4388	380.24					1500	123.30		0.00	400
4418	369.26					350	28.77	60	2.15	120
4445	0.00	4310	187.49		0.00		0.00		0.00	
4472	389.22		0.00		0.00	300	24.66	50	1.79	330
4485	81.14	6187	269.13	1168	29.90	53	4.36	1.6	0.06	305
4502	389.22		0.00		0.00	340	27.95	80	2.86	160
4515	414.17		0.00		0.00	350	28.77	80	2.86	410
4515	269.46	24700	1074.45	4460	114.18	630	51.79	5	0.18	560
4524	289.42		0.00		0.00	1000	82.20		0.00	830
4524	391.22		0.00		0.00	200	16.44		0.00	540
4541	374.25	28110	1222.79	293	7.50	293	24.08		0.00	433
4542	0.00	50200	2183.70		0.00	300	24.66		0.00	289
4544	289.42	32700	1422.45		0.00	1500	123.30		0.00	250
4549	386.23		0.00		0.00	200	16.44	70	2.51	530
4549	494.01		0.00		0.00	2000	164.40	100	3.58	671
4550	346.76	27375	1190.81	3187	81.59	579	47.59	40	1.43	281
4554	399.20		0.00		0.00	350	28.77	80	2.86	480
4566	407.18		0.00		0.00	200	16.44	60	2.15	305
4567	364.27		0.00		0.00	250	20.55	30	1.07	390
4567	349.30	26915	1170.80	2812	71.99	452	37.15	32	1.15	265
4572	404.19					3000	246.60		0.00	534
4575	435.13					200	16.44		0.00	

Appendix 8 SAEM Hydrochemistry Data

Wellnr.	HCO3 mel	Cl mgl	Cl mel	SO4 mgl	SO4 mel	Total Cation	Total Anion	Na+K mel	Comment	Reference
1850	0.00	22700.0	640.14	988.00	20.55	188.51	660.69	472.18	oil well	SGAL
2019	0.00	16500.0	465.30	40.00	0.83	0.00	466.13			SGAL
2219	0.00	30800	868.56	3350	69.68	224.14	938.24			
2300	0.00	25100	707.82	3070	63.86	148.53	771.68			
2364	0.00	30500	860.10	3460	71.97	220.26	932.07			SGAL
3005	4.92	60300	1700.46	360	7.49	241.21	1712.87			SGAL
3067	0.00	4230	119.29		0.00	0.00	119.29		I, Br	SGAL
3655	3.94	5320	150.02	250	5.20	118.59	159.16	40.57		SGAL
3670	7.22	58600	1652.52	90	1.87	420.83	1661.61	1240.77		SGAL
3709	1.64	16000	451.20	70	1.46	111.55	454.30	342.75		SGAL
3578	6.56	18200	513.24	850	17.68	97.53	537.48	439.95		SGAL
3912		58400		940					Artesian	SGAL
4123	5.41	28400	800.88	550	11.44	197.08	817.73	620.65		SGAL
4362	0.98	65300	1841.46	170	3.54	422.98	1845.98	1423.00		SGAL
4388	6.56	58900	1660.98	115	2.39	503.54	1669.93	1166.39		SGAL
4418	1.97	53200	1500.24	130	2.70	400.18	1504.91	1104.73		SGAL
4445	0.00	7100	200.22	257	5.35	187.49	205.57	18.08		SGAL
4472	5.41	55400	1562.28	110	2.29	415.67	1569.98	1154.31		SGAL
4485	5.00	13672	385.55	178	3.70	384.59	394.25		copy	SGAL
4502	2.62	57500	1621.50	90	1.87	420.03	1626.00	1205.96		SGAL
4515	6.72	58600	1652.52	110	2.29	445.80	1661.53	1215.73		SGAL
4515	9.18	55500	1565.10	190	3.95	1510.05	1578.24	68.18		SGAL
4524	13.61	46900	1322.58	249	5.18	371.62	1341.37	969.75		SGAL
4524	8.86	60400	1703.28	192	3.99	407.66	1716.13	1308.47		SGAL
4541	7.10	56100	1582.02	385	8.01	1628.62	1597.13			SGAL
4542	4.74	77400	2182.68	173	3.60	2208.36	2191.02	-17.34		SGAL
4544	4.10	50400	1421.28	76	1.58	1835.17	1426.96	-408.21	?????	SGAL
4549	8.69	57500	1621.50	110	2.29	405.17	1632.48			SGAL
4549	11.00	57100	1610.22	115	2.39	661.99	1623.62	961.63		SGAL
4550	4.61	56622	1596.74	277	5.76	1668.18	1607.11		Mn: 8.2	SGAL
4554	7.87	60400	1703.28	130	2.70	430.83	1713.86	1283.02		SGAL
4566	5.00	52500	1480.50	115	2.39	425.77	1487.89	1062.12		SGAL
4567	6.40	28700	809.34	90	1.87	385.89	817.61	431.71	TDS ?	SGAL
4567	4.35	52895	1491.64	373	7.76	1630.39	1503.74			SGAL
4572	8.76	67160	1893.91	192	3.99	650.79	1906.66	1255.87		SGAL
4575	0.00	45800	1291.56	2204	45.84	451.57	1337.40	885.84	incomplete	SGAL

Appendix 8 SAEM Hydrochemistry Data

Wellnr.	KB	Date	Location	inter.depth	mean.d	Formation	pH	density	TDS mgl	Ca mgl
4584	184	25.4.50	Surbourg		271	Pi	6	1.064		4400
4585	173	8.10.51	Kutzh.N		840	LK	6.4	1.067	102500	7300
4587	164	6.6.50	Walbourg		247	Pi	6.5	1.053		3340
4587	164	14.6.50	Walbourg		740	J	6.5	1.074		7400
4592	189	11.8.50	Heidenboesch		645	ZD	5	1.05		7780
4593	181		Hoelschloch		1015	J		1.073	110000	
4594		4.6.	Lampertsloch		481	ZD	6.5	1.052		5240
4599	178	1.7.50	Surbourg		90	Ps	6.5	1.011		440
4599	173	8.8.50	Surbourg		259	Ps	6	1.044	64300	5000
4599	173	4.9.50	Surbourg		324	Ps	6.5	1.053	78700	6000
4599	173	22.9.50	Surbourg		440	Pi	6	1.066	99800	7720
4599	173	23.10.50	Surbourg		670	ZD	6.5	1.083	152000	8580
4601	169	8.5.51	Hoelschloch		670	LK	6.2	1.07	99300	7900
4603	181	21.7.50	Pechelbronn		599	ZD	6	1.059		6720
4606	199		Ramsbachw		550	ZD	6	1.047	71240	4760
4608	181	25.11.50	Ramsbachw		852	LK	5.5	1.068		7340
4608	181	10.11.50	Ramsbachw		867	LK	5	1.066	99840	7300
4608	181	30.9.50	Ramsbachw		876	LK	5.5	1.054	60800	5000
4608	181	21.10.50	Ramsbachw		876	LK	5.5	1.036	4300	4760
4611	183	26.9.50	Surbourg		715	ZD	5.5	1.087	137000	9400
4616	155		Kutzh.		972	LK	5.5	1.054	72700	5400
4617	187	9.10.50	Pechelbronn		560	ZD	5.5	1.06	94860	5600
4619	151	8.5.51	Soultz		865	LK	6.3	1.072	104000	7500
4620	147	24.10.51	Soultz		850	MK	6.3	1.072	113600	6800
4625	168	2.10.50	Pechelbronn		340.5	Pi	8	1.015	24400	7600
4625	168	2.10..50	Pechelbronn		430	ZD	6	1.06	92810	6700
4631	187	5.10.50	Preuschdorf		111	Ps	7	1.005	3120	300
4631	187	30.10.50	Preuschdorf		260	Ps	6.5	1.014	21160	960
4631	187	30.10.50	Preuschdorf		400	CR	5	1.08	128000	10100
4631	187	30.10.50	Preuschdorf		470	ZD	5.5	1.078	112000	8200
4631	187	30.10.50	Preuschdorf		550	ZD	5.5	10.77	95400	7600
4632	160	22.11.50	Soultz		395	Pi	6	1.024	39240	1600
4633	150	8.11.50	Walbourg		290	Ps	5.5	1.051	81640	3300
4634	173	8.5.51	Soultz		837	LK	5.5	1.062	96400	6100
4639	167	8.5.51	Soultz		800	LK/MK	6.5	1.071	104200	
4640	178	16.1.51	Pechelbronn		300	Pi	6	1.057	78200	

Appendix 8 SAEM Hydrochemistry Data

Wellnr.	Ca mel	Na mgl	Na mel	K mgl	K mel	Mg mgl	Mg mel	Fe2 mgl	Fe2 mel	HCO3 mgl
4584	219.56					3000	246.60		0.00	250
4585	364.30					350	28.77	120	4.30	360
4587	166.67					3000	246.60		0.00	540
4587	369.26					2000	164.40		0.00	1600
4592	388.22					1500	123.30		0.00	710
4593	0.00					1500	123.30	50	1.79	176
4594	261.48					2200	180.84		0.00	30
4599	21.96					2000	164.40		0.00	200
4599	249.50					1000	82.20	50	1.79	90
4599	299.40					1500	123.30		0.00	540
4599	385.23					1500	123.30		0.00	90
4599	428.14					750	61.65		0.00	70
4601	394.21					400	32.88		0.00	270
4603	335.33					1000	82.20		0.00	90
4606	237.52					200	16.44		0.00	510
4608	366.27					150	12.33		0.00	750
4608	364.27					200	16.44	400	14.32	213
4608	249.50					200	16.44	80	2.86	70
4608	237.52					1000	82.20		0.00	204
4611	469.06					500	41.10	40	1.43	85
4616	269.46					70	5.75	50	1.79	590
4617	279.44					1500	123.30	120	4.30	300
4619	374.25					400	32.88	50	1.79	300
4620	339.32					300	24.66	80	2.86	360
4625	379.24					20	1.64		0.00	110
4625	334.33					760	62.47		0.00	18
4631	14.97					100	8.22		0.00	150
4631	47.90					200	16.44		0.00	40
4631	503.99					1500	123.30			204
4631	409.18					1200	98.64		0.00	130
4631	379.24					1500	123.30		0.00	100
4632	79.84					350	28.77	130	4.65	67
4633	164.67					1000	82.20		0.00	
4634	304.39					200	16.44		0.00	380
4639	0.00					350	28.77		0.00	330
4640	0.00						0.00		0.00	330

Appendix 8 SAEM Hydrochemistry Data

Wellnr.	HCO3 mel	Cl mgl	Cl mel	SO4 mgl	SO4 mel	Total Cation	Total Anion	Na+K mel	Comment	Reference
4584	4.10	52100	1469.22	1530	31.82	466.16	1505.14	1038.98		SGAL
4585	5.90	54300	1531.26	110	2.29	397.37	1539.45	1142.09		SGAL
4587	1500.00	44400	1252.08	1150	23.92	413.27	2776.00	2362.73	?	SGAL
4587	26.24	63500	1790.70	130	2.70	533.66	1819.64	1285.98		SGAL
4592	11.64	41100	1159.02	530	11.02	511.52	1181.69	670.17		SGAL
4593	2.89	63900	1801.98	464	9.65	125.09	1814.52		incomplete	SGAL
4594	0.49	44000	1240.00	192	3.99	442.32	1244.49	802.17		SGAL
4599	3.28	10600	298.92	30	0.62	186.36	302.82	116.47		SGAL
4599	1.48	37200	1049.04	1720	35.78	333.49	1086.29	752.80		SGAL
4599	90.00	43700	1232.34	300	6.24	422.70	1328.58	905.88		SGAL
4599	1.48	54300	1531.26	380	7.90	508.53	1540.64	1032.11		SGAL
4599	1.15	99300	2800.26	380	7.90	489.79	2809.31	2319.52		SGAL
4601	4.43	61100	1723.02	130	2.70	427.09	1730.15	1303.06		SGAL
4603	1.48	57900	1632.78	370	7.70	417.53	1641.95	1224.42		SGAL
4606	8.36	80600	2272.92	150	3.12	253.96	2284.40	2030.44		SGAL
4608	12.30	81600	2301.12	60	1.25	378.60	2314.67	1936.07		SGAL
4608	3.49	44400	1252.08	326	6.78	395.03	1262.35	867.32		SGAL
4608	1.15	30200	851.64	76	1.58	268.80	854.37	585.56		SGAL
4608	3.35	38340	1081.19	96	2.00	319.72	1086.53	766.81		SGAL
4611	1.39	108000	3045.60	80	1.66	511.59	3048.66	2537.07		SGAL
4616	9.68	4800	135.36	380	7.90	277.00	152.94	-124.06	??	SGAL
4617	4.92	48900	1378.98	130	2.70	407.04	1386.60	979.57		SGAL
4619	4.92	58900	1660.98	150	3.12	408.92	1669.02	1260.10		SGAL
4620	5.90	60000	1692.00	130	2.70	366.84	1700.61	1333.76		SGAL
4625	1.80	12400	349.68	690	14.35	380.88	365.84	-15.05	fault	SGAL
4625	0.30	69100	1948.62	369	7.68	396.80	1956.59	1559.79	fault	SGAL
4631	2.46	1790	50.48	520	10.82	23.19	63.75	40.56		SGAL
4631	0.66	14500	408.90	1920	39.94	64.34	449.49	385.15	fault	SGAL
4631	100.00	95800	2701.56	380	7.90	627.29	2809.46	2182.17		SGAL
4631	0.00	95800	2701.56	230	4.78	507.82	2706.34	2198.52		SGAL
4631	1.64	92300	2602.86		0.00	502.54	2604.50			SGAL
4632	1.10	33700	950.34	110	2.29	113.26	953.73	840.46		SGAL
4633	0.00	60400	1703.28	960	19.97	246.87	1723.25			SGAL
4634	6.23	51830	1461.61	130	2.70	320.83	1470.54			SGAL
4639	5.41	58600	1652.52	11	0.23	28.77	1658.16			SGAL
4640	5.41	49700	1401.54	570	11.86		1418.81		fault	SGAL

Appendix 8 SAEM Hydrochemistry Data

Wellnr.	KB	Date	Location	inter.depth	mean.d	Formation	pH	density	TDS mgl	Ca mgl
4642	156	9.5.51	Soultz		818.5	K	6.5	1.107	101400	5000
4651	153	14.2.51	Walbourg		285	Ps	6	1.055		3600
4653	176	8.5.51	Soultz		803	K	6.5	1.069	972000	7300
4655	200	9.2.51	Kreuzecke		26	SG	6	1		200
4655	200	9.4.51	Kreuzecke		554	CR	5.5	1.075	103900	6200
4655	200	26.4.51	Kreuzecke		620	ZD	5	1.084	122500	7200
4656	189	9.5.51	Heidenboesch		572	ZD	5.5	1.096	130110	6800
4657	168	17.4.51	Dürrenbach		525	CR	5.9	1.083	112600	8200
4661	152	27.3.51	Bruchmühle		183	Ps	6	1.021	39400	800
4663	172	9.4.51	Ingelmatt		256	Pi	7	1.02	30400	900
4664	157	30.4.51	Kutzh.S		484	ZD	8.1	1.043	63800	4500
4670	168	3.12.50	Pechelbronn		210	Pm	6.7	1.037	52500	440
4670	168	9.7.51	Pechelbronn		805	K	5.3	1.98	138200	8700
4675	177	13.6.51	Kreuzecke		251	Pi	11	1.012	21500	800
4681	149	30.5.51	Kutzh.		504	ZD	8.5	1.049	63200	4400
4682	163	21.4.51	Bruderhaus		294	Pm		1.017	26800	
4682		26.4.51	Schweighausen		370	Pm	6.5	1.018	27100	400
4710	159	24.7.51	Kutzh.s		351	ZD	8	1.031	48100	1700
4710	159	17.7.51	Kutzh.s		460	ZD	8.2	1.046	63100	5400

Appendix 8 SAEM Hydrochemistry Data

Wellnr.	Ca mel	Na mgl	Na mel	K mgl	K mel	Mg mgl	Mg mel	Fe2 mgl	Fe2 mel	HCO3 mgl
4642	249.50					120	9.86	100	3.58	610
4651	179.64					1500	123.30		0.00	100
4653	364.27					70	5.75	190	6.80	420
4655	9.98					200	16.44		0.00	610
4655	309.38					1500	123.30		0.00	120
4655	359.28					350	28.77		0.00	120
4656	339.32					120	9.86		0.00	90
4657	409.18					8200	674.04		0.00	150
4661	39.92					120	9.86		0.00	200
4663	44.91					70	5.75		0.00	30
4664	224.55					120	9.86		0.00	80
4670	21.96					350	28.77	50	1.79	
4670	434.13					200	16.44	80	2.86	60
4675	39.92					750	61.65		0.00	60
4681	219.56					750	61.65		0.00	20
4682	0.00						0.00		0.00	
4682	19.96					750	61.65		0.00	110
4710	84.83					350	28.77		0.00	204
4710	269.46					350	28.77		0.00	40

Appendix 8 SAEM Hydrochemistry Data

Wellnr.	HCO3 mel	Cl mgl	Cl mel	SO4 mgl	SO4 mel	Total Cation	Total Anion	Na+K mel	Comment	Reference
4642	10.00	57500	1621.50	110	2.29	262.94	1633.79	1370.85	fault	SGAL
4651	1.64	87000	2453.40	0	0.00					SGAL
4653	6.89	57800	1629.96	90	1.87	376.83	1638.72	1261.89	fault	SGAL
4655	10.00	350	9.87	380	7.90	26.42	27.78	1.36		SGAL
4655	1.97	71000	2002.20	280	5.82	432.68	2009.99	1577.31	fault at 590	SGAL
4655	1.97	65300	1841.46	190	3.95	388.05	1847.38	1459.33		SGAL
4656	1.48	78900	2224.98	260	5.41	349.18	2231.86	1882.68		SGAL
4657	2.46	67500	1903.50	210	4.37	1083.22	1910.33	827.11		SGAL
4661	3.28	17800	501.96	260	5.41	49.78	510.65	460.86		SGAL
4663	0.49	19200	541.44	300	6.24	50.66	548.17	497.51		SGAL
4664	1.31	33700	950.34	490	10.19	234.41	961.84	727.43		SGAL
4670	0.00	27690	780.86	70	1.46	52.52	782.31			SGAL
4670	0.98	88800	2504.16	170	3.54	453.43	2508.68	2055.25	70C, GR?	SGAL
4675	0.98	8870	250.13	1050	21.84	101.57	272.96	171.39	productive	SGAL
4681	0.33	3900	109.98	210	4.37	281.21	114.68	-166.53	anhydrite	SGAL
4682	0.00	14200	400.44	760	15.81	0.00	416.25			SGAL
4682	1.80	15900	448.38	2110	43.89	81.61	494.07	412.46		SGAL
4710	3.35	29100	820.62	90	1.87	113.60	825.84	712.24		SGAL
4710	0.66	37300	1051.86	190	3.95	298.23	1056.47	758.24		SGAL

Appendix 8 SAEM Hydrochemistry Data

Wellnr.	KB	Date	Location	mean.depth	Formation	pH	Density	TDS mgl	Ca mgl	Ca mel	NaCl mgl	Na mgl
Don 15			Soufflenheim	506								73000
Don 16	119	2.9.55	Soufflenheim	491			1.100					74000
Don 8	119		Soufflenheim	519								77000
Hag 2	156	17.2.56	Haguenau	1414	Pm							97000
Kalt 1	142	62	Haguenau									12000
Kalt 1	142	7.2.62	Haguenau	683			1.160					80000
Kalt 1	142	7.2.62	Haguenau	655								101000
Kil 1	130	6.3.59	Kilstett	1267								49000
Obermod 1	178	17.8.55	Obermodern	122-143	K		1.002					
Obermod 1	178	17.8.55	Obermodern	335	LK		1.010	23400				9200
Obermod 1	178	3.9.55	Obermodern	541	Bsdst		1.005					790
Obermod 1	178	19.9.55	Obermodern	883	Permian		1.008	5850				2300
Schaff 3	126	14.1.59	Kesseldorf	942			1.120					37000
Scheib 1	134	8.1.56	Scheibenhardt	979	Pm		1.107					63000
Scheib 101	148		Niederlauterb	822								60000
Scheib 102	140	10.12.58	Niederlauterb	2085	MK		1.120					17000
Scheib 2	145	22.5.56	Niederlauterb	605								46000
Scheib 2	145		Niederlauterb	958			1.123					87000
Scheib 2	145		Niederlauterb	998	PS		1.122					83000
Schirr 1		21.9.55	Schirrheim	459			1.080					47000
Schirr 10	138		Schirrheim	737	PS		1.160					76000
Soufflll			Soufflenheim	1110	J							53700
Schweig 2	279	20.3.75	Niederlauterb			7.9		9800	470	23.45		2900
WINTZ 1	172	28.5.57	Wintzenbach	370			1.040					26000

Appendix 9 PREPA Hydrochemistry Data

Wellnr.	Na mel	K mgl	K mel	Mg mgl	Mg mel	Fe2 mgl	Fe2 mel	CO3 mgl	CO3 mel	HCO3 mgl	HCO3 mel	Cl mgl	Cl mel
Don 15	3175.50											112000	3158.40
Don 16	3219.00											114000	3214.80
Don 8	3349.50											120000	3384.00
Hag 2	4219.50											149000	4201.80
Kalt 1	522.00											18000	507.60
Kalt 1	3480.00											124000	3496.80
Kalt 1	4393.50											156000	4399.20
Kil 1	2131.50											76000	2143.20
Obermod 1													
Obermod 1	400.20											14000	394.80
Obermod 1	34.37											1200	33.84
Obermod 1	100.05											3500	98.70
Schaff 3	1609.50											57000	1607.40
Scheib 1	2740.50											97000	2735.40
Scheib 101	2610.00											92000	2594.40
Scheib 102	739.50											27000	761.40
Scheib 2	2001.00											71000	2002.20
Scheib 2	3784.50											135000	3807.00
Scheib 2	3610.50											127000	3581.40
Schirr 1	2044.50											72000	2030.40
Schirr 10	3306.00											120000	3384.00
SoufflI												108810	
Schweig 2	126.15	140.00	3.58	76.00	6.25	43.00	1.54					4500	126.90
WINTZ 1	1131.00											41000	1156.20

Appendix 9 PREPA Hydrochemistry Data

Wellnr.	SO4 mgl	SO4 mel	Total Cation	Total Anion	Comment
Don 15					
Don 16					
Don 8					
Hag 2					
Kalt 1					
Kalt 1					
Kalt 1					
Kil 1					
Obermod 1					artesian
Obermod 1					
Obermod 1					
Obermod 1					
Schaff 3					
Scheib 1					
Scheib 101					
Scheib 102					
Scheib 2					
Scheib 2					
Scheib 2					
Schirr 1					
Schirr 10					
Souffll	646.00				
Schweig 2	1200.00	24.96	160.97	151.86	CO2:170
WINTZ 1					

Wellnr.	BGR.Nr	KB	Date	Location	Source	mean.d	Formation	pH	density	TDS mgl	Ca mgl	Ca mel
3262	6012	148	00.5.85	K	well	435	ZD	7.10	cal.	21336.4	410.00	20.46
4275	6052	175	21.6.81	Merkwiller	well	120	Ps	7.10		962	54.00	2.69
AEP Lobsann	6005	292	14.8.81	Marienbronn	well	46.2	Bsdst	5.90			9.00	0.45
Aerodrome	3038	149	12.58.72	Haguenau	well	61	Plio	5.90		80	9.00	0.45
Aluxan	3047	145	19.2.87	Betschdorf	well	32	Plio	7.00	cal.	588.17	113.00	5.64
Bein 1	3037	115	9.10.86	Beinheim	well	11	Plio	6.90		410	120.00	5.99
Beinheim	6037		9.10.86	Beinheim	well	31	Plio	6.90		410	120.00	5.99
Betschdorf	6047		19.2.87	Betschdorf	well	25	Plio	7.00	cal.	587.4	113.00	5.64
Bischwill	3041	125	17.10.67	Bischwiller	well	40	Plio	7.30		300	88.00	4.39
Bischwiller	6041		3.7.72	Bischwiller	well	30	Plio	7.30		300		0.00
Bitche	6021	285	1.7.65	Bitche	well	47	Bsdst	5.70		36.5	6.20	0.31
Celtic	6016	204	20.4.65	Niederbronn	spring	7	Bsdst	6.60		38	5.00	0.25
Celtic	6016	204	00.8.86	Niederbronn	spring	7	Bsdst	6.50	cal.	43.05	6.00	0.30
Celtic	6016	204	28.10.86	Niederbronn	spring	7	Bsdst	6.60		52	6.00	0.30
Drachen E	6001	326	11.8.67	Drachenbronn	well	140	Bsdst	6.80		81	14.00	0.70
Drachen E	6001	326	11.8.67	Drachenbronn	well	140	Bsdst			79	2.80	0.14
Four a Chaux	6026	229	10.11.34	Lembach	well	72	MK			850		
Four a Chaux	6026	229	21.11.34	Lembach	well	72	MK			370		
Four a Chaux	6026	229	18.1.35	Lembach	well	142	MK			610		
Four a Chaux	6026	229	2.3.35	Lembach	well	188	Bsdst			240		
Four a Chaux	6026	229	4.4.35	Lembach	well	236	Bsdst			160		
Four a Chaux	6026	229	16.2.87	Lembach	well	220	Bsdst	7.20		240	35.00	1.75
Fried/3969	6051		2.6.87	Kutzenhausen	well	490	P inf.			8676	100.00	4.99
Fried/3969	6051		27.8.87	Kutzenhausen	well	490	P inf.	7.90		8688	96.00	4.79
Gambs F2		129	13.4.78	Gambsheim	well	50	Plio	7.40		428	89.60	4.47
GPK-1	6055		00.12.87	Soultz	well	1817	Base	6.40		80000	6185.00	308.63
H 1	6003	295	10.6.69	Hochwald	well	167	Bsdst	6.85		100	5.80	0.29
H 1	6003	295	10.6.69	Hochwald	well	167	Bsdst	6.65		51	7.00	0.35
H II	6004	304	6.5.76	Hochwald	well	190	Bsdst	7.00		52	11.00	0.55
H II	6004	304	0.5.85	Hochwald	well	190	Bsdst	6.90	cal.	64.14	11.00	0.55
Haguenau	6038		4.5.72	Haguenau	well	31	Plio	5.90		80	9.00	0.45
Hardt 1	6025	153	14.12.61	Wissembourg	well	41	T	6.90		280	80.00	3.99
Helions II	6049/1	161	29.3.78	Pechelbronn	well	1146	MK	5.10		15579	1200.00	59.88
Helions II	6049/2	161	5.2.83	Pechelbronn	well	1146	MK	6.60		20000	1460.00	72.85
Helions II	6049/3	161	31.3.83	Pechelbronn	well	1146	MK			19900	1520.00	75.85

Appendix 10 BGR Hydrochemistry Data

Wellnr.	Na mgl	Na mel	K mgl	K mel	Mg mgl	Mg mel	Fe2 mgl	Fe2 mel	HCO3 mgl	HCO3 mel	Cl mgl	Cl mel
3262	7260.00	315.81	36.00	0.92	270.00	22.19	7.40	0.26	250.00	4.10	13100.0	369.42
4275	153.00	6.66	3.00	0.08	34.00	2.79		0.00	620.00	10.17	81.0	2.28
AEP Lobsann		0.00		0.00		0.00	0.02	0.00	18.00	0.30	7.0	0.20
Aerodrome	6.00	0.26	2.00	0.05	3.00	0.25	0.90	0.03	12.00	0.20	8.0	0.23
Aluxan	9.00	0.39	0.40	0.01	18.00	1.48	0.77	0.03	428.00	7.02	14.0	0.39
Bein 1	8.00	0.35	2.00	0.05	12.00	0.99	0.50	0.02	330.00	5.41	17.0	0.48
Beinheim	8.00	0.35	2.00	0.05	12.00	0.99		0.00	330.00	5.41	17.0	0.48
Betschdorf	9.00	0.39	0.40	0.01	18.00	1.48		0.00	428.00	7.02	14.0	0.39
Bischwill	6.50	0.28	2.00	0.05	9.10	0.75	0.08	0.00	305.00	5.00	9.4	0.27
Bischwiller		0.00		0.00		0.00		0.00		0.00		0.00
Bitche	4.50	0.20	2.50	0.06	0.80	0.07	0.05	0.00	15.50	0.25	8.5	0.24
Celtic	2.00	0.09	2.10	0.05	2.00	0.16	0.08	0.00	20.00	0.33	5.0	0.14
Celtic	2.00	0.09	2.00	0.05	2.00	0.16	0.05	0.00	20.00	0.33	4.0	0.11
Celtic	3.00	0.13	2.00	0.05	3.00	0.25	0.02	0.00	23.00	0.38	4.0	0.11
Drachen E	3.00	0.13	3.00	0.08	6.00	0.49	0.46	0.02	64.00	1.05	2.0	0.06
Drachen E	1.00	0.04	3.00	0.08	2.00	0.16	0.15	0.01	31.00	0.51	2.0	0.06
Four a Chaux		0.00		0.00		0.00		0.00		0.00		0.00
Four a Chaux		0.00		0.00		0.00		0.00		0.00		0.00
Four a Chaux		0.00		0.00		0.00		0.00		0.00		0.00
Four a Chaux		0.00		0.00		0.00		0.00		0.00	3.0	0.08
Four a Chaux		0.00		0.00		0.00		0.00		0.00	4.0	0.11
Four a Chaux	2.00	0.09	2.00	0.05	11.00	0.90	0.02	0.00	165.00	2.71	2.0	0.06
Fried/3969	3100.00	134.85	18.00	0.46	54.00	4.44		0.00	410.00	6.72	4990.0	140.72
Fried/3969	3130.00	136.16	19.00	0.49	50.00	4.11		0.00	360.00	5.90	5030.0	141.85
Gambs F2	30.00	1.31	2.80	0.07	12.00	0.99	0.03	0.00	238.00	3.90	76.8	2.17
GPK-1	22175.00	964.61	2435.00	62.34	130.00	10.69		0.00	500.00	8.20	48440.0	1366.01
H I	2.50	0.11	3.50	0.09	6.20	0.51	0.45	0.02	45.80	0.75	3.0	0.08
H I	1.00	0.04	3.00	0.08	2.00	0.16	0.29	0.01	30.50	0.50	2.0	0.06
H II	2.00	0.09	1.50	0.04	4.00	0.33	0.18	0.01	52.00	0.85	2.0	0.06
H II	1.00	0.04	2.00	0.05	2.00	0.16	0.14	0.01	44.00	0.72	1.0	0.03
Haguenau	6.00	0.26	2.00	0.05	3.00	0.25		0.00	12.00	0.20	8.0	0.23
Hardt 1	3.00	0.13	2.00	0.05	10.00	0.82	0.03	0.00	270.00	4.43	6.0	0.17
Helions II	4120.00	179.22	480.00	12.29	89.00	7.32		0.00	290.00	4.76	8840.0	249.29
Helions II	5400.00	234.90	820.00	20.99	1600.00	131.52	5.60	0.20	310.00	5.08	10600.0	298.92
Helions II	5180.00	225.33	780.00	19.97	130.00	10.69	4.70	0.17	310.00	5.08	10600.0	298.92

Appendix 10 BGR Hydrochemistry Data

Wellnr.	SO4 mgl	SO4 mel	Total Cation	Total Anion	O2	SiO2	dH	fH	µS/cm	Comment
3262	3.00	0.06	359.65	373.58		6.40	119.70		31200	oil well
4275	1.00	0.02	12.22	12.47					1160	
AEP Lobsann	7.00	0.15	0.45	0.64					60	
Aerodrome	25.00	0.52	1.04	0.94	1.00	12.70	0.70		100	
Aluxan	5.00	0.10	7.55	7.52	1.80	18.00	7.10		641	
Bein 1	50.00	1.04	7.39	6.93	4.80	9.00	6.70		560	
Beinheim	50.00	1.04	7.37	6.93					560	
Betschdorf	5.00	0.10	7.52	7.52					641	
Bischwill	19.00	0.40	5.48	5.66	0.64	14.00		26	418	PT
Bischwiller		0.00	0.00	0.00					420	
Bitche	0.80	0.02	0.64	0.51	9.40	5.20		2	53	
Celtic	4.00	0.08	0.56	0.55		9.40			50	
Celtic	7.00	0.15	0.60	0.59			2?		70	
Celtic	7.00	0.15	0.73	0.64	10.00	7.00			75	
Drachen E	14.00	0.29	1.42	1.40	2.40	12.00		6	120	
Drachen E	1.00	0.02	0.43	0.59	2.80			6	110	
Four a Chaux	370.00	7.70	0.00	7.70						
Four a Chaux	82.00	1.71	0.00	1.71						
Four a Chaux	200.00	4.16	0.00	4.16						
Four a Chaux	18.00	0.37	0.00	0.46						
Four a Chaux	7.00	0.15	0.00	0.26						
Four a Chaux	4.00	0.08	2.79	2.85	7.20	11.00	2.60		270	
Fried/3969	4.00	0.08	144.74	147.53					13600	leaking well/gas
Fried/3969	2.00	0.04	145.54	147.79					14200	
Gambs F2	36.00	0.75	6.84	6.82	1.16	10.50		27	580	PT
GPK-1	171.00	3.56	1346.27	1377.76						thermal well
H 1	8.00	0.17	1.01	1.00	8.80	25.00		4	95	
H 1	1.20	0.02	0.64	0.58	9.40	17.00		3	60	
H II	4.00	0.08	1.01	0.99	9.50	11.50		4	80	PT
H II	3.00	0.06	0.81	0.81		5.10	2.00		75	
Haguenau	25.00	0.52	1.01	0.94					100	
Hardt 1	10.00	0.21	5.00	4.81	4.70	10.00	4.80		390	
Helions II	560.00	11.65	258.70	265.69					10000	71C, 13.5 m3/h
Helions II	840.00	17.47	460.47	321.48		38.50	86.00		25900	72C, 23 m3/h
Helions II	720.00	14.98	332.00	318.98		39.50	87.00		24600	10.8 m3/h

Appendix 10 BGR Hydrochemistry Data

Wellnr.	BGR.Nr	Reference
3262	6012	BGR
4275	6052	SGAL/BGR
AEP Lobsann	6005	SGAL/BGR
Aerodrome	3038	SGAL/BGR
Aluxan	3047	BGR
Bein 1	3037	SGAL/BGR
Beinheim	6037	SGAL/BGR
Betschdorf	6047	SGAL/BGR
Bischwill	3041	SGAL/BGR
Bischwiller	6041	SGAL/BGR
Bitche	6021	SGAL/BGR
Celtic	6016	Fabre
Celtic	6016	SGAL/BGR
Celtic	6016	SGAL/BGR
Drachen E	6001	SGAL/BGR
Drachen E	6001	SGAL/BGR
Four a Chaux	6026	SGAL/BGR
Four a Chaux	6026	SGAL/BGR
Four a Chaux	6026	SGAL/BGR
Four a Chaux	6026	SGAL/BGR
Four a Chaux	6026	SGAL/BGR
Four a Chaux	6026	BGR
Fried/3969	6051	SGAL/BGR
Fried/3969	6051	SGAL/BGR
Gambs F2		SGAL/BGR
GPK-1	6055	BGRM/BGR
H 1	6003	SGAL/BGR
H 1	6003	SGAL/BGR
H II	6004	SGAL/BGR
H II	6004	BGR
Haguenau	6038	SGAL/BGR
Hardt 1	6025	SGAL/BGR
Helions II	6049	SGAL
Helions II	6049	SGAL/BGR
Helions II	6049	SGAL/BGR

Appendix 10 BGR Hydrochemistry Data

Wellnr.	BGR.Nr	KB	Date	Location	Source	mean.d	Formation	pH	density	TDS mgl	Ca mgl	Ca mel
Helions II	6049/4	161	23.8.83	Pechelbronn	well	1146	MK	6.40		20500	1460.00	72.85
Helions II	6049/5	161	5.12.83	Pechelbronn	well	1146	MK	6.30		20000	1500.00	74.85
Helions II	6049/6	161	26.3.84	Pechelbronn	well	1146	MK	6.20		20700	1490.00	74.35
Helions II	6049/7	161	20.8.84	Pechelbronn	well	1146	MK	6.10		20500	1500.00	74.85
Helions II	6049/8	161	3.12.84	Pechelbronn	well	1146	MK	6.20		20800	1530.00	76.35
Helions II	6049/9	161	11.3.85	Pechelbronn	well	1146	MK	6.20		21000	1500.00	74.85
Helions II	6049/10	161	00.5.85	Pechelbronn	well	1146	MK	6.20	cal.	18514.1	1420.00	70.86
Helions II	6049/11	161	14.3.86	Pechelbronn	well	1146	MK	6.20		21660	1600.00	79.80
Helions II	6049/12	161	27.8.86	Pechelbronn	well	1146	MK	5.80		21200	1610.00	80.30
Helions II	6049/13	161	9.12.86	Pechelbronn	well	1146	MK	6.10		21800	1660.00	82.80
Helions II	6049/14	161	18.2.87	Pechelbronn	well	1146	MK	5.90	cal.	19922.5	1610.00	80.34
Helions II	6049/15	161	23.3.87	Pechelbronn	well	1146	MK	6.00		21800	1660.00	82.80
Helions II	6049/16	161	28.8.87	Pechelbronn	well	1146	MK	5.80		20720	1640.00	81.80
Herrlis F2		126	8.1.81	Offendorf	well	46	Plio	7.50		505	120.00	5.99
Hochwald	6034		1.10.81	Hochwald	well	1	Bsdst	5.30				0.00
Kutz		128	31.10.79	Kutzenhausen	well	33	Plio	7.00		460	118.00	5.89
Lauter F1		153	23.6.82	Mothern	well	11.7	Q	7.00		500	118.00	5.89
Lauter F2		153	23.6.82	Mothern	well	11.4	Q	7.10		454	126.40	6.31
Lembach 'E	6029		12.10.76	Lembach	well	1	Bsdst	5.80				
Lembach 'E	6030		12.10.76	Lembach	well	1	Bsdst	6.00				0.00
Lembach 'N	6027		12.10.76	Lembach	well	1	Bsdst	6.00				
Lembach 'N	6028		12.10.76	Lembach	well	1	Bsdst	6.00				0.00
Lembach 'NW	6031		12.10.76	Lembach	well	1	Bsdst	6.00				0.00
Lembach 'NW	6032		12.10.76	Lembach	well	1	Bsdst	5.90				0.00
Lichteneck			7.8.86	Niederbronn	spring		Bsdst	6.50			6.30	0.31
Liebfrauent	6011	175	5.7.86	Woerth	well	130	Bsdst	7.90		200	21.00	1.05
Mar 101	6006	267	6.4.82	Marienbronn	well	46		8.90		760	22.00	1.10
Mar 101	6006	267	00.8.86	Marienbronn	well	906		7.70	cal.	2911.25	77.00	3.84
Mariental	3039	143	15.3.72	Haguenau	well	68	Plio	6.40		36	4.00	0.20
Mattenmühle	6054		2.6.87	Soultz	well	10	SG	7.00		2199	108.00	5.39
Mitschd	6000	221	30.3.73	Mitschdorf	well	200	Bsdst	6.30		50	8.00	0.40
Mitschd	6000	221	00.5.85	Mitschdorf	well	200	Bsdst	6.40		42.4	7.10	0.35
Mitschd	6000	221	16.2.87	Mitschdorf	well	200	Bsdst	7.00		31.96	5.00	0.25
Mors 3a	6017	187	3.12.84	Morsbronn	well	400	MK	6.70		6600	460.00	22.95
Mors 3a	6017	187	00.5.85	Morsbronn	well	400	MK	6.70	cal.	5873.3	450.00	22.46

Appendix 10 BGR Hydrochemistry Data

Wellnr.	Na mgl	Na mel	K mgl	K mel	Mg mgl	Mg mel	Fe2 mgl	Fe2 mel	HCO3 mgl	HCO3 mel	Cl mgl	Cl mel
Helions II	5140.00	223.59	770.00	19.71	140.00	11.51	5.40	0.19	320.00	5.25	10400.0	293.28
Helions II	5300.00	230.55	760.00	19.46	130.00	10.69	5.40	0.19	310.00	5.08	10300.0	290.46
Helions II	5360.00	233.16	800.00	20.48	140.00	11.51	7.20	0.26	320.00	5.25	10700.0	301.74
Helions II	5600.00	243.60	850.00	21.76	130.00	10.69	4.70	0.17	300.00	4.92	10900.0	307.38
Helions II	5280.00	229.68	760.00	19.46	170.00	13.97	5.20	0.19	310.00	5.08	10900.0	307.38
Helions II	5300.00	230.55	600.00	15.36	180.00	14.80	4.95	0.18	300.00	4.92	10800.0	304.56
Helions II	4840.00	210.54	500.00	12.80	120.00	9.86	4.10	0.15	310.00	5.08	10700.0	301.74
Helions II	5400.00	234.90	600.00	15.30	140.00	11.40			315.00	5.20	11300.0	318.80
Helions II	5800.00	252.30	580.00	14.80	150.00	12.30			300.00	4.90	11600.0	327.20
Helions II	5600.00	243.60	600.00	15.30	120.00	9.90			310.00	5.10	11800.0	332.90
Helions II	5260.00	228.81	565.00	14.46	123.00	10.11	4.50	0.16	303.00	4.97	11600.0	327.12
Helions II	5680.00	247.10	640.00	16.40	125.00	10.30			315.00	5.20	12000.0	338.50
Helions II	5660.00	246.20	580.00	14.80	125.00	10.30			300.00	4.90	11800.0	332.90
Herrlis F2	15.50	0.67	2.80	0.07	16.30	1.34	0.13	0.00	314.80	5.16	42.0	1.18
Hochwald		0.00		0.00		0.00		0.00		0.00	7.0	0.20
Kutz	9.50	0.41	3.00	0.08	21.60	1.78	0.93	0.03	405.00	6.64	15.2	0.43
Lauter F1	31.50	1.37	12.20	0.31	12.20	1.00	0.03	0.00	376.00	6.17	50.6	1.43
Lauter F2	19.50	0.85	18.60	0.48	14.20	1.17	0.08	0.00	405.00	6.64	31.2	0.88
Lembach 'E									7.00	0.11	6.0	0.17
Lembach 'E		0.00		0.00		0.00		0.00	15.00	0.25	6.0	0.17
Lembach 'N									15.00	0.20	3.0	0.10
Lembach 'N		0.00		0.00		0.00		0.00	16.00	0.26	4.0	0.11
Lembach 'NW		0.00		0.00		0.00		0.00	10.00	0.16	5.0	0.14
Lembach 'NW		0.00		0.00		0.00		0.00	10.00	0.16	5.0	0.14
Lichteneck	1.80	0.08	2.30	0.06	2.10	0.17	0.05	0.00	20.00	0.33	3.9	0.11
Liebfrauent	13.00	0.57	4.00	0.10	8.00	0.66	3.10	0.11	90.00	1.48	9.0	0.25
Mar 101	220.00	9.57	18.00	0.46	10.00	0.82	1.30	0.05	280.00	4.59	71.0	2.00
Mar 101	890.00	38.72	36.00	0.92	33.00	2.71	0.25	0.01	580.00	9.51	1250.0	35.25
Mariental	3.00	0.13	1.00	0.03	1.00	0.08	0.80	0.03	18.00	0.30	2.0	0.06
Mattenmühle	582.00	25.32	5.00	0.13	40.00	3.29		0.00	490.00	8.04	880.0	24.82
Mitschd	5.00	0.22	1.50	0.04	1.00	0.08	0.03	0.00	28.00	0.46	2.0	0.06
Mitschd	1.40	0.06	1.90	0.05	1.00	0.08		0.00	27.00	0.44	1.0	0.03
Mitschd	1.00	0.04	2.00	0.05	0.70	0.06	0.76	0.03	19.00	0.31	2.0	0.06
Mors 3a	1630.00	70.91	360.00	9.22	46.00	3.78	2.40	0.09	320.00	5.25	2960.0	83.47
Mors 3a	1480.00	64.38	170.00	4.35	31.00	2.55	2.30	0.08	310.00	5.08	2860.0	80.65

Appendix 10 BGR Hydrochemistry Data

Wellnr.	SO4 mgl	SO4 mel	Total Cation	Total Anion	O2	SiO2	dH	fH	µS/cm	Comment
Helions II	690.00	14.35	327.86	312.88	0.30	38.50	84.00		25600	69.4C, 10.3 m3/h
Helions II	660.00	13.73	335.74	309.27	1.10	40.00			25800	69.4C, 11.2 m3/h
Helions II	680.00	14.14	339.76	321.13	0.80	41.00			24700	70.2C, 11.9 m3/h
Helions II	660.00	13.73	351.06	326.03	1.80	38.00	86.00		25500	70.3C, 11.6 m3/h
Helions II	680.00	14.14	339.64	326.61	0.20	40.00	91.00		36500	69C, 10.6
Helions II	670.00	13.94	335.73	323.42	0.50	40.00	90.00		25600	69.2C, 10.2 m3/h
Helions II	620.00	12.90	304.21	319.72		21.20	80.00		26300	thermal
Helions II	640.00	13.30	341.40	337.30	2.00	40.00			26800	71.6C
Helions II	660.00	13.70	359.70	345.80	0.80	40.00			26200	72.1C
Helions II	670.00	13.90	351.60	351.90	1.00	37.00			26300	72
Helions II	457.00	9.51	333.88	341.59	0.30	40.00	90.50		30200	72.4
Helions II	610.00	12.70	356.60	356.40	1.10	34.00			27600	72C
Helions II	615.00	12.80	353.10	350.60	0.20	38.00			33000	72
Herrlis F2	68.00	1.41	8.08	7.76	2.50	10.00		37	620	PT
Hochwald	14.00	0.29	0.00	0.49					70	
Kutz	50.00	1.04	8.19	8.11	6.60	12.50		38	610	PT
Lauter F1	36.00	0.75	8.57	8.34	4.60	8.70		35	688	PT
Lauter F2	38.50	0.80	8.80	8.32	2.30	9.50		38	684	PT
Lembach 'E	16.00	0.33	0.00	0.62					64	
Lembach 'E	5.00	0.10	0.00	0.52					66	
Lembach 'N	1.00								36	
Lembach 'N	2.00	0.04	0.00	0.42					40	
Lembach 'NW	4.00	0.08	0.00	0.39					53	
Lembach 'NW	4.00	0.08	0.00	0.39					53	
Lichteneck	7.00	0.15	0.63	0.58			1.40		70	
Liebfrauent	26.00	0.54	2.48	2.27	8.90	12.50	1.70		160	
Mar 101	190.00	3.95	12.00	10.55		16.00		10	980	TOTAL,trace
Mar 101	45.00	0.94	46.20	45.70			18.40		4050	polluted by inj
Mariental	5.00	0.10	0.47	0.46	1.80	11.50	0.30	2	42	PT
Mattenmühle	94.00	1.96	34.12	34.81					3600	dug well
Mitschd	0.00	0.00	0.74	0.52	10.00	14.00	1.25	2	65	PT
Mitschd	3.00	0.06	0.55	0.53		6.00	1.20		60	
Mitschd	1.50	0.03	0.43	0.40	10.30	13.00	1.20		50	
Mors 3a	610.00	12.69	106.94	101.41	0.40	19.50	27.00		8700	thermal
Mors 3a	570.00	11.86	93.82	97.59	0.40	12.60	24.90		9000	thermal

Appendix 10 BGR Hydrochemistry Data

Wellnr.	BGR.Nr	Reference
Helions II	6049	SGAL/BGR
Helions II	6049	SGAL/BGR
Helions II	6049	SGAL/BGR
Helions II	6049	SGAL/BGR
Helions II	6049	SGAL/BGR
Helions II	6049	SGAL/BGR
Helions II	6049	BGR
Helions II	6049/11	BGR
Helions II	6049/12	BGR
Helions II	6049/13	BGR
Helions II	6049	BGR
Helions II	6049	BGR
Helions II	6049/16	BGR
Herrlis F2		SGAL/BGR
Hochwald	6034	SGAL/BGR
Kutz		SGAL/BGR
Lauter F1		SGAL/BGR
Lauter F2		SGAL/BGR
Lembach 'E	6029	SGAL/BGR
Lembach 'E	6030	SGAL/BGR
Lembach 'N	6027	SGAL/BGR
Lembach 'N	6028	SGAL/BGR
Lembach 'NW	6031	SGAL/BGR
Lembach 'NW	6032	SGAL/BGR
Lichteneck		BGR
Liebfrauent	6011	BGR
Mar 101	6006	SGAL/BGR
Mar 101	6006	BGR
Mariental	3039	SGAL/BGR
Mattenmühle	6054	BGR
Mitschd	6000	SGAL/BGR
Mitschd	6000	BGR
Mitschd	6000	BGR
Mors 3a	6017	SGAL/BGR
Mors 3a	6017	SGAL/BGR

Appendix 10 BGR Hydrochemistry Data

Wellnr.	BGR.Nr	KB	Date	Location	Source	mean.d	Formation	pH	density	TDS mgl	Ca mgl	Ca mel
Mors 3a	6017	187	12.2.87	Morsbronn	well	400	MK	6.10	cal.	5626.3	450.00	22.46
Mors 3b	6018	185	28.3.78	Morsbronn	well	680	Bsdst			4626	310.00	15.47
Mors 3b	6018	185	3.12.84	Morsbronn	well	680	Bsdst	7.30		5300	320.00	15.97
Mors 3b	6018	185	00.5.85	Morsbronn	well	680	Bsdst	7.30		4727	310.00	15.47
Mors 3b	6018	185	00.0.87	Morsbronn	well	680	Bsdst	6.43	cal.	4647.8	298.00	14.87
Moth F1	6024	111	23.6.82	Mothern	well	12	Q	7.10		450	130.00	6.49
Oberhoffen	3040	143	15.3.72	Haguenau	well	68	Plio	6.40		40	6.00	0.30
Pet.Pierre		245	5.7.76	Petite Pierre	well	162	Bsdst	7.00		134	20.80	1.04
Pfaffenb	6030	325	12.10.76	Lembach	spring		Bsdst					
Pfaffens	6029	367	12.10.76	Lembach	spring		Bsdst	5.80				
Phillipsb	6019	218	14.8.85	Phillipsbourg	well	70	Bsdst	8.20	cal.	132.05	15.00	0.75
Phillipsb	6019	218	27.8.65	Phillipsbourg	well	70	Bsdst	7.90	cal.	131.85	14.60	0.73
RG1	6053		22.5.87	Kutzenhausen	well	10	Ps	7.10		3542	75.00	3.74
Riesthal	6020	285	14.8.86	Phillipsbourg	spring		Bsdst	5.70	cal.	58.08	7.00	0.35
Roe	3046	119	25.11.77	Roeschwoog	well	15	Plio		cal.	757.54	120.00	5.99
Roe S1	6036	119	11.8.86	Roeschwoog	well	28	Plio	7.00		600	120.00	5.99
Roeschw	6036		11.8.86	Roeschwoog	well	15	Plio	7.00		600	120.00	5.99
Roeschw	6046		25.11.77	Roeschwoog	well	8	Plio			757.4	120.00	5.99
Romaine	6015	210		Niederbronn	well	11	Bsdst		cal.	5362.03	340.00	16.97
Romaine	6015	210	4.4.78	Niederbronn	well	11	Bsdst	6.80		5250	360.00	17.96
Romaine	6015	210	24.2.77	Niederbronn	well	11	Bsdst	6.72		5090	371.20	18.52
Romaine	6015	210	00.5.85	Niederbronn	well	11	Bsdst	6.80	cal.	4835.8	348.00	17.37
Romaine	6015	210	28.10.86	Niederbronn	well	11	Bsdst	6.60		5170	370.00	18.46
Romaine	6015	210	18.2.87	Niederbronn	well	11	Bsdst	6.60	cal.	4918.5	349.00	17.42
Rothb III	3042	201	8.6.78	Rothbach	well	180	Bsdst	7.10		128	20.80	1.04
Rothb IV	3043	201	1.3.79	Rothbach	well	172	Bsdst	6.70		104	12.80	0.64
Rothbach	6042		13.5.70	Rothbach	well	68	Bsdst	6.30		77	14.00	0.70
Rothbach	6043		14.9.71	Rothbach	well	35	Quat	6.90		64	12.00	0.60
Saline	6050			Soultz			Ps	5.90	cal.	4890.1	40.00	2.00
Schreiner	3048	163	19.2.87	Soultz	well	10	Q	7.10	cal.	708.62	162.00	8.08
Schweigh	3045	155	12.3.70	Schweighouse	well	23	Plio	5.30		64	9.00	0.45
Schweighaus.	6045		12.3.70	Schweighausen	well	12	Plio	5.30		64	9.00	0.45
Seltz 43		113	30.4.80	Seltz	well	13	Q	7.40		412	93.60	4.67
Seltz 44		113	14.4.81	Seltz	well	11.5	Q	7.40		346	88.80	4.43
Sept Font.	6007	268	00.5.86	Hochwald	spring	906	Bsdst	7.60	cal.	111.1	22.00	1.10
Soufl FII	6023	135	15.9.78	Soufflenheim	well	64	T	6.40		72	8.40	0.42

Appendix 10 BGR Hydrochemistry Data

Wellnr.	Na mgl	Na mel	K mgl	K mel	Mg mgl	Mg mel	Fe2 mgl	Fe2 mel	HCO3 mgl	HCO3 mel	Cl mgl	Cl mel
Mors 3a	1490.00	64.82	164.00	4.20	33.00	2.71	2.30	0.08	303.00	4.97	2750.0	77.55
Mors 3b	1260.00	54.81	150.00	3.84	26.00	2.14		0.00	290.00	4.76	2240.0	63.17
Mors 3b	1380.00	60.03	260.00	6.66	34.00	2.79	2.24	0.08	300.00	4.92	2430.0	68.53
Mors 3b	1280.00	55.68	150.00	3.84	25.00	2.06	2.00	0.07	300.00	4.92	2300.0	64.86
Mors 3b	1310.00	56.99	142.00	3.64	25.00	2.06	1.80	0.06	305.00	5.00	2300.0	64.86
Moth F1	20.00	0.87	19.00	0.49	14.00	1.15	0.08	0.00	410.00	6.72	31.0	0.87
Oberhoffen	1.00	0.04	1.00	0.03	1.00	0.08	0.60	0.02	15.00	0.25	2.0	0.06
Pet.Pierre	3.50	0.15	2.00	0.05	10.10	0.83	0.08	0.00	97.60	1.60	6.0	0.17
Pfaffenb		0.00		0.00		0.00		0.00	15.00	0.25	6.0	0.17
Pfaffens		0.00		0.00		0.00		0.00	7.00	0.11	6.0	0.17
Phillipsb	3.00	0.13	3.00	0.08	10.00	0.82	0.05	0.00	92.00	1.51	4.0	0.11
Phillipsb	5.30	0.23	2.50	0.06	8.40	0.69	0.05	0.00	91.50	1.50	8.0	0.23
RG1	1140.00	49.59	9.00	0.23	37.00	3.04		0.00	430.00	7.05	1850.0	52.17
Riesthal	3.00	0.13	4.00	0.10	4.00	0.33	0.08	0.00	7.00	0.11	7.0	0.20
Roe	98.00	4.26	7.40	0.19	10.00	0.82	0.14	0.01	230.00	3.77	200.0	5.64
Roe S1	41.00	1.78	7.00	0.18	14.00	1.15	0.12	0.00	300.00	4.92	94.0	2.65
Roeschw	41.00	1.78	7.00	0.18	14.00	1.15		0.00	300.00	4.92	94.0	2.65
Roeschw	98.00	4.26	7.40	0.19	10.00	0.82		0.00	230.00	3.77	200.0	5.64
Romaine	1230.00	53.51	270.00	6.91	50.00	4.11	3.03	0.11	1200.00	19.68	2200.0	62.04
Romaine	1320.00	57.42	140.00	3.58	71.00	5.84	2.40	0.09	310.00	5.08	2860.0	80.65
Romaine	1300.00	56.55	140.00	3.58	62.88	5.17	5.86	0.21	302.00	4.95	2709.0	76.39
Romaine	1250.00	54.38	117.00	3.00	62.40	5.13	2.40	0.09	305.00	5.00	2690.0	75.86
Romaine	1340.00	58.29	130.00	3.33	65.00	5.34	3.20	0.11	300.00	4.92	2780.0	78.40
Romaine	1300.00	56.55	116.00	2.97	59.00	4.85	2.50	0.09	307.00	5.03	2740.0	77.27
Rothb III	3.00	0.13	3.00	0.08	7.40	0.61	0.20	0.01	100.00	1.64	3.3	0.09
Rothb IV	4.00	0.17	4.00	0.10	4.00	0.33	0.13	0.00	63.40	1.04	2.4	0.07
Rothbach	3.00	0.13	6.00	0.15	5.00	0.41		0.00	73.00	1.20	5.0	0.14
Rothbach	3.00	0.13	3.00	0.08	3.00	0.25		0.00	55.00	0.90	4.0	0.11
Saline	1870.00	81.35	7.00	0.18	2.00	0.16		0.00	31.00	0.51	2940.0	82.91
Schreiner	10.00	0.44	1.60	0.04	22.00	1.81	0.02	0.00	404.00	6.63	86.0	2.43
Schweigh	5.00	0.22	3.00	0.08	3.00	0.25	0.01	0.00	6.00	0.10	8.0	0.23
Schweighaus.	5.00	0.22	3.00	0.08	3.00	0.25		0.00	6.00	0.10	3.0	0.08
Seltz 43	38.00	1.65	2.60	0.07	9.60	0.79	0.03	0.00	281.00	4.61	58.0	1.64
Seltz 44	29.00	1.26	3.40	0.09	7.20	0.59	0.03	0.00	280.60	4.60	37.0	1.04
Sept Font.	3.00	0.13	2.00	0.05	2.00	0.16	0.10	0.00	74.00	1.21	5.0	0.14
Souffl FII	19.00	0.83	1.50	0.04	1.69	0.14	0.92	0.03	48.80	0.80	19.4	0.55

Appendix 10 BGR Hydrochemistry Data

Wellnr.	SO4 mgl	SO4 mel	Total Cation	Total Anion	O2	SiO2	dH	fH	µS/cm	Comment
Mors 3a	434.00	9.03	94.26	91.55	0.40	19.00	25.10		9000	thermal, F-
Mors 3b	350.00	7.28	76.26	75.20					6850	thermal,F-
Mors 3b	370.00	7.70	85.53	81.14	0.10	19.00	18.40		7200	thermal,F-
Mors 3b	360.00	7.49	77.12	77.27		10.30	17.50		7500	thermal
Mors 3b	266.00	5.53	77.61	75.39			16.90		6850	thermal
Moth F1	4.00	0.08	9.00	7.68	2.30	9.50	7.50		690	
Oberhoffen	8.00	0.17	0.47	0.47	0.10	12.00	0.40		50	PT,trace,2 wells
Pet.Pierre	6.00	0.12	2.07	1.89	9.10	8.00		9	240	PT
Pfaffenb	5.00	0.10	0.00	0.52			0.42		66	
Pfaffens	16.00	0.33	0.00	0.62			0.46		64	
Phillipsb	5.00	0.10	1.78	1.73		8.60	4.20		160	
Phillipsb	1.50	0.03	1.72	1.76		12.80		7		
RG1	0.20	0.00	56.60	59.23					6600	shallow survey/oil
Riesthal	26.00	0.54	0.91	0.85		20.00	.2?		100	
Roe	92.00	1.91	11.27	11.33			9.20		930	see copy
Roe S1	55.00	1.14	9.11	8.71	3.90	8.50	7.10		750	see copy
Roeschw	55.00	1.14	9.10	8.71					750	
Roeschw	92.00	1.91	11.26	11.33					930	
Romaine	69.00	1.44	81.60	83.16						faille, Li,Sr
Romaine	77.00	1.60	84.89	87.34	0.90		23.8?		6700	Br,I
Romaine	81.00	1.68	84.04	83.03	1.10	13.50		119	6802	
Romaine	61.00	1.27	79.95	82.13		7.90	63.00		7970	
Romaine	85.00	1.77	85.54	85.08	0.50	14.00	23.8?		7200	
Romaine	45.00	0.94	81.87	83.24		45.00	22.3?		7940	
Rothb III	3.00	0.06	1.86	1.80	9.20	15.50		8	144	PT
Rothb IV	3.00	0.06	1.25	1.17	9.70	13.50		6	112	PT
Rothbach	4.00	0.08	1.39	1.42					100	
Rothbach	5.00	0.10	1.05	1.12					80	
Saline	0.10	0.00	83.68	83.42					1850	salt-work
Schreiner	23.00	0.48	10.37	9.53	9.00	16.00	9.90		930	
Schweigh	25.00	0.52	0.99	0.84	4.50	4.50	0.60		100	
Schweighaus.	25.00	0.52	0.99	0.70					100	
Seltz 43	48.00	1.00	7.18	7.24	2.40	7.00		27	625	PT
Seltz 44	35.00	0.73	6.37	6.37	2.20	7.20		25	544	PT
Sept Font.	3.00	0.06	1.45	1.42		6.20	3.40		130	
Souffl FII	3.00	0.06	1.46	1.41	1.96	16.00		3	110	

Appendix 10 BGR Hydrochemistry Data

Wellnr.	BGR.Nr	Reference
Mors 3a	6017	BGR
Mors 3b	6018	SGAL/BGR
Mors 3b	6018	BGR
Mors 3b	6018	BGR
Mors 3b	6018	BGR
Moth F1	6024	SGAL/BGR
Oberhoffen	3040	SGAL/BGR
Pet.Pierre		SGAL/BGR
Pfaffenb	6030	SGAL/BGR
Pfaffens	6029	SGAL/BGR
Phillipsb	6019	BGR
Phillipsb	6019	SGAL/BGR
RG1	6053	BGR
Riesthal	6020	SGAL/BGR
Roe	3046	SGAL/BGR
Roe S1	6036	SGAL/BGR
Roeschw	6036	SGAL/BGR
Roeschw	6046	SGAL/BGR
Romaine	6015	Carle
Romaine	6015	SGAL/BGR
Romaine	6015	SGAL/BGR
Romaine	6015	BGR
Romaine	6015	BGR
Romaine	6015	BGR
Rothb III	3042	SGAL/BGR
Rothb IV	3043	SGAL/BGR
Rothbach	6042	SGAL/BGR
Rothbach	6043	SGAL/BGR
Saline	6050	SGAL/BGR
Schreiner	3048	BGR
Schweigh	3045	SGAL/BGR
Schweighaus.	6045	SGAL/BGR
Seltz 43		SGAL/BGR
Seltz 44		SGAL/BGR
Sept Font.	6007	BGR
Souffl FII	6023	SGAL/BGR

Appendix 10 BGR Hydrochemistry Data

Wellnr.	BGR.Nr	KB	Date	Location	Source	mean.d	Formation	pH	density	TDS mgl	Ca mgl	Ca mel
Souffl S1	6022	135	5.12.69	Soufflenheim	well	70	T	6.40		68	11.00	0.55
Vosges 1		275	7.8.86	Riesthal	spring		Bsdst	6.20	cal.	56.98	6.80	0.34
Weiler 1	6014	173	6.12.74	Wissembourg	well	80	Bsdst	8.30		96	18.00	0.90
Weiler 2	6013	173	11.4.75	Wissembourg	well	120	P	7.40		144	15.00	0.75
Weitbr III		150	20.6.77	Weitbruch	well	63	Plio	7.00		316	66.00	3.29

Appendix 10 BGR Hydrochemistry Data

Wellnr.	Na mgl	Na mel	K mgl	K mel	Mg mgl	Mg mel	Fe2 mgl	Fe2 mel	HCO3 mgl	HCO3 mel	Cl mgl	Cl mel
Souffl S1	8.00	0.35	1.50	0.04	2.00	0.16	1.40	0.05	43.00	0.71	10.0	0.28
Vosges 1	3.10	0.13	3.60	0.09	3.50	0.29	0.08	0.00	7.00	0.11	6.9	0.19
Weiler 1	5.00	0.22	2.00	0.05	6.00	0.49		0.00	85.00	1.39	5.0	0.14
Weiler 2	18.00	0.78	2.50	0.06	6.00	0.49	0.37	0.01	84.00	1.38	13.0	0.37
Weitbr III	16.00	0.70	1.30	0.03	12.20	1.00	0.81	0.03	239.00	3.92	27.0	0.76

Appendix 10 BGR Hydrochemistry Data

Wellnr.	SO4 mgl	SO4 mel	Total Cation	Total Anion	O2	SiO2	dH	fH	µS/cm	Comment
Soufll S1	8.00	0.17	1.15	1.15		13.10	0.70		100	
Vosges 1	26.00	0.54	0.86	0.85			1.80		103	
Weiler 1	2.00	0.04	1.66	1.58	10.10	9.20	1.40		140	artesian
Weiler 2	9.00	0.19	2.10	1.93	8.10	11.40	1.20		160	confined
Weitbr III	19.50	0.41	5.05	5.09	5.00	13.00		22	408	PT

Wellnr.	BGR.Nr	Reference
Souffl S1	6022	SGAL/BGR
Vosges 1		BGR
Weiler 1	6014	SGAL/BGR
Weiler 2	6013	SGAL/BGR
Weitbr III		SGAL/BGR

Wellnr.	BGR.Nr	KB	Date	Location	Source	mean.d	Formation	pH	density	TDS mgl	Ca mgl
Pfaffenr.	11402/1	n/a	20.9.78	Pfaffenrot	well	25	Bsdst.	5.6			
Herrenalb	11405/1	n/a	28.6.82	Herrenalb	well	820	Upp.Carbon	8.1		630	13
Bad.Pflutt.II	11701/1	n/a	24.11.81	Bad.Pfluttersloch	well	500	Devonian	7.1	1.003	3500	150
Bad.Pflutt. I	11702/1	n/a	24.11.81	Bad. Pfluttersloch	well	200	Low.Carbon	7.1	1.002	2700	110
Baden-Oos	11704/1	n/a	1.8.77	Baden-Oos	well	390	Ps	7.2		3500	
Weiten.	11901/1	n/a	13.7.73	Weitenung	well	50	Pleistocene	7.5		300	84
Schw.-Greff	11902/1	n/a	23.9.71	Schw.-Greffern	well	25	Pleistocene	7.3		427	88
Balzhof.	11903/1	n/a	22.5.68	Balzhofen	well	25	Pleistocene	7.3		414	86
Steinb.	11904/1	n/a	8.4.67	Steinbach	well	10	Pleistocene	7.5		430	110
Hügels.	11905/1	n/a	22.2.72	Hügelscheim	well	15	Pleistocene	7.3		260	
Rotenf.	12001/1	n/a	16.7.76	Rotenfels	well	196	Devonian ?	7.6		5100	220
Kuppen	12002/1	n/a	17/9/76	Kuppenheim	well	15	Pleistocene	7.2			
Rast	12005/1	n/a	23.9.76	Rastatt	well	12	Pleistocene	6.2		533	100
Bischofs.	12006/1	n/a	23.9.76	Bischhofsweiler	well	6	Pleistocene	7.4		490	110
Otters	12102/1	n/a	8.3.77	Ottersdorf	well	36	Pleistocene	7.4		481	99
Hoefen	11305/1	n/a	16.1.69	Hoefen	well	200	Carbon				25
Bruch-1a		n/a	3.9.86	Bruchsal	therm.		Bsdst.	5.4			7530

Appendix 11 GL BW Hydrochemistry Data

Wellnr.	Ca mel	Na mgl	Na mel	K mgl	K mel	Mg mgl	Mg mel	HCO3 mgl	HCO3 mel	Cl mgl
Pfaffenr.								15.5	0.25	8
Herrenalb	0.65	160	6.96	11	0.28	25	2.06	230	3.77	170
Bad.Pflutt.II	7.49	990	43.07	100	2.56	7.3	0.60	160	2.62	1800
Bad.Pflutt. I	5.49	760	33.06	52	1.33	3.6	0.30	160	2.62	1300
Baden-Oos	0.00		0.00		0.00		0.00	250	4.10	1400
Weiten.	4.19		0.00		0.00	2.4	0.20	240	3.94	16
Schw.-Greff	4.39	6.2	0.27	2.2	0.06	10	0.82	270	4.43	14
Balzhof.	4.29	6	0.26	0.9	0.02	9.7	0.80	280	4.59	13
Steinb.	5.49		0.00		0.00	12	0.99	300	4.92	28
Hugels.	0.00		0.00		0.00		0.00	190	3.12	9
Rotenf.	10.98	1400	60.90	130	3.33	31	2.55	220	3.61	2700
Kuppen	0.00		0.00		0.00		0.00	310	5.08	11
Rast	4.99	13	0.57	4.1	0.10	14	1.15	320	5.25	16
Bischofs.	5.49		0.00		0.00	8.6	0.71	330	5.41	19
Otters	4.94	6.1	0.27	1.2	0.03	12	0.99	310	5.08	13
Hoefen	1.2	6.2	0.3	0.9	0	12	1	130	2.1	2.8
Bruch-1a		32100		3540		377		512		76290

Appendix 11 GL BW Hydrochemistry Data

Wellnr.	Cl mel	SO4 mgl	SO4 mel	Total Cation	Total Anion	O2	SiO2	µS/cm	Reference
Pfaffenr.	0.23	2.3	0.05	0.00	0.53	11.5	36	36	GL-BW
Herrenalb	4.79	40	0.83	9.95	9.40	0.1	15	890	GL-BW
Bad.Pflutt.II	50.76	160	3.33	53.71	56.71	0.5	100	5100	GL-BW
Bad.Pflutt. I	36.66	150	3.12	40.18	42.40	0.43	100	4100	GL-BW
Baden-Oos	39.48	370	7.70	0.00	51.28			3500	GL-BW
Weiten.	0.45		0.00	4.39	4.39	5.1	10		GL-BW
Schw.-Greff	0.39	37	0.77	5.54	5.59	0.5	7.7	450	GL-BW
Balzhof.	0.37	17	0.35	5.37	5.31	1.7	15	680	GL-BW
Steinb.	0.79		0.00	6.48	5.71	9.8	11		GL-BW
Hügels.	0.25	21	0.44	0.00	3.81	8.9	4		GL-BW
Rotenf.	76.14	260	5.41	77.75	85.16		14	9000	GL-BW
Kuppen	0.31	24	0.50	0.00	5.89	8.4	13	340	GL-BW
Rast	0.45	43	0.89	6.81	6.59	11.00		500	GL-BW
Bischofs.	0.54		0.00	6.20	5.95				GL-BW
Otters	0.37	39	0.81	6.22	6.26	3.10	7.20	500	GL-BW
Hoefen	0.1	8.2	0.2	2.50	2.40			210	GL-BW
Bruch-1a		334				0.01	8.5		Matthess'86

Appendix 11 GL BW Hydrochemistry Data

Wellnr.	BGR.Nr	KB	Location	Source	mean.d	Formation	pH	density	TDS mgl	Ca mel	Na mel	K mel
3262	6012	148	K	well	435	ZD	7.10			20.46	315.81	0.92
4275	6052		Merkwiller	well	120	Ps	7.10		962	2.69	6.66	0.08
AEP Lobsann	6005	292	Marienbronn	well	46.2	Bsdst	5.90			0.45	0.00	0.00
Aerodrome	3038	149	Haguenau	well	61	Plio	5.90		80	0.45	0.26	0.05
Aluxan	3047	145	Betschdorf	well	32	Plio	7.00			5.64	0.39	0.01
Bein 1	3037	115	Beinheim	well	11	Plio	6.90		410	5.99	0.35	0.05
Beinheim	6037		Beinheim	well	31	Plio	6.90		410	5.99	0.35	0.05
Betschdorf	6047		Betschdorf	well	25	Plio	7.00			5.64	0.39	0.01
Bischwill	3041	125	Bischwiller	well	40	Plio	7.30		300	4.39	0.28	0.05
Bischwiller	6041		Bischwiller	well	30	Plio	7.30		300	0.00	0.00	0.00
Bitche	6021	285	Bitche	well	47	Bsdst	5.70		36.5	0.31	0.20	0.06
Celtic	6016	204	Niederbronn	spring	7	Bsdst	6.60		38	0.25	0.09	0.05
Celtic	6016	204	Niederbronn	spring	7	Bsdst	6.50			0.30	0.09	0.05
Celtic	6016	204	Niederbronn	spring	7	Bsdst	6.60		52	0.30	0.13	0.05
Drachen E	6001	326	Drachenbronn	well	140	Bsdst	6.80		81	0.70	0.13	0.08
Drachen E	6001	326	Drachenbronn	well	140	Bsdst			79	0.14	0.04	0.08
Four a Chaux	6026	229	Lembach	well	72	MK			850		0.00	0.00
Four a Chaux	6026	229	Lembach	well	72	MK			370		0.00	0.00
Four a Chaux	6026	229	Lembach	well	142	MK			610		0.00	0.00
Four a Chaux	6026	229	Lembach	well	188	Bsdst			240		0.00	0.00
Four a Chaux	6026	229	Lembach	well	236	Bsdst			160		0.00	0.00
Four a Chaux	6026	229	Lembach	well	220	Bsdst	7.20		240	1.75	0.09	0.05
Fried/3969	6051		Kutzenhausen	well	490	P inf.				4.99	134.85	0.46
Fried/3969	6051		Kutzenhausen	well	490	P inf.	7.90		8688	4.79	136.16	0.49
Gambs F2		129	Gambsheim	well	50	Plio	7.40		428	4.47	1.31	0.07
GPK-1	6055		Soultz	well	1817	Base	6.40		80000	308.63	964.61	62.34
H 1	6003	295	Hochwald	well	167	Bsdst	6.85		100	0.29	0.11	0.09
H 1	6003	295	Hochwald	well	167	Bsdst	6.65		51	0.35	0.04	0.08
H II	6004	304	Hochwald	well	190	Bsdst	7.00		52	0.55	0.09	0.04
H II	6004	304	Hochwald	well	190	Bsdst	6.90			0.55	0.04	0.05
Haguenau	6038		Haguenau	well	31	Plio	5.90		80	0.45	0.26	0.05
Hardt 1	6025	153	Wissembourg	well	41	T	6.90		280	3.99	0.13	0.05
Helions II	6049	161	Pechelbronn	well	1146	MK	5.10			59.88	179.22	12.29
Helions II	6049	161	Pechelbronn	well	1146	MK	6.60		20000	72.85	234.90	20.99
Helions II	6049	161	Pechelbronn	well	1146	MK			19900	75.85	225.33	19.97
Helions II	6049	161	Pechelbronn	well	1146	MK	6.40		20500	72.85	223.59	19.71

Appendix 12 Schoeller Classification (BGR, SAEM data)

Wellnr.	BGR.Nr	Mg mel	Fe2 mel	HCO3 mel	Cl mel	SO4 mel	Chloride	Sulfate	√ (SO4xCa)	3√(HCO3+CO3)^2*Ca
3262	6012	22.19	0.26	4.10	369.42	0.06	HC	N	1.13	7.01
4275	6052	2.79	0.00	10.17	2.28	0.02	NC	N	0.24	6.53
AEP Lobsann	6005	0.00	0.00	0.30	0.20	0.15		N	0.26	0.34
Aerodrome	3038	0.25	0.03	0.20	0.23	0.52	NC	N	0.48	0.26
Aluxan	3047	1.48	0.03	7.02	0.39	0.10	NC	N	0.77	6.53
Bein 1	3037	0.99	0.02	5.41	0.48	1.04	NC	N	2.50	5.60
Beinheim	6037	0.99	0.00	5.41	0.48	1.04	NC	N	2.50	5.60
Betschdorf	6047	1.48	0.00	7.02	0.39	0.10	NC	N	0.77	6.53
Bischwill	3041	0.75	0.00	5.00	0.27	0.40	NC	N	1.32	4.79
Bischwiller	6041	0.00	0.00	0.00	0.00	0.00				
Bitche	6021	0.07	0.00	0.25	0.24	0.02	NC	N	0.07	0.27
Celtic	6016	0.16	0.00	0.33	0.14	0.08	NC	N	0.14	0.30
Celtic	6016	0.16	0.00	0.33	0.11	0.15	NC	N	0.21	0.32
Celtic	6016	0.25	0.00	0.38	0.11	0.15	NC	N	0.21	0.35
Drachen E	6001	0.49	0.02	1.05	0.06	0.29	NC	N	0.45	0.92
Drachen E	6001	0.16	0.01	0.51	0.06	0.02	NC	N	0.05	0.33
Four a Chaux	6026	0.00	0.00	0.00	0.00	7.70		A		
Four a Chaux	6026	0.00	0.00	0.00	0.00	1.71		N		
Four a Chaux	6026	0.00	0.00	0.00	0.00	4.16		N		
Four a Chaux	6026	0.00	0.00	0.00	0.08	0.37		N		
Four a Chaux	6026	0.00	0.00	0.00	0.11	0.15		N		
Four a Chaux	6026	0.90	0.00	2.71	0.06	0.08	NC	N	0.38	2.34
Fried/3969	6051	4.44	0.00	6.72	140.72	0.08	AC	N	0.64	6.09
Fried/3969	6051	4.11	0.00	5.90	141.85	0.04	AC	N	0.45	5.51
Gambs F2		0.99	0.00	3.90	2.17	0.75	NC	N	1.83	4.08
GPK-1	6055	10.69	0.00	8.20	1366.01	3.56	VHC	N	33.13	27.48
H 1	6003	0.51	0.02	0.75	0.08	0.17	NC	N	0.22	0.55
H 1	6003	0.16	0.01	0.50	0.06	0.02	NC	N	0.09	0.44
H II	6004	0.33	0.01	0.85	0.06	0.08	NC	N	0.21	0.74
H II	6004	0.16	0.01	0.72	0.03	0.06	NC	N	0.19	0.66
Haguenau	6038	0.25	0.00	0.20	0.23	0.52	NC	N	0.48	0.26
Hardt 1	6025	0.82	0.00	4.43	0.17	0.21	NC	N	0.91	4.28
Helions II	6049	7.32	0.00	4.76	249.29	11.65	HC	A	26.41	11.06
Helions II	6049	131.52	0.20	5.08	298.92	17.47	HC	A	35.68	12.35
Helions II	6049	10.69	0.17	5.08	298.92	14.98	HC	A	33.70	12.52
Helions II	6049	11.51	0.19	5.25	293.28	14.35	HC	A	32.34	12.61

Appendix 12 Schoeller Classification (BGR, SAEM data)

Wellnr.	BGR.Nr	IBE	Cl/Na
3262	6012	0.15	1.17
4275	6052	-1.80	0.34
AEP Lobsann	6005		
Aerodrome	3038	-0.16	0.86
Aluxan	3047	0.01	1.01
Bein 1	3037	0.27	1.38
Beinheim	6037	0.27	1.38
Betschdorf	6047	0.01	1.01
Bischwill	3041	-0.07	0.94
Bischwiller	6041		
Bitche	6021	0.18	1.22
Celtic	6016	0.38	1.62
Celtic	6016	0.23	1.30
Celtic	6016	-0.16	0.86
Drachen E	6001	-1.31	0.43
Drachen E	6001	0.23	1.30
Four a Chaux	6026		
Four a Chaux	6026		
Four a Chaux	6026		
Four a Chaux	6026	1.00	
Four a Chaux	6026	1.00	
Four a Chaux	6026	-0.54	0.65
Fried/3969	6051	0.04	1.04
Fried/3969	6051	0.04	1.04
Gambs F2		0.40	1.66
GPK-1	6055	0.29	1.42
H 1	6003	-0.29	0.78
H 1	6003	0.23	1.30
H II	6004	-0.54	0.65
H II	6004	-0.54	0.65
Haguenau	6038	-0.16	0.86
Hardt 1	6025	0.23	1.30
Helions II	6049	0.28	1.39
Helions II	6049	0.21	1.27
Helions II	6049	0.25	1.33
Helions II	6049	0.24	1.31

Appendix 12 Schoeller Classification (BGR, SAEM data)

Wellnr.	BGR.Nr	KB	Location	Source	mean.d	Formation	pH	density	TDS mgl	Ca mel	Na mel	K mel
Helions II	6049	161	Pechelbronn	well	1146	MK	6.30		20000	74.85	230.55	19.46
Helions II	6049	161	Pechelbronn	well	1146	MK	6.20		20700	74.35	233.16	20.48
Helions II	6049	161	Pechelbronn	well	1146	MK	6.10		20500	74.85	243.60	21.76
Helions II	6049	161	Pechelbronn	well	1146	MK	6.20		20800	76.35	229.68	19.46
Helions II	6049	161	Pechelbronn	well	1146	MK	6.20		21000	74.85	230.55	15.36
Helions II	6049	161	Pechelbronn	well	1146	MK	6.20			70.86	210.54	12.80
Helions II	6049	161	Pechelbronn	well	1146	MK	6.10		21800	82.83	243.60	15.36
Helions II	6049	161	Pechelbronn	well	1146	MK	5.90			80.34	228.81	14.46
Herrlis F2		126	Offendorf	well	46	Plio	7.50		505	5.99	0.67	0.07
Hochwald	6034		Hochwald	well	1	Bsdst	5.30			0.00	0.00	0.00
Kutz		128	Kutzenhausen	well	33	Plio	7.00		460	5.89	0.41	0.08
Lauter F1		153	Mothern	well	11.7	Q	7.00		500	5.89	1.37	0.31
Lauter F2		153	Mothern	well	11.4	Q	7.10		454	6.31	0.85	0.48
Lembach 'E	6029		Lembach	well	1	Bsdst	5.80					
Lembach 'E	6030		Lembach	well	1	Bsdst	6.00			0.00	0.00	0.00
Lembach 'N	6027		Lembach	well	1	Bsdst	6.00					
Lembach 'N	6028		Lembach	well	1	Bsdst	6.00			0.00	0.00	0.00
Lembach 'NW	6031		Lembach	well	1	Bsdst	6.00			0.00	0.00	0.00
Lembach 'NW	6032		Lembach	well	1	Bsdst	5.90			0.00	0.00	0.00
Lichteneck			Niederbronn	spring		Bsdst	6.50			0.31	0.08	0.06
Liebfrauent	6011/2	175	Woerth	well	130	Bsdst	7.90		200	0.70	0.10	0.10
Mar 101	6006	267	Marienbronn	well	46		8.90		760	1.10	9.57	0.46
Mar 101	6006	267	Marienbronn	well	906		7.70			3.84	38.72	0.92
Mariental	3039	143	Haguenau	well	68	Plio	6.40		36	0.20	0.13	0.03
Mattenmühle	6054		Soultz	well	10	SG	7.00		2199	5.39	25.32	0.13
Mitschd	6000	221	Mitschdorf	well	200	Bsdst	6.30		50	0.40	0.22	0.04
Mitschd	6000	221	Mitschdorf	well	200	Bsdst	6.40			0.35	0.06	0.05
Mitschd	6000	221	Mitschdorf	well	200	Bsdst	7.00			0.25	0.04	0.05
Mors 3a	6017	187	Morsbronn	well	400	MK	6.70		6600	22.95	70.91	9.22
Mors 3a	6017	187	Morsbronn	well	400	MK	6.70			22.46	64.38	4.35
Mors 3a	6017	187	Morsbronn	well	400	MK	6.10			22.46	64.82	4.20
Mors 3b	6018	185	Morsbronn	well	680	Bsdst				15.47	54.81	3.84
Mors 3b	6018	185	Morsbronn	well	680	Bsdst	7.30		5300	15.97	60.03	6.66
Mors 3b	6018	185	Morsbronn	well	680	Bsdst	7.30			15.47	55.68	3.84
Mors 3b	6018	185	Morsbronn	well	680	Bsdst	6.43			14.87	56.99	3.64
Moth F1	6024	111	Mothern	well	12	Q	7.10		450	6.49	0.87	0.49

Appendix 12 Schoeller Classification (BGR, SAEM data)

Wellnr.	BGR.Nr	Mg mel	Fe2 mel	HCO3 mel	Cl mel	SO4 mel	Chloride	Sulfate	√ (SO4xCa)	3√(HCO3+CO3)^2*Ca
Helions II	6049	10.69	0.19	5.08	290.46	13.73	HC	A	32.06	12.46
Helions II	6049	11.51	0.26	5.25	301.74	14.14	HC	A	32.43	12.70
Helions II	6049	10.69	0.17	4.92	307.38	13.73	HC	A	32.06	12.19
Helions II	6049	13.97	0.19	5.08	307.38	14.14	HC	A	32.86	12.54
Helions II	6049	14.80	0.18	4.92	304.56	13.94	HC	A	32.30	12.19
Helions II	6049	9.86	0.15	5.08	301.74	12.90	HC	A	30.23	12.23
Helions II	6049	9.86	0.21	5.08	332.76	13.94	HC	A	33.98	12.89
Helions II	6049	10.11	0.16	4.97	327.12	9.51	HC	A	27.63	12.57
Herrlis F2		1.34	0.00	5.16	1.18	1.41	NC	N	2.91	5.42
Hochwald	6034	0.00	0.00	0.00	0.20	0.29		N		
Kutz		1.78	0.03	6.64	0.43	1.04	NC	N	2.47	6.38
Lauter F1		1.00	0.00	6.17	1.43	0.75	NC	N	2.10	6.07
Lauter F2		1.17	0.00	6.64	0.88	0.80	NC	N	2.25	6.53
Lembach 'E	6029			0.11	0.17	0.33		N		
Lembach 'E	6030	0.00	0.00	0.25	0.17	0.10		N		
Lembach 'N	6027			0.20	0.10					
Lembach 'N	6028	0.00	0.00	0.26	0.11	0.04		N		
Lembach 'NW	6031	0.00	0.00	0.16	0.14	0.08		N		
Lembach 'NW	6032	0.00	0.00	0.16	0.14	0.08		N		
Lichteneck		0.17	0.00	0.33	0.11	0.15	NC	N	0.21	0.32
Liebfrauent	6011/2	0.20	0.11	0.80	0.10	0.30	NC	N	0.45	0.80
Mar 101	6006	0.82	0.05	4.59	2.00	3.95	NC	N	2.08	2.85
Mar 101	6006	2.71	0.01	9.51	35.25	0.94	LC	N	1.90	7.03
Mariental	3039	0.08	0.03	0.30	0.06	0.10	NC	N	0.14	0.26
Mattenmühle	6054	3.29	0.00	8.04	24.82	1.96	LC	N	3.25	7.03
Mitschd	6000	0.08	0.00	0.46	0.06	0.00	NC	N		0.44
Mitschd	6000	0.08	0.00	0.44	0.03	0.06	NC	N	0.15	0.41
Mitschd	6000	0.06	0.03	0.31	0.06	0.03	NC	N	0.09	0.29
Mors 3a	6017	3.78	0.09	5.25	83.47	12.69	AC	A	17.07	8.58
Mors 3a	6017	2.55	0.08	5.08	80.65	11.86	AC	A	16.32	8.34
Mors 3a	6017	2.71	0.08	4.97	77.55	9.03	AC	A	14.24	8.22
Mors 3b	6018	2.14	0.00	4.76	63.17	7.28	AC	A	10.61	7.05
Mors 3b	6018	2.79	0.08	4.92	68.53	7.70	AC	A	11.09	7.28
Mors 3b	6018	2.06	0.07	4.92	64.86	7.49	AC	A	10.76	7.21
Mors 3b	6018	2.06	0.06	5.00	64.86	5.53	AC	N	9.07	7.19
Moth F1	6024	1.15	0.00	6.72	0.87	0.08	NC	N	0.73	6.64

Appendix 12 Schoeller Classification (BGR, SAEM data)

Wellnr.	BGR.Nr	IBE	Cl/Na
Helions II	6049	0.21	1.26
Helions II	6049	0.23	1.29
Helions II	6049	0.21	1.26
Helions II	6049	0.25	1.34
Helions II	6049	0.24	1.32
Helions II	6049	0.30	1.43
Helions II	6049	0.27	1.37
Helions II	6049	0.30	1.43
Herrlis F2		0.43	1.76
Hochwald	6034	1.00	
Kutz		0.04	1.04
Lauter F1		0.04	1.04
Lauter F2		0.04	1.04
Lembach 'E	6029		
Lembach 'E	6030		
Lembach 'N	6027		
Lembach 'N	6028		
Lembach 'NW	6031		
Lembach 'NW	6032		
Lichteneck		0.29	1.40
Liebfrauent	6011/2	0.00	1.00
Mar 101	6006	-3.78	0.21
Mar 101	6006	-0.10	0.91
Mariental	3039	-1.31	0.43
Mattenmühle	6054	-0.02	0.98
Mitschd	6000	-2.86	0.26
Mitschd	6000	-1.16	0.46
Mitschd	6000	0.23	1.30
Mors 3a	6017	0.15	1.18
Mors 3a	6017	0.20	1.25
Mors 3a	6017	0.16	1.20
Mors 3b	6018	0.13	1.15
Mors 3b	6018	0.12	1.14
Mors 3b	6018	0.14	1.16
Mors 3b	6018	0.12	1.14
Moth F1	6024	0.00	1.00

Appendix 12 Schoeller Classification (BGR, SAEM data)

Wellnr.	BGR.Nr	KB	Location	Source	mean.d	Formation	pH	density	TDS mgl	Ca mel	Na mel	K mel
Oberhoffen	3040	143	Haguenau	well	68	Plio	6.40		40	0.30	0.04	0.03
Pet.Pierre		245	Petite Pierre	well	162	Bsdst	7.00		134	1.04	0.15	0.05
Pfaffenb	6030	325	Lembach	spring		Bsdst					0.00	0.00
Pfaffens	6029	367	Hochwald	spring		Bsdst	5.80				0.00	0.00
Phillipsb	6019	218	Phillipsbourg	well	70	Bsdst	8.20			0.75	0.13	0.08
Phillipsb	6019	218	Phillipsbourg	well	70	Bsdst	7.90			0.73	0.23	0.06
RG1	6053		Kutzenhausen	well	10	Ps	7.10		3542	3.74	49.59	0.23
Riesthal	6020	285	Phillipsbourg	spring		Bsdst	5.70			0.35	0.13	0.10
Roe	3046	119	Roeschwoog	well	15	Plio				5.99	4.26	0.19
Roe S1	6036	119	Roeschwoog	well	28	Plio	7.00		600	5.99	1.78	0.18
Roeschw	6036		Roeschwoog	well	15	Plio	7.00		600	5.99	1.78	0.18
Roeschw	6046		Roeschwoog	well	8	Plio				5.99	4.26	0.19
Romaine	6015	210	Niederbronn	well	11	Bsdst				16.97	53.51	6.91
Romaine	6015	210	Niederbronn	well	11	Bsdst	6.80		5250	17.96	57.42	3.58
Romaine	6015	210	Niederbronn	well	11	Bsdst	6.72		5090	18.52	56.55	3.58
Romaine	6015	210	Niederbronn	well	11	Bsdst	6.80			17.37	54.38	3.00
Romaine	6015	210	Niederbronn	well	11	Bsdst	6.60		5170	18.46	58.29	3.33
Romaine	6015	210	Niederbronn	well	11	Bsdst	6.60			17.42	56.55	2.97
Rothb III	3042	201	Rothbach	well	180	Bsdst	7.10		128	1.04	0.13	0.08
Rothb IV	3043	201	Rothbach	well	172	Bsdst	6.70		104	0.64	0.17	0.10
Rothbach	6042		Rothbach	well	68	Bsdst	6.30		77	0.70	0.13	0.15
Rothbach	6043		Rothbach	well	35	Quat	6.90		64	0.60	0.13	0.08
Saline	6050		Soultz			Ps	5.90			2.00	81.35	0.18
Schreiner	3048	163	Soultz	well	10	Q	7.10			8.08	0.44	0.04
Schweigh	3045	155	Schweighouse	well	23	Plio	5.30		64	0.45	0.22	0.08
Schweighaus.	6045		Schweighausen	well	12	Plio	5.30		64	0.45	0.22	0.08
Seltz 43		113	Seltz	well	13	Q	7.40		412	4.67	1.65	0.07
Seltz 44		113	Seltz	well	11.5	Q	7.40		346	4.43	1.26	0.09
Sept Font.	6007	268	Hochwald	spring		Bsdst	7.60			1.10	0.13	0.05
Souffl FII	6023	135	Soufflenheim	well	64	T	6.40		72	0.42	0.83	0.04
Souffl S1	6022	135	Soufflenheim	well	70	T	6.40		68	0.55	0.35	0.04
Vosges 1		275	Riesthal	spring		Bsdst	6.20			0.34	0.13	0.09
Weiler 1	6014	173	Wissembourg	well	80	Bsdst	8.30		96	0.90	0.22	0.05
Weiler 2	6013	173	Wissembourg	well	120	P	7.40		144	0.75	0.78	0.06
Weitbr III		150	Weitbruch	well	63	Plio	7.00		316	3.29	0.70	0.03
4485		173	Hoelschloch	oil well	1214	Bsdst	7.30	1.015	24190	81.14	269.13	29.90
4515		147	Soultz	oil well	860	MK	7.30	1.070	92599	269.46	1074.44	114.18

Appendix 12 Schoeller Classification (BGR, SAEM data)

Wellnr.	BGR.Nr	Mg mel	Fe2 mel	HCO3 mel	Cl mel	SO4 mel	Chloride	Sulfate	√ (SO4xCa)	3√(HCO3+CO3)^2*Ca
Oberhoffen	3040	0.08	0.02	0.25	0.06	0.17	NC	N	0.22	0.26
Pet.Pierre		0.83	0.00	1.60	0.17	0.12	NC	N	0.36	1.39
Pfaffenb	6030	0.00	0.00	0.25	0.17	0.10		N		
Pfaffens	6029	0.00	0.00	0.11	0.17	0.33		N		
Phillipsb	6019	0.82	0.00	1.51	0.11	0.10	NC	N	0.28	1.19
Phillipsb	6019	0.69	0.00	1.50	0.23	0.03	NC	N	0.15	1.18
RG1	6053	3.04	0.00	7.05	52.17	0.00	AC		0.12	5.71
Riesthal	6020	0.33	0.00	0.11	0.20	0.54	NC	N	0.43	0.17
Roe	3046	0.82	0.01	3.77	5.64	1.91	NC	N	3.39	4.40
Roe S1	6036	1.15	0.00	4.92	2.65	1.14	NC	N	2.62	5.25
Roeschw	6036	1.15	0.00	4.92	2.65	1.14	NC	N	2.62	5.25
Roeschw	6046	0.82	0.00	3.77	5.64	1.91	NC	N	3.39	4.40
Romaine	6015	4.11	0.11	19.68	62.04	1.44	AC	N	4.93	18.73
Romaine	6015	5.84	0.09	5.08	80.65	1.60	AC	N	5.36	7.74
Romaine	6015	5.17	0.21	4.95	76.39	1.68	AC	N	5.59	7.69
Romaine	6015	5.13	0.09	5.00	75.86	1.27	AC	N	4.69	7.57
Romaine	6015	5.34	0.11	4.92	78.40	1.77	AC	N	5.71	7.65
Romaine	6015	4.85	0.09	5.03	77.27	0.94	AC	N	4.04	7.61
Rothb III	3042	0.61	0.01	1.64	0.09	0.06	NC	N	0.25	1.41
Rothb IV	3043	0.33	0.00	1.04	0.07	0.06	NC	N	0.20	0.88
Rothbach	6042	0.41	0.00	1.20	0.14	0.08	NC	N	0.24	1.00
Rothbach	6043	0.25	0.00	0.90	0.11	0.10	NC	N	0.25	0.79
Saline	6050	0.16	0.00	0.51	82.91	0.00	AC	N	0.06	0.80
Schreiner	3048	1.81	0.00	6.63	2.43	0.48	NC	N	1.97	7.08
Schweigh	3045	0.25	0.00	0.10	0.23	0.52	NC	N	0.48	0.16
Schweighaus.	6045	0.25	0.00	0.10	0.08	0.52	NC	N	0.48	0.16
Seltz 43		0.79	0.00	4.61	1.64	1.00	NC	N	2.16	4.63
Seltz 44		0.59	0.00	4.60	1.04	0.73	NC	N	1.80	4.54
Sept Font.	6007	0.16	0.00	1.21	0.14	0.06	NC	N	0.26	1.17
Souffl FII	6023	0.14	0.03	0.80	0.55	0.06	NC	N	0.16	0.65
Souffl S1	6022	0.16	0.05	0.71	0.28	0.17	NC	N	0.30	0.65
Vosges 1		0.29	0.00	0.11	0.19	0.54	NC	N	0.43	0.16
Weiler 1	6014	0.49	0.00	1.39	0.14	0.04	NC	N	0.19	1.20
Weiler 2	6013	0.49	0.01	1.38	0.37	0.19	NC	N	0.37	1.12
Weitbr III		1.00	0.03	3.92	0.76	0.41	NC	N	1.16	3.70
4485		4.36	0.06	5.00	385.55	3.70	HC	N	17.33	12.66
4515		51.79	0.18	9.18	1565.10	3.95	VHC	N	32.62	28.32

Appendix 12 Schoeller Classification (BGR, SAEM data)

Wellnr.	BGR.Nr	IBE	Cl/Na
Oberhoffen	3040	0.23	1.30
Pet.Pierre		0.10	1.11
Pfaffenb	6030	1.00	
Pfaffens	6029	1.00	
Phillipsb	6019	-0.16	0.86
Phillipsb	6019	-0.02	0.98
RG1	6053	0.05	1.05
Riesthal	6020	0.34	1.51
Roe	3046	0.24	1.32
Roe S1	6036	0.33	1.49
Roeschw	6036	0.33	1.49
Roeschw	6046	0.24	1.32
Romaine	6015	0.14	1.16
Romaine	6015	0.29	1.40
Romaine	6015	0.26	1.35
Romaine	6015	0.28	1.40
Romaine	6015	0.26	1.34
Romaine	6015	0.27	1.37
Rothb III	3042	-0.40	0.71
Rothb IV	3043	-1.57	0.39
Rothbach	6042	0.07	1.08
Rothbach	6043	-0.16	0.86
Saline	6050	0.02	1.02
Schreiner	3048	0.82	5.58
Schweigh	3045	0.04	1.04
Schweighaus.	6045	-1.57	0.39
Seltz 43		-0.01	0.99
Seltz 44		-0.21	0.83
Sept Font.	6007	0.07	1.08
Souffl FII	6023	-0.51	0.66
Souffl S1	6022	-0.23	0.81
Vosges 1		0.31	1.44
Weiler 1	6014	-0.54	0.65
Weiler 2	6013	-1.14	0.47
Weitbr III		0.09	1.09
4485		0.30	1.43
4515		0.31	1.46

Appendix 12 Schoeller Classification (BGR, SAEM data)

Wellnr.	BGR.Nr	KB	Location	Source	mean.d	Formation	pH	density	TDS mgl	Ca mel	Na mel	K mel
4541		150	Soultz	oil well	950	MK	7.80	1.070	100634	374.25	1222.79	7.50
4544		171	Pechelbronn	oil well	250	P inf.	6.00	1.057	90000	289.42	1014.00	
4550		150	Soultz	oil well	980	Bsdst	6.90	1.072	105300	399.20	1190.81	81.59
4567		147	Soultz	oil well	871	MK	6.80		97314	349.30	1170.80	71.99

Appendix 12 Schoeller Classification (BGR, SAEM data)

Wellnr.	BGR.Nr	Mg mel	Fe2 mel	HCO3 mel	Cl mel	SO4 mel	Chloride	Sulfate	√ (SO4xCa)	3√(HCO3+CO3)^2*Ca
4541		24.08		7.10	1582.02	8.01	VHC	N	54.70	26.62
4544		123.30		4.10	1421.28	1.58	VHC	N	21.38	16.94
4550		47.59	1.48	4.61	1596.74	5.76	VHC	N	47.95	20.40
4567		37.15	1.15	4.35	1491.64	7.76	VHC	A	52.06	18.77

Appendix 12 Schoeller Classification (BGR, SAEM data)

Wellnr.	BGR.Nr	IBE	Cl/Na
4541		0.23	1.29
4544		0.29	1.40
4550		0.25	1.34
4567		0.22	1.27

Appendix 12 Schoeller Classification (BGR, SAEM data)

Well No.	BGR No.	Location	Formation	B	F	Br	I	NH4	Li	Rb	Cs	Sr	Ba	Th
Mitschd	6000/1	Mitschdorf	Bsdst											
Mitschd	6000/2	Mitschdorf	Bsdst											
Mitschd	6000/3	Mitschdorf	Bsdst	0.04	<0.1	<0.02	<0.5		<0.003			<0.1		
Drachen E	6001/1	Drachenbronn	Bsdst											
Drachen E	6001/2	Drachenbronn	Bsdst											
H I	6003/1	Hochwald	Bsdst					**all in**	**mg/l**					
H I	6003/2	Hochwald	Bsdst											
H II	6004/1	Hochwald	Bsdst											
H II	6004/2	Hochwald	Bsdst											
H II	6004/3	Hochwald	Bsdst	0.001	<0.1	<0.1	<0.05	0.008	0.005	<0.001		0.035	0.37	<0.001
AEP Lobsann	6005/1	Marienbronn	Bsdst											
AEP Lobsann	6005/2	Marienbronn	Bsdst											
Mar 101	6006/1	Marienbronn	MK											
Mar 101	6006/2	Marienbronn	MK											
Sept Font.	6007/1	Hochwald	Bsdst											
Sept Fontaine	6007/2	Hochwald	Bsdst	0.01	<0.1	<0.1	<0.05	0.008	0.005	<0.001		0.05	0.26	<0.001
Liebfrauental	6011/1	Woerth	Bsdst		0.1									
Liebfrauental	6011/2	Woerth	Bsdst	<0.01		<0.1		0.3	0.008	0.009	0.002	0.05	0.08	<0.001
3262	6012/1	K	ZD	10	1.1	127	3.3		10.5					
3262	6012/2	K	ZD	12.6	1.2	90	2.7	12.6	15.2	0.014	0.004	72		
3262	6012/3	K	ZD									54	17.4	<0.001
Weiler 2	6013	Wissembourg	P		0.85									
Romaine	6015/1	Niederbronn	Bsdst						0.65			0.74		
Romaine	6015/2	Niederbronn	Bsdst		0.08	7.7	0.085		40					
Romaine	6015/3	Niederbronn	Bsdst											
Romaine	6015/4	Niederbronn	Bsdst		0.24									
Romaine	6015/5	Niederbronn	Bsdst	1.9	0.1	20.7	0.15		4.8			13.7		
Celtic	6016/1	Niederbronn	Bsdst											<0.008
Celtic	6016/2	Niederbronn	Bsdst											
Celtic	6016/3	Niederbronn	Bsdst		0.06									
Mors 3a	6017/1	Morsbronn	MK		1.7			2						
Mors 3a	6017/2	Morsbronn	MK											
Mors 3a	6017/3	Morsbronn	MK	3.5	1.8	16.2	0.15		6.2			14.4		
Mors 3b	6018/1	Morsbronn	Bsdst	1.4	1.6				6.5					
Mors 3b	6018/2	Morsbronn	Bsdst		1.6									

Appendix 13 Trace element content of formation waters in the Vosges, Hochwald and Pechelbronn-Soultz Basin

Well No.	BGR No.	U	Al	V	Cr	Fe	Mn	Co	Ni	Cu	Zn	Cd	Pb	Ag
Mitschd	6000/1					0.03	<0.01							
Mitschd	6000/2					0.76	0.02							
Mitschd	6000/3		0.005			<0.02	<0.01	<0.001	<0.001	<0.0002	0.02	<0.0002	0.001	
Drachen E	6001/1					0.46	<0.01							
Drachen E	6001/2					0.29	0.1							
H 1	6003/1					0.45	0.05							
H 1	6003/2					0.15	<0.01							
H II	6004/1					0.17	0.01							
H II	6004/2					0.14	<0.01							
H II	6004/3	<0.001	0.003	<0.001	<0.001	<0.02	<0.01	0.001	<0.001		0.003	<0.0002	<0.001	<0.001
AEP Lobsann	6005/1					0.02								
AEP Lobsann	6005/2													
Mar 101	6006/1					1.3	0.02							
Mar 101	6006/2		0.9			0.25	0.05							
Sept Font.	6007/1					0.1	<0.01	0.001	<0.001		0.003	<0.0002		
Sept Fontaine	6007/2	<0.001	0.14	<0.001	<0.001	0.03	0.01	0.001	<0.001				<0.001	<0.001
Liebfrauental	6011/1		0.79			3.1	0.19							
Liebfrauental	6011/2	<0.001	0.04	<0.001	<0.001			0.001	<0.001		0.1	<0.0002	<0.001	<0.001
3262	6012/1					7.4	0.16							
3262	6012/2				0.01	7.6	0.13	0.012	0.029		0.005	0.003	0.01	
3262	6012/3	<0.001	0.14	0.31	0.007								<0.001	0.001
Weiler 2	6013					0.37	0.04							
Romaine	6015/1		14.5			3.03	0.46							
Romaine	6015/2					2.4	0.46							
Romaine	6015/3					2.4	0.39							
Romaine	6015/4		0.16			3.2	0.47							
Romaine	6015/5		<0.01			2.5	0.38	<0.003	<0.01	0.02	0.06	<0.0002	0.001	
Celtic	6016/1	<0.0005				0.08								
Celtic	6016/2					0.05	<0.01							
Celtic	6016/3		0.01			0.02	<0.01							
Mors 3a	6017/1		0.085			2.4	0.56							
Mors 3a	6017/2					2.3	0.51							
Mors 3a	6017/3		0.005			2.3	0.48	<0.003	<0.003	0.005	0.03	<0.0002	0.002	
Mors 3b	6018/1													
Mors 3b	6018/2		0.068			2.24	0.4							

Appendix 13 Trace element content of formation waters in the Vosges, Hochwald and Pechelbronn-Soultz Basin

Well No.	BGR No.	As	Sb	Se
Mitschd	6000/1			
Mitschd	6000/2			
Mitschd	6000/3	0.015	<0.001	
Drachen E	6001/1			
Drachen E	6001/2			
H I	6003/1			
H I	6003/2			
H II	6004/1			
H II	6004/2			
H II	6004/3	0.015	<0.002	<0.0002
AEP Lobsann	6005/1			
AEP Lobsann	6005/2			
Mar 101	6006/1			
Mar 101	6006/2			
Sept Font.	6007/1			
Sept Fontaine	6007/2	0.012	<0.002	<0.0002
Liebfrauental	6011/1	1.4		
Liebfrauental	6011/2	0.65	0.03	<0.002
3262	6012/1			
3262	6012/2	0.002	<0.001	0.001
3262	6012/3	0.003	<0.002	<0.002
Weiler 2	6013			
Romaine	6015/1			
Romaine	6015/2			
Romaine	6015/3			
Romaine	6015/4			
Romaine	6015/5	0.072	0.031	
Celtic	6016/1			
Celtic	6016/2			
Celtic	6016/3			
Mors 3a	6017/1			
Mors 3a	6017/2			
Mors 3a	6017/3	1.3	0.007	
Mors 3b	6018/1			
Mors 3b	6018/2			

Appendix 13 Trace element content of formation waters in the Vosges, Hochwald and Pechelbronn-Soultz Basin

Well No.	BGR No.	Location	Formation	B	F	Br	I	NH4	Li	Rb	Cs	Sr	Ba	Th
Mors 3b	6018/3	Morsbronn	Bsdst											
Mors 3b	6018/4	Morsbronn	Bsdst	3	1.6	12.8	0.1		5.5			11		
Phillipsb	6019/1	Phillipsbourg	Bsdst											
Phillipsb	6019/2	Phillipsbourg	Bsdst											
Riesthal	6020	Phillipsbourg	Bsdst											
Bitche	6021	Bitche	Bsdst											
Souffl S1	6022	Soufflenheim	T											
Souffl FII	6023	Soufflenheim	T		0.06									
Moth F1	6024	Mothern	Q		0.22									
Hardt 1	6025	Wissembourg	T											
Four a Chaux	6026/5	Lembach	MK	0.03	<0.1	<0.2	<0.05		0.005			<0.1		
Lembach 'N	6027	Lembach	Bsdst											
Lembach 'N	6028	Lembach	Bsdst											
Lembach 'E	6029	Lembach	Bsdst											
Lembach 'E	6030	Lembach	Bsdst											
Lembach 'NW	6031	Lembach	Bsdst											
Lembach 'NW	6032	Lembach	Bsdst											
Hochwald	6034	Hochwald	Bsdst											
Roeschw S1	6036	Roeschwoog	Plio		0.06				0.28			0.6	0.075	
Beinheim S1	6037	Beinheim	Plio		0.1				0.022			0.27	0.053	
Haguenau	6038	Haguenau	Plio											
Haguenau 55	6039	Haguenau	Plio											
Bischwiller	6041	Bischwiller	Plio											
Rothbach F1	6042	Rothbach	Bsdst											
Rothbach F2	6043	Rothbach	Quat											
Schweighaus.	6045	Schweighause	Plio											
Roeschw 21	6046/1	Roeschwoog	Plio											
Roeschw 21	6046/2	Roeschwoog	Plio						0.6			0.74		
Roeschw 21	6046/3	Roeschwoog	Plio						0.52			0.69		
Betsch/Aloxar	6047	Betschdorf	Plio	0.03	<0.1	0.02	<0.05		0.011			0.3		
Schreiner	6048	Soultz	Ps	0.03	0.1	0.6	0.05		0.013			0.4		
Helions II	6049/1	Pechelbronn	MK/Bsdst	2.1	2.6			4	23					
Helions II	6049/2	Pechelbronn	MK/Bsdst	6.7	5.3			6.2	46			53	2.4	
Helions II	6049/3	Pechelbronn	MK/Bsdst	6.1	2.8	46	0.42	5.7	42			51	1.2	
Helions II	6049/4	Pechelbronn	MK/Bsdst	8.2	2.6	47.5	0.32	5	36			68	1.2	
Helions II	6049/5	Pechelbronn	MK/Bsdst	8.8	2.8	29	0.32	5.6	33			70	3.3	

Appendix 13 Trace element content of formation waters in the Vosges, Hochwald and Pechelbronn-Soultz Basin

Well No.	BGR No.	U	Al	V	Cr	Fe	Mn	Co	Ni	Cu	Zn	Cd	Pb	Ag
Mors 3b	6018/3					2	0.39							
Mors 3b	6018/4		0.01			1.8	0.37	0.01	<0.003	0.03	0.03	<0.0002	0.004	
Phillipsb	6019/1					<0.05	<0.05							
Phillipsb	6019/2													
Riesthal	6020					0.08	0.01							
Bitche	6021					0.05	<0.01							
Souffl S1	6022					1.4	0.05							
Souffl FII	6023					0.92	0.03							
Moth F1	6024					0.076	0.002							
Hardt 1	6025					0.03	0.02							
Four a Chaux	6026/5		0.02			<0.02	<0.01	<0.001	<0.001	0.001	0.028	<0.0001	0.002	
Lembach 'N	6027					0.01								
Lembach 'N	6028					<0.01								
Lembach 'E	6029					0.02								
Lembach 'E	6030					0.01								
Lembach 'NW	6031					0.02								
Lembach 'NW	6032					0.02								
Hochwald	6034					<0.01								
Roeschw S1	6036		0.013		0.004	0.12	0.03		0.1	0.006	0.018	<0.0001	<0.001	
Beinheim S1	6037		0.02		0.004	0.056	0.02		0.002	0.008	0.016	<0.0001	<0.001	
Haguenau	6038					0.9	<0.01							
Haguenau 55	6039					0.8	<0.01							
Bischwiller	6041													
Rothbach F1	6042					0.19	0.25							
Rothbach F2	6043					0.46	0.1							
Schweighaus.	6045					<0.01	<0.01							
Roeschw 21	6046/1					<0.01	<0.01							
Roeschw 21	6046/2					0.02	0.006							
Roeschw 21	6046/3					0.14								
Betsch/Aloxar	6047		0.4			0.77	0.08	<0.001	<0.001	0.0035	0.057	<0.0001	0.002	
Schreiner	6048		0.01			0.02	<0.01	<0.001	0.001	0.0006	0.125	<0.0001	0.001	
Helions II	6049/1													
Helions II	6049/2		1.95		0.09	5.6	1.6		0.067	0.038	0.072	0.038	0.058	
Helions II	6049/3		1.35		0.072	4.7	1.6		0.07	0.04	0.052	0.02	0.026	
Helions II	6049/4		1.63		0.004	5.4	1.8		0.03	0.06	0.71	0.0006	0.008	
Helions II	6049/5		0.77		0.04	5.4	1.7		0.024	0.04	0.31	0.006	0.026	

Appendix 13 Trace element content of formation waters in the Vosges, Hochwald and Pechelbronn-Soultz Basin

Well No.	BGR No.	As	Sb	Se
Mors 3b	6018/3			
Mors 3b	6018/4	1.1	<0.001	
Phillipsb	6019/1			
Phillipsb	6019/2			
Riesthal	6020			
Bitche	6021			
Souffl S1	6022			
Souffl FII	6023			
Moth F1	6024			
Hardt 1	6025			
Four a Chaux	6026/5	0.022	<0.001	
Lembach 'N	6027			
Lembach 'N	6028			
Lembach 'E	6029			
Lembach 'E	6030			
Lembach 'NW	6031			
Lembach 'NW	6032			
Hochwald	6034			
Roeschw S1	6036			
Beinheim S1	6037			
Haguenau	6038			
Haguenau 55	6039			
Bischwiller	6041			
Rothbach F1	6042			
Rothbach F2	6043			
Schweighaus.	6045			
Roeschw 21	6046/1			
Roeschw 21	6046/2			
Roeschw 21	6046/3			
Betsch/Aloxar	6047	0.012	0.001	
Schreiner	6048	0.0018	<0.001	
Helions II	6049/1			
Helions II	6049/2	1.5		0.001
Helions II	6049/3	1.5		0.001
Helions II	6049/4	1.4		0.004
Helions II	6049/5	1.5		0.002

Appendix 13 Trace element content of formation waters in the Vosges, Hochwald and Pechelbronn-Soultz Basin

Well No.	BGR No.	Location	Formation	B	F	Br	I	NH4	Li	Rb	Cs	Sr	Ba	Th
Helions II	6049/6	Pechelbronn	MK/Bsdst	6.3	2.3	30.5	0.29	6.2	50			88	0.76	
Helions II	6049/7	Pechelbronn	MK/Bsdst	7	2.1	36	0.17	5.2	42			75	1.5	
Helions II	6049/8	Pechelbronn	MK/Bsdst	6.6	2	36	0.17	5.2	42			70	2.1	
Helions II	6049/9	Pechelbronn	MK/Bsdst	7.5	2.4	31	0.37	6.4	32			67	1	
Helions II	6049/10	Pechelbronn	MK/Bsdst											
Helions II	6049/11	Pechelbronn	MK/Bsdst	6.2	2.1	34	0.33	6.4	32			66	1.8	
Helions II	6049/12	Pechelbronn	MK/Bsdst	7	2.1	35.5	0.36	6.6	37			79	2.12	
Helions II	6049/13	Pechelbronn	MK/Bsdst	7.1	2.3	35.5	0.36	6.6	37			67		1.2
Helions II	6049/14	Pechelbronn	MK/Bsdst	6.6	2.5	61.5		5.4	14.6			74		
Helions II	6049/15	Pechelbronn	MK/Bsdst	7.2	2.05	32	0.28	6	39			75		
Helions II	6049/16	Pechelbronn	MK/Bsdst	7.1	2.5	50	0.6	4.5	30	3	1.65	54	0.64	<0.001
Saline	6050	Soultz	Ps			0.04	0.007	9.2						
Fried/3969	6051	Kutzenhausen	Pi			26	0.7	6.1	4			13		
Fried/3969	6051	Kutzenhausen	Pi	8.6	1.8	35	0.9	5.7	6.8	0.006	0.004	13	2.3	<0.001
4275	6052	Merkwiller	Ps			0.6	0.1	1.1	0.7	0.005	0.003	2.1		
4275	6052/2	Merkwiller	Ps	2.5	0.5	0.7	0.1	1.1	0.7	0.005	0.003	2.4	0.2	<0.001
RG1	6053	Kutzenhausen	Ps			8.7	0.6	4.2	2.5			9.1		
Mattenmühle	6054	Soultz	SG	1.5	0.2	6.1		2.2	0.9			3.8		
Mattenmühle	6054	Soultz	SG	1.6	0.2	6.6		2.8	1.1	0.005	0.003	3.6	0.07	0.001
GPK-1	6055	Soultz	Base	18.8	2.7	190		28	119			360		
Hoel-1 1)	Cl:86200	Hoelschloch	GR			900	16		37			243		
Bruch-1a 2)		Bruchsal	Bsdst			309	8.7		227			261		

1) courtesy of TOTAL 2) Matthess, 1986

Appendix 13 Trace element content of formation waters in the Vosges, Hochwald and Pechelbronn-Soultz Basin

Well No.	BGR No.	U	Al	V	Cr	Fe	Mn	Co	Ni	Cu	Zn	Cd	Pb	Ag
Helions II	6049/6		0.43		0.04	7.2	2		0.052	0.036	0.15	<0.0001	<0.001	
Helions II	6049/7		0.83		0.036	4.7	1.7		<0.001	0.04	0.162	<0.0001	<0.001	
Helions II	6049/8		0.21		0.042	5.2	1.8		0.028	0.044	0.3	0.016	0.016	
Helions II	6049/9		0.48		0.04	4.95	1.8						<0.001	
Helions II	6049/10					4.1	1.5							
Helions II	6049/11		0.48		0.026	5.2	1.7		0.012	0.046	0.106	<0.0001	<0.001	
Helions II	6049/12		0.21		0.01	5.9	2		0.014	0.04	0.34	0.002	<0.001	
Helions II	6049/13		0.18		0.03	6	1.5		0.04	0.04	0.112	0.006	0.006	
Helions II	6049/14		<0.01			4.5	1.5	<0.01	<0.05	0.01	0.07	<0.0002	0.01	
Helions II	6049/15		0.16		0.04	6.2	1.6		0.02	0.04	0.08	0.002	<0.024	
Helions II	6049/16	<0.001	0.1	0.3	0.007	4.8	1.7	0.041	0.078		0.4	0.005	<0.001	<0.001
Saline	6050		2			1.3								
Fried/3969	6051													
Fried/3969	6051	<0.001	0.007	0.12	0.002	13.2	0.13	0.003	0.003		0.025	0.003	<0.001	<0.001
4275	6052													
4275	6052/2	<0.001	0.13	0.005	0.001	7.1	0.35	0.002	0.001		0.013	0.002	<0.001	<0.001
RG1	6053													
Mattenmühle	6054					0.8	0.04	<0.001	0.002	<0.001	0.005		0.6	
Mattenmühle	6054	<0.001	0.55	0.01	0.001	0.75	0.04	0.004	<0.001		0.01	0.003	0.002	<0.001
GPK-1	6055													
Hoel-1 1)	Cl:86200													
Bruch-1a 2)														

1) courtesy of TOTAL

Appendix 13 Trace element content of formation waters in the Vosges, Hochwald and Pechelbronn-Soultz Basin

Well No.	BGR No.	As	Sb	Se
Helions II	6049/6	1.5		0.002
Helions II	6049/7	2		0.01
Helions II	6049/8	1.2		0.002
Helions II	6049/9	1.6		0.002
Helions II	6049/10			
Helions II	6049/11	2		0.006
Helions II	6049/12	1.2		0.003
Helions II	6049/13	1.6		0.004
Helions II	6049/14	2		0.004
Helions II	6049/15	2.7		0.003
Helions II	6049/16	2.1	0.02	
Saline	6050			
Fried/3969	6051			
Fried/3969	6051	0.003	<0.002	<0.002
4275	6052			
4275	6052/2	0.04	<0.002	<0.002
RG1	6053			
Mattenmühle	6054	0.001	<0.001	0.001
Mattenmühle	6054	0.003	<0.002	<0.002
GPK-1	6055			
Hoel-1 1)	Cl:86200			
Bruch-1a 2)				

1) courtesy of TOTAL

Appendix 13 Trace element content of formation waters in the Vosges, Hochwald and Pechelbronn-Soultz Basin

Zone	BGR No.	Well no.	KB	Location	Date	Formation	Water level m	Yield m3/h	mean depth m	Source
VOSGES	6021	Bitche	285	Bitche	14.8.85	Bsdst	4.65	160	29-47	well
	6019	Phillip	218	Phillipsburg	14.8.85	Bsdst	37.82	24	15-70	well
	6020	Riesthal	285	Riesthal	7.8.86	Bsdst		15		spring
	6016/1	Celtic	204	Niederbronn	7.8.86	Bsdst		10.8		spring
	6016/2	Celtic	204	Niederbronn	18.2.87	Bsdst		10.8		spring
ZABERNER FRAC.ZONE	6015/1	Romaine	215	Niederbronn	13.8.86	Bsdst		13.5		spring/spa
	6015/2	Romaine	215	Niederbronn	18.2.87	Bsdst		13.5		spring/spa
LEMBACH GRABEN	6026/1	F.Chaux	229	Lembach	16.2.87	Bsdst&MK	artes.	7	41	well, unused
	6011/1	F1	175	Liebfrauental	17.2.87	Bsdst & MK	artes.	125	24-116	well
	6011/2	F1	175	Liebfrauental	21.6.87	Bsdst & MK	artes.	125	24-116	well
	6011/3	F1	175	Liebfrauental	5.12.87	Bsdst & MK	artes.	125	24-116	well
HOCHWALD HORST	6010/1	Pfaffensl.	367	Pfaffenschlick	9.1185	Bsdst				spring
	6008/1	AEP Drachen	350	Drachenbronn	00.11.85	Bsdst				spring
	6009/1	Brülbächel	290	Hochwald	15.11.85	Bsdst		11		spring
RHINE FAULT	6007/1	Sept Font.	268	Hochwald	4.6.85	Bsdst		30		spring
	6007/2	Sept Font.	268	Hochwald	9.11.85	Bsdst		30		spring
	6007/3	Sept Font.	268	Hochwald	27.8.87	Bsdst				spring
	6001/1	Drachen E	325	Drachenbronn	14.11.85	Bsdst	48	35	50-110	well
	6002/1	Drachen W	350	Drachenbronn	9.11.85	Bsdst		10		well
	6003/1	H1	295	Hochwald	15.11.85	Bsdst	3.5	28	53-167	well
	6004/1	H II	304	Hochwald	12.8.85	Bsdst	9.25	10	50-170	well
	6000/1	Mitsch. F2	221	Mitschdorf	12.8.85	Bsdst	artes.	80	48-187	well
	6000/2	Mitsch. F2	221	Mitschdorf	16.2.87	Bsdst	artes.	80	48-187	well
	6017/1	Mors 3a	187	Morsbronn	00.00.77	MK	artes.		324-392	well,spa
	6017/2	Mors 3a	187	Morsbronn	13.8.85	MK	artes.		324-392	well,spa
	6017/3	Mors 3a	187	Morsbronn	17.2.87	MK	artes.	49	324-392	well,spa
	6018/1	Mors 3b	185	Morsbronn	00.00.77	Bsdst	artes.		465-680	well,spa
	6018/2	Mors 3b	185	Morsbronn	00.00.77	Bsdst	artes.		465-680	well,spa
	6018/3	Mors 3b	185	Morsbronn	28.3.78	Bsdst	artes.		465-680	well,spa
	6018/4	Mors 3b	185	Morsbronn	13.8.85	Bsdst	artes.		464-680	well,spa
	6018/5	Mors 3b	185	Morsbronn	17.2.87	Bsdst	artes.	9	465-680	well,spa

Appendix 14 Isotope Data

Zone	BGR No.	Temperature (C)	pH	EC S/cm x E-6	Cl mg/l	SO4 mg/l	HCO3 mg/l	CO2 mg/l	O18 o/oo SMOW	D o/oo SMOW
VOSGES	6021	12.7	5.6	50	7	1	8		-10.57	-57
	6019	13.9	8.2	160	4	5	92		-8.99	-61
	6020	11	6.2	70	4	7	20		-9.04	-61.8
	6016/1	11	6.5	70	4	7	20		-9.06	-62.8
	6016/2	9.8							-8.99	-59.8
ZABERNER FRAC.ZONE	6015/1	18.2	6.8	6900	2690	61	305		-9.28	-66
	6015/2	18.1	6.6	7900	2740	45	307	98	-9.18	-62.7
LEMBACH GRABEN	6026/1	16	7.2	270	2	4	165	18	-8.62	-62.8
	6011/1	12.6	6.7	130					-8.85	-60.4
	6011/2	12.8	6.2	130	5	19	81	28	-8.54	-63.4
	6011/3								-8.85	-63.6
HOCHWALD HORST	6010/1									
	6008/1									
	6009/1	9.6	5.8	60	5	11				
RHINE FAULT	6007/1	12	7.6	130	5	3	74		-8.69	-62
	6007/2									
	6007/3	11.2	6.1	70	5	3	23	26	-8.85	-61.6
	6001/1	11	6.8	110	2	16	61	17		
	6002/1									
	6003/1	11.2	6.7	60	2	1	31	13		
	6004/1	12.7	6.9	75	1	3	44		-8.84	-62
	6000/1		6.4	60	1	3	27		-8.8	-61
	6000/2	13.3	7	50	2	2	19	14	-8.82	-61.5
	6017/1								-9.9	
	6017/2		6.7	9000	2860	570	310		-9.7	-68
	6017/3	41.2	6.1	9000	2750	430	300	97	-9.59	-67.4
	6018/1								-9.77	
	6018/2								-10	
	6018/3	41.9	6.8	6850	2240	350	290	200	-9.6	-69
	6018/4		6.7	7500	360	300			-10	-68
	6018/5	39.5	6.4	7700	2300	270	300	73	-9.77	-67.8

Appendix 14 Isotope Data

Zone	BGR No.	H3 TU	C13 o/oo PDB	C14 (pmc)	C14, convent. age in years	C14 corrected Ingr.-Pears. Eq.	S34 o/oo CD	Reference
VOSGES	6021							BGR
	6019							BGR
	6020	44.8 ±1.2						BGR
	6016/1	20.1 ±1.4						BGR
	6016/2	21.5 ±1.4						BGR
ZABERNER FRAC.ZONE	6015/1	<1.8						BGR
	6015/2	<2.2	-6.4	8.6 ±0.3	19720 ±305	8380		BGR
LEMBACH GRABEN	6026/1	<1.2	-15	43.2 ±0.5	6730 ±85	2640		SGAL
	6011/1	<2.1						SGAL
	6011/2	<1.8	-23.2	80.7 ±2.9	1725 ±285	1123		SGAL
	6011/3							SGAL
HOCHWALD HORST	6010/1	66 ±6						SGAL
	6008/1	67 ±6						SGAL
	6009/1	43 ±4						SGAL
RHINE FAULT	6007/1	8 ±0.6						BGR
	6007/2	8 ±2						SGAL
	6007/3	7.5 ±1	-19.6	81.6 ±1.5	1635 ±150	recent		BGR
	6001/1	2 ±1						SGAL
	6002/1	12 ±2						SGAL
	6003/1	12 ±2						SGAL
	6004/1	3.3 ±1	-18.8	67.4 ±2.3	3165 ±275	860		BGR
	6000/1							BGR
	6000/2	<2.2	-19.7	85.6 ±1.1	1250 ±105	> 150		BGR
	6017/1						16.22	SGAL
	6017/2							BGR
	6017/3	<2.1	-5.7	3.6 ±0.3	26685 ±635	14800		BGR
	6018/1							SGAL
	6018/2						16.01	SGAL
	6018/3	2 ±1					17.4	SGAL
	6018/4							BGR
	6018/5	<1.4	-5.4	3.5 ±0.3	26900 ±600	14600		BGR

Appendix 14 Isotope Data

Zone	BGR No.	Well no.	KB	Location	Date	Formation	Water level m	Yield m3/h	mean depth m	Source
	6006/1	Mar 101	267	Marienbronn	7.8.86	Bsdst	artes.		842-878	injec.well
	6006/2	Mar 101	267	Marienbronn	23.5.87	Bsdst	artes.	0.7	842-878	injec.well
	6049/1	Helion II	161	Pechelbronn	29.3.78	Bsdst & MK	artes.	13.5	905-1146	well
	6049/17	Helion II	161	Pechelbronn	12.8.85	Bsdst & MK	artes.		905-1146	well
	6049/14	Helion II	161	Pechelbronn	18.2.87	Bsdst & MK	artes.	18.5	905-1146	well
	6049/18	Helion II	161	Pechelbronn	22.5.87	Bsdst & MK	artes.	18.2	905-1146	well
PECHEL-	6049/19	Helion II	161	Pechelbronn	20.6.87	Bsdst & MK	artes.	18.2	905-1146	well
BRONN	6049/20	Helion II	161	Pechelbronn	6.12.87	Bsdst & MK	artes.	18.2	905-1146	well
	6052/1	4275	176	Pechelbronn	21.6.87	Ps	artes.	little	85-148	oil well
SOULTZ	6051/1	3969	163	Kutzenhausen	2.6.87	ZD	artes.	little	482-505	oil well
	6051/2	3969	163	Kutzenhausen	21.6.87	ZD	artes.	little	482-505	oil well
	6051/3	3969	163	Kutzenhausen	6.12.87	ZD	arts.	little		
BASIN	6012/1	3262	148	Kutzenhausen	12.8.85	ZD	artes.		429-435	oil well
	6012/2	3262	148	Kutzenhausen	2.6.87	ZD	artes.	0.04	429-435	oil well
	2976/1	4616	155	Kutzenhausen	26.10.87	LK-Base	4 bar	1.6	970-1494	oil well
	2976/2	4616	155	Kutzenhausen	26.10.87	LK-Base	4 Bar	1.6	970-1494	oil well
	BGRM	GPK-1	150	Soultz	00.00.88	Basement			1817	geothermal wel
	6053/1	RG1	150	Soultz	22.5.87	Ps	>+0.34	0.2	10-Sep	shallow well
	6054/1	Mattenm.	144	Soultz	2.6.87	SG	artes.	0.3	0-10	dug well
	6048/1	Schreiner	163	Soultz	12.2.87	Quat.		1.5	10-Jul	water well
	6047/1	Aloxan	145	Betschdorf	19.2.87	Quat.		4	17-32	water well
	GTB-Br 1a	Bruch-1a	±120	Bruchsal		Bsdst			1742-1875	geotherm.well
BLACK	GTB-Br 2	Bruch-2	±120	Bruchsal		Permian			2440-2470	geotherm.well
		Wildbad	±500	Wildbad		Rotliegend	artes.		104	therm. well
FOREST		Bad Herrenalb	±450	Herrenalb			artes.		600	therm. well
		Bad Rotenfelfs	±200	Rotenfels			artes.		123	therm. well
		Friedrichquelle	±200	Baden-Baden			artes.			therm. well

Zone	BGR No.	Temperature (C)	pH	EC S/cm x E-6	Cl mg/l	SO4 mg/l	HCO3 mg/l	CO2 mg/l	O18 o/oo SMOW	D o/oo SMOW
	6006/1	25	7.7	4050	1250	45	580		-7.63	-60.2
	6006/2	17.1		4600	1230				-7.36	-59.9
	6049/1	71	5.1	10000	8840	560	287	200	-9.6	-69.9
	6049/17	70	6.2	25900	10700	620	310		-8.57	-66
	6049/14	72.4	5.9	302000	11600	460	300	99	-8.64	-62.4
	6049/18	72.4							-8.41	-59.3
PECHEL-	6049/19	72.5	5.8	31100					-8.76	-58.7
BRONN	6049/20								-8.68	-65.8
	6052/1	11	7.1	1600	81	11	620	41	-8.31	-59.1
SOULTZ	6051/1	13.5		13600					-8.57	-58.7
	6051/2	13.5	7.8	14700	4990	4	410	20	-9.04	-63.5
	6051/3								-8.98	-64.5
BASIN	6012/1		7.1	31200	13100	<3	250		-8.03	-60
	6012/2	15.7	7.4	32900	12300	7	250		-7.89	-54
	2976/1	120	5.5		48000	380	590	surface	-6.69	-52.8
	2976/2	120	6.4		48400	170	500	1388	-7.9	-48.2
	BGRM 1								-0.3	-25.3
	6053/1	12.7	7.1	6600	1850	0.2	430		-8.45	-55.9
	6054/1	12.7	7	3500	890	88	510	44	-7.97	-53.4
	6048/1	12.2	7	990	86	23	400	30	-7.91	-56.7
	6047/1	12.2	7	640	14	5	430	50	-8.02	-56.4
	GTB-Br 1a								-3.06	-37.2
BLACK	GTB-Br 2								-2.99	-35.5
		35.5							-9.5	-64.4
FOREST		32							-10.1	-68.7
		19							-9.3	-65.7
		42.9							-9.7	-66.1

Appendix 14 Isotope Data

Zone	BGR No.	H3 TU	C13 o/oo PDB	C14 (pmc)	C14, convent. age in years	C14 corrected Ingr.-Pears. Eq.	S34 o/oo CD	Reference
	6006/1							BGR
	6006/2	13 ±0.7						BGR
	6049/1	4 ±1					17.6 ±0.2	SGAL
	6049/17	<1.8	-2.8	2.1 ±0.4	31100 +1800/	15150	-1460	BGR
	6049/14	<1.8	-4.1	1.6 ±0.3	31930 +1545/	20000	-1215	BGR
	6049/18							BGR
PECHEL-	6049/19							BGR
BRONN	6049/20							BGR
	6052/1	4.9 ±0.9	-15.5	28.1 ±1.1	10200 ±300	6400		BGR
SOULTZ	6051/1	<2.1						BGR
	6051/2	2.4	-4.6	6 ±0.8	22580 ±1030	8000		BGR
	6051/3							BGR
BASIN	6012/1	<1.8						BGR
	6012/2	<2	1.1	1 ±0.7	>33835	CH4 contam.		BGR
	2976/1	29 ±1.4			values ???			BGRM
	2976/2	29 ±3						BGRM
	BGRM	6 ±3			Vuataz et al. 88			Vuataz'88
	6053/1	<1.9						BGR
	6054/1	<2.1	-14.3	46.4 ±0.4	6165 ±75	1600		BGR
	6048/1	28.0 ±0.8	-13.9	90.1 ±0.9	835 ±80	recent		BGR
	6047/1	<2.5	-14.1	70.1 ±0.8	2850 ±95	1000		BGR
	GTB-Br 1a	1.6 ±0.6	-2.31	<1.6	>30000			Matthess'86
BLACK	GTB-Br 2	0.9 ±0.7	-6.2	<2	>30000			Matthess'86
								Friedrichsen
FOREST								Friedrichsen
								Friedrichsen
								Friedrichsen

Wellnr.	Location	KB	end depth, m	inter.depth, m	mean depth, m	Formation	Temp.[C]	Comment
2933	K	153	533	503-523	513		45	SAEM
2951	K	164	490	415-430	422.5		hot	SAEM
2951	K	164	490	479-490	484.5			SAEM
3031	Hoel	178	553		522			SAEM
3050	Kn	153	474		474			SAEM
3054	Ks	146	420		381			SAEM
3075	Hoel	167	600		600	ZD	53.3	SAEM
3076	Hoel	177	560		560	ZD	56.7	SAEM
3119	Ks	148	402	390-396	393			SAEM
3121	Hoel	179			357		38.7	SAEM
3128	Kn	146	490				N/A	SAEM
3133	Hoel	152	550				N/A	SAEM
3134	Hoel	179	465				N/A	SAEM
3164	Kn	168	550	503-505	504			SAEM
3165	Pech	201	466				N/A	SAEM
3175	Hoel	176	354				N/A	SAEM
3176	Hoel	189		600-610	605		50.4	SAEM
3180	Pech	180	570	560-570	565	ZD	60	SAEM
3188	Pech	197	511				N/A	SAEM
3201	Hoel	181	545		540			SAEM
3204	Walbourg	152					N/A	SAEM
3214	Pech	209	450				N/A	SAEM
3220	Hoel	177	360				N/A	SAEM
3230	Hoel	188	550				N/A	SAEM
3265	Hoel	157	406	395-406	400.5		47.4	SAEM
3318	Hinzbach	168			903		82	SAEM
3368	Hoel	171	550	540-550	545			SAEM
3373		146	558	477-519	498		50	SAEM
3401	Ks	178	600		579		45-50	SAEM
3406	Hoel	186	495	423-438	430.5			SAEM
3406	Hoel	186	495		485			SAEM
3441	Hoel	173	660		645			SAEM
3553	Hoel	171	445		335			SAEM
3578	Soultz	154	532		532			SAEM
3613	Kn	158	525		460			SAEM
3647	Kn	168	998		735	K	75.1	SAEM

Appendix 15 Subsurface temperature data

Wellnr.	Location	KB	end depth, m	inter.depth, m	mean depth, m	Formation	Temp.[C]	Comment
3647	Kn	168	998		998	LK	97.5	SAEM
3661	Soultz	176	919		80	Pi	29.8	SAEM
3661	Soultz	176	921		450	ZD	61.5	SAEM
3661	Soultz	176	921		820	K	103	SAEM
3661	Soultz	176	921		865	K	110	SAEM
3661	Soultz	176	921		910	K	112	SAEM
3661	Soultz	176	921		998	LK	117	SAEM
3716	Ohlungen	182			769		53	SAEM
3717	Birlenbach	750	749		700		40	SAEM
3719	Ohlungen	184			9	50	63	see 4547,SAEM
3728	Kreuzecke	178		696-719	702.5		64	SAEM
3793	Kreuzecke	201			790		68.5	SAEM
3804	Kreuzecke	155			660	ZD	58	SAEM
3804	Kreuzecke	155			960	J	75	SAEM
3937	Pech	164					N/A	SAEM
3956	K	176	1573		1463	Bsdst	109	Fault, after 38h
3956	K	176	1573		1500	Bsdst	112	Fault,after 18h
4036	Pech	185	1309				N/A	
4152	Pech	186	1230		1000	J	53.5	
4487	Ohlungen	195	778		774	LK	50	Fault
4500	Soultz	149	971		900	MK	112	11.3/100m
4502	Ks	179	940					n/A
4515	Soultz	146	864		200	P sup.	47	
4515	Soultz	146	864		400	ZD	68	
4515	Soultz	146	864		600	ZD	87	
4515	Soultz	146	864		800	K	100	11.9.49
4515	Soultz	146	864		857	MK	104	5.1.50 avalaible
4515	Soultz	146	864		300		62	SAEM, 22.5.50
4515	Soultz	146	864		500		82.5	
4515	Soultz	146	864		700		102	
4515	Soultz	146	864		857		109.7	
4516	Soultz	187	930		800	K	92	
4541	Soultz	150	950	847-890	868.5	LK	95	
4541	Soultz	150	950	895-905	940	MK	106	SGAL
4547	Ohlungen	193	876		870	MK	60	see 3719
4548	Hochstett	200	1157	1095-1130		MK	66.5	61-72C

Appendix 15 Subsurface temperature data

Wellnr.	Location	KB	end depth, m	inter.depth, m	mean depth, m	Formation	Temp.[C]	Comment
4550	Soultz	150			650	K	63	SAEM
4550	Soultz	150			695	K(f)	66	SAEM
4550	Soultz	150			750	K	69	SAEM
4550	Soultz	150			800	K	76	SAEM
4550	Soultz	150			900	MK	83	SAEM
4550	Soultz	150			960	MK	93	SAEM
4550	Soultz	150	1050		1000	Bsdst	108	SAEM
4554	Soultz	156	857		500	ZD	73.6	Schädel '84
4554	Soultz	156	857		700	J	93.6	SAEM
4554	Soultz	156	857		857	MK	110	SAEM
4555	Soultz	155	873		857	MK	112	SAEM
4555	Soultz	155	873		500	ZD	73	SAEM
4579	Soultz	164	993		970	MK	90	SAEM
4581	Soultz	210	949		940	MK	99.2	SAEM
4583	Soultz	158	1049	885-960		MK	92	SAEM
4583	Soultz	158	1049	984-991	987.5	Bsdst	100	SAEM
4583	Soultz	158	1049	992-1011	1001.5	Bsdst	108	SAEM
4583	Soultz	158	1049	1011-1029	1020	Bsdst	110	SAEM
4583	Soultz	158	1049	1030-1049	1039.5	Bsdst	111	SAEM
4589	Soultz	174	849		843	K	99	fault
4590	Soultz	178	1050	956-976	966	K	83.3	Fault zone
4590	Soultz	178	1050	1016-1021	1018.5	Bsdst	89	SAEM
4590	Soultz	178	1050	1020-1025	1022.5	Bsdst	89	SAEM
4597	Hochstett	200	1065	1019-1040	1029.5	MK	57	SAEM
4597	Hochstett	200	1065	1040-1065	1052.5	MK	61	SAEM
4598	Soultz	148	855	841-855	848	MK	93.5	fault
4601	Hoel	169	1010	999-1010	1004.5	MK	99	?
4602	Kn	182	1065	969-1010	990	LK	88	
4602	Kn	182	1065	1041-1065	1053	MK	95	
4606	Soultz	197	991	928-959	943	MK	114.5	fault, SAEM
4607	Soultz	159	907.8		898	MK	105	fault, SAEM
4609	Ks	147	982	862-899	878	MK	97	fault, SAEM
4609	Ks	147	982		920	Bsdst	99	SGAL
4609	Ks	147	982	962-982	972	Bsdst	102	SAEM
4609	Ks	147	982	968-977	972.5	Bsdst	103	SAEM
4613	Soultz	162	1050	982-1015	998.5	MK	102	SAEM

Appendix 15 Subsurface temperature data

Wellnr.	Location	KB	end depth, m	inter.depth, m	mean depth, m	Formation	Temp.[C]	Comment
4613	Soultz	162	1050	1014-1027	1020.5	MK	112	SAEM
4613	Soultz	162	1050	1027-1037	1032	MK	115.5	SAEM
4616	Soultz	155	1500	850-874	862	K	72	SAEM
4616	Soultz	155	1500	998-1008	1003	MK	77	SAEM
4616	Soultz	155	1500	1009-1028	1018.5	MK	80	SAEM
4616	Soultz	155	1500	1029-1042	1035.5	MK	81	SAEM
4616	Soultz	155	1500	1042-1060	1051	MK	87	SAEM
4616	Soultz	155	1500	1115-1145	1130	Bdst	99.5	SAEM
4616	Soultz	155	1500	1192-1196	1194	Bsdst	119	SAEM, fault
4616	Soultz	155	1500	1374-1387	1381	Bsdst	123	SAEM
4616	Soultz	155	1500		600		70	BRGM '88
4616	Soultz	155	1500		700	K	82	BRGM '88
4616	Soultz	155	1500		800	MK	93.3	BRGM '88
4616	Soultz	155	1500		900	MK	100.8	BRGM '88
4616	Soultz	155	1500		1000	MK	110	BRGM '88
4616	Soultz	155	1500		1100	MK	115	BRGM '88
4616	Soultz	155	1500		1200	Bsdst	119	BRGM '88
4616	Soultz	155	1500		1350	Bsdst	123	BRGM '88
4618	Berst	218	954	865-898	881.5	LK	60	SAEM
4619	Soultz	151	873	803-825	814	K	81	fault,SAEM,3h
4619	Soultz	151	873	842-876	859	MK	78	fault,SAEM,3h
4620	Soultz	147	837	831-850	840.5	MK	97	fault,SAEM
4620	Soultz	147	837	855-858	856.5	MK	100	SAEM
4626	Soultz	181	890		890	MK	102	SAEM
4630	Merk	170	1185	749-779	764	K	80	SAEM
4630	Merk	170	1185	889-910	899.5	LK	105	SAEM
4635	Berst	175	831		775	LK	75	SAEM
4636	Soultz	147	914	841-859	850	LK	84.5	fault,SAEM
4636	Soultz	147	914	880-900	890	MK	86	fault,SAEM
4636	Soultz	147	914	901-914	907.5	MK	90	fault,SAEM
4639	Soultz	107	848	795-809	802	LK	87	fault,SAEM
4639	Soultz	107	848	835-840	837.5	MK	89.5	SAEM
4642	Soultz	156	871	832-852	842	MK	94.5	SAEM
4648	Pech	194	892	809-833	823	MK		fault,SAEM
4648	Pech	194	892	882-892	887	MK	64.5	SAEM
4653	Soultz	176	873	816-832	824	LK	85.5	SAEM

Appendix 15 Subsurface temperature data

Wellnr.	Location	KB	end depth, m	inter.depth, m	mean depth, m	Formation	Temp.[C]	Comment
4662	Hoel	167	1205	1129-1156	1142.5	LK	102	SAEM
4662	Hoel	167	1205	1185-1205	1195	MK	109	SAEM
4670	Merk	168	806	779-805	792	K	70/75	SAEM
4677	Pech	184	832	793-832	812.5	J	70	SAEM,fault
4685	Soultz	179	1089	953-977	965	LK	81	SAEM
4687	Berstheim	203	1557	900-928	914	LK	57	SAEM
4687	Berstheim	203	1557	1039-1093	1065	Bsdst	67	SAEM
4687	Berstheim	203	1557	1537-1555	1546	Bsdst	75	SAEM
4712	Ritt	176	1853	1658-1680	1669	MK	159	SAEM
4712	Ritt	176	1853	1746-1762	1754	MK	155	SAEM
4712	Ritt	176	1853	1763-1777	1770	MK	159	SAEM
4713	Pech	168	772	756-778	767	K	68	SAEM
4716	Souflenh.	131	1868		1295	J	68	SAEM
4716	Souflenh.	131	1868		1465	K	88	SAEM
4716	Souflenh.	131	1868		1505	K	91	SAEM
4716	Souflenh.	131	1868		1537	K	100	SAEM
4716	Souflenh.	131	1868		1650	LK	105	SAEM
4716	Souflenh.	131	1868		1691	MK	109	SAEM
4716	Souflenh.	131	1868		1723	MK	106	SAEM
4716	Souflenh.	131	1868		1744	MK	110	SAEM
4716	Souflenh.	131	1868		1764	MK	110	SAEM
4742	Souflenh.	134	1656		1150	J	93	SAEM
4742	Souflenh.	134	1656		1171	J	80	SAEM
4747	Ritt	158	1656	1214-1229	1221.5	J	103	SAEM
4749	Roeschwoog	119	2505	752-785	763.5	NS	39	SAEM
4749	Roeschwoog	119	2505	1022-1049	1035.5	SG	68	SAEM
4749	Roeschwoog	119	2505	2476-2506	2491	MK	137	
4755	Soufflenh.	164	1407	1117-1140	1128.5	ZD	70	SAEM
4756	Soufflenh.	133	1164	1066-1094	1080	ZD	77	SAEM
4759	Soufflenh.	134	1133	1131-1141	1136	ZTrans	82	SAEM,fault zone
4761	Walbourg	165	802	630-654	642	J	49	SAEM,fault
4761	Walbourg	165	802	763-792	782.5	J	61	SAEM
4761	Walbourg	165	802	798-828	813	J	69	SAEM
4762	Soufflenh.	134	2130	804-813	808.5	Pm	60.5	SAEM,faults
4762	Soufflenh.	134	2130	1090-1113	1105.5	J	71.5	SAEM
4762	Soufflenh.	134	2130	1525-1552	1538	LK	126	SAEM

Appendix 15 Subsurface temperature data

Wellnr.	Location	KB	end depth, m	inter.depth, m	mean depth, m	Formation	Temp.[C]	Comment
4765	Forstfeld	116	2150	1565-1605	1685	ZD	72	SAEM
4770	Schirrheim	121	1700	1490-1541	1515.5	J	78	SAEM,faults
4770	Schirrheim	121	1700	1494-1551	1517.5	J	79	SAEM
4770	Schirrheim	121	1700	1555-1591	1573	K	100?	SAEM,fault
4774	Beinheim	116	2520	1493-1460	1523.5	Pm	94	SAEM
4774	Beinheim	116	2520	2058-2090	2074	ZD	110	SAEM
4774	Beinheim	116	2520	2342-2359	2350.5	ZD	127.7	SAEM
4775	Schirrheim	222	1700	1620-1670	1645	J	111	SAEM
4776	Ritters.	137	1592	550-567	558.5	Pm	53	SAEM
4776	Ritters.	137	1592	829-852	840.5	ZD	70	SAEM
4776	Ritters.	137	1592	1312-1337	1324.5	J	96	SAEM
4776	Ritters.	137	1592	1440-1457	1448.5	K	116	SAEM
4776	Ritters.	137	1592	1514-1530	1522	LK	124	SAEM
4776	Ritters.	137	1592	1556-1575	1565.5	MK	125	
4776	Ritters.	137	1592	1576-1591	1583.5	MK	140	SAEM
4776	Ritters.	137	1592					
4777	Beinheim	115	1301	1258-1285	1271.5	P sup.	76	SAEM,fault
4778	Beinheim	118	1084	1058-1088	1073	P sup.	63	SAEM,fault
4780	Schirrheim	121	1580	492-515	503.5	P sup.	53	SAEM,fault
4781	Schirrheim	122	800	756-780	768	Pm	49	SAEM
4782	Schirrheim	122	900	538-560	549	P sup.	32	SAEM
4783	Schirrheim	120	1560	997-1014	1005.5	ZD	58	SAEM
4783	Schirrheim	120	1560	1526-1540	1533	J	83	SAEM
4783	Schirrheim	120	1560	1538-1560	1549	K	84.5	SAEM
4788	Schirrheim	121	572.3	532-572	552	P sup.	40	SAEM
4795	Schönenburg				500		36	PREPA, Lauer 76
Alt 1	Altenstadt	155			500	Pi	29	PREPA, Lauer 76
Croet 1	Croetwiller	175			500	SG	42	PREPA, Lauer 76
Croet 2	Coretwiller	175			500	SG	35	PREPA, Lauer 76
Dief-1	4796	223	440	356-396	371	MK	21	PREPA,fault
Dief-1	4796	223	440	400-431	415.5	Bsdst	21	PREPA,fault
Dief-2	Dieffenbach	238	1210	1009-1035	1017	MK	62	
Do-10	Donau	120	1525	494-500	497	Pm	52	PREPA,fault
Do-10	Donau	120	1525	504-525	514.5	Pi	63	PREPA,fault
Do-11	Donau	119	510	478-490	484	Ps	42	PREPA,fault
Do-16	Donau	119	511					PREPA,fault

Appendix 15 Subsurface temperature data

Wellnr.	Location	KB	end depth, m	inter.depth, m	mean depth, m	Formation	Temp.[C]	Comment
Do-8	Donau	119	529	488-511	499.5	Ps	38	PREAP,fault
Do-9	Donau	119	505	475-491	483	Pm	37	PREPA,fault
Do-9	Donau	119	505	492-504	498	ZD	42	PREPA,fault
Hag-1	Haguenau	150	1540		50		13.7	PREPA, Delattre '68
Hag-1	Haguenau	150	1540		100		14.11	PREPA, Delattre '68
Hag-1	Haguenau	150	1540		200		16.14	PREPA, Delattre '68
Hag-1	Haguenau	150	1540		300		20.08	PREPA, Delattre '68
Hag-1	Haguenau	150	1540		400		24.66	PREPA, Delattre '68
Hag-1	Haguenau	150	1540		500		31.55	PREPA, Delattre '68
Hag-1	Haguenau	150	1540		600		38.83	PREPA, Delattre '68
Hag-1	Haguenau	150	1540		700		43.64	
Hag-1	Haguenau	150	1540		800		49.45	
Hag-1	Haguenau	150	1540	1393-1425	1409	J	52	PREPA,fault
Hag-1	Haguenau	150	1540	1439-1463	1451	J	74	PREPA,fault
Hag-1	Haguenau	150	1540	1420-1438	1429	J	69	PREPA,fault
Hag-2	Haguenau	156	1444	1399-1430	1414.5	J	70	PREPA,fault
Helion	Pechelbronn	156	1146	904.5	904.5	MK	70	SGAL, well head
Helion	Pechelbronn	161	1146		1146	Bsdst	72	SGAL, well head
Hun-1	Hunspach	150	643	542-576	559		55	PREPA,fault
Huns 101	Hunspach	150		542-576		PS	55	PREPA, Lauer 76
Kalt 1	Kaltenhausen	142			500	PS	29	PREPA, Delattre '68
Kil-1	Kilstett	130	1808		1808	J	66	PREPA
Kubelm 1	Kubelmühl				500		40	PREPA, Lauer 76
Mar 101	Marienbronn	266	904		904	Bsdst	80	Total
Mors 3a	Morsbronn	190	400.3		400	well head	42	SGAL
Mors 3b	Morsbronn	190	580		580	well head	41.8	SGAL
Niederr 101	Niederrödern				500		31	PREPA, Lauer 76
Oberhof	Oberhoffen	124	55					PREPA,fault
Oberl 2	Oberlauterbach	168			500	SG	35	PREPA, Lauer 76
Oberr 1	Oberrödern	134			500		47.5	PREPA, Lauer 76
Obersee 1	Oberssebach	174			500	NS	46	PREPA, Lauer 76
Reim 1	Reimersw.	186	708		708	J	77	PREPA
Reim 1	Reimersw.	186	708		50		15.44	
Reim 1	Reimersw.	186	708		100		20.95	
Reim 1	Reimersw.	186	708		200		33.31	
Ritt 4	Rittershoffen	138			500	PS	42	PREPA, Lauer 76

Appendix 15 Subsurface temperature data

Wellnr.	Location	KB	end depth, m	inter.depth, m	mean depth, m	Formation	Temp.[C]	Comment
Roh-1	Rohrlach	151	1185		1183	K	99	PREPA
Schaff 2	Schaffhausen	126			500	SG	32	PREPA, Lauer 76
Schaff 3	Schaffhausen	126			500	SG	30	PREPA, Lauer 76
Scheib-18	Scheibenhardt	156			50		10.8	PREPA, Delattre '68
Scheib-18	Scheibenhardt	156			100			PREPA, Delattre '68
Scheib-20	Scheibenhardt	157			50		11.06	PREPA, Delattre '68
Scheib-20	Scheibenhardt	157			100		13.83	PREPA, Delattre '68
Scheib-20	Scheibenhardt	157			200		20.83	PREPA, Delattre '68
Scheib-20	Scheibenhardt	157			300		27.8	PREPA, Delattre '68
Scheib-20	Scheibenhardt	157			400		34.08	PREPA, Delattre '68
Scheib-20	Scheibenhardt	157			500		40.42	PREPA, Delattre '68
Scheib-20	Scheibenhardt	157			600		46.35	PREPA, Delattre '68
Scheib-9	Scheibenhardt	157	744	599-603	601		41	PREPA
Stundw 1	Stundwiller	144			500	SG	42	PREPA, Lauer 76
Wintz 1	Wintzenbach 1	172			500		34.5	PREPA, Lauer 76

Appendix 15 Subsurface temperature data

				f=fault(s)		W/mC	m2C/W	C	mW/m2
wellnr.	location	KB	End.Depth	Formation	Depth/base	therm.Conduc.	therm. Resis.	meas.temp.	heat flow
3647	Kutz.N	168	1000	Tert	400	2.1	190.5		
				Tert/f	625	2.1	297.6		
				J	735	2.7	338.4	75.1	189.4
				J	775	2.7	353.2		
				J	800	2.7	362.4		
				K	1000	2.7	436.5	97.5	198.2
3661	Soultz	176	921	NS	55	1.8	30.6		
				PS	80	2.1	42.5	29.8	442.8
				PS	376	2.1	183.4		
				ZD	400	2.1	194.8		
				ZD	450	2.1	218.7	61.5	231.0
				J	542	2.1	262.5		
				K	721	2.7	328.8		
				K	800	2.7	358.0		
				K	820	2.7	365.4	103	251.8
				MK	921	2.8	401.5	117	264.0
				MK	1000	2.8	429.7		
				Base	1400	2.9	567.6		
3956	Kutz.	176	1573	PS	400	2.1	190.5		
				PS	576	2.1	274.3		
				CR	682	2.1	324.8		
				ZD	800	2.1	381.0		
				ZD	945	2.1	450.0		
				J	1000	2.7	470.4		
				J	1125	2.7	516.7		
				K/f	1200	2.7	544.4		
				MK/f	1300	2.8	580.2		
				Bdst	1463	2.8	638.4	109	153.5
				Bdst	1530	2.9	661.5		
				Perm	1561	2.9	672.2	112	150.3
4152	Kleinfrank	186	1230	Q	12	1.7	7.1		

Appendix 16 Cumulative thermal resistance and calculated heat flow values for various depths in the study area

				f=fault(s)		W/mC	m2C/W	C	mW/m2
wellnr.	location	KB	End.Depth	Formation	Depth/base	therm.Conduc.	therm. Resis.	meas.temp.	heat flow
					922	2.1	440.4		
					1000	2.7	469.3	53.5	90.6
					1068	2.7	494.5		
					1127	2.7	516.3		
					1230	2.7	554.5		
4487	Ohlungen	195	778	Q	36	1.7	21.2		
				PS,CR,ZD	400	2.1	194.5		
				PS,CR,ZD	604	2.1	291.7		
				J/f	720	2.7	334.6		
				K	750	2.7	345.7	64	153.3
				K	778	2.7	356.1		
				MK	779	2.8	356.5		
				MK	800	2.8	364.0		
4500	Soultz	149	971	PS	400	2.1	190.5	45	179.0
				PS/f	495	2.1	235.7		
				ZD	524	2.1	249.5		
				J	681	2.7	307.7		
				K	800	2.7	351.7		
				K	891	2.7	385.4		
				LK	900	2.8	388.7	112	259.9
				LK	918	2.8	395.1		
				MK	971	2.8	414.0		
4515	Soultz	146	864	Q	13	1.7	7.6		
	19.11.49			PS	200	2.1	96.7	47	372.3
				ZD	400	2.1	191.9	68	297.0
				ZD	600	2.1	287.2	87	264.7
				ZD	649	2.1	310.5		
				J	772	2.7	356.1		
				K	792	2.7	363.5		
				LK	800	2.8	366.3	100	243.0
				LK/f	802	2.8	367.0		
				MK	857	2.8	386.7	109.7	255.2

Appendix 16 Cumulative thermal resistance and calculated heat flow values for various depths in the study area

				f=fault(s)		W/mC	m2C/W	C	mW/m2
wellnr.	location	KB	End.Depth	Formation	Depth/base	therm.Conduc.	therm. Resis.	meas.temp.	heat flow
				MK	865	2.8	389.5		
4515	Soultz 22.5.88	146	864	Q	13	1.7	7.6		
				PS	200	2.1	96.7	47	377.5
				ZD	400	2.1	191.9	71.5	317.8
				ZD	600	2.1	287.2	92	283.8
				ZD	649	2.1	310.5		
				ZD	700	2.1	334.8	102	273.3
				J	772	2.7	361.5		
				K	792	2.7	368.9		
				LK	800	2.8	371.7	107	259.6
				LK/f	802	2.8	372.4		
				MK	857	2.8	392.1	109.7	253.0
				MK	865	2.8	394.9		
4516	Soultz	187	930	PS	397	2.1	189.0		
				CR	400	2.1	190.5		
				CR	430	2.1	204.8		
				ZD/f	570	2.1	271.4		
				J/f	713	2.7	324.4		
				K	800	2.7	356.6	92	227.1
				K	910	2.7	397.4		
				LK	930	2.8	404.5		
				MK	950	2.8	411.6		
	Soultz	150	930	PS	400	2.1	190.5		
4541				PS	479	2.1	228.1		
				CR	550	2.1	261.9		
				ZD/f	785	2.1	373.8		
				K	800	2.7	379.4		
				K	852	2.7	398.6		
				LK	868.5	2.8	404.5	92	200.2
				LK	879	2.8	408.3		
				MK	900	2.8	415.8	95	202.0
				MK	950	2.8	433.6	106	219.1

Appendix 16 Cumulative thermal resistance and calculated heat flow values for various depths in the study area

				f=fault(s)		W/mC	m2C/W	C	mW/m2
wellnr.	location	KB	End.Depth	Formation	Depth/base	therm.Conduc.	therm. Resis.	meas.temp.	heat flow
4547	Ohlungen	193	876	Q	26	1.7	15.3		
				SG	93	2.1	47.2		
				PS	345	2.1	167.2		
				CR	395	2.1	191.0		
				ZD	600	2.1	288.6		
				J/f	785	2.7	357.1		
				K	800	2.7	362.7		
				K/f	820	2.7	370.1		
				MK	855	2.8	382.6		
				Bdst	870	2.9	387.8	60	126.4
				Bdst	876	2.9	389.9		
4548	Hochstett	200	1157	Q	51	1.7	30.0		
				SG	208	2.1	104.8		
				PS	400	2.1	196.2		
				PS	637	2.1	309.0		
				CR/f	641	2.1	311.0		
				CR/f	653	2.1	316.7		
				J	800	2.7	371.1		
				J/f	890	2.7	404.4		
				K	1062	2.7	468.1		
				LK	1033	2.8	457.8		
				MK	1112.5	2.8	486.2	66.5	114.2
				MK	1157	2.8	502.1		
4550	Soultz	150	1050	Q	12	1.7	7.1		
				Ps	339	2.1	162.8		
				CR	400	2.1	191.8		
				CR	385	2.1	184.7		
				ZD	648	2.1	309.9	63	167.8
				J/f	695	2.7	327.3	66	168.0
				J/f	750	2.7	347.7	69	166.8
				J/f	762	2.7	352.1		
				J/f	800	2.7	366.2	76	177.5

Appendix 16 Cumulative thermal resistance and calculated heat flow values for various depths in the study area

				f=fault(s)		W/mC	m2C/W	C	mW/m2
wellnr.	location	KB	End.Depth	Formation	Depth/base	therm.Conduc.	therm. Resis.	meas.temp.	heat flow
				K/f	854	2.7	386.2		
				K/f	900	2.7	403.2	83	178.5
				MK/f	955	2.8	422.9		
				Mk/f	960	2.8	424.7	93	193.1
				Bdst	1000	2.9	438.5	108	221.2
				Bdst	1050	2.9	455.7		
4554	Soultz		857	PS	384	2.1	182.9		
				CR	400	2.1	190.5		
				CR	438	2.1	208.6		
				ZD	500	2.1	238.1	73.6	262.9
				ZD	679	2.1	323.3		
				J	700	2.7	331.1	93.6	249.5
				J/f	772	2.7	357.8		
				K/f	792	2.7	365.2		
				LK	800	2.8	368.0		
				LK	815	2.8	373.4		
				MK	857	2.8	388.4	110	254.9
				MK	873	2.8	394.1		
4555	Soultz	155	873	PS	348	2.1	165.7		
				CR	402	2.1	191.4		
				ZD	500	2.1	238.1	73	260.4
				ZD	629	2.1	299.5		
				J/f	755	2.7	346.2		
				K	800	2.7	362.9		
				K/ff	830	2.7	374.0		
				LK/f	835	2.8	375.8		
				MK	857	2.8	383.6	112	263.3
				MK	873	2.8	389.3		
4579	Soultz	164	993	Q	6	1.7	3.5		
				PS	400	2.1	191.1		
				PS	598	2.1	285.4		
				CR	662	2.1	315.9		

Appendix 16 Cumulative thermal resistance and calculated heat flow values for various depths in the study area

				f=fault(s)		W/mC	m2C/W	C	mW/m2
wellnr.	location	KB	End.Depth	Formation	Depth/base	therm.Conduc.	therm. Resis.	meas.temp.	heat flow
				ZD	800	2.1	381.6		
				ZD	942	2.1	449.2		
				J/f	942	2.7	449.2		
				K/f	963	2.7	457.0		
				MK	970	2.8	459.5	90	171.9
				MK	1022	2.8	478.1		
4581	Soultz	210	949	PS	400	2.1	190.5		
				PS/f	450	2.1	214.3		
				ZD	601	2.1	286.2		
				J	808	2.7	362.9		
				K	940	2.7	411.7		
				MK	970	2.8	422.5	99.2	208.8
4583	Soultz	158	1049	PS	354	2.1	168.6		
				CR	400	2.1	190.5		
				CR	417	2.1	198.6		
				ZD	665	2.1	316.7		
				J	800	2.7	366.7		
				J	805	2.7	368.5		
				K/f	901	2.7	404.1		
				MK	922.5	2.8	411.8	92	196.7
				MK	965	2.8	426.9		
				Bdst	987.5	2.9	434.7	100	204.7
				Bdst	1000	2.9	439.0		
				Bdst	1001.5	2.9	439.5	108	220.7
				Bdst	1020	2.9	445.9	110	222.0
				Bdst	1039.5	2.9	452.6	111	220.9
				Bdst	1049	2.9	455.9		
4589	Soultz	174	849	Q	20	1.7	11.8		
				PS	324	2.1	156.5		
				CR	370	2.1	178.4		
				ZD	400	2.1	192.7		
				ZD	635	2.1	304.6		

Appendix 16 Cumulative thermal resistance and calculated heat flow values for various depths in the study area

				f=fault(s)		W/mC	m2C/W	C	mW/m2
wellnr.	location	KB	End.Depth	Formation	Depth/base	therm.Conduc.	therm. Resis.	meas.temp.	heat flow
				J/f	727	2.7	338.7		
				K	800	2.7	365.7		
				K/f	843	2.7	381.7	99	230.6
				K/f	849	2.7	383.9		
4590	Soultz	178	1050	Q	53	1.7	31.2		
				PS	400	2.1	196.4		
				PS	423	2.1	207.4		
				CR	468	2.1	228.8		
				ZD	757	2.1	366.4		
				J	800	2.7	382.3		
				J/f	885	2.7	413.8		
				K	966	2.7	443.8	83.3	162.9
				K/f	972	2.7	446.0		
				MK/f	1000	2.8	456.0		
				Bdst	1018.5	2.9	462.4	89	168.7
				Bdst	1022.5	2.9	463.8	89	168.2
4597	Hochstett	200	1065	Q	40	1.7	23.5		
				SG	180	2.1	90.2		
				PS	400	2.1	195.0		
				PS	560	2.1	271.1		
				CR	605	2.1	292.6		
				ZD	750	2.1	361.6		
				J	800	2.7	380.1		
				J	930	2.7	428.3		
				K/f	980	2.7	446.8		
				LK	1000	2.8	454.0		
				LK	1010	2.8	457.5		
				MK	1029.5	2.8	464.5	57	99.0
				MK	1052.5	2.8	472.7	61	105.8
				MK	1060	2.8	475.4		
4598	Soultz	148	855	PS	358	2.1	170.5		
				CR	405	2.1	192.9		

Appendix 16 Cumulative thermal resistance and calculated heat flow values for various depths in the study area

				f=fault(s)		W/mC	m2C/W	C	mW/m2
wellnr.	location	KB	End.Depth	Formation	Depth/base	therm.Conduc.	therm. Resis.	meas.temp.	heat flow
				ZD	636	2.1	302.9		
				J/f	776	2.7	354.7		
				K	800	2.7	363.6		
				K/f	851	2.7	382.5		
				MK	848	2.8	381.4	93.5	216.3
				MK/f	855	2.8	383.9		
				MK	1000	2.8	435.7		
4601	Hoelschl	168	1010	PS	400	2.1	190.5		
				PS	535	2.1	254.8		
				CR	607	2.1	289.0		
				ZD	800	2.1	381.0		
				ZD	825	2.1	392.9		
				J/f	855	2.7	404.0		
				K/f	922	2.7	428.8		
				LK	948	2.8	438.1		
				MK	1004	2.8	458.1	99	192.1
				MK	1010	2.8	460.2		
4602	Kutz.N	182	1065	PS	400	2.1	190.5		
				PS	562	2.1	267.6		
				CR	641	2.1	305.2		
				ZD	800	2.1	381.0		
				ZD/f	893	2.1	425.2		
				K/f	972	2.7	454.5		
				LK	990	2.8	460.9	88	167.1
				LK	998	2.8	463.8		
				MK	1053	2.8	483.4	95	173.8
				MK	1065	2.8	487.7		
4606	Soultz	197	991	PS	383	2.1	182.4		
				CR	400	2.1	190.5		
				CR	429	2.1	204.3		
				ZD	690	2.1	328.6		
				J	800	2.7	369.3		

Appendix 16 Cumulative thermal resistance and calculated heat flow values for various depths in the study area

				f=fault(s)		W/mC	m2C/W	C	mW/m2
wellnr.	location	KB	End.Depth	Formation	Depth/base	therm.Conduc.	therm. Resis.	meas.temp.	heat flow
				J	810	2.7	373.0		
				K/f	930	2.7	417.5		
				LK/f	944	2.8	422.5		
				MK	943	2.8	422.1	114.5	245.2
				MK/f	991	2.8	439.2		
4607	Soultz	159	907.8	PS	306	2.1	145.7		
				CR/f	340	2.1	161.9		
				ZD	400	2.1	190.5		
				ZD	605	2.1	288.1		
				J	774	2.7	350.7		
				K	800	2.7	360.3		
				K	862	2.7	383.3		
				MK	898	2.8	396.1	104	234.8
				MK	907	2.8	399.4		
				MK	1000	2.8	432.6		
4609	Kutz.S	147	982	Q	10	1.7	5.9		
				PS	340	2.1	163.0		
				CR	390	2.1	186.8		
				ZD	400	2.1	191.6	39.7	149.8
				ZD	610	2.1	291.6		
				J/f	720	2.7	332.3		
				K	800	2.7	362.0		
				K/f	865	2.7	386.0		
				MK	878	2.8	390.7	97	220.1
				MK/f	965	2.8	421.8		
				Bdst	972	2.9	424.2	102	214.5
				Bdst	972.5	2.9	424.3	103	216.8
				Bdst	982	2.9	427.6		
				Bdst	1000	2.9	433.8		
				Bdst	1250	2.9	520.0		
				Base	1500	3.1	600.7		
4613	Soultz	162	1050	Q	12	1.7	7.1		

Appendix 16 Cumulative thermal resistance and calculated heat flow values for various depths in the study area

				f=fault(s)		W/mC	m2C/W	C	mW/m2
wellnr.	location	KB	End.Depth	Formation	Depth/base	therm.Conduc.	therm. Resis.	meas.temp.	heat flow
				PS	316	2.1	151.8		
				CR	357	2.1	171.3		
				ZD	400	2.1	191.8		
				ZD	637	2.1	304.7		
				J	803	2.7	366.2		
				K/f	960	2.7	424.3		
				LK	980	2.8	431.5		
				MK	998.5	2.8	438.1	102	207.7
				MK	1020.5	2.8	445.9	112	226.5
				MK	1032	2.8	450.0	115.5	232.2
				MK	1050	2.8	456.5		
4616	Soultz	155	1500	Q	17	1.7	10.0		
				PS	323	2.1	155.7		
				CR	389	2.1	187.1		
				ZD	400	2.1	192.4		
				ZD	654	2.1	313.3		
				J/f	786	2.7	362.2		
				K	800	2.7	367.4		
				K	862	2.7	390.4	72	156.3
				K	972	2.7	431.1		
				LK	989	2.8	437.2		
				MK	1003	2.8	442.2	77	149.3
				MK	1051	2.8	459.3	87	165.5
				MK/f	1107	2.8	479.3		
				Bdst	1130	2.9	487.3	99.5	181.6
				Bdst	1194	2.9	509.3	119	212.0
				Bdst	1380	2.9	573.5	123	195.0
				Basement	1500	2.3	625.6		
4618	Berstheim	218	954	PS	400	2.1	190.5		
				PS	469	2.1	223.3		
				CR	505	2.1	240.5		
				ZD	639	2.1	304.3		
				J	800	2.7	363.9		

Appendix 16 Cumulative thermal resistance and calculated heat flow values for various depths in the study area

				f=fault(s)		W/mC	m2C/W	C	mW/m2
wellnr.	location	KB	End.Depth	Formation	Depth/base	therm.Conduc.	therm. Resis.	meas.temp.	heat flow
				J/f	825	2.7	373.2		
				K/f	872	2.7	390.6		
				LK	881	2.8	393.8	60	124.4
				LK	894	2.8	398.4		
				MK	954	2.8	419.9		
				MK	1000	2.8	436.3		
4619	Soultz	151	873	Q	9	1.7	5.3		
				PS	347	2.1	166.2		
				CR	398	2.1	190.5		
				ZD	660	2.1	315.3		
				J/f	785	2.7	361.6		
				K	800	2.7			
				K	814	2.7	372.3	81	188.0
				K/f	845	2.7	383.8		
				LK/f	849	2.8	385.2		
				MK	859	2.8	388.8	78	172.3
				MK/f	873	2.8	393.8		
				Bdst	1000	2.9	437.6		
4620	Soultz	147	837	Q	12	1.7	7.1		
				PS	351	2.1	168.5		
				CR	392	2.1	188.0		
				ZD	400	2.1	191.8		
				ZD	632	2.1	302.3		
				K	800	2.7	364.5		
				K/ff	837	2.7	378.2		
				MK	840.5	2.8	379.5	97	226.6
				MK	856.5	2.8	385.2	100	231.1
				MK/f	858	2.8	385.7		
				MK	1000	2.8	436.4		
4626	Soultz	181	890	Q	6	1.7	3.5		
				PS	384	2.1	183.5		
				CR	400	2.1	191.1		

Appendix 16 Cumulative thermal resistance and calculated heat flow values for various depths in the study area

				f=fault(s)		W/mC	m2C/W	C	mW/m2
wellnr.	location	KB	End.Depth	Formation	Depth/base	therm.Conduc.	therm. Resis.	meas.temp.	heat flow
				CR	434	2.1	207.3		
				ZD	575	2.1	274.5		
				J/f	670	2.7	309.7		
				K	800	2.7	357.8		
				K	860	2.7	380.0		
				LK	886	2.8	389.3		
				MK	890	2.8	390.8	102	232.9
				MK	1000	2.8	430.0		
4630	Pechelbronn	170	1185	PS	356	2.1	169.5		
				CR	400	2.1	190.5		
				CR	449	2.1	213.8		
				ZD	675	2.1	321.4		
				J/f	680	2.7	323.3		
				K	764	2.7	354.4	80	194.7
				K	800	2.7	367.7		
				K	888	2.7	400.3		
				LK	889	2.8	400.7	105	234.6
				LK	916	2.8	410.3		
				Mk	1000	2.8	440.3		
				MK	1185	2.8	506.4		
4635	Berstheim	175	831	SG/f	83	2.1	39.5		
				PS	400	2.1	190.5		
				PS	428	2.1	203.8		
				CR	476	2.1	226.7		
				ZD/f	610	2.1	290.5		
				J/f	742	2.7	339.4		
				K/f	771	2.7	350.1		
				LK	775	2.8	351.5	75	182.1
				LK	800	2.8	360.5		
				LK	831	2.8	371.5		
				MK	835	2.8	373.0		
				MK	1000	2.8	431.9		

Appendix 16 Cumulative thermal resistance and calculated heat flow values for various depths in the study area

				f=fault(s)		W/mC	m2C/W	C	mW/m2
wellnr.	location	KB	End.Depth	Formation	Depth/base	therm.Condu	therm. Resis.	meas.temp.	heat flow
4636	Soultz	147	914	Q	49	1.7	28.8		
				PS	325	2.1	160.3		
				CR	361	2.1	177.4		
				ZD	400	2.1	196.0		
				ZD	625	2.1	303.1		
				J	748	2.7	348.7		
				K	800	2.7	367.9		
				K/ff	840	2.7	382.7		
				LK	850	2.8	386.3	84.5	190.3
				LK	855	2.8	388.1		
				MK	890	2.8	400.6	86	187.2
				MK	907.5	2.8	406.8	90	194.2
				MK/f	914	2.8	409.2		
				MK	1000	2.8	439.9		
4639	Soultz	107	848	Q	16	1.7	9.4		
				PS	377	2.1	181.3	37	137.8
				CR	400	2.1	192.3		
				CR	416	2.1	199.9		
				ZD	621	2.1	297.5		
				J	718	2.7	333.4		
				K	802	2.7	364.5	87	208.5
				K/f	826	2.7	373.4		
				MK	837.5	2.8	377.5	89.5	207.9
				MK	848	2.8	381.3		
				MK	1000	2.8	435.6		
				Bdst	1500	2.9	608.0		
4642	Soultz	156	871	Q	4	1.7	2.4		
				PS	360	2.1	171.9	41	154
				CR	409	2.1	195.2		
				ZD	605	2.1	288.5		
				J	750	2.7	342.2		
				K	800	2.7	360.8		

Appendix 16 Cumulative thermal resistance and calculated heat flow values for various depths in the study area

				f=fault(s)		W/mC	m2C/W	C	mW/m2
wellnr.	location	KB	End.Depth	Formation	Depth/base	therm.Conduc.	therm. Resis.	meas.temp.	heat flow
				K/f	823	2.7	369.3		
				LK/f	837	2.8	374.3		
				MK	842	2.8	376.1	94.5	222.0
				MK/f	852	2.8	379.6		
				MK	1000	2.8	432.5		
				Bdst	1400	2.9	570.4		
				Base	1500	3.1	602.7		
4648	Pechelbronn	194	892	Q	6	1.7	3.5		
				PS	375	2.1	179.2		
				CR	400	2.1	191.1		
				CR	474	2.1	226.4		
				ZD	690	2.1	329.2		
				J/f	745	2.7	349.6		
				K	800	2.7	370.0		
				K/ff	818	2.7	376.7		
				LK	823	2.8	378.4	58	124.2
				LK/f	836	2.8	383.1		
				MK	887	2.8	401.3	64.5	133.3
				MK	892	2.8	403.1		
				MK	1000	2.8	441.7		
4653	Soultz	176	873	Q	21	1.7	12.4		
				PS	400	2.1	192.8	36	129.6
				PS	411	2.1	198.1		
				CR	432	2.1	208.1		
				ZD/f	634	2.1	304.3		
				J/f	700	2.7	328.7		
				K	800	2.7	365.7		
				K/f	816	2.7	371.7		
				LK	824	2.8	374.5	85.5	198.9
				LK	843	2.8	381.3		
				MK	843	2.8	381.3		
				MK	1000	2.8	437.4		
				Bdst	1200	2.9	506.3		

Appendix 16 Cumulative thermal resistance and calculated heat flow values for various depths in the study area

				f=fault(s)		W/mC	m2C/W	C	mW/m2
wellnr.	location	KB	End.Depth	Formation	Depth/base	therm.Conduc.	therm. Resis.	meas.temp.	heat flow
				Base	1500	2.9	609.8		
4662	Hoelschl	167	1205	Ps	400	2.1	190.5		
				PS	548	2.1	261.0		
				CR	647	2.1	308.1		
				ZD	800	2.1	381.0		
				ZD	913	2.1	434.8		
				J	1000	2.7	467.0		
				J	1120	2.7	511.4		
				LK	1142	2.8	519.3	102	175.2
				LK	1145	2.8	520.4		
				MK	1195	2.8	538.2	109	182.1
4670	Pechelbronn	168	806	PS	354	2.1	168.6		
				CR	400	2.1	190.5		
				CR	436	2.1	207.6		
				ZD	556	2.1	264.8		
				J	733	2.7	330.3		
				K	792	2.7	352.2	70	167.5
				K	805	2.7	357.0		
				MK	1000	2.8	426.6		
4677	Pechelbronn	184	832	PS	393	2.1	187.1		
				PS	400	2.1	190.5		
				CR	500	2.1	238.1		
				ZD	647	2.1	308.1		
				J/f	753	2.7	347.4		
				K	800	2.7	364.8		
				K	812	2.7	369.2	70	159.8
				K	805	2.7	366.6		
				MK	1000	2.8	436.3		
4685	Soultz	179	1089	PS	380	2.1	181.0		
				PS	400	2.1	190.5		
				CR	432	2.1	205.7		

Appendix 16 Cumulative thermal resistance and calculated heat flow values for various depths in the study area

				f=fault(s)		W/mC	m2C/W	C	mW/m2
wellnr.	location	KB	End.Depth	Formation	Depth/base	therm.Conduc.	therm. Resis.	meas.temp.	heat flow
				ZD	726	2.1	345.7		
				J	800	2.7	373.1		
				J	885	2.7	404.6		
				K	965	2.7	434.2	81	161.2
				K	1000	2.7	447.2		
				K	1089	2.7	480.2		
4687	Berstheim	203	1557	SG	30	2.1	14.3		
				PS	272	2.1	129.5		
				CR	306	2.1	145.7		
				ZD	400	2.1	190.5		
				ZD	451	2.1	214.8		
				J	771	2.7	333.3		
				K	800	2.7	344.0		
				K	906	2.7	383.3		
				LK	914	2.8	386.1	57	119.1
				LK	926	2.8	390.4		
				MK	1000	2.8	416.9		
				MK/f	1030	2.8	427.6		
				Bdst	1065	2.9	439.6	67	127.4
				Bdst	1546	2.9	605.5	75	105.7
				Bdst	1557	2.9	609.3		
4712	Ritt 1	176	1853	Q	105	1.7	61.8		
				SG	400	2.1	202.2		
				SG	490	2.1	245.1		
				PS	800	2.1	392.7		
				PS	1000	2.1	488.0		
				PS/CR/ZD	1220	2.1	592.7		
				J	1480	2.7	689.0		
				K/f	1653	2.7	753.1		
				MK	1770	2.8	794.9	159	186.2
				MK/f	1830	2.8	816.3		
				Bdst	1853	2.9	824.2		

Appendix 16 Cumulative thermal resistance and calculated heat flow values for various depths in the study area

				f=fault(s)		W/mC	m2C/W	C	mW/m2
wellnr.	location	KB	End.Depth	Formation	Depth/base	therm.Conduc.	therm. Resis.	meas.temp.	heat flow
4713	Pechelbronn	168	772	Q	5	1.7	2.9		
				PS	365	2.1	174.4		
				CR	400	2.1	191.0		
				CR	456	2.1	217.7		
				ZD	635	2.1	302.9		
				J/f	683	2.7	320.7		
				K	767	2.7	351.8	68	162.0
				K	772	2.7	353.7		
				K	800	2.7	364.1		
				MK	1000	2.8	435.5		
4716	Soufflenh.	131	1868	Q	50	1.7	29.4		
				SG	360	2.1	177.0		
				PS	400	2.1	196.1		
				PS	746	2.1	360.8		
				ZD	800	2.1	386.6		
				ZD	1000	2.1	481.8		
				ZD	1186	2.1	570.4		
				J	1295	2.7	610.7	68	
				J	1455	2.7	670.0		
				K	1465	2.7	673.7	88	114.3
				K	1505	2.7	688.5	91	116.2
				K	1537	2.7	700.4	100	127.1
				K	1638	2.7	737.8		
				LK	1650	2.8	742.1	105	126.7
				LK	1668	2.8	748.5		
				MK	1691	2.8	756.7	109	129.5
				MK	1723	2.8	768.1	106	123.7
				MK	1744	2.8	775.6	110	127.6
				MK	1830	2.8	806.3		
				Bdst	1868	2.9	819.4		
4742	Soufflenh.	134	1656	Q	68	1.7	40.0		
				SG	312	2.1	156.2		
				PS	400	2.1	198.1		

Appendix 16 Cumulative thermal resistance and calculated heat flow values for various depths in the study area

				f=fault(s)		W/mC	m2C/W	C	mW/m2
wellnr.	location	KB	End.Depth	Formation	Depth/base	therm.Conduc.	therm. Resis.	meas.temp.	heat flow
				PS	755	2.1	367.1		
				ZD	800	2.1	388.6		
				ZD	1000	2.1	483.8		
				ZD	1108	2.1	535.2		
				J	1150	2.7	550.8	93	148.9
				J	1398	2.7	642.6		
				K	1556	2.7	701.2		
				LK	1593	2.8	714.4		
				MK	1650	2.8	734.7		
4747	Ritt 2	158	1655	Q	87	1.7	51.2		
				SG	400	2.1	200.2		
				SG	464	2.1	230.7		
				PS	800	2.1	390.7		
				PS	860	2.1	419.3		
				CR	985	2.1	478.8		
				ZD	1000	2.1	485.9		
				ZD	1194	2.1	578.3		
				J	1221.5	2.7	588.5	103	156.3
				J	1444	2.7	670.9		
				K	1605	2.7	730.5		
				LK	1629	2.8	739.1		
				MK	1655	2.8	748.4		
4749	Roeschwoog	119	2505	Q	12	1.7	7.1		
				CN	400	1.8	222.6		
				CN	763.5	1.8	424.6	39	66.0
				CN	800	1.8	444.8		
				CN	995	1.8	553.2		
				SG	1000	2.1	540.1		
				SG	1035.5	2.1	572.5	68	99.6
				SG	1458	2.1	773.6		
				PS	1880	2.1	974.6		
				J	2287	2.7	1125.3		
				K	2467	2.7	1192.0		

Appendix 16 Cumulative thermal resistance and calculated heat flow values for various depths in the study area

				f=fault(s)		W/mC	m2C/W	C	mW/m2
wellnr.	location	KB	End.Depth	Formation	Depth/base	therm.Conduc.	therm. Resis.	meas.temp.	h[illegible]ow
				LK	2491	2.8	1200.6	137	[illegible].9
				MK	2505	2.8	1205.6		
4755	Soufflenh.	164	1407	Q	66	1.7	38.8		
				SG	320	2.1	159.8		
				PS	400	2.1	197.9		
				PS	775	2.1	376.4		
				ZD	800	2.1	388.3		
				ZD	1000	2.1	483.6		
				ZD	1128.5	2.1	544.8	70	108.3
				ZD	1136	2.1	548.3		
				J	1407	2.7	648.7		
4759	Roeschwoog	134	1133	Q	52	1.7	30.6		
				CN	83	1.8	47.8		
				SG	313	2.1	157.3		
				PS	400	2.1	198.8		
				PS	763	2.1	371.6		
				ZD	800	2.1	389.2		
				ZD	1000	2.1	484.5		
				J/f	1136	2.7	534.8	82	132.7
4761	Walbourg	165	802	SG	181	2.1	86.2		
				PS	400	2.1	190.5		
				PS	520	2.1	247.6		
				J	642	2.7	292.8	49	129.8
				J/f	752	2.7	333.5		
				J	782.5	2.7	344.8	61	145.0
				K	800	2.7	351.3		
				K	813	2.7	356.1	69	162.9
				MK	1000	2.8	422.9		
4762	Soufflenh.	134	2130	Q	80	1.7	47.1		
				SG	400	2.1	199.4		
				SG	536	2.1	264.2		

Appendix 16 Cumulative thermal resistance and calculated heat flow values for various depths in the study area

				f=fault(s)		W/mC	m2C/W	C	mW/m2
wellnr.	location	KB	End.Depth	Formation	Depth/base	therm.Conduc.	therm. Resis.	meas.temp.	heat flow
				PS	800	2.1	389.9		
				PS	808	2.1	393.7	60.5	125.7
				PS	830	2.1	404.2		
				ZD	1000	2.1	485.2		
				ZD/f	1037	2.1	502.8		
				J	1105.5	2.7	528.1	71.5	114.6
				J	1356	2.7	620.9		
				LK	1538	2.8	685.9	126	167.7
				LK	1551	2.8	690.6		
4765	Forst 1	116	2150	Q	90	1.7	52.9		
				CN	400	1.8	225.2		
				CN	500	1.8	280.7		
				SG	800	2.1	423.6		
				SG	1000	2.1	518.8		
				SG	1015	2.1	526.0		
				PS	1240	2.1	633.1		
				ZD	1685	2.1	845.0	72	72.2
				ZD	1880	2.1	937.9		
				J	1885	2.7	939.7		
4770	Schirrheim	121	1700	Q	43	1.7	25.3		
				SG	400	2.1	195.3		
				SG	499	2.1	242.4		
				PS	750	2.1	362.0		
				ZD	800	2.1	385.8		
				ZD	1000	2.1	481.0		
				ZD	1130	2.1	542.9		
				J	1515.5	2.7	685.7	78	97.7
				J	1517.5	2.7	686.4	79	99.1
				J	1565	2.7	704.0		
				K	1745	2.7	770.7		
				LK	1770	2.8	779.6		
				MK	1830.5	2.8	801.2		

Appendix 16 Cumulative thermal resistance and calculated heat flow values for various depths in the study area

				f=fault(s)		W/mC	m2C/W	C	mW/m2
wellnr.	location	KB	End.Depth	Formation	Depth/base	therm.Conduc.	therm. Resis.	meas.temp.	heat flow
4774	Beinheim	116	2520	Q	102	1.7	60.0		
				CN	400	1.8	225.6		
				CN	570	1.8	320.0		
				SG	800	2.1	429.5		
				SG	1000	2.1	524.8		
				SG	1023	2.1	535.7		
				Ps	1523.5	2.1	774.0	94	107.2
				PS	1617	2.1	818.6		
				ZD	2074	2.1	1036.2	110	95.5
				ZD	2350.5	2.1	1167.9	127.7	99.9
				ZD	2465	2.1	1222.4		
				J	2520	2.7	1242.8		
4775	Schirrheim	222	1700	Q	135	1.7	79.4		
				CN	286	1.8	163.3		
				SG	400	2.1	217.6		
				SG	516	2.1	272.8		
				PS	800	2.1	408.1		
				PS	1000	2.1	503.3		
				PS	1005	2.1	505.7		
				ZD	1302	2.1	647.1		
				J	1645	2.7	774.1	111	129.2
				J	1670	2.7	783.4		
4776	Ritt 3	137	1592	Q	25	1.7	14.7		
				SG	390	2.1	188.5		
				PS	400	2.1	193.3		
				PS	558.5	2.1	268.8	53	156.3
				PS	775	2.1	371.8		
				ZD	800	2.1	383.8		
				ZD	840.5	2.1	403.0	70	146.4
				ZD	1000	2.1	479.0		
				ZD	1044	2.1	499.9		
				J	1324.5	2.7	603.8	96	140.8
				J	1342	2.7	610.3		

Appendix 16 Cumulative thermal resistance and calculated heat flow values for various depths in the study area

				f=fault(s)		W/mC	m2C/W	C	mW/m2
wellnr.	location	KB	End.Depth	Formation	Depth/base	therm.Conduc.	therm. Resis.	meas.temp.	heat flow
				K	1448.5	2.7	649.8	116	161.6
				K	1517	2.7	675.1		
				LK	1522	2.8	676.9	124	166.9
				LK	1542	2.8	684.1		
				MK	1565.5	2.8	692.5	125	164.6
				MK	1583.5	2.8	698.9	140	184.6
				MK	1592	2.8	701.9		
4777	Beinheim	115	1301	Q	100	1.7	58.8		
				CN	400	1.8	225.5		
				CN	594	1.8	333.3		
				SG	800	2.1	431.4		
				SG	954	2.1	504.7		
				PS	1000	2.1	526.6		
				PS/f	1271	2.1	655.6	76	99.1
4778	Beinheim	118	1084	Q	80	1.7	47.1		
				CN	400	1.8	224.8		
				CN	718	1.8	401.5		
				SG	800	2.1	440.6		
				SG	805	2.1	442.9		
				PS	1000	2.1	535.8		
				PS/f	1073	2.1	570.6	63	91.1
4780	Schirrheim	121	1580	Q	120	1.7	70.6		
				SG	400	2.1	203.9		
				SG	495	2.1	249.2		
				PS	503.5	2.1	253.2	53	165.9
				PS/f	544	2.1	272.5		
4781	Schirrheim	122	800	Q/Plio	230	1.7	135.3		
				SG	400	2.1	216.2		
				SG	432	2.1	231.5		
				PS	768	2.1	391.5	49	97.1
				PS	800	2.1	406.7		

Appendix 16 Cumulative thermal resistance and calculated heat flow values for various depths in the study area

				f=fault(s)		W/mC	m2C/W	C	mW/m2
wellnr.	location	KB	End.Depth	Formation	Depth/base	therm.Conduc.	therm. Resis.	meas.temp.	heat flow
4782	Schirrheim	122	900	Q/Plio	110	1.7	64.7		
				SG	260	2.1	136.1		
				PS	400	2.1	202.8		
				PS	549	2.1	273.8	32	76.7
				PS	572	2.1	284.7		
4783	Schirrheim	120	1560	Q/Plio	130	1.7	76.5		
				SG	400	2.1	205.0		
				SG/f	517	2.1	260.8		
				PS	755	2.1	374.1		
				ZD	400	2.1	205.0		
				ZD	1000	2.1	490.8		
				ZD	1005.5	2.1	493.4	58	95.3
				ZD	1177	2.1	575.0		
				J	1533	2.7	706.9	83	101.9
				J	1549	2.7	712.8	84.5	103.1
				J	1560	2.7	716.9		
4788	Schirrheim	121	572.3	Q/Pio	220	1.7	129.4		
				SG	245	2.1	141.3		
				PS	400	2.1	215.1		
				PS	552	2.1	287.5	40	100.9
				PS	572	2.1	297.0		
4796	Dieff 1 rhinefault hochwald	223	440	Q	5	1.7	2.9		
				PS	207	2.1	99.1		
				CR	320	2.1	152.9		
				ZD/f	361	2.1	172.5		
				MK	371	2.8	176.0	21	56.8
				MK	400	2.8	186.4		
				MK	409	2.8	189.6		
				Bdst	415.5	2.9	191.8	21	52.1
				Bdst/f	440	2.9	200.3		
				Base	800	3.1	316.4		

Appendix 16 Cumulative thermal resistance and calculated heat flow values for various depths in the study area

				f=fault(s)		W/mC	m2C/W	C	mW/m2
wellnr.	location	KB	End.Depth	Formation	Depth/base	therm.Conduc.	therm. Resis.	meas.temp.	heat flow
Dief 2	Dieffenb	237	1035	Q	5	1.7	2.9		
				PS	325	2.1	155.3		
				CR	400	2.1	191.0		
				CR	423	2.1	202.0		
				ZD	645	2.1	307.7		
				J	800	2.7	365.1		
				J	835	2.7	378.1		
				K	985	2.7	433.6		
				MK	1000	2.8	439.0		
				MK/f	1035	2.8	451.5	62	113.0
DO 10	Donau	120	520	Q	42	1.7	24.7		
				SG	268	2.1	132.3		
				PS	400	2.1	195.2		
				PS	497	2.1	241.4	52	169.9
				PS	525	2.1	254.7	63	204.2
				PS/f	525	2.1	254.7		
DO 11	Donau	119	515	Q	55	1.7	32.4		
				SG	249	2.1	124.7		
				PS	400	2.1	196.6		
				PS/f	484	2.1	236.6	42	131.0
				PS/f	515	2.1	251.4		
DO 8	Donau	119	529	Q	37	1.7	21.8		
				SG	273	2.1	134.1		
				PS	400	2.1	194.6		
				PS	511	2.1	247.5	38	109.1
				PS	529	2.1	256.1		
DO 9	Donau	119	504.1	Q/Plio	70	1.7	41.2		
				SG	395	2.1	195.9		
				PS/f	504	2.1	247.8	42	125.1

Appendix 16 Cumulative thermal resistance and calculated heat flow values for various depths in the study area

				f=fault(s)		W/mC	m2C/W	C	mW/m2
wellnr.	location	KB	End.Depth	Formation	Depth/base	therm.Conduc.	therm. Resis.	meas.temp.	heat flow
Hag1	Haguenau	150	1540	Q	60	1.7	35.3		
				SG	337	2.1	167.2		
				PS	400	2.1	197.2		
				PS	800	2.1	387.7		
				PS	880	2.1	425.8		
				CR/ZD	1405	2.1	675.8		
				J	1409	2.7	677.3	52	60.5
				J	1429	2.7	684.7	69	84.7
				J	1451	2.7	692.8	74	90.9
				J	1540	2.7	725.8		
Hag 2	Haguenau	156	1444	Q/Plio	62	1.7	36.5		
				SG	340	2.1	168.9		
				PS	400	2.1	197.4		
				PS	800	2.1	387.9		
				PS	845	2.1	409.3		
				ZD	1000	2.1	483.1		
				ZD	1373	2.1	660.8		
				J	1444	2.7	687.1	70	85.9
Helion	Pechelbronn	161	1146	Q	9	1.7	5.3		
				PS	299	2.1	143.4		
				CR	382	2.1	182.9		
				ZD	400	2.1	191.5		
				ZD	547	2.1	261.5		
				J	702	2.7	318.9		
				K	800	2.7	355.2		
				K	900	2.7	392.2		
				LK	927	2.8	401.9		
				MK	1000	2.8	427.9		
				MK	1103	2.8	464.7		
				Bdst	1146	2.9	479.6	71	125.1
Hun 1	Hunspach	150	643	PS	576	2.1	274.3	55	160.4

Appendix 16 Cumulative thermal resistance and calculated heat flow values for various depths in the study area

				f=fault(s)		W/mC	m2C/W	C	mW/m2
wellnr.	location	KB	End.Depth	Formation	Depth/base	therm.Conduc.	therm. Resis.	meas.temp.	heat flow
Kilst 1	Kilstett	130	1809	Q	190	1.7	111.8		
				SG	400	2.1	211.8		
				SG	602	2.1	308.0		
				PS	800	2.1	402.2		
				PS	1000	2.1	497.5		
				PS	1172	2.1	579.4		
				ZD	1565	2.1	766.5		
				J	1809	2.7	856.9	66	64.2
Mors 3a	Morsbronn	190	400.3	Q	5.5	1.7	3.2		
				PS/f	49	2.1	23.9		
				J/f	199	2.7	79.5		
				K	282	2.7	110.2		
				LK	304	2.8	118.1		
				MK/f	392	2.8	149.5		
				Mk	400	2.8	152.4	42	203.4
Mors 3b	Morsbronn	190	680	Q	6.5	1.7	3.8		
				PS/f	72	2.1	35.0		
				J/f	210	2.7	86.1		
				K/f	272	2.7	109.1		
				MK	400	2.8	154.8		
				MK	457	2.8	175.2		
				Bdst	575	2.9	215.8	42	143.6
				Bdst/f	680	2.9	252.1		
Reim 1	Reimerswi.	186	708.7						
				Q	28	1.7	16.5		
				SG	180	2.1	88.9		
				PS	342	2.1	166.0		
				Cr	400	2.1	193.6		
				CR/f	438	2.1	211.7		
				ZD	668	2.1	321.2		
				J	709	2.7	336.4	77	196.2

Appendix 16 Cumulative thermal resistance and calculated heat flow values for various depths in the study area

				f=fault(s)		W/mC	m2C/W	C	mW/m2
wellnr.	location	KB	End.Depth	Formation	Depth/base	therm.Conduc.	therm. Resis.	meas.temp.	heat flow
Roh 1	Rohwiller	151	1185	SG	191	2.1	91.0		
				PS	400	2.1	190.5		
				PS	588	2.1	280.0		
				CR	633	2.1	301.4		
				ZD	736	2.1	350.5	57	131.3
				ZD	800	2.1	381.0		
				ZD	847	2.1	403.3		
				J	945	2.7	439.6	80	157.0
				J	1000	2.7	460.0		
				J	1081	2.7	490.0		
				K	1183	2.7	527.8	96	161.1
				K	1185	2.7	528.5		

Appendix 16 Cumulative thermal resistance and calculated heat flow values for various depths in the study area

												given
			m	m	m	m	g/cm3			Cel.	kPa/m	m
												subsuface
wellnr	KB	loc	end.depth	inter.d	mean.d	form.	density	est.	TDS mgl	Temp	vert.grad.	w-level
4486	215	Ohlungen	1060		1010	J	1.033				10.135	180
4487	195	Ohlungen			775	MK	1.050			50	10.302	159
4491	189	Dieffenbach			623		1.087				10.665	69
4500	149	Soultz		982-987	985	MK	1.080	y			10.596	
4502	179	Ks	940		900	MK	1.069				10.488	10
4502	179	Ks	940		929	MK	1.070				10.498	0
4506	171	Pechelb		522-550	536	ZD	1.060				10.400	0
4506	171	Pechelb	771	599-613	606	ZD	1.051				10.311	0
4515	147	Soultz			857.7	MK	1.072		101200		10.517	
4516	187	Soultz			903	LK	1.065				10.449	0
4531	200	Kreuz		623-643	633	ZD	1.082				10.616	560
4541	150	Soultz NW		925-950	937	M.K.	1.070		100654		10.498	
4548	200	Hoch		1085-1095	1090	LK	1.050				10.302	
4548	200	Hochstett	1157	1064-1085	1074.5	LK	1.050				10.302	
4548	200	Hochstett	1157	1119-1143	1131	LK	1.050				10.302	
4548	200	Hochstett	1157	1143-1157	1150	MK	1.050	y			10.302	
4550	150	Soultz			985	Bsdst	1.072				10.517	
4550	150	Soultz			1029	Bsdst	1.071				10.508	
4554	156	Soultz			869	MK	1.072		105300		10.517	
4555	150	Soultz	873		300	CR	1.040	y			10.203	
4555	150	Soultz	873		500	ZD	1.068	y			10.478	
4555	150	Soultz	873		859	MK	1.070	y		112	10.498	
4567	147	Pechelb			871	MK	1.070		97314		10.498	
4581	210			948-932	940	Km	1.063				10.429	
4583	158	Kn		985-991	988	Bsdst	1.069		104700	87.7	10.488	
4585	168	Kn	939	923-939	931	MK	1.067		102500		10.468	
4589	174	Soultz	849	825-849	834	K	1.070	y			10.498	
4590	178	Soultz	1050	1035-1050	1042	Bsdst	1.070			112.2	10.498	
4590	178	Soultz	1050	1029-1035	1032	Bsdst	1.038				10.184	90
4597	200	Hoch		975-997	986	K	1.049				10.292	
4597	200	Hoch		1040-1065	1053	LK	1.044				10.243	
4598	148	Soultz	851	842-855	848.5	MK	1.070	y			10.498	

Appendix 17 Equivalent and environmental hydraulic head data

	values	calculated values:						good: 1 fair: 2 poor: 3	
	kPa	m	kPa	m	m	m	m		
wellnr	press	z	cal.press.r	hf	hr	press.hf	press.hr	Quality	Comment
4486		-795	8411.85	63	35.00	858	830	2	
4487		-580	6345.75	67	36.00	647	616	2	fault
4491		-434	5908.16	168	120.00	602	554	2	
4500	10297	-836		214	135.79	1050	972	2	higher
4502		-721	9334.28	231	169.00	952	890	2	log
4502		-750	9752.43	244	179.00	994	929	1	artesian,fault
4506		-365	5574.22	203	171.00	568	536	1	artesian
4506		-435	6248.68	202	171.00	637	606	1	artesian
4515	9365	-710.7		244	179.73	955	890	2	
4516	6962	-716	9435.19	246	187.00	962	903	1	artesian,p too low
4531		-433	774.93	-354	-360.00	79	73	3	
4541	10395	-787		273	203.21	1060	990	2	SiO2: 18; Mn: 11
4548	10346	-890		165	114.31	1055	1004	3	dens. is low!
4548	10346	-874.5		181	129.81	1055	1004	2	dens. is low!
4548	11376	-931		229	173.30	1160	1104	2	dens. is low!
4548	11728	-950		246	188.47	1196	1138	2	dens. is low!
4550	10297	-835		215	144.04	1050	979	2	
4550	10003	-879		141	72.98	1020	952	3	too low
4554	9807	-713		287	219.46	1000	932	2	log
4555	4874	-150		347	327.68	497	478		
4555	5825	-350		244	205.92	594	556		
4555	9218	-709		231	169.09	940	878	2	log,rapp
4567	9613.8	-724		256	191.79	980	916		
4581	9316	-730		220	163.27	950	893	2	
4583	11003	-830		292	219.11	1122	1049	2	
4585	9806	-763		237	173.73	1000	937	2	gaz!!
4589	8139	-660		170	115.31	830	775	3	
4590	11571	-864		316	238.23	1180	1102	3	dens.low/fault
4590		-854	9593.16	124	88.00	978	942	3	dens. low/fissures
4597	8659	-786		97	55.35	883	841	3	density?
4597	10364	-853		204	158.84	1057	1012	2	density?
4598	9169	-700.5		234	172.92	935	873	2	

Appendix 17 Equivalent and environmental hydraulic head data

												given
			m	m	m	m	g/cm3			Cel.	kPa/m	m subsuface
wellnr	KB	loc	end.depth	inter.d	mean.d	form.	density	est.	TDS mgl	Temp	vert.grad.	w-level
4601	169	Hoel		922-950	936	LK	1.070			74	10.498	
4602	182	Kn	1065	969-1010	984.5	LK	1.070	y		88	10.498	
4602	182	Kn	1065	1042-1065	1053	MK	1.100	y		95	10.792	
4606	199	Ramsbachw		986-990	988	MK	1.044				10.243	
4606	199	Ramsbachw		928-960	944	MK	1.066	y			10.459	
4607	159	Soultz	907.8	866-893	879.5	MK	1.070	y		104.5	10.498	
4607	159	Soultz	907.8	893-903	898	MK	1.070	y		104.5	10.498	
4609	147	Ks	982	862-899	881	K	1.070	y			10.498	
4609	147	Ks	982	901-931	916	K	1.072				10.517	
4613	162	Ramsb		1014-1027	1030.5	MK	1.070				10.498	
4616	155	K	1500	850-874	862	Gres R.	1.050	y		72	10.302	
4616	155	K	1500	970.7-982.2	976.5	LK	1.050			96	10.302	
4616	155	K	1500	1115-1145	1130	Bdst	1.100	y		99.5	10.792	
4616	155	K	1500	1192-1196	1194	Bsdst	1.100	y		119	10.792	
4616	155	K	1500	1222-1250	1237	Bsdst	1.100	y		105	10.792	
4616	155	K	1500	1375-1387	1381	Base	1.122	y		111	11.008	
4619	151	Soultz			874	MK	1.072		104000		10.517	
4620	147	Soultz		855-858	856.5	MK	1.072		103700	100	10.517	
4630	170	Hoelschl	1185	889-910	900	LK	1.080	y		105	10.596	
4632	160	Soultz N	418		378	P.inf	1.024		39240		10.046	120
4635	175	Berstheim	831	763-786	775	LK	1.063	y		72	10.429	
4635	175	Berstheim	831	742-767	754.5	K	1.063	y		79	10.429	
4642	156	Soultz SW		832-852	842	LK	1.070		101400	94.5	10.498	
4648	194	Pechelb	892	809-833	821	LK/f	1.070	y			10.498	
4648	194	Pechelb	892	834-852	843	MK	1.070	y			10.498	20
4648	194	Pechelb	892	883-892	884	MK	1.070	y		65	10.498	
4662	167	Bruchmühle	1205	1130-1157	1143.5	LK	1.100	y		102	10.792	
4662	167	Bruch	1205	1185-1205	1195	MK	1.100	y	30400	109	10.792	
4670	168	Pechelb	805	780-805	795.5	K	1.098				10.772	
4677	184	Pechelb		794-832	813	K	1.070	y			10.498	
4685	179	Soultz	1200		1200	Bsdst	1.086				10.655	0
4687	203	Berst NE	1557	901-928	914	LK	1.043		66850	57	10.233	

Appendix 17 Equivalent and environmental hydraulic head data

	values			calculated values:				good: 1 fair: 2 poor: 3	
	kPa	m	kPa	m	m	m	m		
wellnr	press	z	cal.press.r	hf	hr	press.hf	press.hr	Quality	Comment
4601	8722	-767		122	63.84	889	831	3	artesian
4602	8918	-802.5		107	47.01	909	850	3	
4602	10045	-871		153	59.77	1024	931	3	rapp.artesian
4606	9898	-789		220	177.35	1009	966	3	au fond
4606	9212	-745		194	135.81	939	881	3	
4607	9604	-720.5		259	194.36	979	915	3	
4607	10388	-739		320	250.54	1059	990	2	
4609	9996	-734		285	218.20	1019	952	2	
4609	9800	-769		230	162.79	999	932	3	log.copy
4613	10693	-868.5		222	150.10	1090	1019	2	
4616	9124	-707		223	178.69	930	886	2	temp is low
4616	11969.4	-821.5		399	340.40	1221	1162	2	temp? gas/oil
4616	8290	-975		-130	-206.84	845	768	3	Packer
4616	12062	-1039		191	78.67	1230	1118	2	
4616	12454	-1082		188	71.99	1270	1154	2	gaz
4616	12847	-1226		84	-58.93	1310	1167	2	mud
4619	7943	-723		87	32.23	810	755	2	fault
4620	9375	-709.5		246	181.88	956	891	2	
4630	8728	-730		160	93.72	890	824	2	
4632		-218	2591.99	46	40.00	264	258	3	
4635	7453	-600		160	114.64	760	715	2	
4635	7208	-579.5		156	111.64	735	691	2	in fault
4642	6570	-686		-16	-60.15	670	626	2	faille
4648	7845	-627		173	120.30	800	747	3	fault
4648		-649	8639.66	232	174.00	881	823		
4648	8927.1	-690		220	160.36	910	850		
4662	11670	-976.5		214	104.85	1190	1081	2	
4662	12062	-1028		202	89.67	1230	1118	3	
4670	5845	-627.5		-31	-84.91	596	543	3	
4677	7355	-629		121	71.62	750	701	3	oil traces
4685		-1021	12785.70	283	179.00	1304	1200	1	depth?
4687	9218	-711		229	189.82	940	901	2	

Appendix 17 Equivalent and environmental hydraulic head data

												given
											kPa/m	m
			m	m	m	m	g/cm3			Cel.		subsuface
wellnr	KB	loc	end.depth	inter.d	mean.d	form.	density	est.	TDS mgl	Temp	vert.grad.	w-level
4687	203	Berst NE	1557	960-990	975	MK						
4687	203	Berst NE	1557	1024-159	1042	Bsdst/f				67		
4687	203	Berst NE	1557	1059-1093	1076	Bsdst	1.100	y	55150	66.6	10.792	
4712	176	Rittenhouse	1853	1658-1680	1669	MK	1.300	y		159	12.754	
4716	131	Soufl	1890	1660-1674	1667	Bsdst	1.300	y		108	12.754	
4742	134	Soufl	1656	1122-1150	1136	J	1.122	y			11.008	
4755	164	Soufl	1407		350	PS	1.040	y			10.203	10
4755	164	Soufl	1407		1080	ZD	1.100	y			10.792	
4755	164	Soufl	1407		1128	ZT	1.100	y			10.792	
4762	134	Soulff	2130	1525-1552	1539	K	1.250	y			12.264	
4770	121	Schirr	1700	1811-1830	1821	J	1.300	y			12.754	
4774	116	Beinheim	2520	1493-1460	1477	J	1.810	y			17.758	
4776	137	Rittenhouse	1592	549-567	560.5	PM	1.068	y		53	10.478	
4776	137	Rittenhouse	1592	1576-1591	1584	MK	1.300	y		140	12.754	
4777	115	Beinheim	1301	1258-1285	1272	PM	1.123	y			11.018	
4778	126	Beinheim	1077	1059-1089	1074	PM	1.310				12.852	
4780	121	Schirr	544	519-544	531	PM	1.280			39	12.558	
4780	121	Schirr	544	492-515	503.5	PS	1.260			59	12.362	
4781	122	Schirr	800	720-753	734	PS	1.063	y			10.429	
4788	121	Schirr	572.3	505-529	517	PS	1.068	y			10.478	
4794	119	Soufl	535	505-529	517	PS	1.068	y			10.478	45
											#VALUE!	
											0.000	
DIEFF 1	223	Dieffenbach	440		376	MK	1.040	y			10.203	
DO 11	119	Donau	510		483	PS	1.050	y			10.302	
DO 16	119	Donau	511		476	PS	1.050	y			10.302	
DO 18	130	Donau	525		481	PS	1.050	y			10.302	
DO 21	119	Donau	539		494	PS	1.050	y			10.302	
DO 22	121	Donau	527		487	PS	1.050	y			10.302	
DO 23	118.5	Donau	517		498	PS	1.050	y			10.302	
DO 25	120	Donau	506		497	PS	1.050	y			10.302	
DO 9	119	Donau	505		497	PS	1.050	y			10.302	

Appendix 17 Equivalent and environmental hydraulic head data

	values	calculated values:						good: 1 fair: 2 poor: 3	
	kPa	m	kPa	m	m	m	m		
wellnr	press	z	cal.press.r	hf	hr	press.hf	press.hr	Quality	Comment
4687	9221.4	-772		168		940			
4687	7652	-839		-59		780			
4687	10983	-873		247	144.69	1120	1018	2	
4712	17750	-1493		317	-101.31	1810	1392	2	
4716	16671	-1536		164	-228.91	1700	1307	2	
4742	11964	-1002		218	84.85	1220	1087	2	
4755		-186	3469.17	168	154.00	354	340	2	
4755	13091	-916		419	297.02	1335	1213	2	
4755	14121	-994		446	314.46	1440	1308	3	too high
4762	17848	-1405		415	50.35	1820	1455	3	high
4770	18613	-1700		198	-240.65	1898	1459	2	dens.?
4774	15583	-1361		228	-483.48	1589	878	2	
4776	5913	-423.5		179	140.82	603	564	2	
4776	16495	-1447		235	-153.71	1682	1293	2	
4777	12773	-1157		145	2.31	1302	1159	2	
4778	11061	-948		180	-87.38	1128	861	2	fault
4780	3868	-410		-16	-101.99	394	308	2	
4780	5240	-382.5		152	41.38	534	424	2	in fault plane
4781	8728	-612		278	224.89	890	837	3	
4788	5756	-396		191	153.33	587	549	3	
4794		-398	4945.69	106	74.00	504	472	3	
DIEFF 1	3373	-153		191	177.57	344	331	2	PREPA/in fault
DO 11	3432	-364		-14	-30.85	350	333	3	PREPA
DO 16	5982	-357		253	223.69	610	581	2	PREPA
DO 18	5982	-351		259	229.69	610	581	2	PREPA
DO 21	6472	-375		285	253.25	660	628	2	PREPA
DO 22	5099	-366		154	128.97	520	495	3	PREPA
DO 23	6178	-379.5		250	220.22	630	600	2	PREPA
DO 25	4903	-377		123	98.95	500	476	2	PREPA
DO 9	5237	-378		156	130.37	534	508	2	PREPA

Appendix 17 Equivalent and environmental hydraulic head data

												given
			m	m	m	m	g/cm3			Cel.	kPa/m	m
wellnr	KB	loc	end.depth	inter.d	mean.d	form.	density	est.	TDS mgl	Temp	vert.grad.	subsuface w-level
HAG 1	150	Haguenau			1409	J	1.300	y			12.754	
HAG 1	150	Haguenau			1450	J	1.300	y			12.754	
HAT 1	140	Hatten	653		640		1.078	y			10.576	
HOEL 1	164	Hoelschloch			750		1.063	y			10.429	
KALT 1	142	Kalthouse	715		651	PS	1.078	y			10.576	
MORS 3a	185	Morsbronn		359-392	375	MK	1.040	y			10.203	15.1
MORS 3b	182	Morsbronn		359-683	491	Bsdst	1.050	y			10.302	18.1
OBERM	178	Obermodern	1367		550	Bsdst	1.068	y			10.478	
OBERM	178	Obermodern	1367		882	Perm	1.070	y			10.498	
OBERM	178	Obermodern	1367		335	Bsdst	1.040	y			10.203	
OBERS 1	174	Oberseebach	1089		991	PS	1.080	y			10.596	
OHL 1	158	Ohlungen			410	J	1.050	y			10.302	
ROHR 1	153	Rohrlach		843-856	849.5	J	1.070	y			10.498	
SCHAFF 3	126	Schaffhouse	1200		941	PS	1.080	y			10.596	
SCHE 1	134	Scheibenh	1042		978	PS	1.080	y			10.596	
SCHE 12	146	Scheibenh			823	PS	1.078	y			10.576	
SCHE 12	146	Scheibenh			855	PS	1.078	y			10.576	
SCHE 13	140	Scheibenh	735		600	SG	1.078	y			10.576	
SCHE 19	131	Scheibenh	928		906.5	SG	1.080	y			10.596	
SCHE 2	145	Scheibenh	1020		606	SG	1.078	y			10.576	
SCHE 3	145	Scheibenh	980		607	SG	1.078	y			10.576	
SCHE 30	157.5	Scheibenh	958		937	PS	1.080	y			10.596	
SCHE 5	145	Scheibenh	720		553	SG	1.068	y			10.478	
SCHE102	140	Scheibenh	2290		2255	Bsdst	1.120	y			10.987	

Appendix 17 Equivalent and environmental hydraulic head data

	values			calculated	values:			good: 1 fair: 2 poor: 3	
	kPa	m	kPa	m	m	m	m		
wellnr	press	z	cal.press.r	hf	hr	press.hf	press.hr	Quality	Comment
HAG 1	19809	-1259		761	294.12	2020	1553	2	PREPA
HAG 1	21280	-1300		870	368.46	2170	1668	2	PREPA
HAT 1	7070	-500		221	168.48	721	668	2	PREPA
HOEL 1	6266	-586		53	14.82	639	601	3	TOTAL,KB?
KALT 1	7551							2	PREPA
MORS 3a		-190	3979.34	216	200.00	406	390	1	SGAL
MORS 3b		-309	5243.49	226	200.00	535	509	1	SGAL:
OBERM	5982	-372		238	198.90	610	571	2	PREPA
OBERM	8825	-704		196	136.65	900	841	2	PREPA
OBERM	3432	-157		193	179.36	350	336	2	PREPA
OBERS 1	9610	-817		163	89.96	980	907	2	PREPA
OHL 1	3102.6	-252		64	49.18	316	301	2	TOTAL
ROHR 1	9282	-696.5		250	187.69	947	884	2	TOTAL,50%shale
SCHAFF 3	12160	-815		425	332.62	1240	1148	2	PREPA
SCHE 1	10002	-844		176	99.95	1020	944	2	PREPA
SCHE 12	8689	-677		209	144.56	886	822	3	PREPA
SCHE 12	8580	-709		166	102.25	875	811	3	PREPA
SCHE 13	6217								PREPA
SCHE 19	7345	-775.5		-27	-82.31	749	693	3	PREPA
SCHE 2	6864	-461		239	188.00	700	649	2	PREPA
SCHE 3	5491	-462		98	57.18	560	519	2	PREPA
SCHE 30	8963	-779.5		134	66.39	914	846	2	PREPA
SCHE 5	4903	-408		92	59.93	500	468	2	PREPA
SCHE102	20593	-2115		-15	-500.41	2100	1615	3	PREPA,dens.??

Appendix 17 Equivalent and environmental hydraulic head data